

University of Nevada, Reno

The Mercedes Au-Ag District, Sonora, Mexico:
Geology, Geochemistry and Structure of a Sierra Madre
Low-sulfidation Epithermal System.

A thesis submitted in partial fulfillment of the requirements for a Master of
Science degree in Geology.

by

Geoffrey K. Burtner

Dr. Tommy B. Thompson/Thesis Advisor

December, 2013

UMI Number: 1550886

All rights reserved

INFORMATION TO ALL USERS

The quality of this reproduction is dependent upon the quality of the copy submitted.

In the unlikely event that the author did not send a complete manuscript and there are missing pages, these will be noted. Also, if material had to be removed, a note will indicate the deletion.



UMI 1550886

Published by ProQuest LLC (2014). Copyright in the Dissertation held by the Author.

Microform Edition © ProQuest LLC.

All rights reserved. This work is protected against unauthorized copying under Title 17, United States Code



ProQuest LLC.
789 East Eisenhower Parkway
P.O. Box 1346
Ann Arbor, MI 48106 - 1346

Copyright by Geoffrey K. Burtner 2013

All Rights Reserved



University of Nevada, Reno
Statewide • Worldwide

THE GRADUATE SCHOOL

We recommend that the thesis
prepared under our supervision by

GEOFFREY K. BURTNER

entitled

**The Mercedes Au-Ag District, Sonora, Mexico: Geology, Geochemistry
And Structure Of A Sierra Madre Low-Sulfidation Epithermal System.**

be accepted in partial fulfillment of the
requirements for the degree of

MASTER OF SCIENCE

Tommy B. Thompson, Ph.D., Advisor

John L. Muntean, Ph.D., Committee Member

Thom Seal, Ph.D., Graduate School Representative

Marsha H. Read, Ph. D., Dean, Graduate School

December, 2013

ABSTRACT

The Mercedes district contains a series of Oligocene-aged low-sulfidation quartz-carbonate veins with economic Au and Ag mineralization. The veins are hosted in dextral-normal faults contained within andesitic flows, flow breccias and lahar deposits within the Sierra Madre Occidental volcanic sequence. These are localized within two structural basins adjacent to a northwest-trending anticline that exposes pre-mineral tuffs and sedimentary units. The vein mineralogy is characterized by a unique ferruginous green quartz and Mn-oxide bearing calcite assemblage along with both primary and supergene Au-Ag mineralization. Three vein systems within the district were studied: the Mercedes, Klondike and Lupita/Diluvio systems. The Mercedes vein contains the highest grades within the district, is highly-brecciated and displays weak and anomalous geochemical zonation patterns attributed to a high degree of hydrothermal and tectonic brecciation and permeability controlled supergene remobilization. The vein possesses a 4-phase paragenesis. Phase I was the major mineralizing phase, introducing native Au as well as unidentified silver minerals (likely both electrum and silver sulfosalts) along with green quartz and pyrite. Phase II began during a hydrothermal/tectonic brecciation event and appears as a dark Mn-oxide bearing calcite and rhodochrosite cement between phase I breccias. Phase III was a later quartz and calcite veinlet event with local amounts of dark carbonate. Phase IV was the final event, and is a post-mineral oxidation event creating hematite after pyrite, limonite, zeolites and cerargyrite. Statistical evaluation of the geochemical data reveals that Au and Ag grades are poorly correlated with one another, due to post-mineral reworking of the silver mineralogy. Au is most strongly correlated with Pb, Cu, Hg, Zn and Se in that order. Ag is somewhat correlated with Se and Hg, with only weak (<0.5)

correlations with other elements. Ca is positively correlated with only C and Mn, supporting the fact that the dark carbonate phase is a Mn-oxide/calcite intergrowth. This interpretation is further supported by XRF analysis of the carbonates and the presence of boxworks of pyrolusite and other Mn-oxides in former carbonate sites leached by acidic groundwaters. The Klondike vein displays a similar mineralogy and paragenesis to the Mercedes vein, but retains a higher degree of structural order that results in a less-permeable system displaying a stronger and more apparent classical geochemical zonation. Geochemical correlations display a similar pattern to Mercedes with Pb, Cu and Hg being the most correlative elemental indicators of Au grade. Ag correlations with these elements are somewhat higher than in Mercedes. The Lupita/Diluvio system is hosted within a listric structure and consists of the fault-hosted Lupita vein and the overlying Diluvio stockwork, hosted within a gravitationally-displaced block of a quartz-lithic tuff that had been structurally prepared for mineralization during its displacement along the Lupita structure. The Lupita/Diluvio system displays a similar mineralogy and paragenesis to the Mercedes and Klondike vein systems. From these data, a number of inferences can be made. First is that the high degree of brecciation and transport within the Mercedes vein has destroyed the classical epithermal geochemical zonation that is somewhat present in the Klondike system and better defined in the Lupita/Diluvio system. This "washing-out" was accomplished through both physical transport and overprinting during multiple hydrothermal pulses. Second, supergene remobilization related to meteoric fluids has altered the grades and distribution of precious metals as well as further modified the geochemical zonation. The presence of cerargyrite and mineralogical evidence suggests that these processes may be related to the poor Ag recoveries (~30%) and erratic Au/Ag ratios within the vein systems. Third, it is apparent that the structural

weaknesses that localized the mineralization on the property reflect the regional structural fabric of both dextral and extensional tectonics.

ACKNOWLEDGEMENTS

This project would not have been possible without the help of many dedicated geologists and educators. I would like to first thank Dr. Tommy Thompson for his advice and guidance throughout the entire fieldwork, research, writing and review process. Also, gratitude goes out to both Dr. John Muntean and Dr. Thom Seal for their thoughtful edits and feedback on this thesis. Further assistance was provided by Dr. Ian Warren, who allowed access to data from his preliminary studies of the Mercedes area and Dr. Willis Hames at Auburn University for providing a $^{40}\text{Ar}/^{39}\text{Ar}$ date on the latite intrusive.

Last and most certainly not least, Yamana Gold and the entire Mercedes exploration and mine geology teams deserve enormous credit for the funding, on-site assistance and gracious hospitality to a gringo during the summer field season. These talented geologists and staff members include:

Mark Hawksworth, Exploration Director

Jose Carlos Beltran Encinas, Exploration Manager

Rodolfo Garcia Duarte, Geologist

Facundo Cazares Hernandez, Geologist

Mike Zbrozek, Geologist

Rene Cerda Tudon, Geologist

Dario Teran, Facilities Manager

David Saucedo, Engineer

 TABLE OF CONTENTS

Abstract	i.
Acknowledgements	iv.
Table of Contents	v.
List of Tables/Figures	vi.
Introduction	1
Methods	4
Regional Geology	9
Assembly of Northern Sonora: Tectonics and Volcanism	9
Cenozoic Extension: The Mexican Basin and Range	10
Other Regional Deposits	13
District Geology	15
Stratigraphy and Unit Descriptions	18
Petrologic Descriptions of Host Andesite	29
Overview of Mineralized Zones	35
The Mercedes Vein	40
Introduction	40
Paragenesis	46
Vein and Mineral Textures	55
Geochemistry	69
The Klondike Vein	87
Introduction	87
Paragenesis	91
Vein and Mineral Textures	97
Geochemistry	105
The Lupita/Diluvio System	116
Introduction	116
Paragenesis	122
Vein and Mineral Textures	125
Geochemistry	138
Structure on the Mercedes Property	149
Mercedes/Barrancas Structure	149
Klondike Structure	152
Lupita/Diluvio Structure	152
Discussion	153
Conclusions	159
Exploration Implications	168
Suggestions for Future Work	170
References	172

LIST OF TABLES/FIGURES

Fig. 1	Location of the Mercedes Property	1
Fig. 2	The Mercedes region.	11
Fig. 3	Regional geologic map.	12
Fig. 4	Mercedes district geologic map.	16
Fig. 5	Lithostratigraphy of the Mercedes property.	17
Fig. 6	Diamictites and mudstones of the Basal Sedimentary Package.	19
Fig. 7	Field photo and photomicrograph of the quartz-lithic tuff unit.	20
Fig. 8	Photos of the host andesite units in outcrop.	22
Fig. 9	Characteristics of the latite flow-dome complex.	25
Fig. 10	Outcrop photo of flow-foliated platy andesite.	27
Fig. 11	Typical porphyritic andesite flow.	30
Fig. 12	Heterolithic andesite debris flow deposit.	30
Fig. 13	Sample An-S-1, thin section, plane polarized light.	31
Fig. 14	Sample An-S-2, thin section, plane polarized light.	32
Fig. 15	Sample C-An-S-5, thin section, crossed nicols.	33
Fig. 16	District geologic map with mineralized zones labeled.	34
Fig. 17	Geologic map of the Mercedes vein zone.	41
Fig. 18	Long section of the Mercedes vein showing true thickness.	42
Fig. 19	Long section of the Mercedes vein showing average Au grade.	43
Fig. 20	Cross-section 9550.	44
Fig. 21	Cross-section 11710	45
Fig. 22	Paragenetic Diagram for the Mercedes Vein.	47
Fig. 23	Examples of phase I mineralization.	49
Fig. 24	Examples of phase II mineralization.	51
Fig. 25	Examples of phase III mineralization.	53
Fig. 26	Cavities coated with goethite after pyrite.	54
Fig. 27	Typical Mercedes vein morphologies, 960 level of the Corona de Oro Zone.	56
Fig. 28	Photomicrographs of andesite.	57
Fig. 29	"Sandy" veinlet from the 910 level of the Corona de Oro ore shoot.	58
Fig. 20	The Mercedes fault.	59
Fig. 31	Mineral textures from Phase I.	61
Fig. 32	Plane polarized light, close-up of boxed area of Fig. 32.	62
Fig. 33	Phase II dark carbonates from the 910 level of the Corona de Oro ore shoot.	64
Fig. 34	Photomicrographs of phase III mineralization.	66
Fig. 35	Iron staining in the 960 level, Mercedes.	68
Fig. 36	Mercedes metals vs. elevation.	74
Fig. 37	Mercedes trace elements vs. elevation	75
Fig. 38	Mercedes section 9550 metals vs. elevation	76
Fig. 39	Mercedes section 9950 trace elements vs. elevation	77
Fig. 40	Mercedes section 8860 metals vs. elevation.	78
Fig. 41	Mercedes section 8860 trace elements vs. elevation.	79
Fig. 42	Covariation of Ag/Zn and Pb/Zn, Mercedes Vein	80

Fig. 43	Mercedes major elements vs. strike.	82
Fig. 44	Mercedes metals vs. strike.	83
Fig. 45	Mercedes trace elements vs. strike.	84
Fig. 46	Correlation matrix for selected elements, Mercedes vein.	86
Fig. 47	Geologic map of the Klondike vein zone.	88
Fig. 48	Cross-section 11080	89
Fig. 49	Klondike vein long section showing true width of the vein.	90
Fig. 50	Klondike vein paragenetic diagram	92
Fig. 51	Klondike vein material.	93
Fig. 52	Vein proximal stockworks demonstrating paragenetic relationships.	93
Fig. 53	Phase II dark carbonate cement of oxidized andesite and local phase I quartz clasts.	94
Fig. 54	Crystalline phase III calcite vein cutting oxidized andesite.	95
Fig. 55	Banded vein material from Klondike.	97
Fig. 56	Typical phase I mineral textures from the Klondike vein.	100
Fig. 57	Typical phase II textures.	102
Fig. 58	Typical phase III textures.	103
Fig. 59	Klondike metals vs. elevation.	107
Fig. 60	Klondike minor elements vs. elevation.	108
Fig. 61	Covariation of Ag/Zn and Pb/Zn, Klondike Vein	109
Fig. 62	Klondike major elements vs. strike.	111
Fig. 63	Klondike metals vs. strike.	112
Fig. 64	Klondike trace elements vs. strike.	113
Fig. 65	Correlation matrix for selected elements, Klondike vein.	115
Fig. 66	Geologic map of the Lupita/Diluvio zone.	117
Fig. 67	Cross-section 5240.	119
Fig. 68	Cross-section 9940.	120
Fig. 69	Paragenetic diagram for the Lupita/Diluvio system.	122
Fig. 70	Outcrop textures of the Lupita vein.	126
Fig. 71	Polyphase banded chalcedonic quartz and dark carbonate vein from the Lupita vein.	127
Fig. 72	Massive carbonate w/ quartz veinlet from Lupita vein.	127
Fig. 73	Lupita vein breccia with clasts of chalcedonic green quartz in a carbonate/hematite matrix.	128
Fig. 74	High level, vuggy vein material from the Lupita vein.	130
Fig. 75	Typical Phase I mineral textures.	132
Fig. 76	Phase II calcite+Mn-oxide intergrowths grown from a selvage of phase I mosaic quartz.	134
Fig. 77	Phase III calcite veinlet cutting with dark selvages cutting Phase I and II breccia.	135
Fig. 78	Phase IV incomplete oxidation of Lupita vein breccia.	136
Fig. 79	Lupita metals vs. elevation.	140
Fig. 80	Lupita trace elements vs. elevation.	141
Fig. 81	Diluvio metals vs. elevation.	124
Fig. 82	Diluvio trace elements vs. elevation.	143
Fig. 83	Covariation of Ag/Zn and Pb/Zn, Lupita Vein	144
Fig. 84	Covariation of Ag/Zn and Pb/Zn, Diluvio System	145
Fig. 85	Interpretation of Diluvio Ag/Zn and Pb/Zn Covariance	146
Fig. 86	Relative Ag/Zn and Pb/Zn Trends, Diluvio System	146

Fig. 87	Correlation matrix for selected elements, Lupita/Diluvio.	148
Fig. 88	"Foliated" clay gouge on the Mercedes fault trace at the 910 level of the Corona de Oro ore shoot.	150
Fig. 89	Stereographic projection of Mercedes fault trace measurements.	151
Fig. 90	Stereographic projection of Klondike fault trace measurements and fault surface.	152
Fig. 91	Structural context of the Mercedes, Klondike and Lupita fault-hosted veins.	156
Fig. 92	Graben linkage structures from Canyonlands, Utah.	157
Fig. 93	Illustrations of geothermal structural regimes.	158
Table 1	Comparison of the Mercedes District to a selection of other epithermal Au-Ag deposits	160
Table 2	Summary of characteristics of the Mercedes, Klondike and Lupita/Diluvio Zones.	161

INTRODUCTION



Figure 1. Location of the Mercedes Property (red star) within the state of Sonora (red outline), Mexico.

Modern mining has occurred sporadically in the Mercedes district since the late 19th century, though gold and silver have been known in the region since it was settled in the early 1600s. There are small, artisanal workings scattered across the property of unknown age but records from the Anaconda Copper Company show that mining was in progress as of the early 20th century in the Klondike, Rey de Oro and Tucabe zones within the district (Hawksworth et al., 2009).

The most productive vein in the district, the Mercedes vein, was discovered and explored in the mid-1930s by the Anaconda Copper Company. This vein was later put into production between 1937 and 1940 by Minera Oro Chico. Modern exploration of

the region began in 1993 by FMC Gold Company and later on in the decade as Meridian Gold Company.

A reverse-circulation drilling program through the early 2000s resulted in promising intercepts culminating in 2005 with a hole piercing the Corona de Oro ore shoot within the Mercedes vein. This hole (M05-031R) intercepted 21 m of 28 ppm Au and 240 ppm Ag (Mercedes Core Logs and Hawksworth et al., 2009).

Further drilling along the Mercedes and Klondike vein systems defined contiguous mineralization along strike and has also identified Au-Ag mineralization in the Lupita vein and two stockwork zones with open-pit potential associated with both the Lupita vein (the Diluvio stockwork) and the Klondike vein (the Rey de Oro stockwork). Underground mining began in 2010 at both the Mercedes and Klondike veins, with the first bars poured in December, 2011. As of late 2011, the district contained proven and probable reserves of 5.30 Mt ore grading at 5.66 ppm Au and 59.3 ppm Ag containing 960,000 oz Au and 10,099,000 oz Ag (Yamana Gold, 2013)

This project focuses on the major mineralized zones of the Mercedes district, namely the Mercedes, Klondike and Lupita/Diluvio zones. Together, they are best described as a low-sulfidation epithermal (Buchanan, 1981; Hayaba et al., 1987; Heald et al., 1987; White and Hedenquist, 1990; Simmons et al., 2005) system that displays both the typical characteristics of such systems as well as characteristics unique to the Mercedes district.

While the district is in full-scale production and has been extensively drilled, there has been little detailed mineralogical and geochemical work done on the property. The availability of both a large library of core and underground access allows for a detailed, three-dimensional analysis of the mineralogy, paragenesis, and trace- and

major-element geochemistry. Conclusions drawn from these data have applications to ongoing exploration for additional resources.

This paper aims to describe and catalog the characteristics of the Mercedes district, one of the northernmost documented epithermal systems in the Sierra Madre metallogenic belt. Four primary lines of investigation are covered within this paper: vein mineralogy and paragenesis, major and trace element geochemistry of the veins, structural controls on mineralization within the district and the nature of the host rocks with an attempt to define an age for this deposit.

Within the broad heading of vein mineralogy and paragenesis, this study will define the mineralogical evolution of the vein systems and define the mineralogy of the precious metals, the textural and compositional variations within the veins and attempt to constrain the characteristics and causes of the high-grade ore shoots.

Study of the major and trace element geochemistry of the veins will attempt to quantify any spatial zonation or correlation between elements in the vein systems, along strike and dip as well as on a district scale, in order to illuminate any patterns which may be exploited for the ongoing exploration in the district.

Further, an initial study of the structure and petrology of the district was undertaken to better understand the nature of the faults localizing the veins and place these structures within a regional context that may provide additional exploration targets. This structural context is supplemented by a petrologic investigation of the volcanic sequence of the district with an attempt to date the mineralization and determine its relationship to the host rocks.

METHODS

The three mineralized zones (Mercedes, Klondike and Diluvio/Lupita) chosen for this study were selected on the basis of the availability of a drill core, underground access (for Mercedes and Klondike), and the possibility that the results of this study can be used to better understand the mineralization of these areas with the goal of enhancing production or further developing the district. Within these zones, cross sections for this study were chosen based on the amount of available core and to ensure an adequate spatial distribution of samples along the strike and dip of the veins. For the Mercedes zone, these selections were hampered by a prior metallurgical study that consumed entire vein intercepts, directly affected sample selection for this study.

In all, 52 diamond drill holes from 13 study cross-sections were used from the 3 zones. The preserved core was largely restricted to vein intercepts, but enclosing country rocks were sampled in some holes. From these, 108 30 μm -thick polished thin-sections were prepared to study the vein mineralogy and textures. A further 8 thin-sections were created of representative samples of the host andesites and lower tuff sequence. Microscopy was performed using Olympus BX51 and BX53 polarizing light microscopes.

Geochemical studies were accomplished using reject assay pulps from the initial resource delineation drilling. 260 pulps from 1 m vein intervals were selected from the Meridian Gold pulp library housed in Hermosillo, Sonora. Samples were chosen on the basis of availability of the sample and reference core, proximity to the study cross sections and position along the vein for adequate vertical and horizontal coverage given the budget of this study. These samples were submitted to ALS-Chemex for 48-element ICP atomic emission and mass spectroscopy (depending on the element), Hg analysis via the cold-vapor method and total C and S via LECO furnace IR spectroscopy following a

4-acid digestion (method ID Codes: ME-MS61m and ME-IR08). Au and Ag assaying was completed by 30 g fire assay with an AA finish where data was missing from the original assay runs.

These samples were put into a 3-dimensional model constructed from down-hole drill surveys using Leapfrog software. Using this model, the true spatial coordinates for the center of each pulp segment was determined and used in conjunction with the chemical data in Microsoft Excel in order to generate the plots showing the geochemical zonation and elemental correlation of the vein systems. Statistical regressions of the data was performed using a power regression to accommodate the log-log plotting of the large variations in the element concentrations. Pearson's product-moment correlation coefficients, calculated by dividing the covariance of the two variables with the product of the respective standard deviations of their arrays, are used to determine the degree of interrelationship between various elements. While statistical tests to interpret the importance of a particular size of correlation exist, this study chose ± 0.5 to be a relevant correlation and ± 0.75 to be significant relationship based on the perceived quality and spread of the assay data as well as a literature review suggesting that these criteria would be sufficient to evaluate the relationships between the elements in the system.

Several factors came into play when attempting to assess the geochemical zonation of the veins. First, inspection of the sampled vein was not always possible as the assay pulps were frequently all that remained of the drill core. This also hampered the use of grade-thickness as different loggers used different criteria to define the vein (presence of breccia, presence of vein quartz, a certain cut-off grade e.g.) and the author of this paper was not able to reconcile these difference given the missing core. Second, observation of the sampling process lead to doubts about the uniformity of each assay

pulp. While the pulps were collected on regular intervals, the collection process involved splitting (not cutting) highly fragmented core with an unknown amount missing and a significant possibility of cross-contamination from other intervals and sampling errors due to the subjective judgment of what was “half” of the core. Mitigation of the handling effects was also impossible due to missing reference core. Numerical techniques (compositing, averaging etc.) to moderate these issues was impossible for the same reasons as the issues themselves.

Adequate resampling of the systems was impossible. Channel samples for grade control in Mercedes and Klondike were only assayed for Au and Ag and assay rejects were unavailable. Additionally, mining had only progressed to the 980 m level at Mercedes and the 1020 m level in Klondike, presenting a limited vertical extent for study. Underground sampling along strike was also unfeasible as any non-working faces had been covered by shotcrete. The Lupita and Diluvio systems are currently undeveloped and direct sampling was impossible. Thus, in order to minimize the errors introduced by the logistical realities of this study, as many samples as were available within budget were used with the assumption that a large sample size would smooth out the outliers created by the unknown factors and allow for a somewhat reasonable dataset for analysis. In order to accomplish this, the entire vein intercept of each drillhole was assayed, but each individual sample interval was maintained as a discrete data point throughout the analysis. Samples were selected with the aid of existing core logs and core photos in an attempt to minimize the amount of wall rock-containing samples. Where records indicate significant brecciation or uncertainties in the location of the vein boundaries, samples were taken starting from the location where green quartz and dark carbonate mineralogies began to dominate the logs.

Two methods are attempted to assess the geochemical zonation of the veins. The first is a direct method (see Berger and Silberman, 1985; Silberman and Berger, 1985; Ruvalcaba-Ruiz and Thompson, 1988), plotting the concentration of the element in question directly against depth. Secondly, a slightly modified version of the method used by Loucks and Petersen (1985) involving graphical interpretations of metal ratios within the vein is used to test the veracity of the direct plotting method. However, the Loucks and Petersen study depended upon detailed a detailed paragenetic study documenting codeposition of the sphalerite, galena and silver-bearing minerals in an unoxidized and unbrecciated ore body with high total sulfide content. Lacking these qualities, the assumption that the Ag, Pb and Zn minerals were deposited together in all vein systems based on the presence of galena and Ag mineralization coexisting in the 1st paragenetic phase within the relatively unoxidized Diluvio system. Further, the thorough oxidation of the Mercedes and Klondike systems documented in this study suggests that any zonation patterns based off relatively mobile Ag and Zn probably reflect an undermined combination of hypogene distribution and supergene remobilization. Using these assumptions, assay pulps were grouped into populations centered every 50 m of elevation and the plots were interpreted according to the graphical method outlined in that study. The reader is directed to the referenced Loucks and Petersen paper for a more detailed treatment of their methodologies and the mathematics involved.

Quantitative XRF spectroscopy was performed on 6 samples selected from the Mercedes and Klondike veins. Separates of the green quartz and dark carbonates were prepared by fracturing bulk samples and further isolating the desired species using a diamond saw to remove unwanted phases. The quartz samples were further prepared via partial digestion with 38% HCl overnight, followed by another digestion of 6 hours

with fresh acid and a tap water rinse to remove any traces of carbonates. The carbonate samples underwent no further treatment and these were submitted to ALS-Chemex. Pulverization was achieved using a zirconia bowl to avoid silica contamination. Major element analysis was conducted after a LiBO_4 fusion by X-ray fluorescence (method ID code: ME-XRF06) as well as total C by LECO furnace IR spectroscopy (method ID code: C-IR07).

Mapping and surveying was completed underground over the duration of the 3-month field season from May-August, 2012. Working faces in the Mercedes and Klondike mines were mapped for gross textural information and sampled for fill-in petrographic and geochemical work. Underground exposures from the 1080 to 960 level were examined in Mercedes, and from the 1160 to 1060 levels in Klondike. The existing Yamana geodatabase was used for the surface geological maps, and these data were verified and added to with surface reconnaissance over the course of the summer.

The data for the structural analysis of the Mercedes and Klondike veins was gathered along accessible underground exposures of the vein-hosting faults using a Brunton International Pocket Transit using a magnetic declination correction of 10° east. Lower-hemisphere stereonet plots were generated using GEOrient software by Rod Holcombe, under the free academic use agreement.

REGIONAL GEOLOGY

Assembly of Northern Sonora: Tectonics and Volcanism

The Mercedes district (Fig. 3) lies atop a basement composed of the Proterozoic crystalline rocks and Paleozoic sediments of the Mazatal province (Molina-Garza and Iriondo, 2007). Starting in the Jurassic the region was heavily affected by synoptic-scale sinistral tectonics, notably the controversial Mojave-Sonora megashear (Centeno-Garcia et al., 2003; Anderson and Silver, 2005), bringing the Papago, Cortes and Caborca terranes from their depositional locations near present-day Nevada and docking them against the North American craton to the southwest of the Mercedes district's present location. The resultant north-northwest directed convergence and accretion, defined by Mesozoic structures throughout central and southern Sonora (Henry, 1986), are also recorded in a number of northeast-trending basement structures inferred to have directed the extensive copper porphyry mineralization in northern Sonora (Turner et al., 1982).

Magmatic activity in the region began in the late Cretaceous in association with the subduction of the Farallon plate to the west of the District (McDowell and Clabaugh, 1981). Products of this magmatism, termed the Lower Volcanic Complex (McDowell and Keizer, 1977), are a suite of intermediate to felsic batholiths and related volcanic rocks exposed and that are correlative throughout the length of the Sierra Madre (Ferrari et al., 2007; Gonzalez-Leon et al., 2000; McDowell and Clabaugh, 1981). The intrusions are thought to be genetically related to a significant endowment of Cu-porphyry and related mineralization represented by the giant Cananea and La Caridad Cu deposits and the Alacran-Nacozari porphyries, skarns and carbonate replacement Cu-Pb-Zn deposits all within 100 km of the Mercedes camp (Damon et al., 1983; Anderson and Silver, 1977).

This first phase of magmatism ceased in the early- to mid-Paleocene and there was a lull in plutonic activity in the Sierra Madre until the Eocene (Ferrari et al., 2007). The resumption of magmatism at 46 Ma was the earliest expression of the "ignimbrite flare-up" that defines the geology of the Sierra Madre Occidental. The silicic eruptive activity peaked from 27 to 33 Ma during the Oligocene and early Miocene resulting in an ignimbrite province 1200 km long, 250 km wide and with local thicknesses exceeding 1000 m of dominantly rhyolitic ignimbrites, tuffs and flows that sum to over 300,000 km³ of material cumulatively termed the Upper Volcanic Supergroup (Ferrari et al., 2007; McDowell and Keizer, 1977).

Cenozoic Extension: The Mexican Basin and Range

Starting around 30 Ma, much of the western part of mainland Mexico began to be affected by the southernmost expressions of Basin and Range extension (Henry and Aranda-Gomez, 1992). This event is particularly significant in regards to the economic geology of northwestern Mexico. Many of the significant epithermal deposits of the region, including the Fresnillo, Guanajuato, Ocampo and Santa Eulalia districts, exhibit the same northwesterly orientations of the veins (Henry and Aranda-Gomez, 1992; this study). The shared orientation between these systems, dated between 26-31 Ma, and the mineralization trends in the Mercedes district suggests that the veins may all be part of the same metallogenic epoch responsible for western Mexico's huge endowment of precious and base-metal deposits.

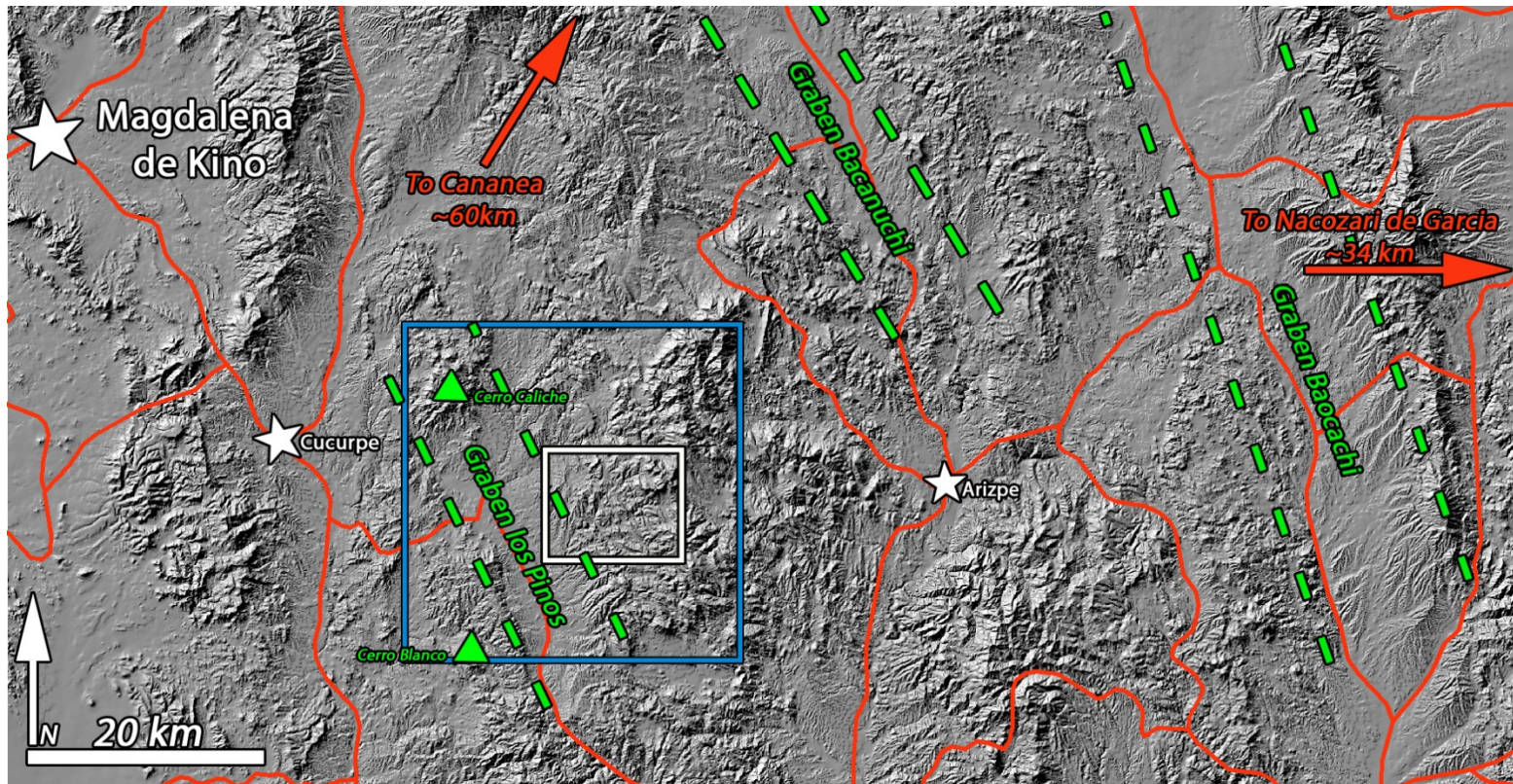


Figure 2. The Mercedes region. Red lines are roads, the larger blue box indicates the extent of the Saracachi quadrangle (Fig. 3). The contained, white box indicates the extent of the district geologic map (Fig. 4). Grabens are labeled and marked with green, dashed lines.

Other Regional Deposits

The region surrounding the Mercedes property has seen mining activity since the mid-1600s. Within the Saracachi quadrangle (Fig. 3), a number of precious and base metal deposits hosted in the local volcanic sequences have seen production, though much of the data on these mines has since been lost. Deposits (1) and (2) in Figure 4 represent the Mercedes and Klondike zones, (3) Santa Clara del Cobre vein system, (4) the El Matadera and La Brisa placers, (5) El Magistral veins and stockworks, (6) the many vein and replacement deposits of Los Japoneses area and (7) El Toro vein deposits. Many of these vein-hosted deposits share the northwest to west strike of the Mercedes deposits. More detailed information can be found in the description of the Saracachi quadrangle map (SGM, 1999) and related documents.

Approximately 30 km north-northwest of the Mercedes property, the Santa Gertrudis district contains disseminated Au mineralization hosted in Cretaceous siliciclastic and carbonate units, interpreted as Carlin-style mineralization with local evidence of epithermal-style quartz+calcite+Au and subeconomic Cu-Mo porphyry mineralization (Alba Pascoe, 1998; Noble et al., 2010). Mineralization is inferred to date between 22-26 Ma and the district produced ~565,000 oz Au from 8.24 Mt of ore grading 2.13 g/t. Current resource estimates are of 13.50 Mt with an average grade of 1.28 g/t Au using a cutoff of 0.30 g/t Au (Noble et al., 2010).

Within 100 km of the Mercedes property, a number of world-class Cu-porphyry with related skarn and manto-type deposits exist. To the north, the Laramide Cananea district holds porphyry and skarn mineralization that has been in production since the early 1900s. Together, La Colorada and Maria deposits contained 516,000 t Cu, 53,760 t Mo and 1.59 Moz Ag (Wodzicki, 2001). Genetically-related Cu-porphyry and high-sulfidation Cu-Au epithermal mineralization at La

Caridad, ~55 km east of Mercedes, is (as of 2008) the most productive Cu system currently in operation in Mexico and dates between 53 and 56 Ma (Valencia et al., 2008).

Sixty-two km west of the Mercedes property, the San Francisco mine and surrounding properties host Au and local Mn mineralization hosted in quartz+tourmaline veins within Mesozoic gneisses and schists along the trace of, and inferred to be coeval with, the Mojave-Sonora megashear zone. Production from 1996 to 2002 extracted 300,000 oz Au and 96,150 oz Ag from a mesothermal/orogenic style ore body (Lewis, 2005)

DISTRICT GEOLOGY

Roughly 2500 m of stratigraphic thickness is exposed throughout the Mercedes property. The mineralized veins are concentrated within biotite-hornblende andesites (Figs. 4 and 5) that are restricted to two basins that are peripheral to two northwest striking antiforms. The antiforms plunge gently ($\sim 10^\circ$) to the northwest and expose a lower sequence of lithic tuffs and Mesozoic sedimentary packages (Fig. 6). These antiforms appear to predate and possibly localize the subsequent andesitic units as no evidence of deformation is seen within the andesites hosting the Mercedes or Klondike vein systems.

Overlying the host andesites is a unique "platy" andesite unit and a latite dome-flow complex, both of which appear to postdate mineralization. A high plateau to the northeast of the mining camp is held up by a sequence of rhyolite ignimbrites and flows and a vesicular basalt sequence, both of which are commonly found as float within the major arroyos that drain the plateau through the property.

The regionally extensive Baucarit Formation of intercalated conglomerates and tuffs encroaches on the northern and western sides of the property (Fig. 4 and 5), locally covering the mineralized host andesites in the Mercedes basin. The conglomeratic Baucarit members contain clasts of all of the units defined above as well as horizons of argillized volcanic ash and tuffs.

Based on mapping and field examination, the major units within the Mercedes district stratigraphic sequence are described below.

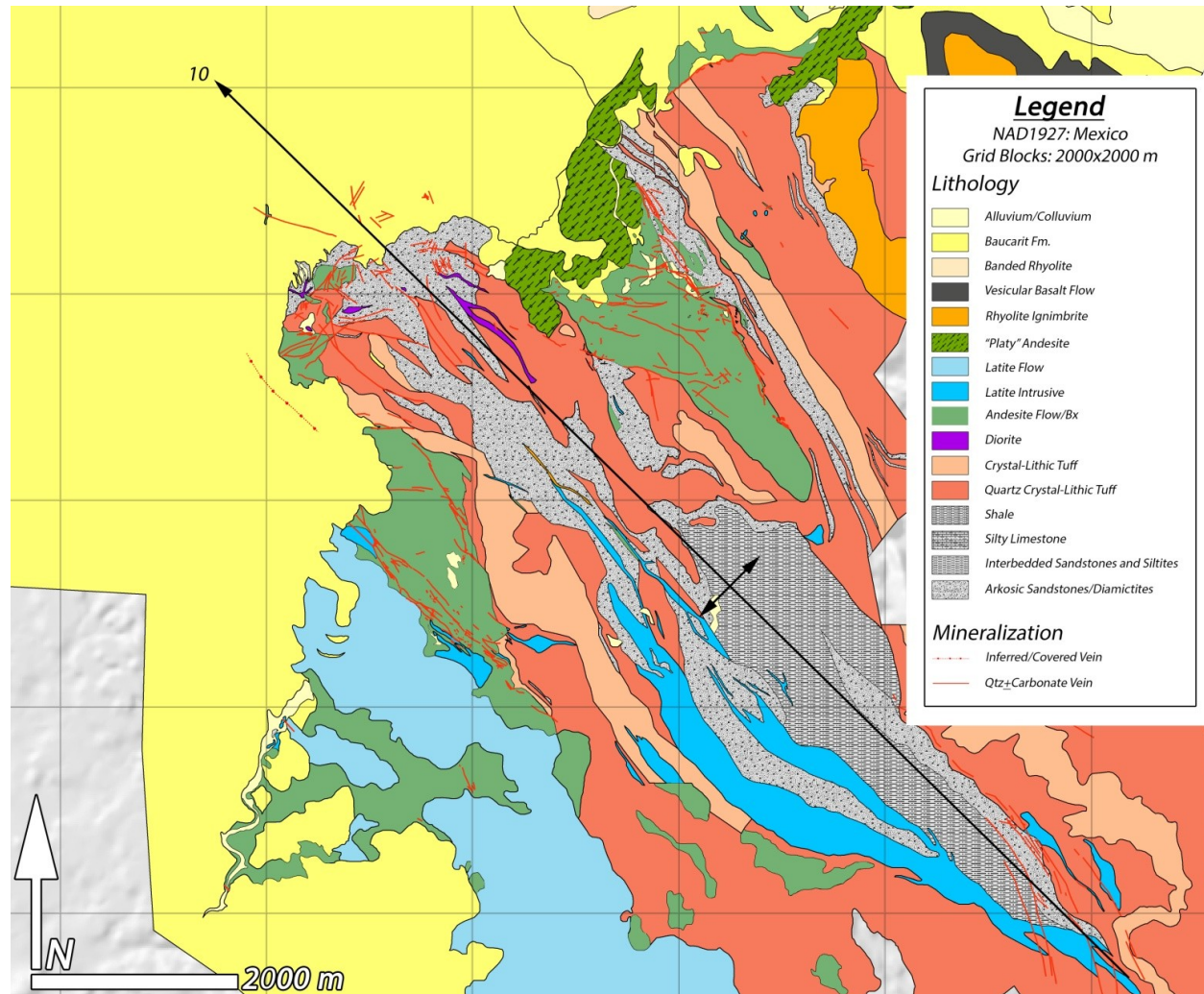


Figure 4. Geologic map of the Mercedes Property. Mineralized veins are represented by red lines. Adapted from Yamana unpublished mapping. (Yamana Exploration Staff, 2012)

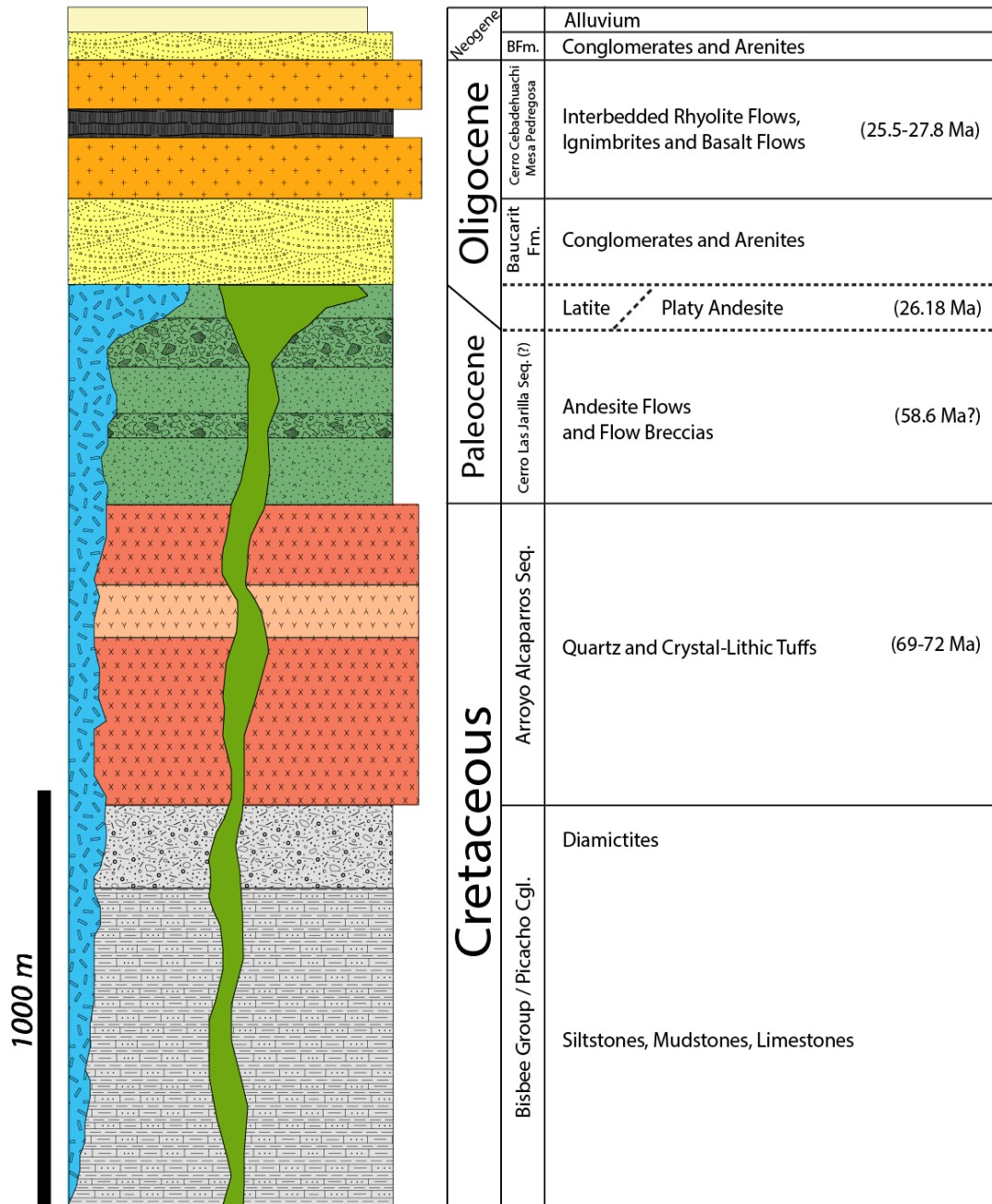


Figure 5. Lithostratigraphy of the Mercedes property. Unit thicknesses from Hawksworth et al., 2009. Formation names and ages as cited below.

Stratigraphy and Unit Descriptions

Basal Sedimentary Package

A suite of interbedded silty limestones, mudstones and diamictites form the oldest rocks exposed on the property (Figs. 5 and 6). The package is exposed only within the northwest-striking anticlines that separate the Mercedes and Klondike basins. Local horizons of graded bedding suggest an aqueous depositional environment and the topmost members of the sequence locally contain a widely-separated (0.5-1 m) stockwork of thin (1-5mm) quartz veinlets of unknown association with the major mineralized vein sequences.

Work by Gonzalez-Leon et al. (2000) in the Arizpe and Bacanuchi quadrangles immediately east and northeast of the Mercedes district suggests that these units are correlative to the early and mid-Cretaceous Bisbee Group sediments and the late Cretaceous Picacho conglomerate .

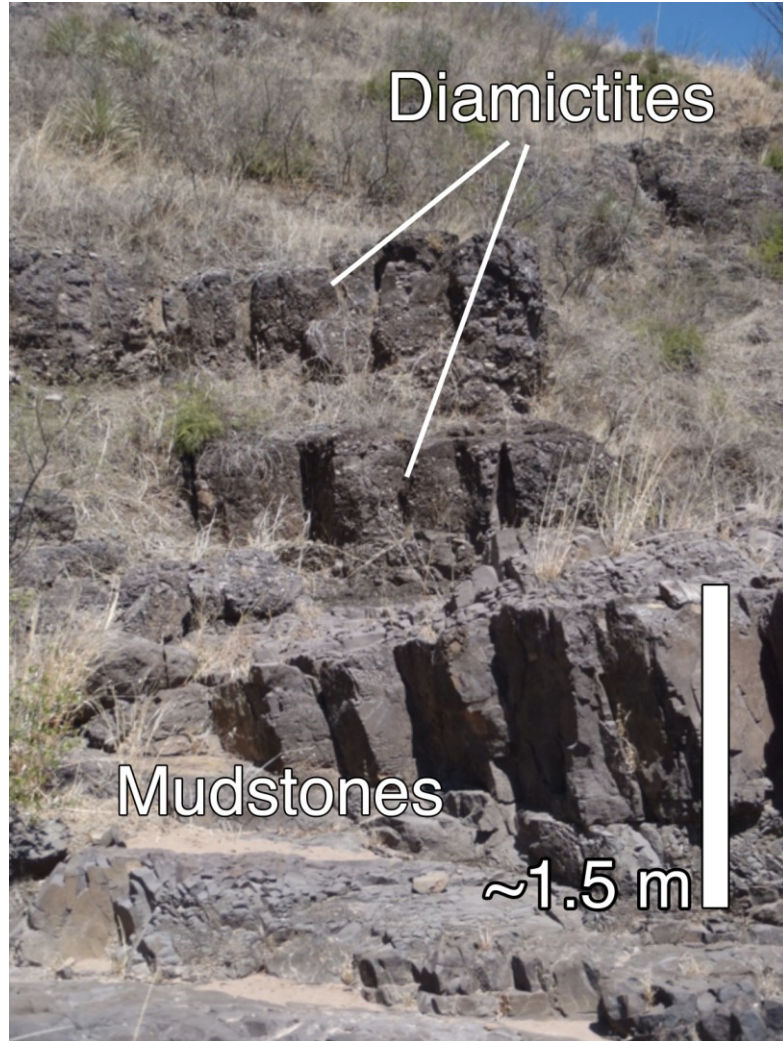


Figure 6. Diamictites and mudstones of the Basal Sedimentary Package.

Lithic Tuff Package

Unconformably overlaying the Mesozoic sediments is a sequence of pinkish, densely-welded lithic tuffs (Fig. 7). They are characterized by an abundance (20-40% by volume) of lithic fragments and local fiamme. The clasts are typically angular and range in size from 1-2 mm up to several centimeters and are composed of rhyolite and possibly andesite porphyry. Lower sections contain up to 10% crystalline quartz grains and sparsely distributed sanidine crystals. There appears to be a somewhat gradational transition between the lower quartz-lithic tuffs and the upper lithic tuffs. These units are also predominantly found within the limbs of the two northwest-trending anticlines that extend across the property.

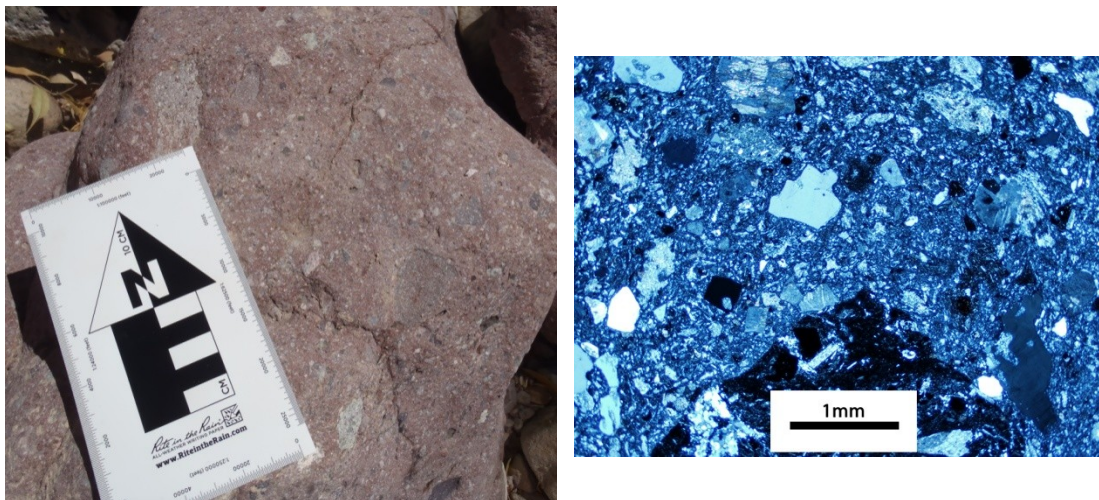


Figure 7. Field photo (left) and photomicrograph under crossed nicols (right) of the Quartz-lithic tuff unit. Note fragmental crystals of quartz and feldspars and lithic fragment (bottom-center under scale, extinct) floating in weakly flow-oriented groundmass.

This is lowest unit in the local stratigraphy that contains epithermal mineralization at Mercedes. Most notably, a fractured block of the lithic tuff forms a half-graben or listrically-displaced mass that hosts the Diluvio stockwork system. Deeper drillholes within the Mercedes zone suggest that Au-Ag mineralization may be present in tuff-hosted continuations of the Mercedes vein.

Although the relationship between these tuffs and other studied units within the region is ambiguous, the stratigraphic relationships on the property suggest that these are a member of the Arroyo Alcaparros igneous sequence, with ages between 72 and 69 Ma (Gonzales-Leon et al., 2000).

Diorite

Several dikes or sills of a dioritic intrusive are reported parallel to the axis of the anticline that separates the Mercedes and Klondike basin, apparently intruding the lithic tuff package. They are volumetrically minor within the district and were not examined in detail as part of this study. Laramide felsic to intermediate plutons are widely reported throughout northern Sonora, and the spatial association with the tuffs and sedimentary units exposed in the core of the uplift suggests a similar provenance for these intrusives. The Sierra El Manzanal granodiorite examined by Gonzalez-Leon et al. (2000) several kilometers to the northeast of the Mercedes district yielded an age of 68 Ma. However, the Rancho Vaqueria quartz monzonite of the same study gave an age of 57 Ma. Given that the identification of the diorite is based on field examination only, it is possible that it could be a representative of either event or of the event related to any one of the volcanic packages on the property.

Host Andesites

The most economically significant unit at the property is a series of andesite flows and flow-breccias (Fig. 8) that host the economic quartz-carbonate Mercedes, Klondike and Lupita veins. These andesites also cover the Diluvio stockwork system and host the Rey de Oro stockwork. Given the importance of these units, a more detailed examination is presented below.

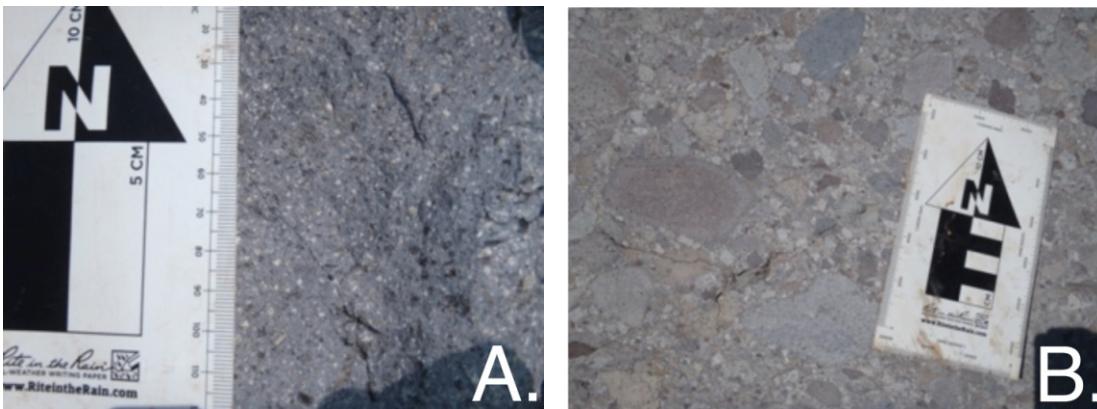


Figure 8. Photos of the host andesite units in outcrop. (A) Porphyritic andesite flow with weak preferred orientation of the longer aspect-ratio hornblendes, approximately 500 m from the Mercedes vein trace. (B) Poorly-sorted, heterolithic andesite debris flow breccia. The two photos were taken about 100 m apart.

Latite

Present mainly in the Mercedes zone is a biotite-alkali feldspar latite porphyry (Fig. 9) dome-flow complex that intrudes and locally overlies the host andesites along the same structural weakness that controlled the emplacement of the Mercedes vein. It is characterized by strongly flow-banded latite porphyry with large, 5-10 mm phenocrysts of concentrically zoned alkali feldspars and smaller 1-2 mm phenocrysts of euhedral biotites and hornblende within a fine-grained matrix of plagioclase and alkali feldspar.

The latite is localized near a vertically-foliated dome or vent structure that deforms the extreme northwestern part of the Mercedes vein and is locally in contact with it. The chilled margins of the pipe are composed of a glassy porphyry that is in contact with the Mercedes vein and contains minor but measurable gold grades. The retention of the glassy nature of the latite in contact with the vein and the presence of minor grades within the unit suggest that the latite is post-mineral and could provide an upper boundary for the age of mineralization at the property.

Fresh samples of the glassy latite (Fig. 9B) were dated using the $^{40}\text{Ar}/^{39}\text{Ar}$ method on two hornblende and two biotite crystals (see Appendix VI). The hornblendes produced an arithmetic mean age of 26.27 ± 0.14 Ma while the biotites produced an arithmetic mean age of 26.14 ± 0.07 Ma for an overall average mean age of 26.15 ± 0.16 Ma. Closure temperatures for these two systems range between $\sim 500\text{-}575^\circ\text{C}$ for hornblende and $\sim 250\text{-}300^\circ\text{C}$ for biotite (Chiaradia et al., 2013) While the lower temperatures of the biotite closure range approach temperatures in the epithermal environment, the retention of vitreous groundmass suggests that the latite has been unaffected by hydrothermal activity and these dates provide an absolute cap on the youngest age of mineralization. Mineralization near this date would coincide with the

earliest expressions of basin and range extension in northern Sonora (Henry and Aranda-Gomez, 1992) and make mineralization roughly contemporaneous with the normal faulting associated with the opening of the nearby Aconchi and Los Pinos grabens.

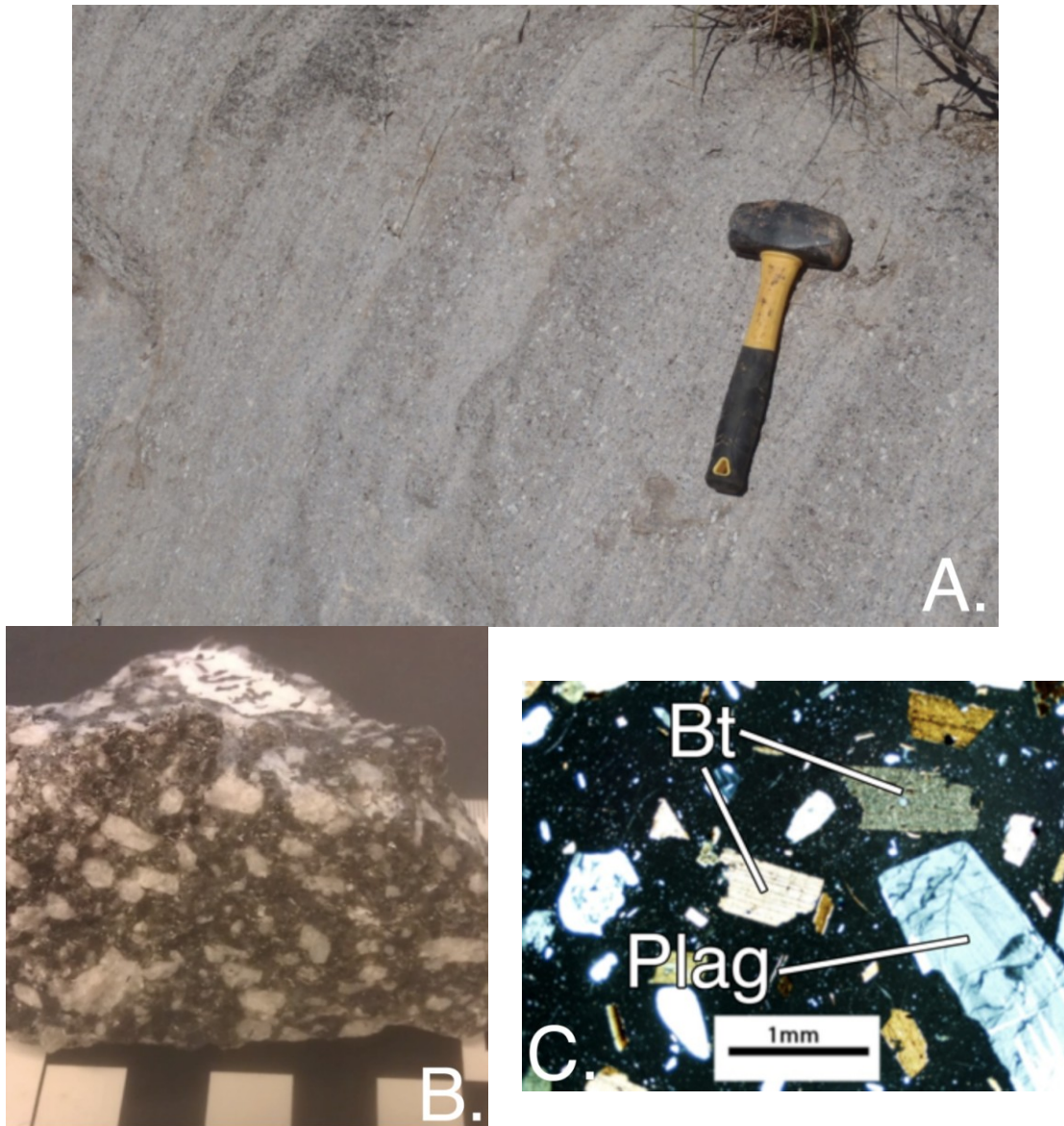


Figure 9. Characteristics of the latite flow-dome complex. (A) Flow-banded latite porphyry outcrop. (B) Sample C-Vit-1. Glassy plagioclase-biotite porphyry from the chilled margin. Scale intervals are 1 cm. (C) Thin section from C-Vit-1 under crossed nicols. Fragmental biotite (Bt) and zoned plagioclase (Plag) in a glassy matrix.

Platy Andesite

Exposed primarily within the northwestern end of the Klondike basin, is the "platy" andesite (Fig. 10). It is an aphanitic to finely porphyritic biotite-hornblende andesite with a parting along flow foliation. Contacts with the underlying host andesite unit are exposed in several locations and the boundary appears to truncate small quartz-carbonate veinlets possibly associated with mineralization in the Klondike zone. It is unconformably overlain by the Baucarit formation. U-Pb geochronology of 12 zircons within this unit indicates a magmatic crystallization age of 26.18 ± 0.11 Ma (Boise State, 2008). This age date is contemporaneous (within error) of the 26.15 ± 0.16 Ma age of the latites in the Mercedes zone, however no contacts between the two units are exposed and a relative timing between the two is undetermined.



Figure 10. Outcrop photo of flow-foliated platy andesite. Hammer for scale.

Rhyolite-Basalt Sequence

The outcrops of this volcanic package in the Mercedes district form part of the westernmost expressions of the Sierra Madre ignimbrite province. The rhyolites are a thick sequence of densely-welded ignimbrites and air-fall tuffs with locally vitric horizons. These are intermingled with at least one vesiculated basalt flow. Regional

reconnaissance by Yamana geologists did not identify any mineralization or prospective alteration within these units.

Based on examination of river cobbles sourced from these units and anecdotal descriptions, it is reasonable to include this package as part of the Upper Volcanic Supergroup of McDowell and Keizer (1977). It is probable that they correlate with the Cerro Cebadehuachi and Mesa Pedregosa volcanics of Gonzalez-Leon et al. (2001), who dated the packages at 25.48-27.77 Ma. The uncertainty of the correlation between the particular units of Gonzalez-Leon and the units mapped on the Mercedes property is reflected in the ages given in Figure 5.

Baucarit Formation

The Baucarit Formation is a regionally-extensive sequence of interbedded arenite, conglomerate, ash-fall deposits and rhyolitic ignimbrites and flows (Gonzalez-Leon et al., 2001). The entire package dips gently (10-20°) to the northwest. Clasts within the conglomeratic horizons are most common in local channel deposits and range in size from gravel to boulders up to a meter in diameter and are composed of rounded to sub-rounded fragments of the underlying andesites, rhyolites and basalts. The formation on the property locally exceeds 200 m in thickness and conformably overlies the host andesites within the Mercedes basin, forming unmineralized cover atop the Barrancas-Lagunas zone of the Mercedes vein.

Petrologic Descriptions of Host Andesite and Alteration

Of all the units at the Mercedes property, the vein-hosting andesites (Figs. 13-16) are the most economically significant. This series hosts the fault-controlled quartz-carbonate Mercedes, Klondike and Lupita veins, as well as several other minor veins and stockworks not covered within the scope of this study.

The andesites are a sequence of flows, flow-breccias and minor lahar deposits exceeding 500 m in thickness and are spatially restricted to two chevron-shaped basins along the limbs of the major northwest-striking anticline on the property that appear to have controlled deposition of the units. The southwestern Mercedes basin hosts the Mercedes vein and a number of smaller vein systems that have seen historic production but are no longer exploited. The northeastern, Klondike basin contains andesites of identical composition, and it is likely that they represent deposits from the same series of eruptive events. The macroscopic textures of the andesites commonly change dramatically over short distances (Figs. 11 and 12), ranging from flow-oriented porphyries to coarsely-fragmented flow breccias and lahar deposits. The orientation of the flow structures also changes sharply, with nearly vertical foliations found within a few meters of sub-horizontal flow bands.

Despite the textural variation, all the andesites across the property are hornblende-plagioclase porphyries (Fig. 13), locally enriched with magnetite as an accessory. Euhedral to subhedral hornblendes are the predominant phenocrysts, forming 10-50% of the rock by volume, and ranging in size from 1-5 mm. They are commonly flow-oriented (Figs. 14 and 15). Lathy plagioclase phenocrysts of largely andesine composition (An_{29} - An_{46} via Michel-Levy method on 37 phenocrysts from 4 samples; Michel-Levy, 1894 and Glazner, 1980) compose another 5-20% of the rock volume. These are also euhedral to subhedral and locally flow-oriented. The phenocrysts are

held in a pilotaxitic matrix dominated by feldspar microlites that commonly maintain the flow banding visible in outcrop-scale exposures.



Figure 11. Typical porphyritic andesite flow with weak flow textures defined by elongate hornblendes.



Figure 12. Heterolithic andesite debris flow deposit with seriate clasts. Both this photograph and that in fig. 11 were taken in an arroyo near the exploration camp, within 100 m of one another.

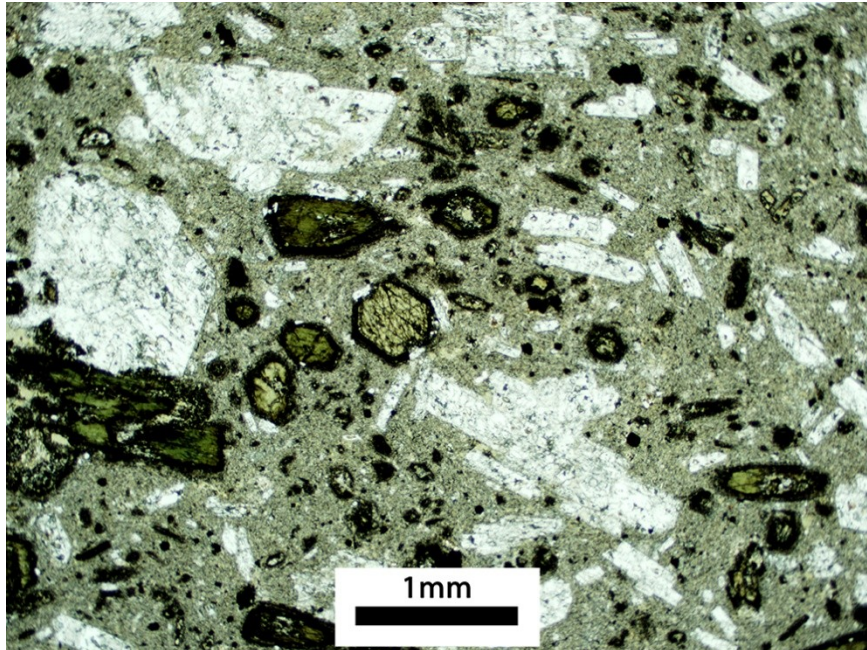


Figure 13. Sample An-S-1, photomicrograph, plane polarized light. Samples from this locality were weakly altered, with reaction rinds around the euhedral hornblendes, weak argillization of the feldspar phenocrysts and local chloritization of the biotites and hornblendes.

All the accessible exposures of the andesites display varying degrees of alteration, with the intensity of alteration visually increasing towards the vein systems. Samples from approximately 1.5 km southwest (perpendicular to strike) of the Mercedes vein contain partially chloritized amphiboles and biotites while samples from the margins of the vein have undergone complete replacement of the ferromagnesian minerals to chlorite and hematite as well as total argillization of the feldspars (Fig. 14). In samples proximal to the vein, minor amounts of epidote are present both as replacement products within the plagioclase phenocrysts and as small disseminations within the altered groundmass commonly present near chloritized biotites and hornblendes. In one surface exposure from near the Mercedes vein, small zeolite accumulations were observed within vugs. The composition is unknown, but the habit and appearance is similar to wairakite samples the author has examined from similar epithermal settings in the Taupo volcanic zone, New Zealand and in Japan. However, it is

also likely that these are a non-hydrothermal zeolite, perhaps related to post-mineral weathering of the andesites or an alteration product related to the weak, regional alteration of the andesites.

It is unclear whether the distal alteration signature corresponds to hydrothermal alteration related to the mineralization event or if it represents authigenic deuteric alteration related to the emplacement of the andesites themselves. Given that even the most distally accessible andesites show clear evidence of alteration in the hornblendes, biotites and feldspars, it is unlikely that the unit within the property can be accurately dated to give an absolute lower boundary on the time of mineralization.

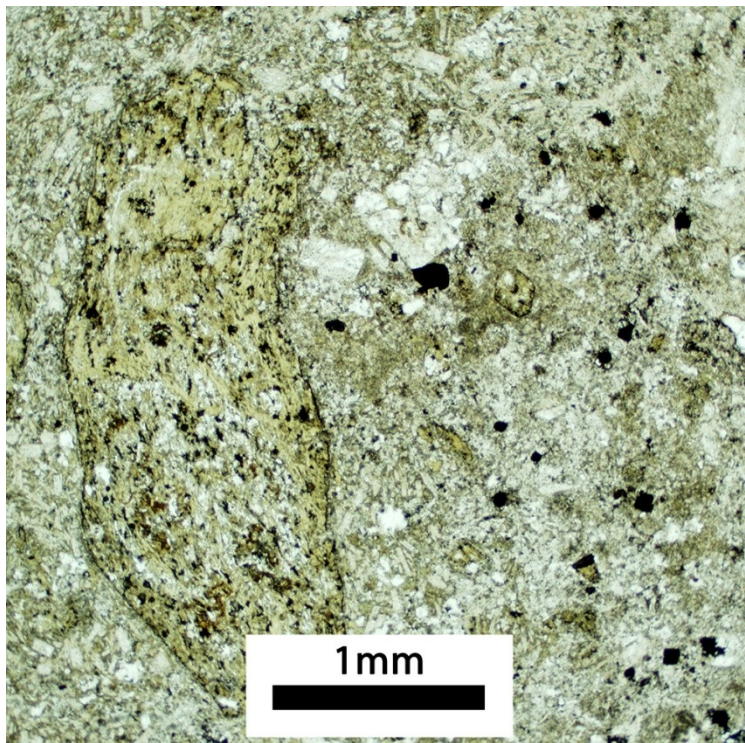


Figure 14. Sample An-S-2, photomicrograph, plane polarized light. Strongly altered andesite porphyry. Hornblendes and biotites have been totally altered to chlorite and feldspars to clays. Cubic opaque shapes are hematite pseudomorphs after magnetite or pyrite.

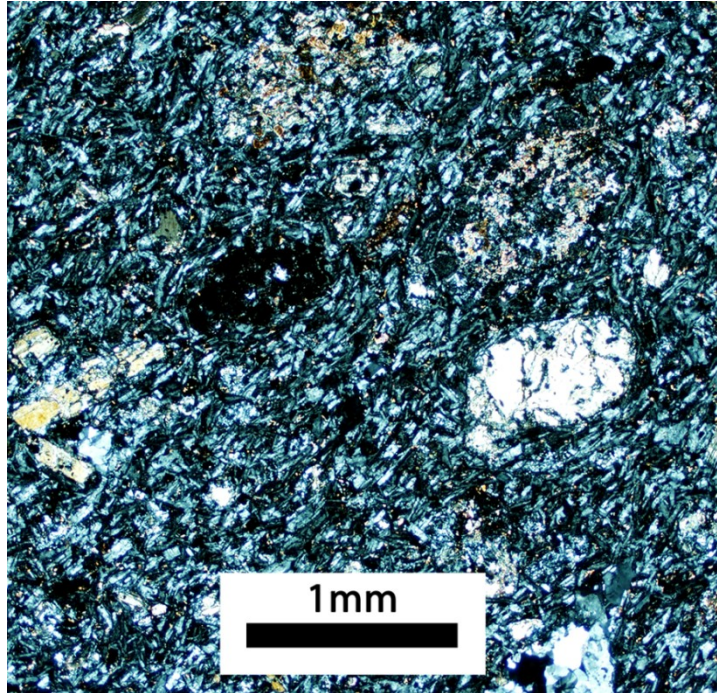


Figure 15. Sample C-An-S-5, photomicrograph, crossed nicols. Strong flow orientations (pilotaxitic texture) of fine-grained plagioclase microlites surrounding partially altered hornblende and plagioclase phenocrysts.

The andesite package likely correlates with the Cerro Las Jarilla sequence studied several kilometers to the northeast by Gonzales-Leon et al. (2001). That study found a $^{40}\text{Ar}/^{39}\text{Ar}$ date of 58.66 ± 0.17 Ma from a biotite phenocryst. However, 1:50,000 scale mapping published by the Servicio Geológico Mexicano in 1999 indicates that these volcanics are late Cretaceous and may correspond to the Arroyo Alcaparros volcanics, also of Gonzales-Leon et al. (2001), and date between 69 and 72 Ma. The uncertainty of the correlation between the units defined by Gonzales-Leon et al. and those on the Mercedes property is reflected on the age given as ≥ 58.6 Ma in Figure 5.

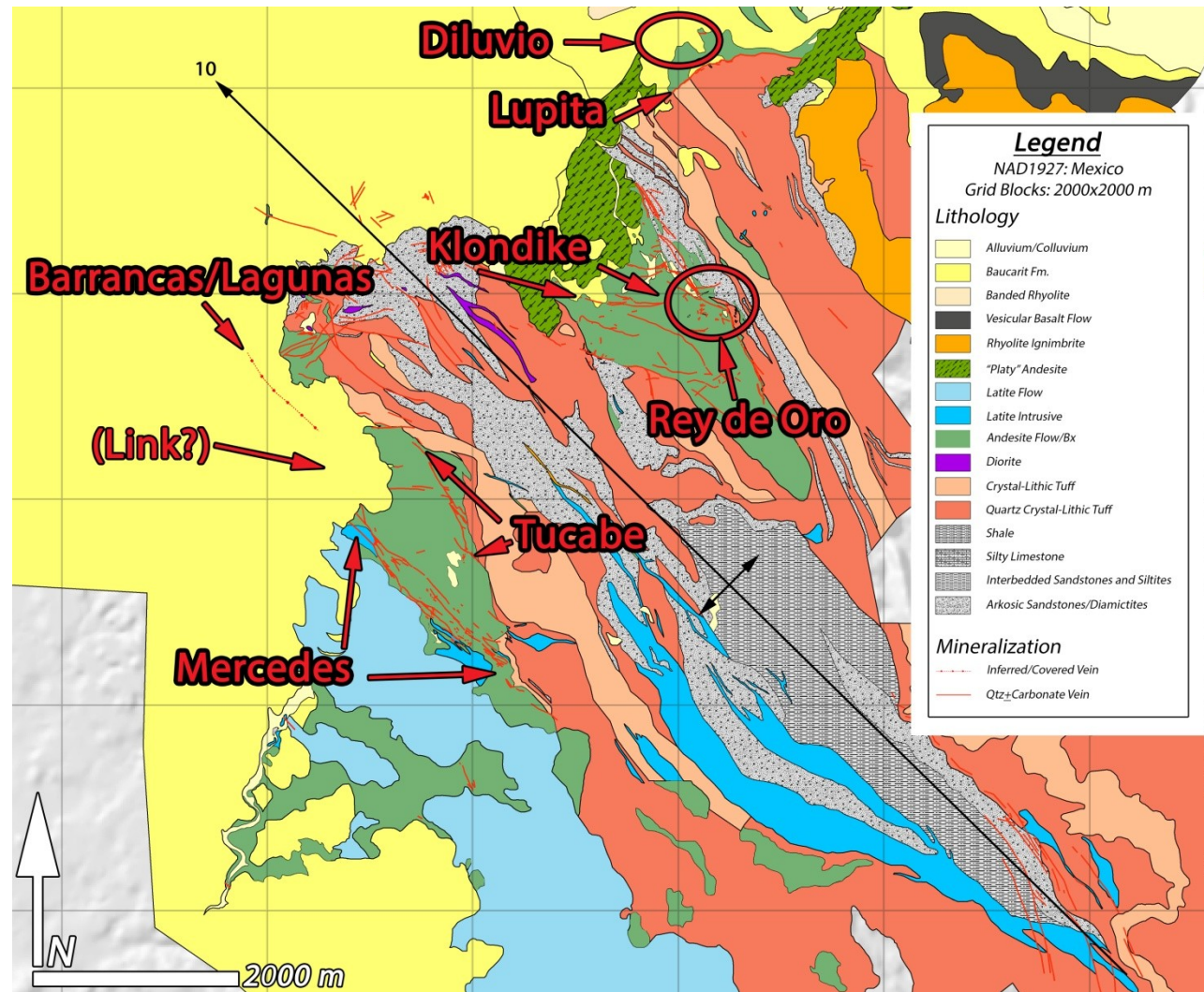


Figure 16. Mercedes district geologic map, adapted from Yamana unpublished mapping. (Yamana Exploration Staff, 2012) Mineralized zones are labeled.

Overview of the Mineralized Zones in the Mercedes District

The Mercedes property contains a number of mineralized veins (Fig. 16), all displaying roughly the same mineralogy of quartz-carbonate veins with anomalous to economic concentrations of Au and Ag. Four of these zones, Mercedes, Klondike, Lupita and Diluvio, will be considered in detail within the scope of this project. Brief descriptions of the other zones compiled from field work of the author and communication with Yamana geologists are included here for completeness. More detailed descriptions of the Mercedes, Klondike, and Lupita vein systems are presented in the next section.

Mercedes

The Mercedes vein is the most laterally extensive and highest grade vein found on the property. Mineralization has been defined over 1640 m of strike (Fig. 16) and 600 m down-dip.

The vein ranges between 1-15 m in true width and is strongly brecciated. It dips steeply, typically between 75-90° south-southwest, though it has been deformed and tilted to the northeast where it contacts the latite intrusion at the northwestern extent of its surface expression (Fig. 16). It is localized by a dextral oblique normal fault and bounded by a strongly milled zone of clay gouge up to 2 m thick along the hanging wall margin. The bulk of the vein is highly brecciated and is composed of unique light to dark olive-green quartz and andesite clasts in a matrix of dark carbonate and local rhodochrosite cement.

Grades in the vein locally exceed 640 ppm Au and 3700 ppm Ag in the high-grade ore shoots, but average 8.7 ppm Au and 95 ppm Ag (Hawksworth et al., 2009). The Au occurs as native Au, whereas the Ag occurs as, cerargyrite, and a number of other Ag-bearing phases (most likely argentojarosite and native Ag). The exact ore mineralogy, both hypogene and the subsequent supergene products, are uncertain due to the lack of high-grade samples available for examination, equipment limitations and the near total oxidation of the vein system.

Minera Oro Chico began mining the vein in 1937 by surface stope and underground methods. The mine was closed in 1940, with decreasing grades at depth cited as the reason for abandonment. However, exploratory drilling in the late 1990s and early 2000s by Meridian Minerals and Yamana Gold discovered the high-grade Corona de Oro ore shoot less than 15 m below the deepest historic workings. The vein contains a resource of more than 600,000 ounces of Au and 6.7 million ounces of Ag at a cut off grade of 2.0 ppm Au-equivalent (Au+Ag/150; Hawksworth et al., 2009). Underground mining began in 2010 with the first production of doré in December 2011.

Barrancas/Lagunas

The Barrancas/Lagunas vein system is present under as much as 150 m of post-ore cover, largely composed of sedimentary and volcanic rocks of the Baucarit Formation. It occurs 800-2000 m along strike to the northwest of the Mercedes vein (Fig. 16, label on figure). Despite a shift of 200 m to the northeast of the projection of the Mercedes vein strike, it appears to be a continuation of the Mercedes vein or possibly an en-echelon vein within the same hydrothermal circulation. It is currently undergoing resource delineation drilling and the construction of a portal/decline.

Mineralogy is similar that of the main Mercedes vein; however, the northwestern end of the Barrancas/Lagunas vein system appears to be much more sheared and discontinuous than the relatively linear Mercedes vein. For the purposes of this paper, the Mercedes and Barrancas/Lagunas systems will be considered to be a continuous extension of the same vein system.

Tucabe

The Tucabe vein runs approximately parallel to the Mercedes vein, 200-500 m to the northeast and is contained within the Mercedes andesite basin. It has a mapped extent of about 500 m and ranges in width from 1-5 m. It is of similar mineralogy to the Mercedes vein, consisting of discontinuous veins and pods of green quartz and dark carbonates.

The vein has seen some historic, artisanal production, but no further exploitation is planned and there are no available data on precious metal grades (Hawksworth et al., 2009)

Klondike

The Klondike system is located in the northeastern end of the andesite-filled basin within a series of flows and flow-breccias similar to that of the Mercedes basin. Mineralization extends more than 800 m along strike and about 400 m vertically. On average the vein strikes north-northwesterly and dips vertically to subvertically between 70-90° SW.

Compared to the Mercedes vein, the Klondike vein is much less brecciated and extensive portions of the vein system are banded. The mineralogy of the vein is similar

to that of Mercedes and the other veins in the district, composed mainly of banded chalcedony, green crystalline quartz, +dark-colored carbonates, and calcite.

The vein zone is between 1 and 50 m in thickness and anastomoses to the southeast where it appears to grade into the Rey de Oro stockwork zone (Fig. 17). Preliminary petrography indicates gold occurs as native Au, and silver occurs as cerargyrite and possibly several other Ag-bearing phases (argentojarosite, native Ag and possibly electrum though Au-Ag correlations suggest that it is only a minor component). Grades are generally lower than that of the Mercedes vein, only locally exceeding 60 ppm Au and 200 ppm Ag. The Klondike system saw minor historic production, with modern production on the vein beginning in 2010. Current resource estimates include 131,000 ounces of Au and 808,000 ounces of Ag at average grades of 6.3 ppm Au and 39 ppm Ag (Hawksworth et al., 2009).

Rey de Oro

The Rey de Oro system is a vein and stockwork system occupying the southeastern portion of the Klondike basin (Fig. 16). It appears to be related to the same structural zone that hosts the the Klondike vein system and is probably contiguous with it as an anastomosing series of veins and veinlets of similar composition to the main Klondike vein. (Hawksworth et al., 2009). Ongoing exploration drilling is currently (2013) testing this scenario.

Rey de Oro experienced small-scale production as both open stope and small underground workings that started on outcrops of the vein and stockwork. Exploratory drilling by Yamana is ongoing for bulk-mineable deposit.

Lupita/Diluvio

The Lupita vein exists outside of the two major andesite basins, approximately 2 km north of the Klondike vein and 5 km northeast of the Mercedes vein. It is unique among the veins on the Mercedes property in that it exists as a curvilinear outcrop that mainly trends mainly east-west. At the surface the vein dips 20-50° north, but drilling suggests the dip shallows to near horizontal at depth.

The vein has a mapped strike extent of about 1,500 m and ranges in thickness between one and five meters along the surface. The vein is similar to both Mercedes and Klondike, composed of banded green quartz+dark carbonate that is locally brecciated. Grades along the vein locally exceed 18 ppm Au and 65 ppm Ag with grades of 1-3 ppm Au and 10-30 ppm Ag being common (Hawksworth et al., 2009)

At the surface, similar to Mercedes and Klondike, andesites form the hanging wall of the Lupita vein and the lithic tuff sequence forms the footwall. This orientation changes at depth, where 300-400 m down-dip, the hanging wall abruptly changes to a highly fractured block of the lithic tuff sequence.

This fractured and mineralized block overlying the Lupita structure is the Diluvio zone and consists of a stockwork of quartz-carbonate veinlets containing anomalous Au-Ag grades. The block is interpreted as a cohesive unit of the lithic tuff sequence that slid along a listric or half-graben type structure and was subsequently buried by later andesitic flows. Grades are generally lower than that of Lupita, with Au in the 0.5-3 ppm and Ag in the 5-20 ppm ranges.

Exploratory drilling is ongoing in both the Lupita and Diluvio zones. A bulk-mineable target is being evaluated at , Diluvio .

THE MERCEDES VEIN

Introduction

The Mercedes vein is the highest-grade and most extensive vein in the Mercedes district. The surface expression extends over 1800 m striking northwest, with an average azimuth of 310°. It dips near vertically, with a range of 74° to the southwest to 70° to the northeast where the latite intrusion has deformed the vein at the northwestern margin of its surface exposure. The vein continues under cover of the Baucarit Formation and is likely contiguous with the Barrancas/Lagunas zone to the northwest, for a total strike length of over 3 km. The vein ranges in width between 1-20 m, with the widest zones (Fig. 17) occupying dilatational zones where the localizing fault changes in strike or dip.

These dilatational zones also constrain the highest grade ore shoots (Fig. 18), named (from southeast to northwest) Casa Blanca, Centinela, Tierra de Nadie, Corona de Oro and Breccia Hill. Of these, the Corona de Oro ore shoot contains the highest grades and grade-thicknesses of the drilled sections of the Mercedes vein. For the purposes of this study, seven representative cross-sections were selected in an attempt to achieve adequate lateral and vertical spacing to delineate the variations in mineralogy, geochemistry and structure along the vein with consideration given to the availability of core and access to underground workings in proximity to the chosen sections. Four sections: 8860, 9100, 9550 (Fig. 20) and 9880 were chosen along the Mercedes vein proper with an additional three: 11110, 11710 (Fig. 21) and 11910 chosen within the Barrancas/Lagunas zone to the northwest of the Mercedes vein exposures. The nomenclature reflects their position within the local exploration grid (Fig. 17).

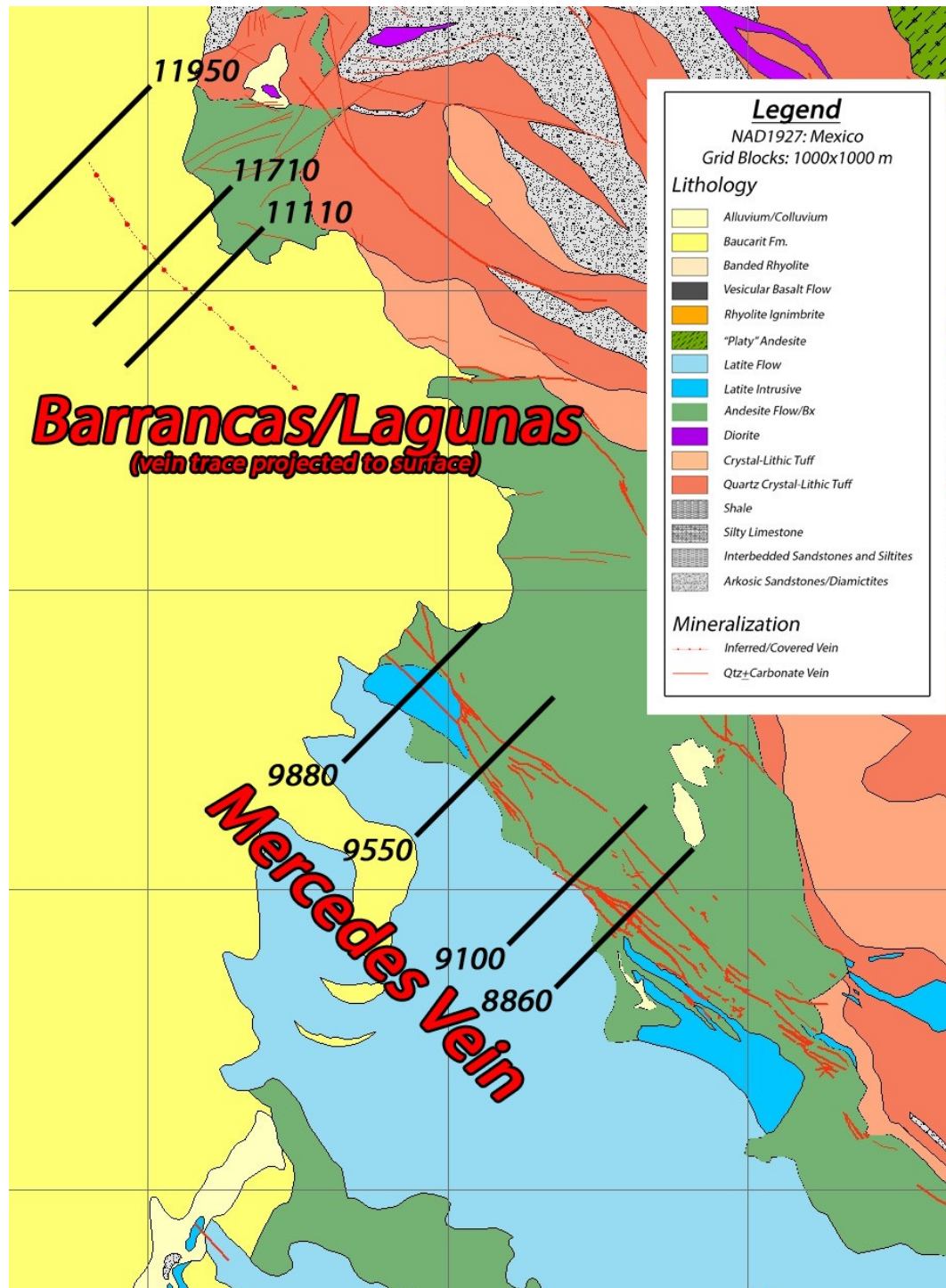


Figure 17. Geologic map of the Mercedes vein zone. Black lines represent the locations of the study cross sections. Nomenclature reflects the position on the Mercedes exploration grid. Adapted from Yamana Geodatabase. (Yamana Exploration Staff, 2012)

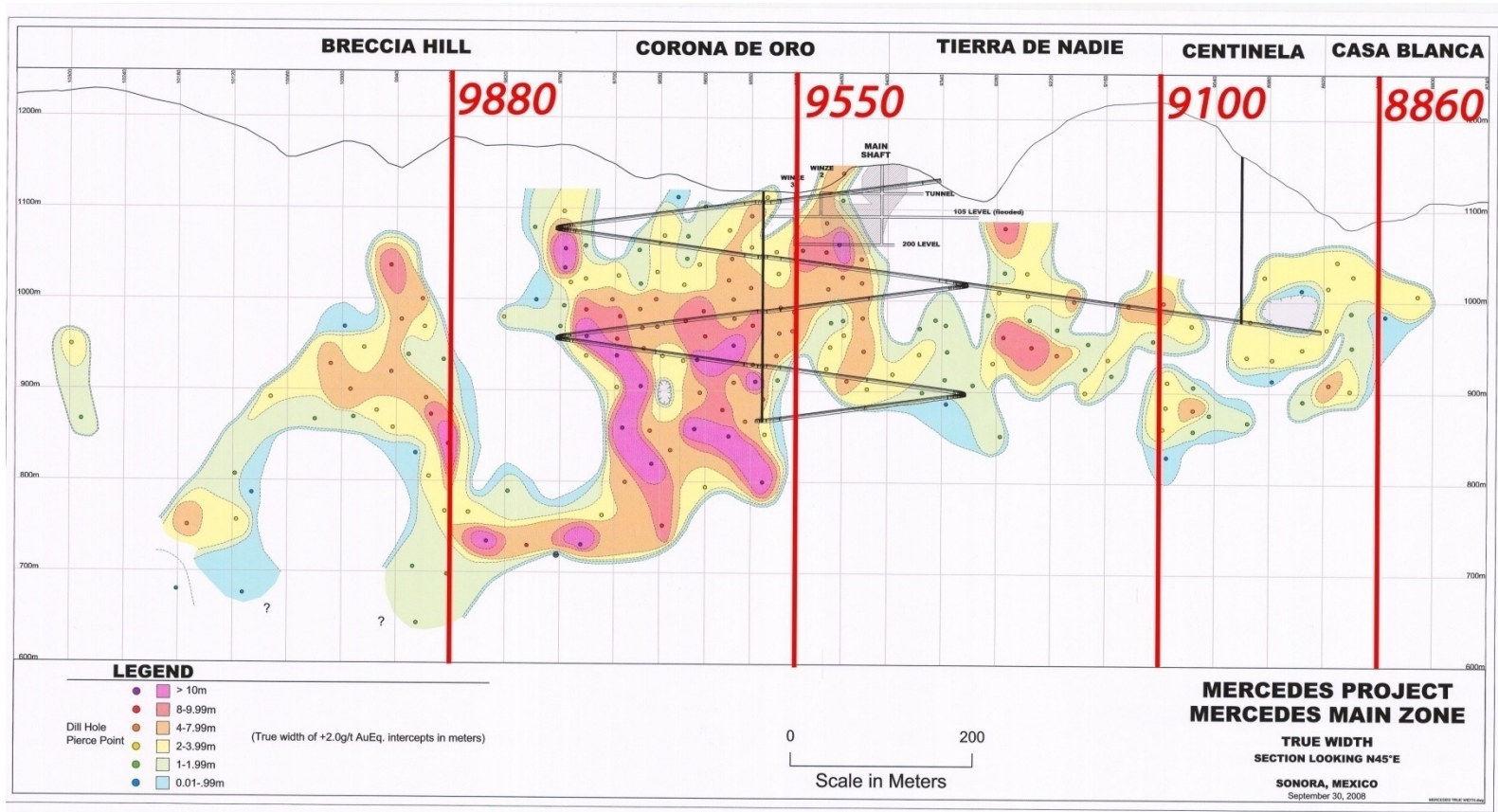


Figure 18. Long section of the Mercedes vein showing true thickness. Study cross sections are marked in red. (Yamana Exploration Staff, unpublished data, 2008).

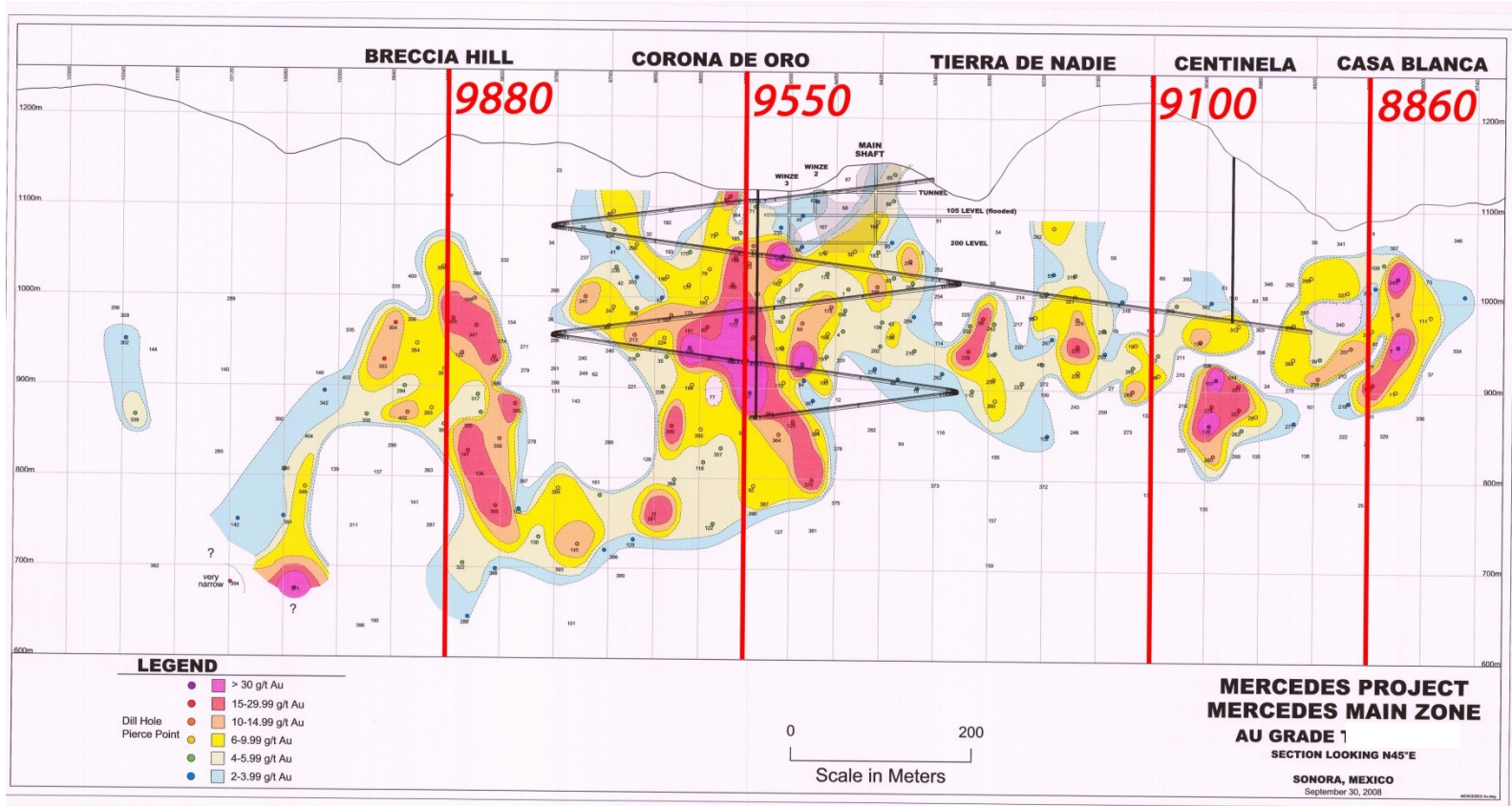


Figure 19. Long section of the Mercedes vein showing average Au grades. Study cross sections are marked in red. Note that original figure title denoting grade-thickness is incorrect. (Yamana Exploration Staff, Unpublished Data, 2008)

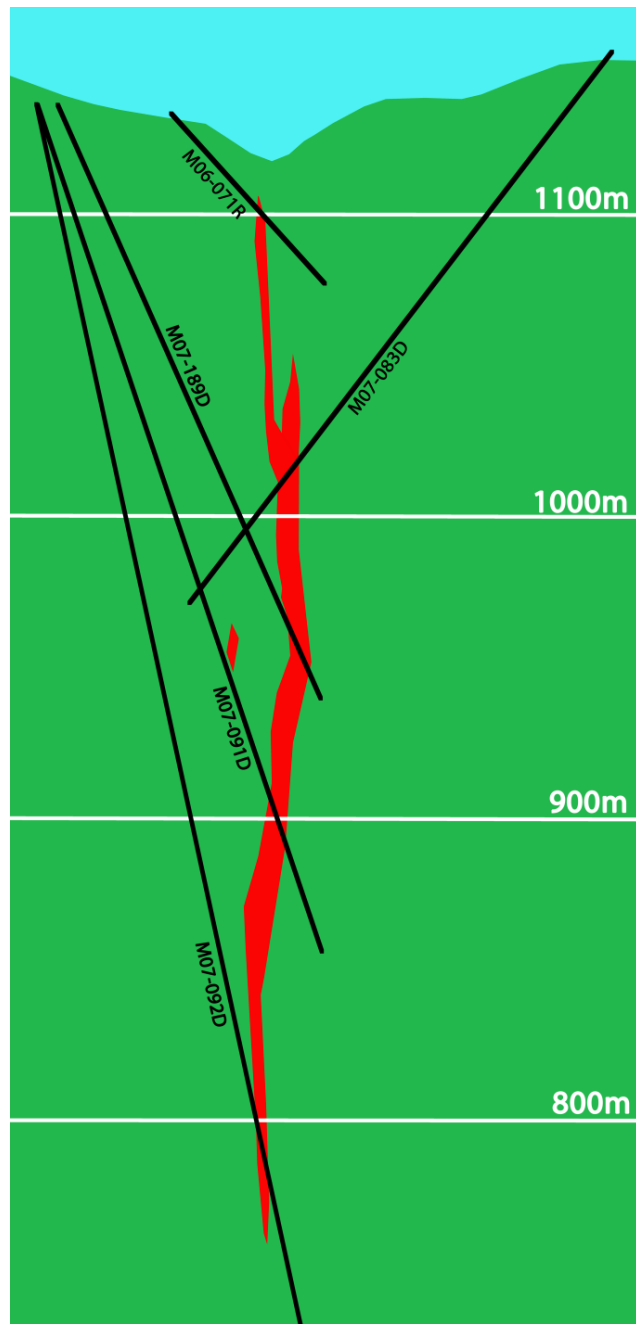


Figure 20. Cross-section 9550 looking northwest along the Mercedes vein through the Corona de Oro ore shoot. Red is vein material defined by core logs, green is the host andesite and the black lines are the drill holes selected for sampling. The elevation is given on the right. Figure created from unpublished interpretive cross-sections (Yamana Exploration Staff, 2008) and original work by the author.

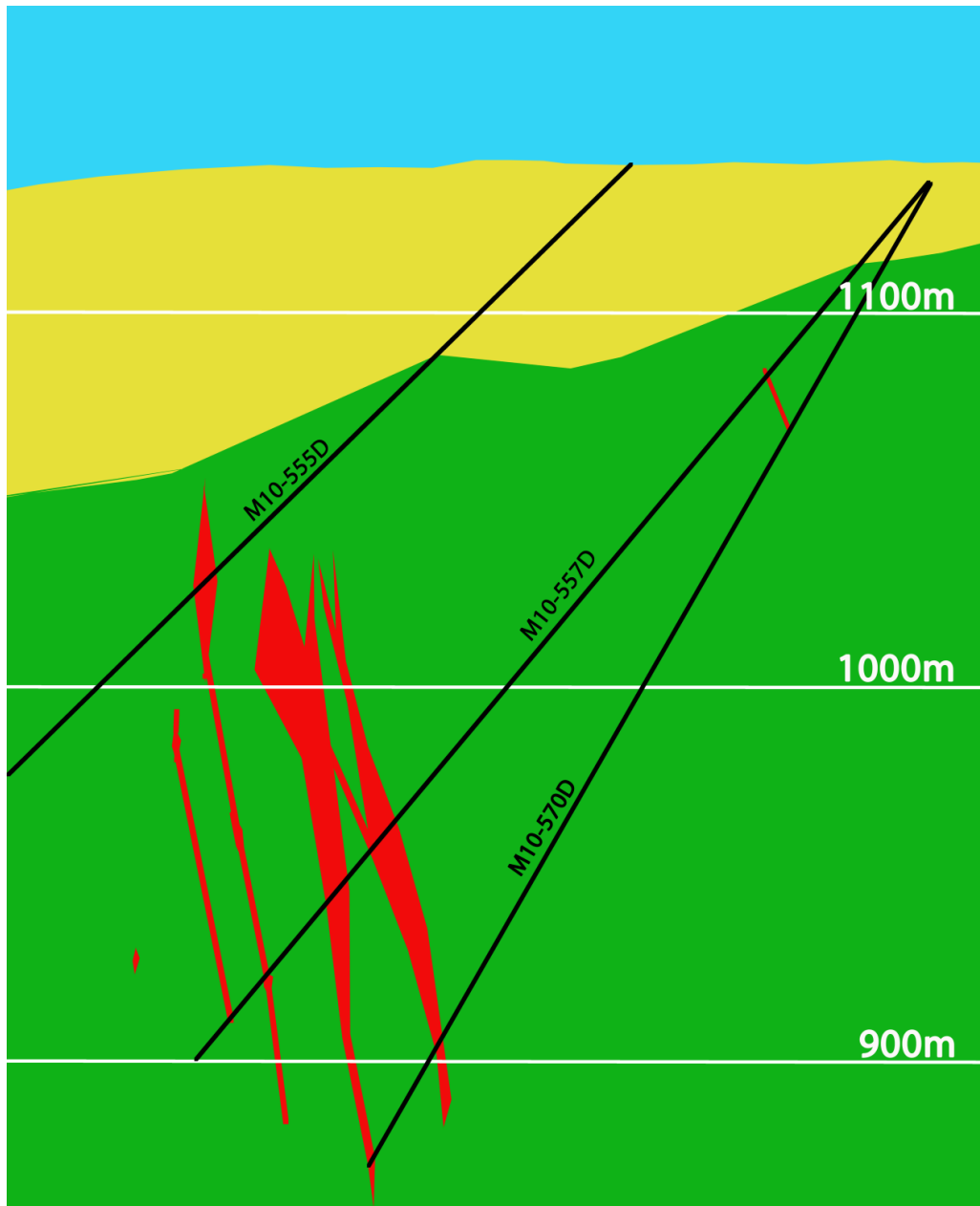


Figure 21. Section 11710 looking northwest through the Barrancas/Lagunas extension of the Mercedes vein. Red is vein material, green is the host andesite, yellow is Baucarit Formation and the black lines are the drill holes selected for sampling. Figure created from unpublished interpretive cross-sections (Yamana Exploration Staff, 2008) and original work by the author.

Paragenesis

The paragenetic sequence of the Mercedes vein (Fig. 22) consists of three major hydrothermal phases followed by a final phase of weathering. At least one significant brecciation event separated Phases I and II, with additional brecciation likely occurring during phase II.

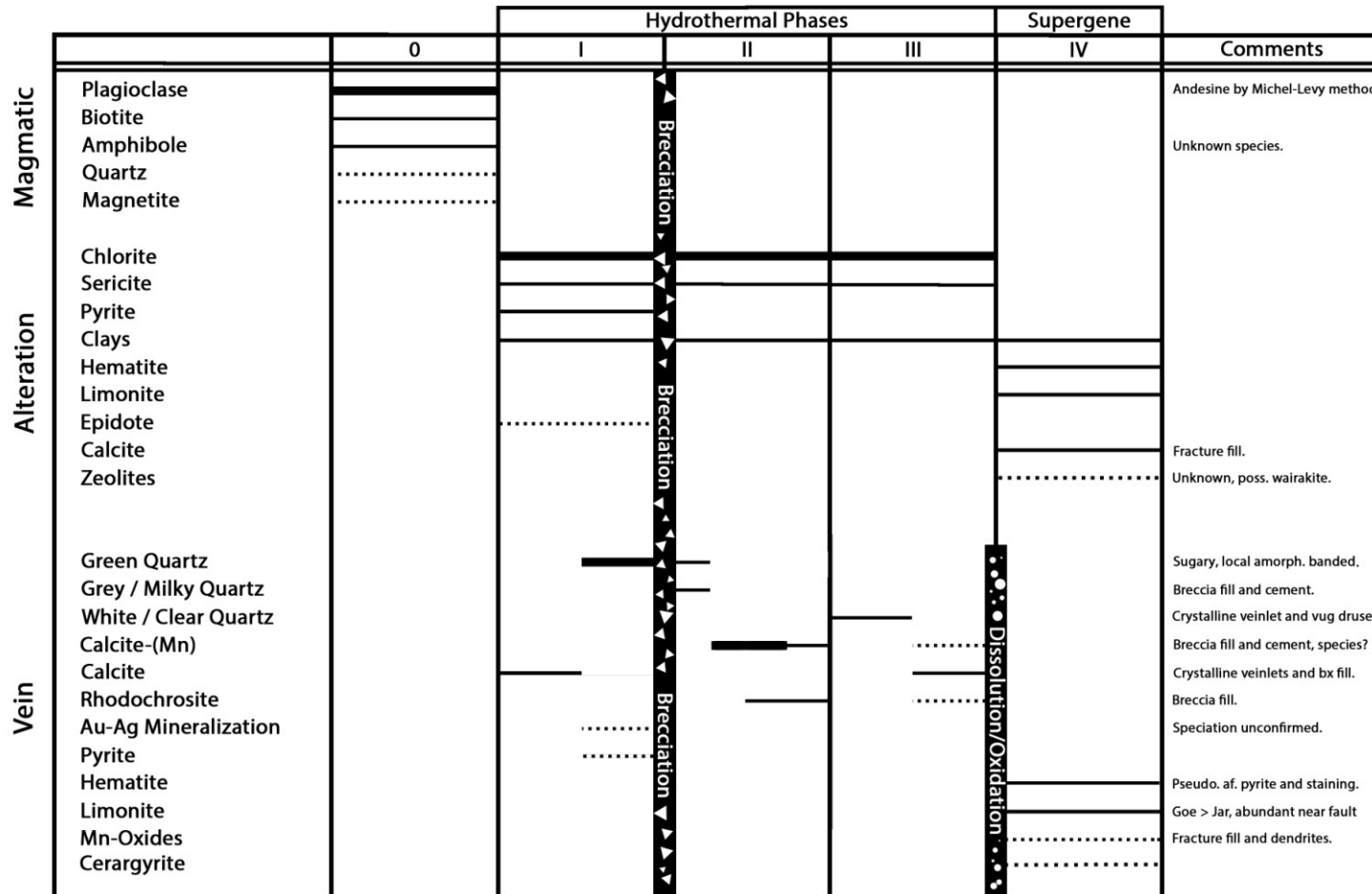


Figure 22. Paragenetic Diagram for the Mercedes Vein. Weight of bars denotes relative abundance of the mineral within each paragenetic phase.

Phase I

The earliest phase in Mercedes is dominated by a light to dark olive green-colored quartz (Fig. 23A-D). Most of the clasts within the vein breccia are composed of this green-colored quartz, up to 80% of the vein volume. It is commonly saccharoidal, but locally clasts of both coarsely crystalline quartz and banded chaledonic textures occur. Phase I also locally forms the selvages of "sandy" veinlets (Fig. 29). Most of the samples examined microscopically show evidence of boiling, by the presence of feathery, vapor-dominant fluid inclusion trails and local jigsaw quartz textures. The green quartz in high-grade zones is commonly found with limonite-coated boxworks (goethite>>jarosite), as well hematite after pyrite. The original Phase I pyrites appear to have been locally cubic euhedra, but these have been completely oxidized during weathering. Though pyrite appears to have been the principal sulfide, some boxworks appear to retain non-pyritic habits. Significantly, remnant tetrahedra and octahedra may be present suggesting that some of the silver mineralization may have been due to silver sulfides or sulfosalts. The qualitative correlation between the saccharoidal green quartz, boxworks of hematite/limonite after sulfides and high Au grades suggests the precious metal mineralization was introduced during Phase I.

Locally, especially within the Casa Blanca ore shoot, Phase I is characterized by zones of intense silicification. None of these areas were easily accessible underground, appearing high in working face, but they appear to be fractured with in-place zones of reddish, massive silica with peripheral clasts of the same material scattered in the vein breccia. Clasts of similar material are found locally throughout the vein breccia away from visible zones of silicification.

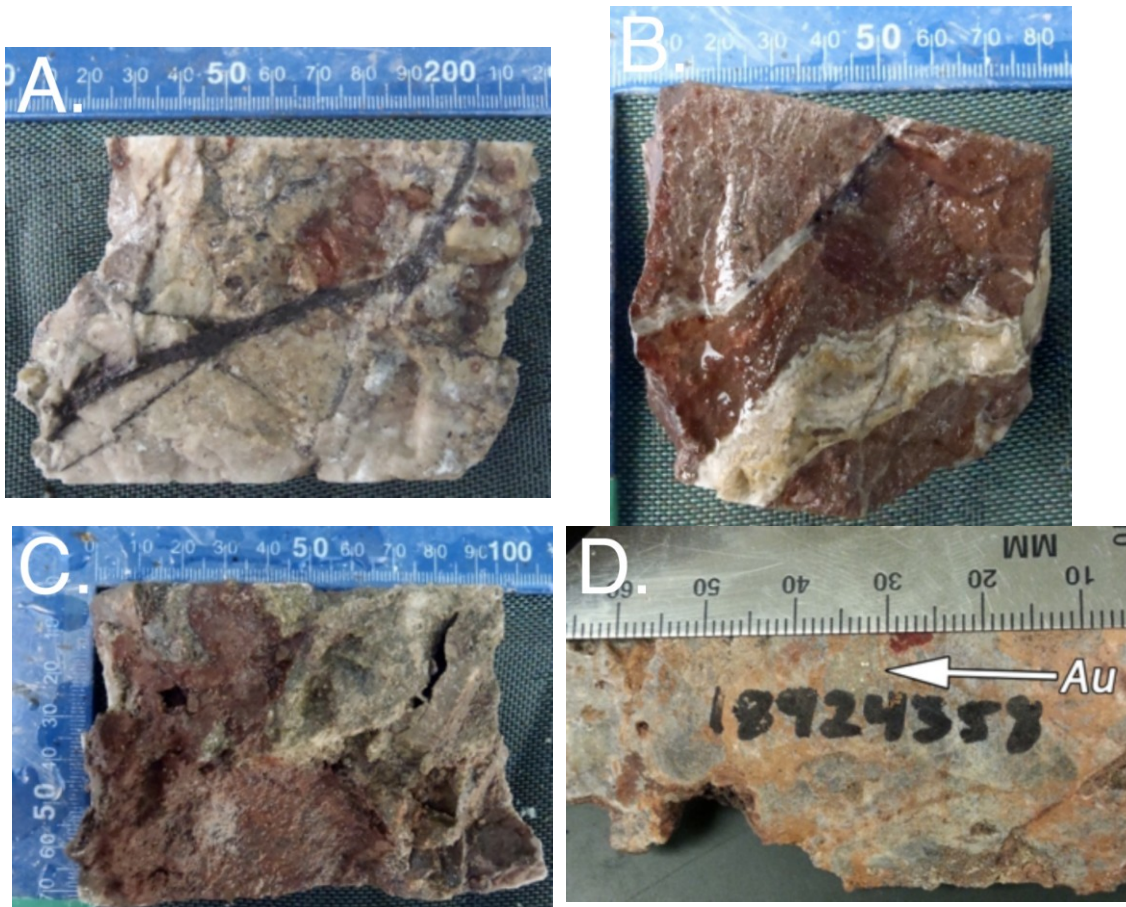


Figure 23. Examples of Phase I mineralization. Scale in mm. (A) Green-colored quartz breccia with red oxidized andesite clasts cut by Phase II carbonate veinlet. 17.47 ppm Au, 75 ppm Ag. 172.35 m, hole M08-315D. (B) Rare example of banded Phase I quartz vein in oxidized andesite wall rock. 243.33 m, hole M07-103D. (C) High-grade saccharoidal dark green quartz and hematitic matrix. 32 ppm Au, 237 ppm Ag. 181.46 m, hole M07-083D. (D) Visible Au in Phase I quartz+hematitic matrix bonanza breccia in the Corona de Oro ore shoot. Sample assayed 652 ppm Au and 463 ppm Ag. From 243.58 m in hole M07-189D.

Phase II

Separating Phase I from Phase II is a major brecciation event. This event appears to have been both hydrothermal, with vertical transport of host andesite and phase I clasts up to 400 m vertically, and tectonic with the appearance of local phase I clasts within the clay gouge in the vein-hosting fault. With the exception of the banded chalcidonic selvages of the "sandy" veinlets, no Phase I material appears to be unbrecciated.

Phase II mineralization consists of an early grey and green quartz stage and a later carbonate stage consisting of a dark, Mn-bearing calcite and rhodochrosite forming a cement that forms the matrix to the clasts of Phase I mineralization (Figs. 24A and 24B). Phase II is also present as finely crystalline quartz veinlets that cross-cut the breccia matrix as well as Phase I intense silicification..

Where not associated with features of Phase I mineralization, Phase II mineralization contains low- to sub-economic grades of Au and Ag, typically <5 ppm Au and <18 ppm Ag. In addition, Phase II lacks the boiling textures that are common in Phase I minerals.

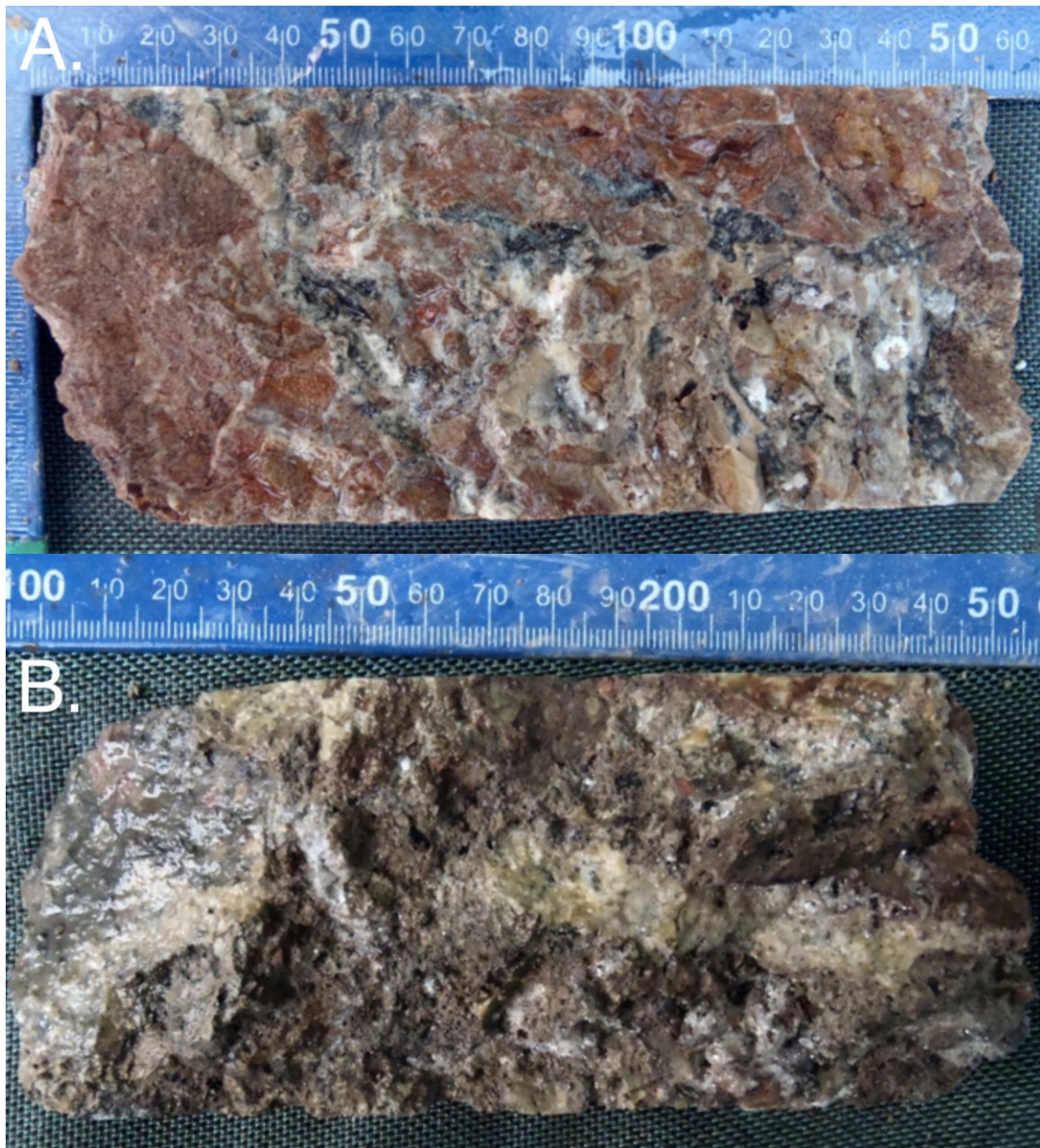


Figure 24. Examples of Phase II mineralization, scale in mm. (A) Oxidized andesite and phase I quartz cemented by dark phase II carbonates and local, lighter Phase III calcite+quartz. From 123.87 m in hole M08-351D. (B) Partially dissolved phase II dark carbonates with remnant spongy Mn-oxides surrounding clasts of green Phase I quartz. 35 ppm Au, 230 ppm Ag. From 245.19 m in hole M07-189D.

Phase III

The third and final phase of epithermal mineralization consists of quartz+carbonate veinlets and drusy quartz vug-fill that cross-cut the more voluminous vein breccia and post-date Phase I and II. There is no evidence of sulfide or precious metal mineralization associated with these veinlets, nor is there any evidence of boiling textures. Few veinlets show any evidence of brecciation or tectonic displacement and they commonly cross-cut (Fig. 25A) the vein system and extend into the wall rocks as a low-density stockwork. Locally, Phase III veinlets can be found in outcrop, up to 50 m away from the vein trace. The veinlets contain boudin-shaped cores of darker carbonate and rhodochrosite surrounded by clear quartz selvages (Fig. 25B).

The stockwork nature of these veinlets and cross-cutting relationships suggest that they may be part of a later hydrothermal event that may or may not be related to the evolution of the ore-forming hydrothermal system at Mercedes.

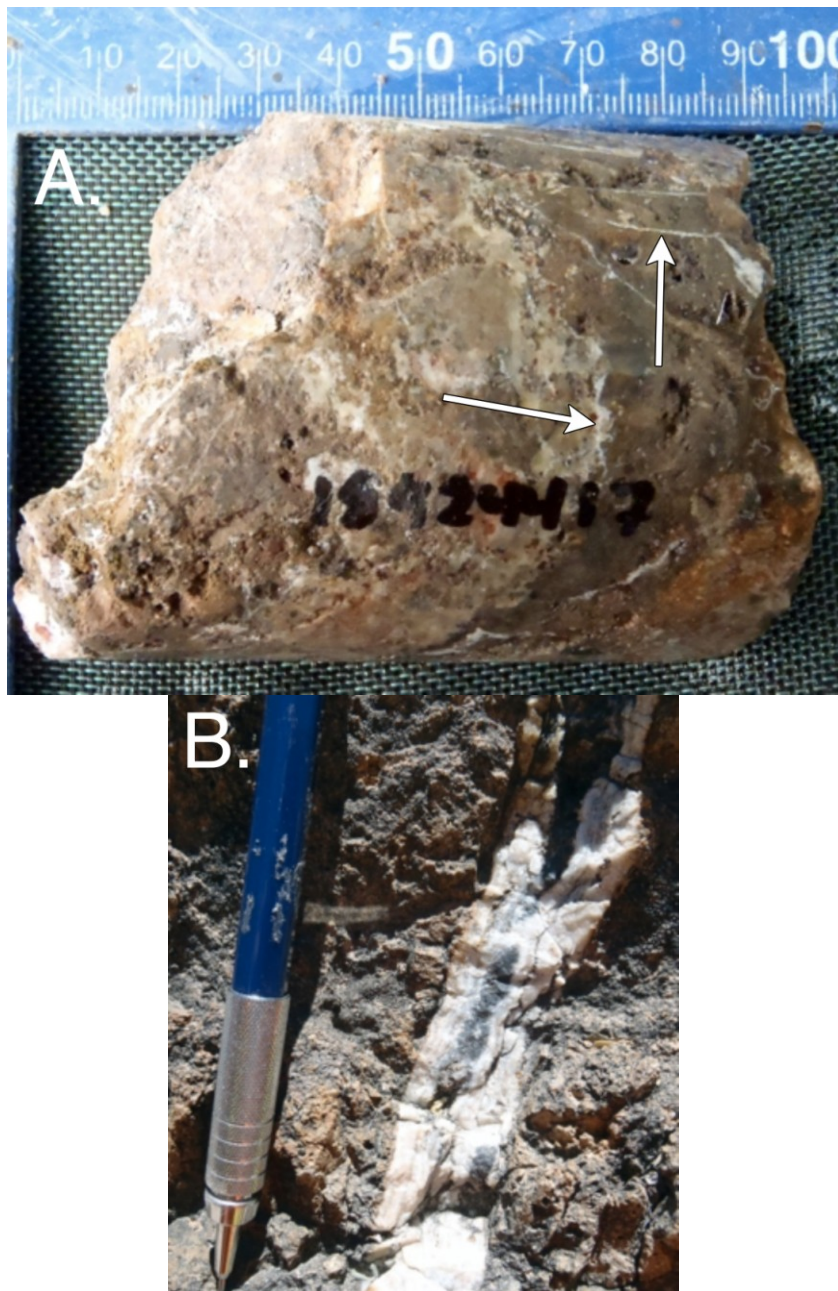


Figure 25. Examples of Phase III mineralization. (A) Thins, white Phase III quartz+calcite veinlets (white arrows) cutting phase I quartz and andesite clasts. From 244.17 m in hole M07-189D. (B) Phase III veinlets with banded quartz selvage and dark grey quartz and dark carbonate centers. Located in an outcrop 50 m west of the trace of the Mercedes vein.

Phase IV

Phase IV consists of the extensive, supergene oxidation event that post-dated hydrothermal mineralization. In addition to the extensive oxidation of the wall rocks, the vein is oxidized at all depths studied. The inferred Phase I sulfides have been oxidized to hematite and limonites (generally goethite with local zones of jarosite, Fig. 26) with the degree of oxidation becoming more intense toward the fault trace. Mn-oxides are also present as fracture fill and dendrites.

In several of the higher-grade core samples, spongy brown cerargyrite is present in close association to the vuggy quartz+hematite that commonly occurs in the high-grade zones.. Cerargyrite represents the only silver mineral that was definitively identified in this study.



Figure 26. Cubical cavities coated with goethite after pyrite (good examples arrowed) due to phase IV processes. From 980 level of the Corona de Oro ore shoot, scale in mm.

Vein and Mineral Textures

The Mercedes vein displays a number of morphological and textural features, on a variety of scales, that are common in low-sulfidation epithermal systems (Dong, et al., 1995; Cooke and Simmons, 2000)

Vein Textures: Macroscopic to Working-face Scale

The Mercedes vein is, in essence, a vein breccia (Fig. 27). In all of the available core and at all the working faces examined in this study, banded-style mineralization was very localized and present only as clasts of the Phase I mineralization. Breccia clasts range in size from sand-sized particles up to 10 cm across. Over 90% of the clasts are Phase I quartz, with the remainder being mostly highly oxidized wall rock clasts of andesite. . The percentage of clasts matrix vary, but the vein is typically 20-50% clasts and 50-80% matrix composed mainly of Phase II carbonate.

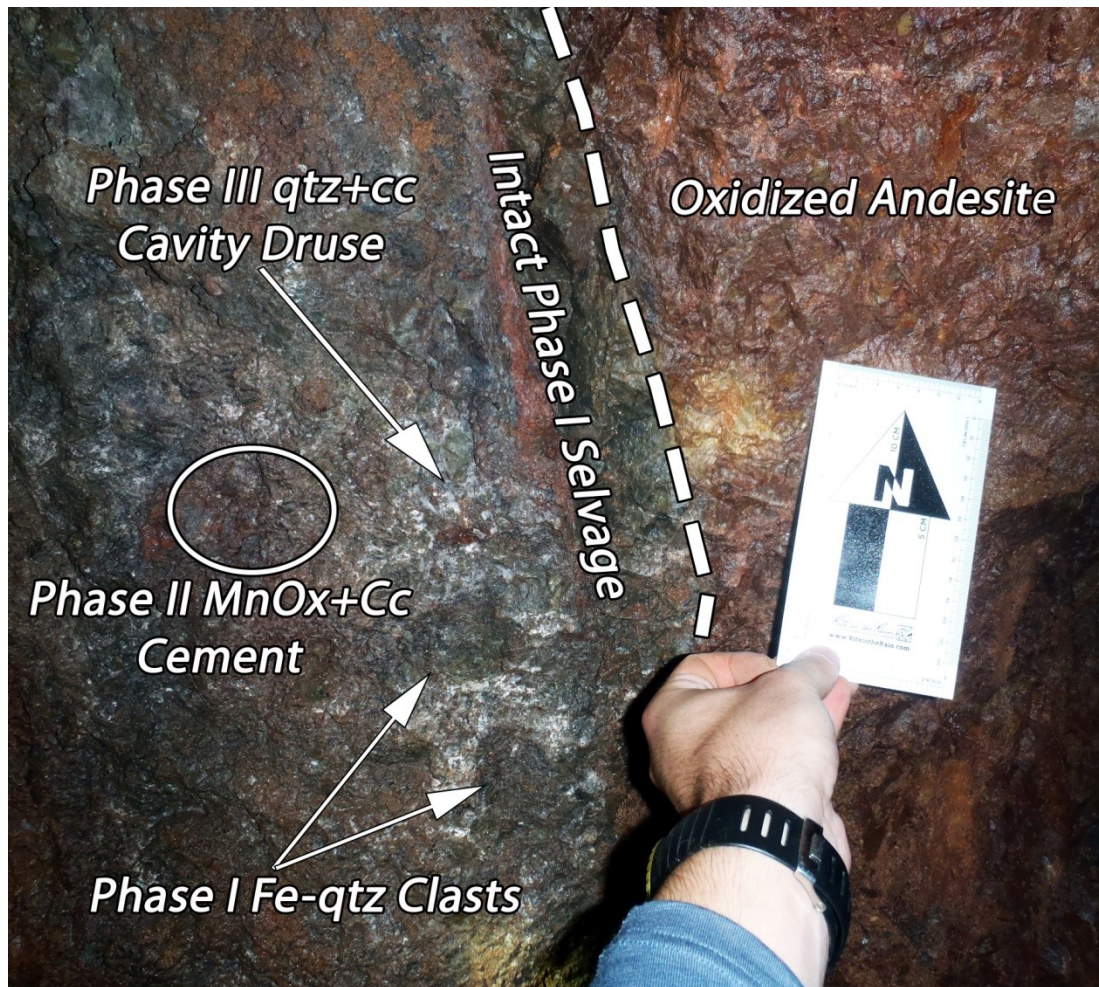


Figure 27. Typical Mercedes vein morphologies, 960 level of the Corona de Oro Zone. qtz=quartz, cc=calcite, MnOx=manganese oxides. Arrow on scale card is 10 cm long.

All the clasts observed show evidence of milling, with most of the quartz clasts ranging from sub-angular to fully rounded. The andesite clasts are more angular. Deep drillholes, notably M08-286D, which intercepted the vein at 653 m elevation, intersect heavily-altered unoxidized andesites with pervasive chlorite-pyrite alteration with a texture that is not seen in higher levels. Oxidized pieces of this material, with the pyrite altered to spidery hematite (Fig. 28A and 28B), are found as clasts within the vein breccia as high as the 1020 level within the mine. This fact paired with the rounding of the clasts implies significant amounts of vertical transport within the vein system, as much as 400 m in some locations.

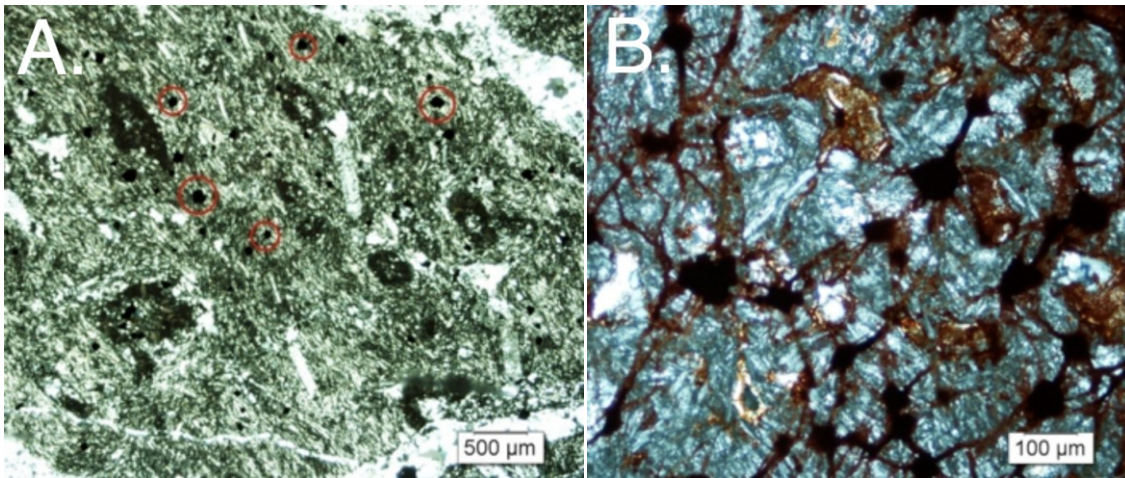


Figure 28. Photomicrographs of andesite. (A) Unoxidized, chloritized andesite from 536.08 m in hole M08-286D, corresponding to an elevation of 653 m. Circled are unoxidized pyrite euhedra. (B) Hematite after pyrite and spidery hematite from an oxidized andesite clast contained within Mercedes vein breccia at the 980 level of the Corona de Oro ore shoot. Similarities in texture between the unoxidized sample and the deep vein sample and observed lack of similar textures in proximity to the vein at all levels examined underground suggest vertical transport of andesite clasts in excess of 330 m.

Further evidence of hydrothermal transport of comes from "sandy" veinlets, one example of which can be seen in Figure 29. These veinlets are uncommon and are contained within the wall rock on the hanging wall of the vein. They appear as narrow pipes up to 5 cm in diameter that contain loosely consolidated, highly-milled pieces of Phase I and Phase II material as moderately-well sorted coarse sand-sized particles. Some of the occurrences contained thin selvages of banded Phase I quartz. They all are oriented parallel to sub-parallel to the main vein, with dips differing no more than 15°. These features are interpreted to be clastic dikelets formed within fractures subordinate to the main vein that have been filled with hydrothermally (Franchini et al., 2011) milled vein material.

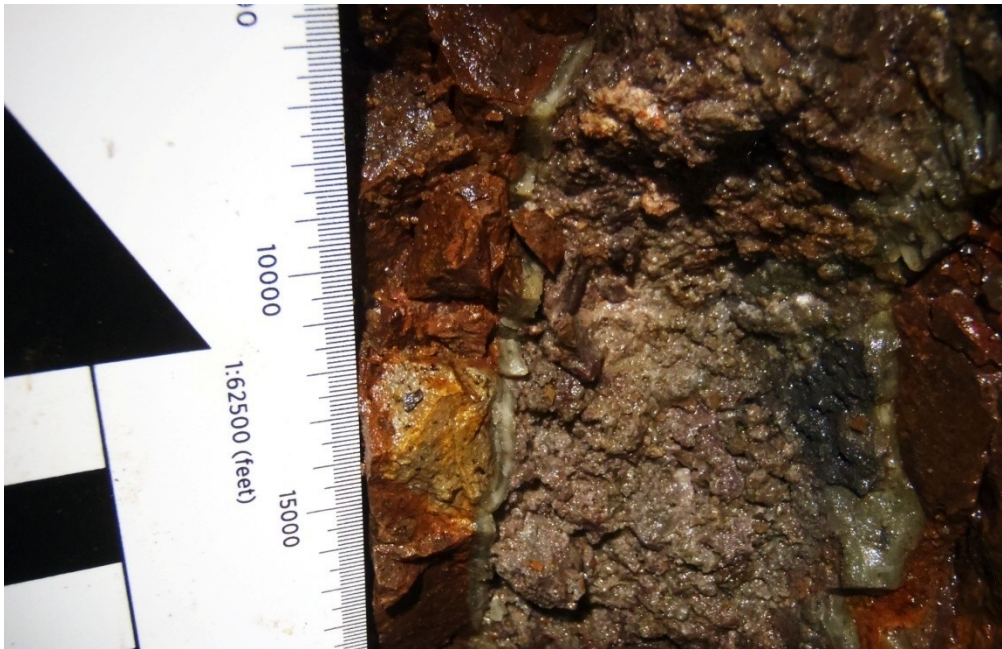


Figure 29. "Sandy" veinlet from the 910 level of the Corona de Oro ore shoot.

The Mercedes vein is localized by a normal fault with a slight component of dextral slip. The fault appears on the hanging wall side of the vein and is characterized by a thick 1-2 m zone of foliated clay gouge with strong soft-sediment deformation textures, flow banding and local slickenlines. Entrained within the gouge are small fragments of both the host andesite and vein breccia. Interestingly, many of the individual biotite and hornblende grains plucked from the andesites and sheltered by the relatively impermeable clays are not completely altered (Fig. 30) hinting that faulting initiated prior to the introduction of the hydrothermal fluids.

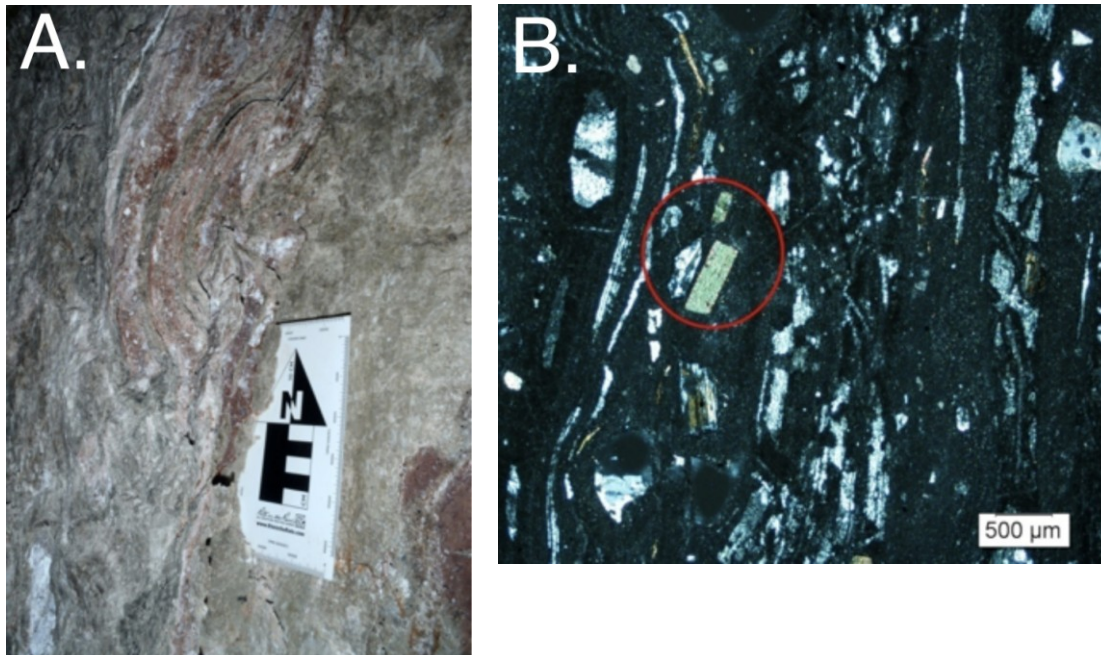


Figure 30. The Mercedes fault. Left: Underground exposure from the 940 level of the Breccia Hill ore shoot, showing clay gouge, flow banding and the typical foliated nature. Right: Thin section of material at left showing strong flow orientation of fresh biotite phenocrysts (circled) in a clay gouge.

High-grade zones that locally grade over 300 ppm Au and contain visible native gold are strongly correlated with a particular set of textural characteristics. These intervals are distinguished by a porous, clast-supported breccia containing clasts of dark olive green, saccharoidal Phase I quartz in a matrix of minor Phase II carbonates and abundant hematite that locally shows boxwork textures that formed from the oxidation of sulfides. These intervals also possess variable Ag: Au ratios, but tend to contain lower than average ratios than the lower-grade zones. Visible Au in these intervals occurs in hematitic zones as irregularly shaped grains up to 5 mm across (Fig. 23D). Conversely, lower grade ore between 5 and 15 ppm Au displays the textures common throughout the vein. The low-grade zones are typically more dense and have a high proportion of Phase II carbonates cementing lesser amounts of light green Phase I quartz clasts.

Macro- and Microscopic Textures: Phase I

The green quartz that dominates the Phase I mineralogy is preserved as clasts within the vein breccia. The most common texture within the clasts is a jigsaw or mosaic patterned quartz (Fig. 31A), resulting from the recrystallization of amorphous silica or chalcedony (Adams, 1920; Dong et al., 1995; Moncada et al., 2012). This texture appears to form a continuum with coarser grained saccharoidal (Figs. 31B, 31C) quartz after platy calcite that is distinctive of the Mercedes high-grade. Locally, clasts of what were originally banded chalcedonic quartz display feathery (Sander and Black, 1988) recrystallization textures containing high proportions of exclusively vapor-phase inclusions (Fig. 31D Fig. 32). In addition to the recrystallization textures, unaltered colloform quartz is irregularly distributed within the vein breccia as well as forming the selvages of the rare "sandy" veinlets.

Samples of phase I quartz examined from all levels of the vein record evidence of vigorous boiling. In particular, the vapor-phase inclusions in the feathery quartz imply rapid depressurization and "flashing" (Moncada et al., 2012) of the hydrothermal fluids. This mechanism has been invoked to explain bonanza-grade Au and Ag deposits in other deposits (Brown, 1986; Dong et al., 1995, Sillitoe, 1993; Cooke and Simmons, 2000; Moncada et al., 2012) and may be responsible for the high-grade ore shoots in Mercedes as well.

The bulk of the Au is submicroscopic, and intercepts greater than 500 ppm Au routinely lacked visible Au at the hand lens or microscopic (i.e. $>5 \mu\text{m}$). Hand-lens visible Au, in both core obtained for this study (Fig. 23D) and specimens kept by the mine geology and exploration staff, was uniformly associated with highly porous, hematitic, green quartz breccia. The individual grains were commonly 1-3 mm in size, with one specimen containing a flake 8 mm across within a hematitic boxwork. All the

grains observed during the course of this study were irregularly shaped, spongy and deeply golden in color, suggesting a high fineness.

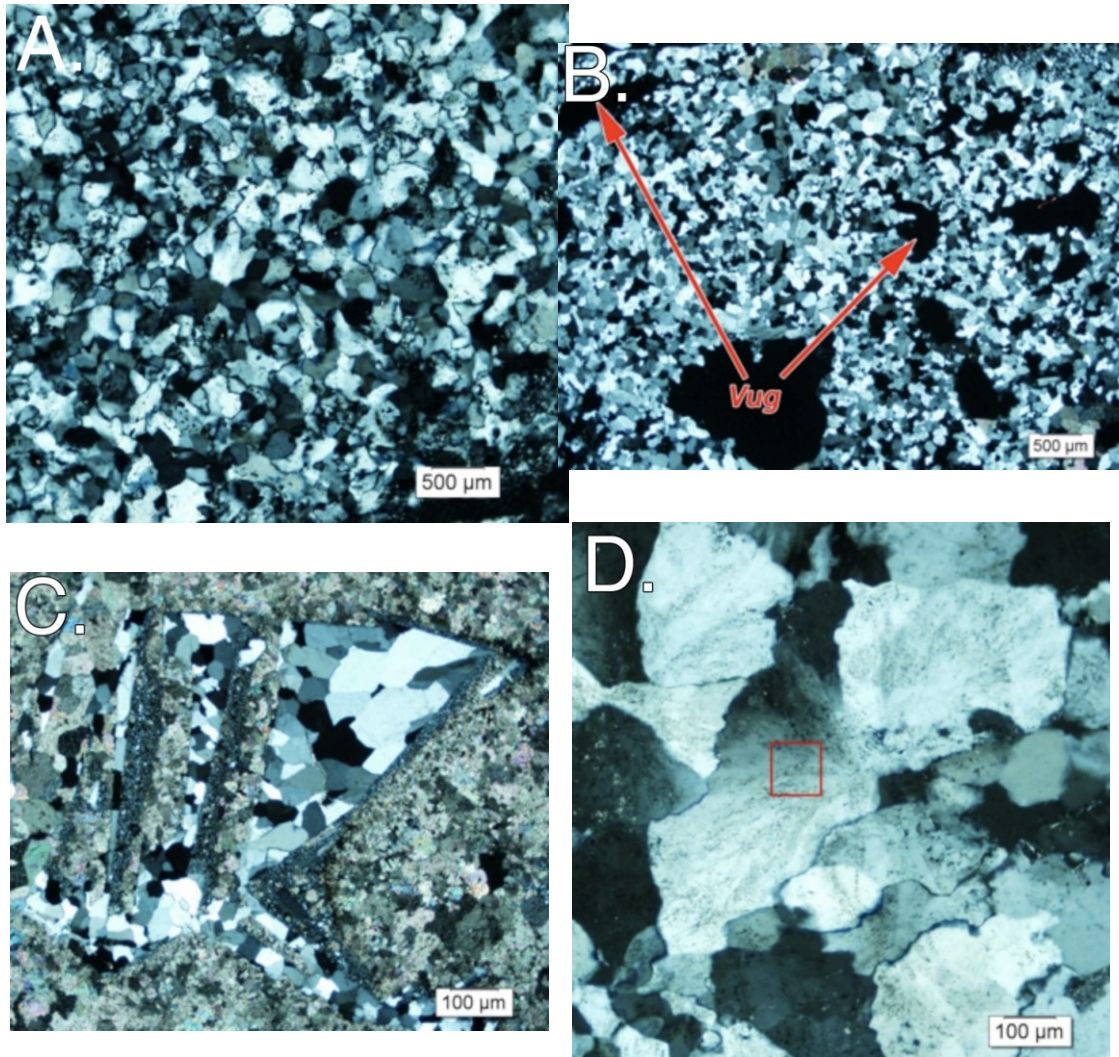


Figure 31. Mineral textures from Phase I. Crossed polars. (A) Jigsaw or Mosaic texture in a phase I green quartz clast. Hole M07-083D, 182.49 m. (B) Vuggy saccharoidal green quartz. Hole M07-083, 182.49 m. 2.55 ppm Au, 228 ppm Ag. (C) Saccharoidal quartz partially replacing platy calcite with infilling later clear quartz. Hole M10-519D, 203.30 m. 6.1 ppm Au, 40 ppm Ag. (D) Feathery quartz with abundant vapor inclusions. Red, boxed zone is the approximate extent of Fig. 32. From 960 Level, Corona de Oro ore shoot.

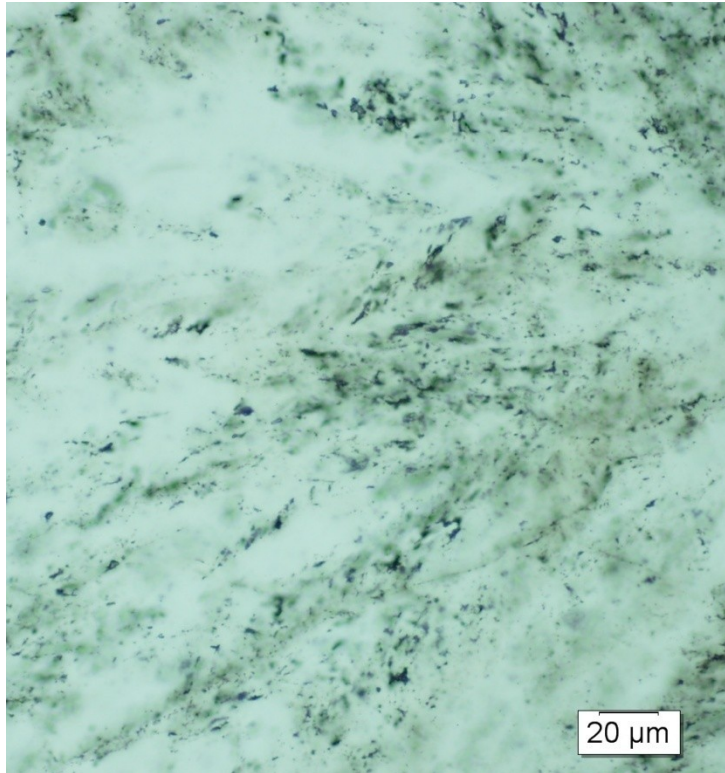


Figure 32. Plane polarized light, close-up of boxed area of Fig. 31, bottom right. Abundant, feathery vapor inclusions indicative of vigorous boiling or "flashing" (Moncada et al., 2012).

Ordinarily, the distribution of boiling textures may provide some sort of guide to the extent of mineralization, as precious metal deposition tends to occur within and slightly above the boiling zone (Buchanan, 1981; Robb, 2005; Camprubi and Albinson, 2007). However, brecciation and transport of the Mercedes vein subsequent to Phase I mineralization makes any interpretation of the extent of boiling impractical. Samples (Fig. 31) from the lower levels of the Mercedes workings, at 960 m elevation, possess equally abundant boiling textures as those higher in the system. Textural evidence supports up to 400 m of vertical transport for wall rock clasts entrained within the vein breccia, during the Phase I/Phase II brecciation event and it is possible that the deepest samples from the mine workings may have been transported similar distances.

Macro- and Microscopic Textures: Phase II

Phase II minerals, dominated by Mn-oxide bearing calcite, record less textural diversity than the Phase I silica minerals. The overwhelming bulk of the Phase II mineralization is composed of massive, fine-grained, crystalline calcite/Mn-oxide intergrowths, as shown in Figure 33. Variable amounts of Mn-oxides (possibly pyrolusite) compose up to 70% of the volume of the darkest carbonate+Mn-oxide masses. These zones commonly intermingle and grade into pink rhodochrosite that commonly has slightly larger grain sizes and much lower amounts of intermixed Mn-oxides than the darker calcites.

In addition to carbonate, minor amounts of grey-green milky quartz veinlets, typically <1 cm in width, with zonal growth or comb textures pinch in and out of the carbonate and seem contemporary with the Phase II mineralization, but the relationship is somewhat ambiguous as local examples may be clasts of Phase I material poorly exposed within the carbonate matrix.

In sharp contrast to the ubiquity of boiling textures in the Phase I minerals, evidence of boiling is absent within the Phase II minerals. None of the diagnostic bladed or acicular textures of calcite under boiling conditions (Simmons and Christenson, 1994; Moncada et al., 2012; Dong et al., 1995) were in the Phase II mineralization from any level of the Mercedes vein. The lack of boiling textures and the related low grades of Au-Ag mineralization within intervals dominated by Phase II (Itoh et al., 2002) suggest that the Au-Ag mineralization was restricted to Phase I.

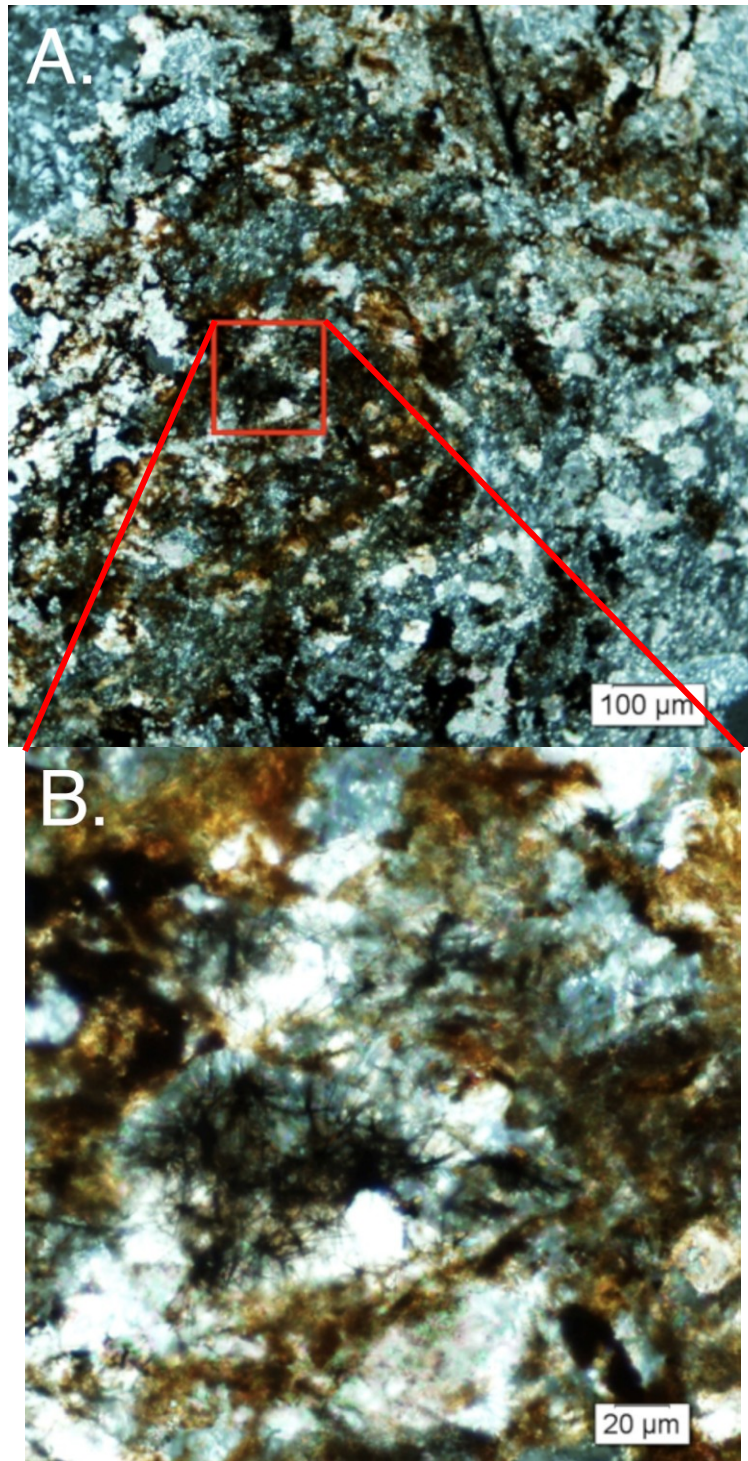


Figure 33. Phase II dark carbonates from the 910 level of the Corona de Oro ore shoot. (A) Brownish Mn-oxides intergrown with calcite. (B) Close-up of boxed area showing acicular inclusions of Mn-oxides in calcite and Mn-oxide disseminated throughout calcite.

Macro- and Microscopic Textures: Phase III

The final phase of hydrothermal mineralization within the Mercedes vein system is represented by a network of small veinlets that cross-cut the vein breccia and the host andesites. They are composed of clear quartz and calcite with very local boudin-shaped pockets of darker, Mn-oxide bearing calcite or rhodochrosite. Veinlets of this style can be found in outcrop several hundred meters from the main vein and may represent downward-drawn fluids introduced during the collapse of the epithermal system or a later hydrothermal event.

Microscopically, the veins contain crystalline calcite with obvious twin-planes and comb-textured quartz (Fig. 34, top) with local growth zoning consisting of increased concentrations of bimodal liquid-vapor inclusions with constant phase ratios (Fig. 34, bottom). These features are interpreted to represent a non-boiling, fluid that was unrelated to deposition of sulfides or precious metals (Moncada et al., 2012).

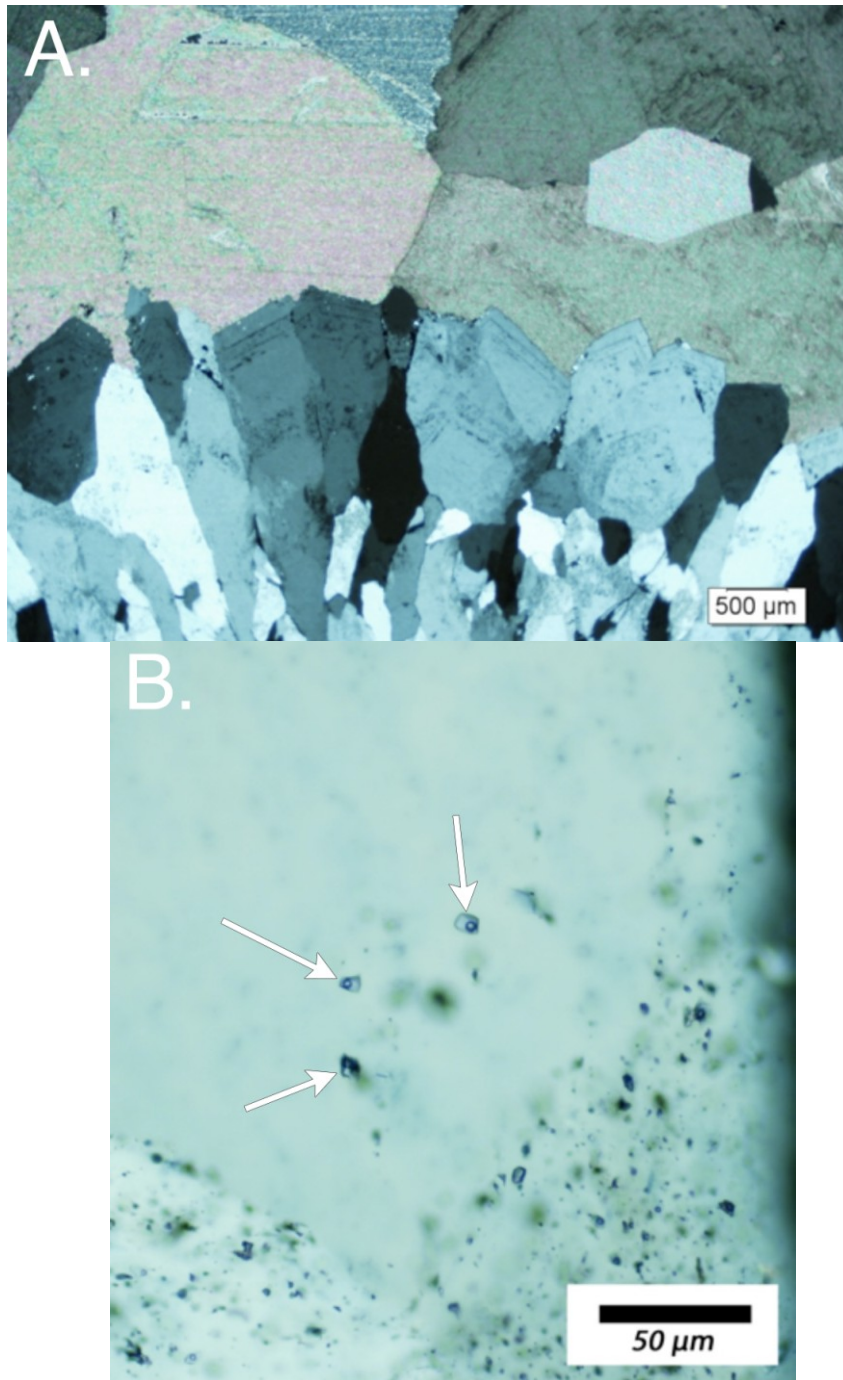


Figure 34. (A) Phase III veinlet with coarse calcite (high birefringance) and zoned, comb-textured quartz (shades of grey). From hole M10-570 at 272.18 m. (B) Rare examples of consistent-ratio fluid/vapor inclusions (arrowed) along growth zones in Phase III quartz. Hole M07-189D, 241.42 m.

Macro- and Microscopic Textures: Phase IV

Unlike phases I-III, the fourth phase of mineralization at the Mercedes mine is related to weathering, and supergene oxidation of many of the sulfides in the Mercedes vein system. The most obvious and extensive results are the total oxidation of the vein sulfides and surrounding wall rocks down to at least 650 m elevation. Hematite and limonites are extremely common, with goethite being the dominant Fe-hydroxide phase. Small zones of jarositic staining are also locally present. The hematite is found as three forms: 1.) a spidery oxidation product of pyrite in transported andesite clasts (see Fig. 28); 2.) Pervasive staining within the wall-rock matrix (Fig. 35); and 3.) boxworks and replacement after vein sulfides associated with the highest grade intervals and local visible Au (see Fig. 23). This indigenous hematite after sulfide is the best visual indicator of the high-grade ore at Mercedes, especially where it occurs in porous zones with material dark green, saccharoidal quartz.

Also present within the Phase IV assemblage are local concentrations of cerargyrite, appearing as spongy brown vug and boxwork fill. According to observations as well as the core logs (Yamana Exploration Staff, unpublished information, 2008-2012), the cerargyrite is closely associated with the high-grade gold zones with indigenous hematite. Unfortunately, much of the high-grade was unavailable for petrologic sampling and none of the high-grade samples studied in thin section contained discernible cerargyrite.



Figure 35. Top: Extensive exotic hematite, goethite and jarosite staining of the andesite wall rocks. A small vein dominated by phase II carbonates runs just to the left of the scale card. From the 960 level of the Corona de Oro ore shoot.

Finally, Mn-oxides are widespread in the vein system as fracture fill, dendrites and spongiform masses that occupy the location of former phase II Mn-bearing calcites that have had the carbonate leached from the matrix leaving intergrown Mn-oxides (Fig. 24B).

Variations in Textures

There does not appear to be a consistent pattern to the distribution of the quartz textures outlined above. This is due to the extensive amount of physical transport during hydrothermal and tectonic disruption that occurred within the vein system. Boiling textures contained within clasts of the early, green quartz are found throughout the entire vertical extent of the vein and there appear to be no intervals in the Mercedes vein where brecciation has not occurred. Along strike to the northwest, the vein structure becomes markedly less coherent in the Barrancas/Lagunas zone. The vein here, as interpreted from drill data (Yamana Exploration Staff, 2010-2012; this study), takes on a poddy, sheared and discontinuous structure. However, within the mineralized sectors the matrix-supported vein breccias appear indistinguishable from the breccias in the Mercedes zone.

Geochemistry

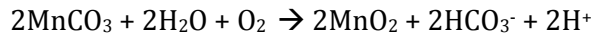
Composition of Green Quartz and Dark Carbonates

Green quartz appears to be uncommon within epithermal systems, and review of the literature has not found another known occurrence within Mexico. In order to determine the cause of the green color and understand the cause of the correlation between the darkest greens and the highest Au grades, three samples of the phase I green quartz were prepared (see Appendix IV) and submitted for XRF analysis. Sample Q-001, from 182.5 m in drillhole M08-083D was the darkest green sample submitted and contained 95.9% SiO₂, 0.32% Fe₂O₃, 0.22% MgO and 0.01% MnO. The sample also contained 0.06% C and 0.48% CaO, suggesting that it was nearly pure quartz with minimal contamination by transition-metal bearing phase II carbonates. The lightest green sample, Q-002 from the 156.2 m interval of hole M12-555 in the Barrancas zone

contained 98.1% SiO₂, 0.09% Fe₂O₃, 0.08% MgO and 0.05% MnO along with 0.06% C and 0.34% CaO. Under a petrographic microscope, the darkest green quartz is visually indistinguishable from lighter green quartz with a similar texture. There does not appear to be any significant mineral inclusions larger than the visual resolution limit (conservatively estimated to be ~5µm) with the microscopes used during this study. This fact, combined with the XRF data, suggests that the greenish color is due to Fe contained within the crystalline matrix of the quartz and not effects due to inclusions of fluid or other minerals. Given the green color (Schwertmann and Cornell, 2000) and the arguably reduced nature of the fluids (Sillitoe and Hedenquist, 2003; Gemmell, 2004) that introduced the phase I precious metals and sulfides, it is possible that the iron is present as Fe⁺² ions. These ions may be accommodated within the quartz as either submicroscopic disseminations of iron(II) oxides/hydroxides or as direct substitution for Si⁺⁴ cations. Both the charge and atomic radius of the Fe⁺² ion (0.76 Å, Railsback, 2003) are approximately 1/2 that of the Si⁺⁴, making some sort of coordination within the Si site conceivable. This variety of quartz, prasiolite, is rare and unknown in Mexico. Considering the scarcity of this quartz variety and the implications that reduced Fe has on the redox properties of the vein chemistry, further investigation using SEM is needed to solve the mystery.

One sample of dark carbonate was also prepared and submitted from the 1040 level of Mercedes for XRF analysis. C-001 returned 46.3% CaO, 9.67% C, 0.89% Fe₂O₃, 0.15% MgO and 3.78% MnO. For reference, stoichiometric calcite contains 56.04 wt% CaO and 43.96 wt% CO₂ (12.00 wt% C). The sample also contained 14.9% SiO₂, likely as small amounts of phase I quartz. The carbonate reacts vigorously with dilute (3%) HCl and has a dark grey to black color. Given the high Mn content and the color, it seems unlikely that it is rhodochrosite or manganoan calcite as these are both diagnostically

pinkish in color. Some samples from the Mercedes system contain zones of spongy pyrolusite and other Mn-oxides that are retained in places that look as if they were once occupied by the phase II dark carbonates; thus it seems that the dark carbonates are in fact an intergrowth of calcite and Mn-oxides, possibly resulting from partial oxidation of rhodochrosite generating pyrolusite and acid according to the equation below:



This interpretation is supported by thin section microscopy clearly showing Mn-oxide minerals contained within the Phase II calcite as a member of Phase II mineralization and separate from later Mn-oxides produced during weathering as part of Phase IV mineralization.

Vertical Zonation

Figures 36 through 41 show the results of ICP-AES and fire assay (Au and Ag) analyses plotted versus the true elevations of 49 drill core assay pulp samples from the main Mercedes vein and 34 from the Barrancas/Lagunas extension. The samples represent the entire accessible vertical extent of the system from 650 m to 1097 m elevation; a vertical range of 450 m.

Weak vertical patterns are evident in both the major metals (Fig. 36: Ag, Au, Cu, Mo, Pb, Zn) and minor elements (Fig. 37: As, Ba, Hg, Sb, Tl). Some of the calculated trends run counter to the classical vertical zonation within epithermal systems (Buchanan, 1981). Base metals (Cu, Pb, Zn) may slightly increase with depth, while Mo decreases. Ag shows a steeper decrease in depth than Au, which stays nearly constant across all elevations. The minor elements As, Ba, Tl and notably Hg all anomalously increase with depth while Sb shows decreasing concentrations.

On the scale of individual study sections, these trends are broadly similar. The zonation for section 9550, as seen in 20 samples from 790 m to 1103 m elevation (Figs. 38 and 39, above) retains the overall increases of Cu, Pb and Zn and a decrease in Mo with depth. Ag displays a steeper decline with depth, while Au increases dramatically. The trace element zonation is the same in this section as in the vein as a whole.

With only 13 samples spread from 933 m to 1089 m, section 8860 (Figs. 40 and 41) displays a very similar zonation, with the exception of the trends in Au and Ag which reverse with Ag slightly increasing with depth and Au slightly decreasing.

The significant scatter in the data and poor statistical fits for the calculated trendlines, suggest that these patterns reflect a system that has been significantly affected by tectonic and hydrothermal vertical transport of vein material and subsequent post-mineral supergene effects on mobile elements.

The method outlined by Loucks and Petersen (1985) for the Ag-dominant veins at Topia, Durango was attempted (Fig. 42) for the geochemical data from the Mercedes vein. No discernible pattern regarding the distribution of Ag/Zn and Pb/Zn ratios can be determined as is shown by the seemingly random “shotgun” pattern of the plotted data.

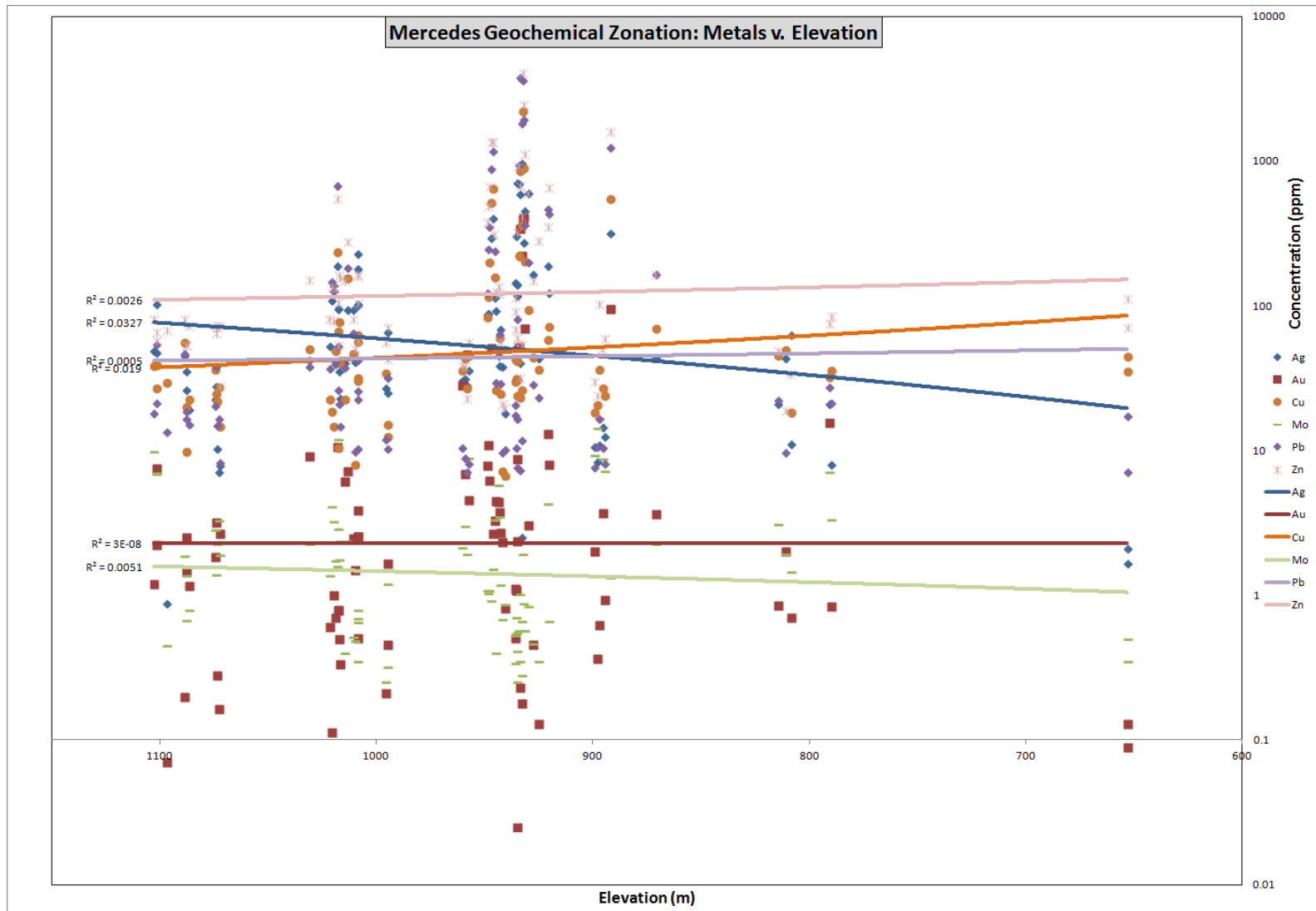


Figure 36. Mercedes metals vs. elevation. Trend lines are power regressions with R-squared values listed. Note log scale on y-axis.

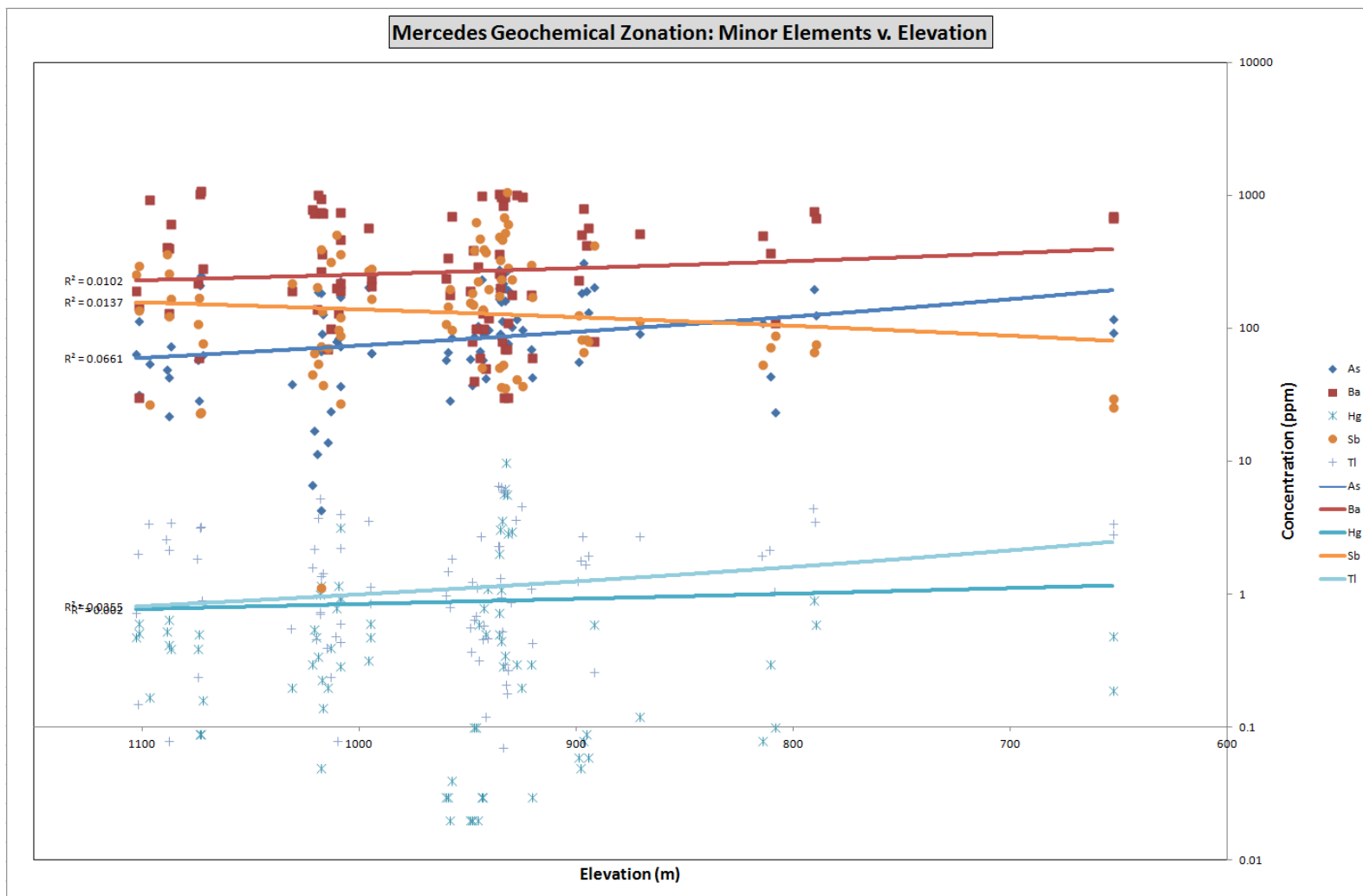


Figure 37. Mercedes trace elements vs. elevation. Trend lines are power regressions with R-squared values listed. Note log scale on y-axis.

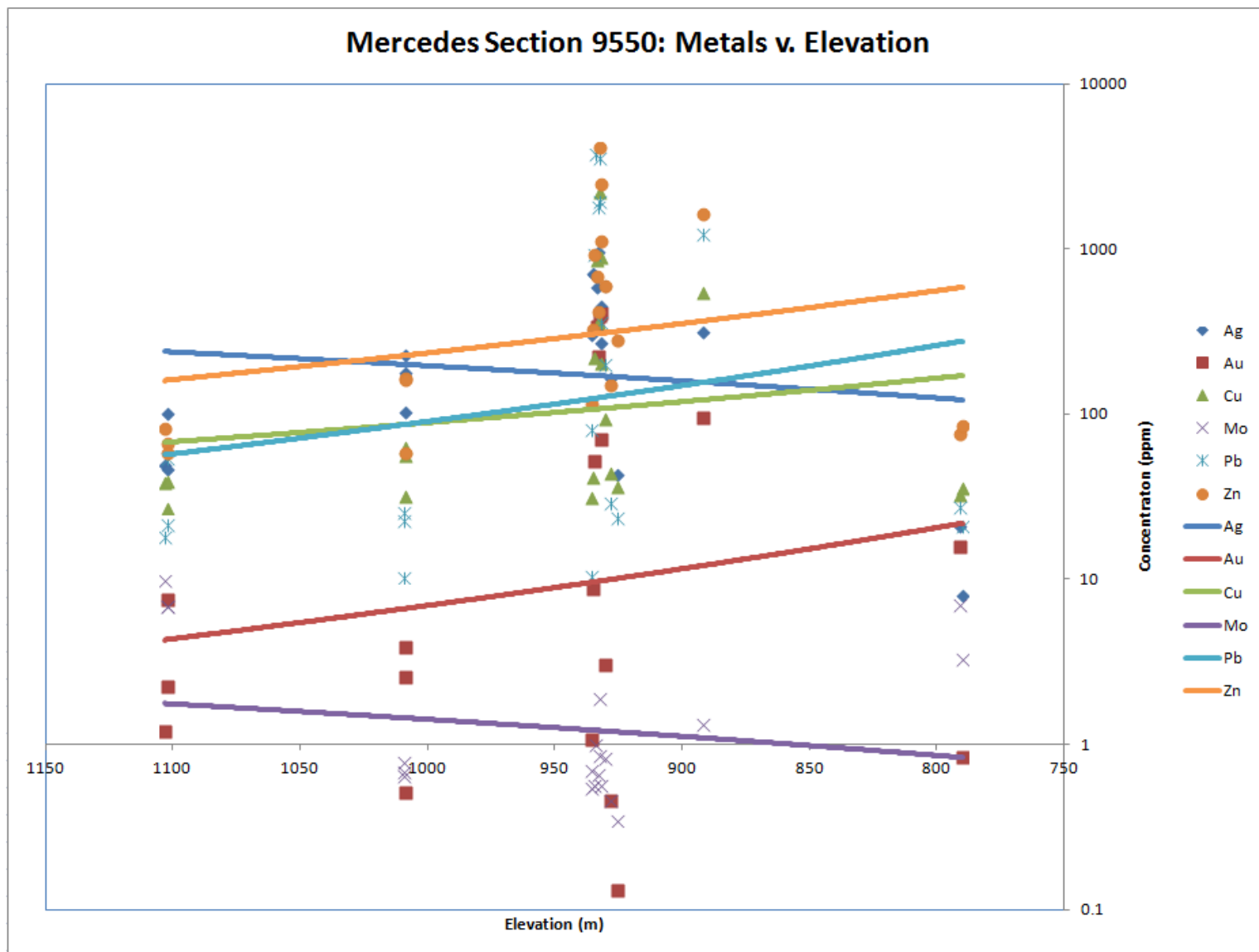


Figure 38. Mercedes section 9550 metals vs. elevation. Trend lines are power regressions with R-squared values listed. Note log scale on y-axis.

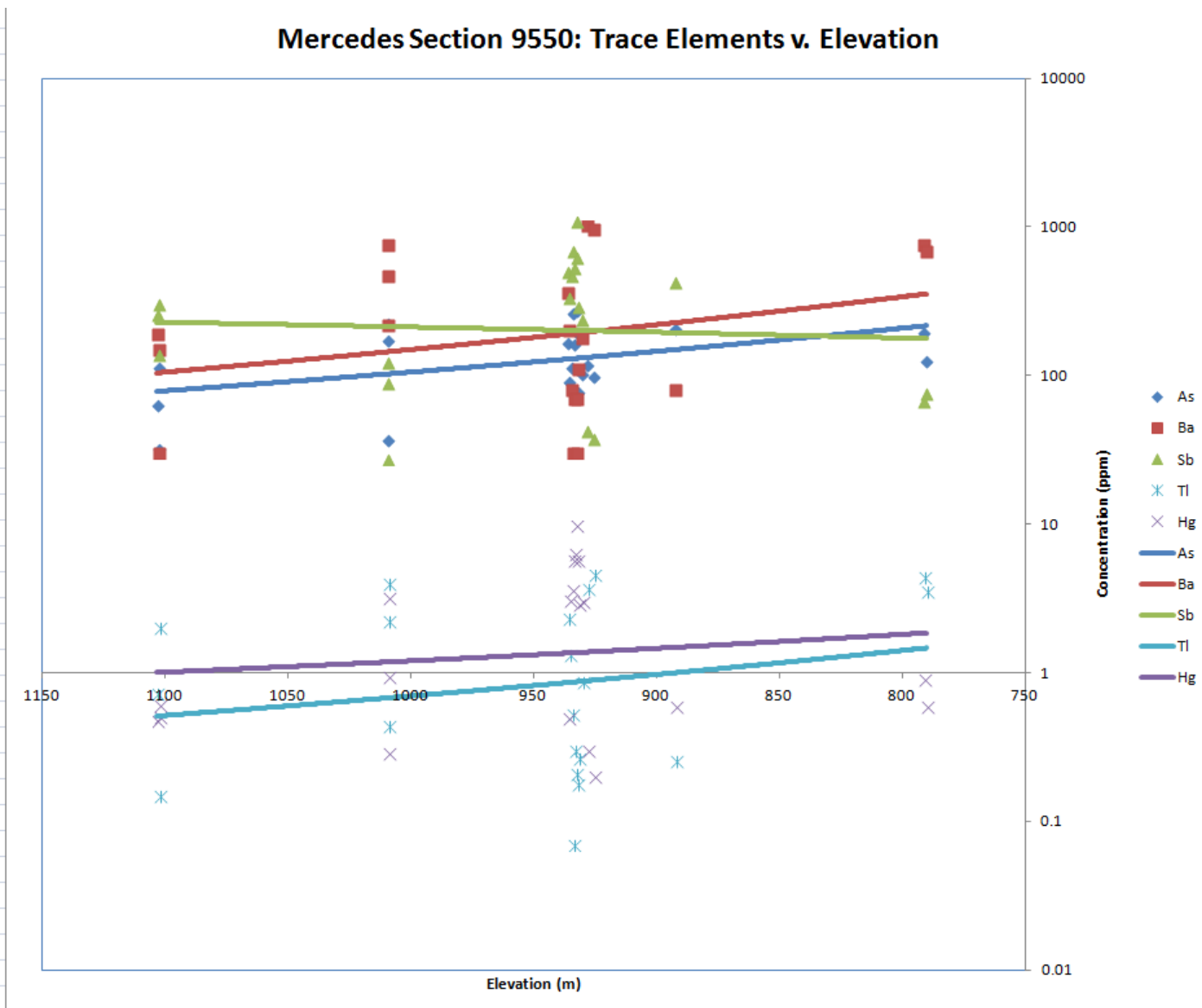


Figure 39. Mercedes section 9950 trace elements vs. elevation. Trend lines are power regressions with R-squared values listed. Note log scale on y-axis.

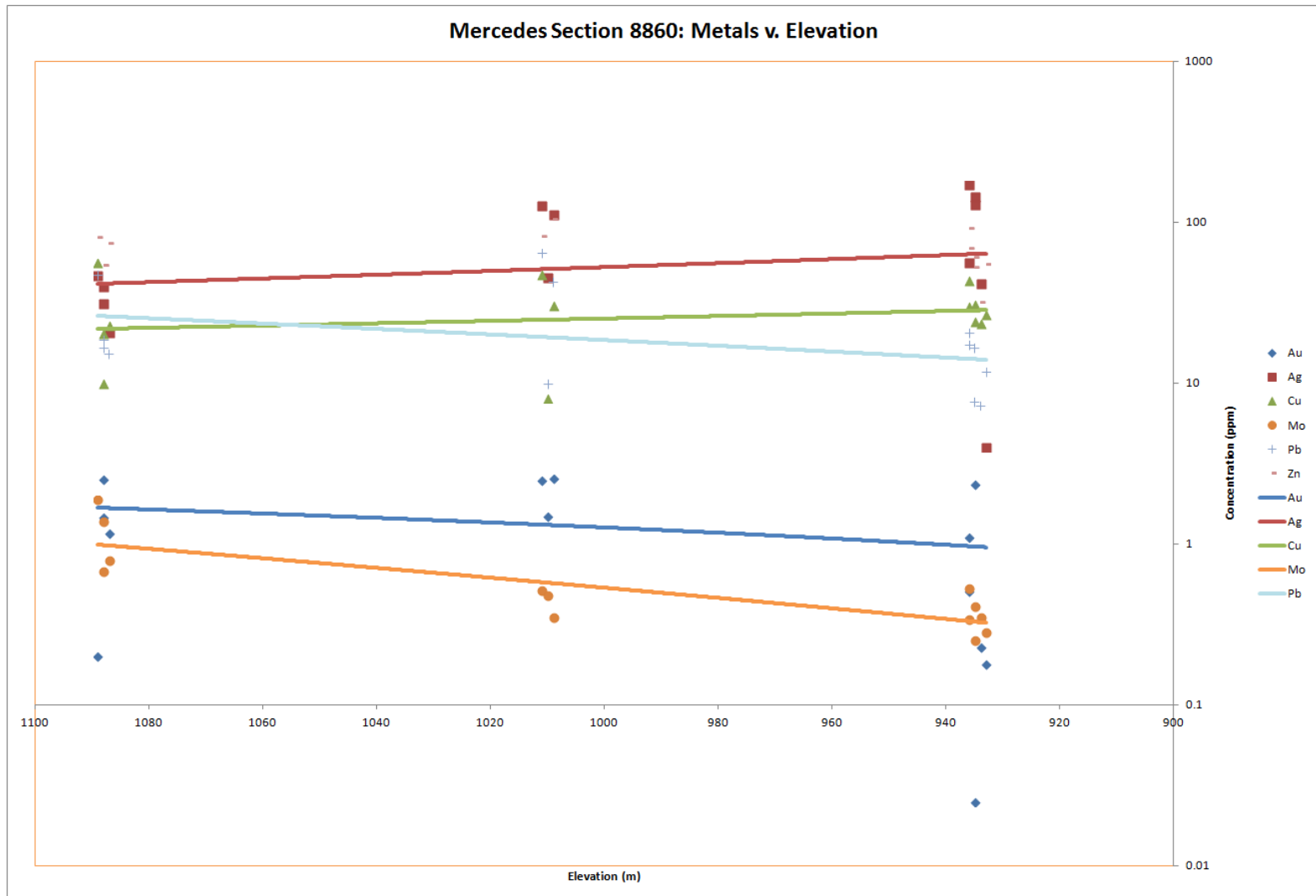


Figure 40. Mercedes section 8860 metals vs. elevation. Trend lines are power regressions with R-squared values listed. Note log scale on y-axis.

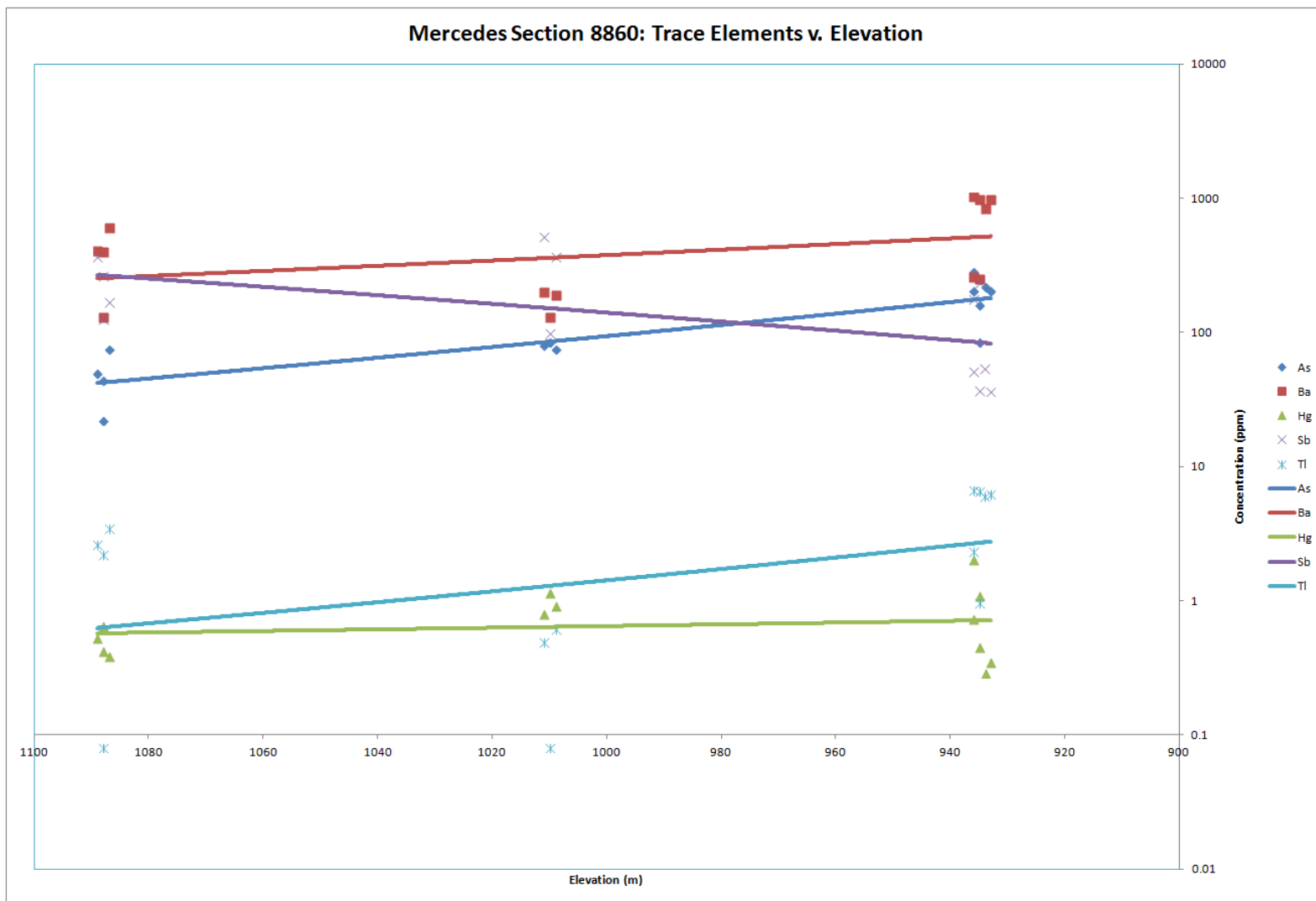


Figure 41. Mercedes section 8860 trace elements vs. elevation. Trend lines are power regressions with R-squared values listed. Note log scale on y-axis.

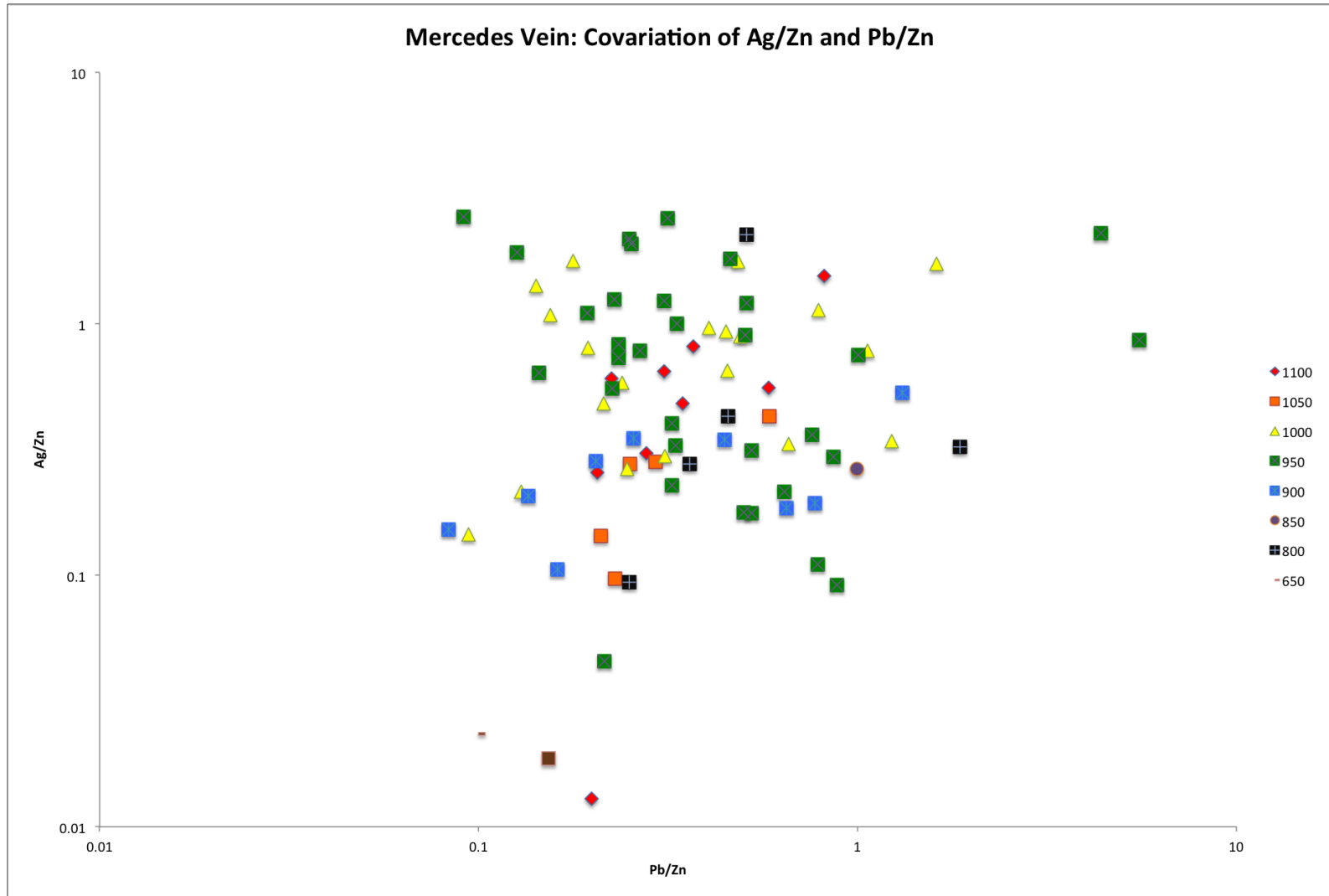


Figure 42. Covariation of Ag/Zn and Pb/Zn ratios with elevation for the Mercedes vein. Color spectrum reflects elevation in meters: red=higher, purple=lower. Method modified from Loucks and Petersen (1985).

Horizontal Zonation

The zonation along strike of the Mercedes vein is non-existent for most elements, despite over 3 km of sampled interval. Major vein component elements (Ca, Fe, Mn, C and S, Fig. 43), most trace elements (Ba, Se and Tl, Fig. 45) and Zn (Fig. 44.) have nearly zero variation along strike.

Au, Cu, Mo, Pb, Zn all show some increase toward the northwest while As, Sb and Ag show a slight decrease. Hg shows a very marked decrease in concentration towards the northwestern Barrancas/Lagunas extension.

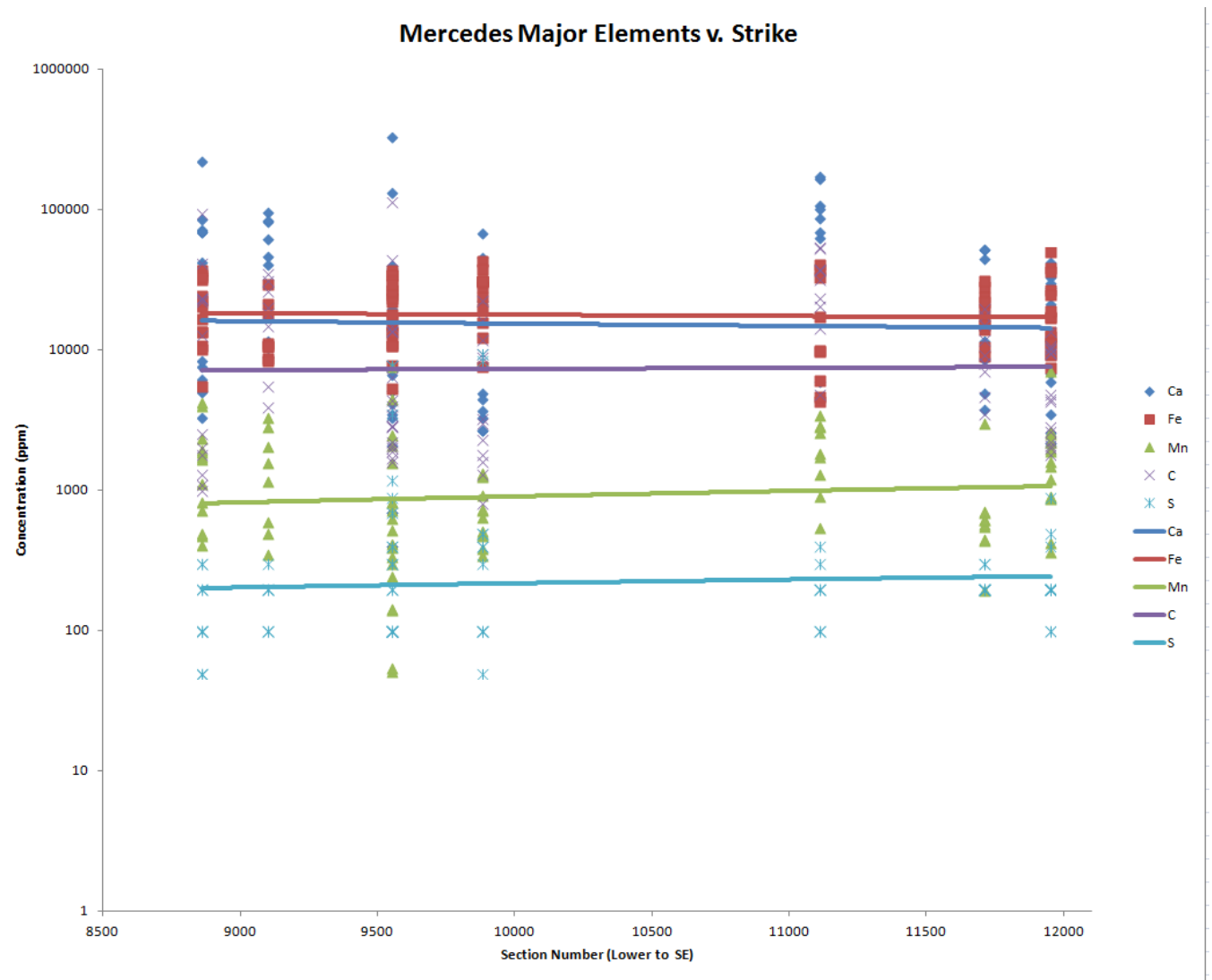


Figure 43. Mercedes major elements vs. strike. Trend lines are power regressions. Note log scale on y-axis.

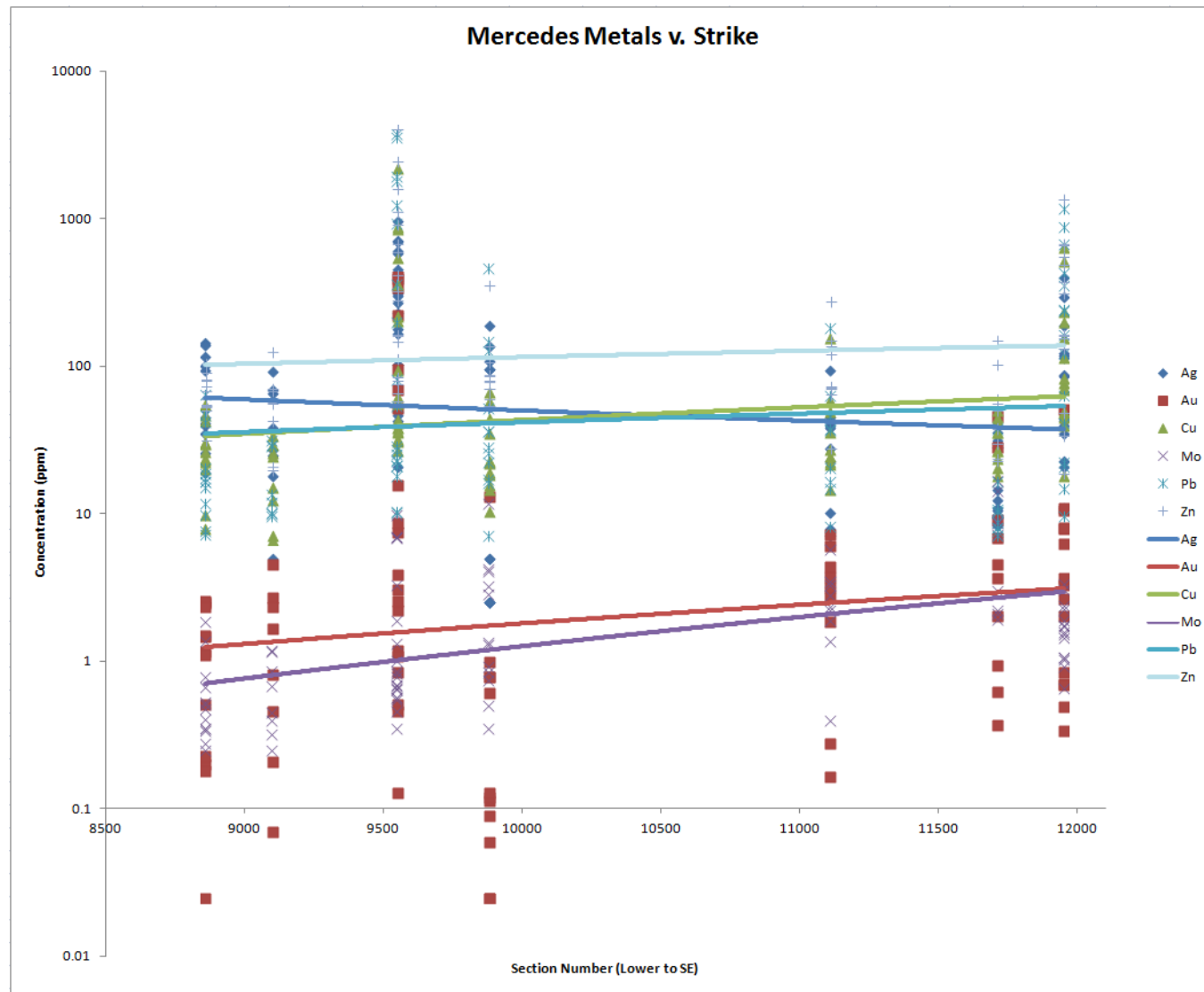


Figure 44. Mercedes metals vs. strike. Trend lines are power regressions listed. Note log scale on y-axis.

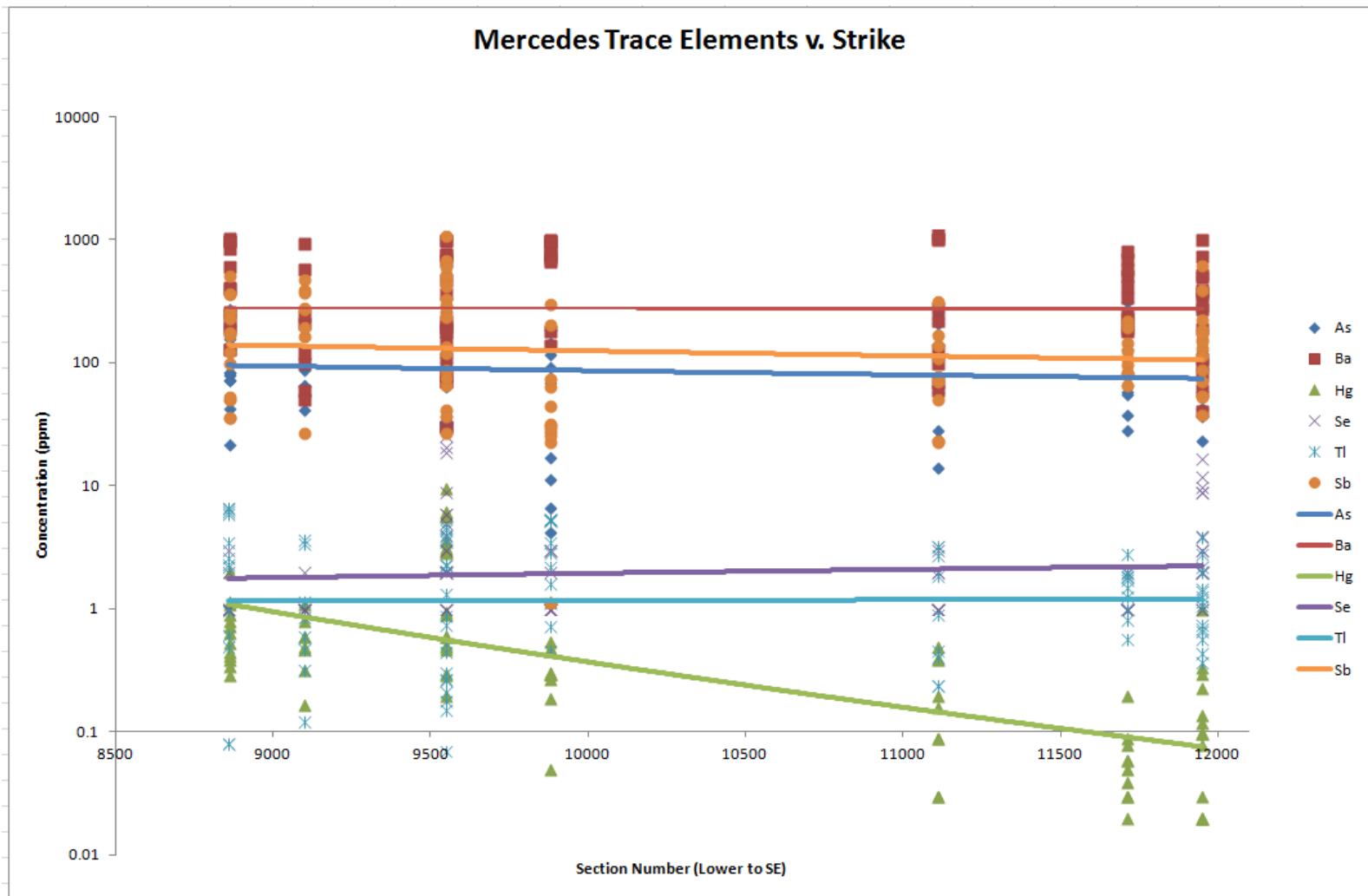


Figure 45. Mercedes trace elements vs. strike. Trend lines are power regressions with. Note log scale on y-axis.

Correlations

Using the same ICP-AES, fire assay and IR spectroscopy data used for the geochemical zonation analysis, correlation analysis was undertaken to determine the associations between the various major and trace elements within the Mercedes vein. Using 83 samples from the entire Mercedes vein, a correlation matrix of the entire 48-element analysis suite in addition to C and S was created (see Appendix V). Figure 46 takes the most salient 18 elements from that analysis for reference. R-values with an absolute value greater than 0.5 are chosen to be statistically relevant while those greater than 0.75 are considered significant.

The most notable correlative relationship is the slight positive correlation (0.517) between Au and Ag. Au is much more strongly correlated with Pb, Hg, Se, Zn and Sb (0.913, 0.856, 0.808, 0.775 and 0.686, respectively). Ag, however, correlates with Se, Hg, Pb and Sb (0.719, 0.706, 0.613 and 0.600) and these relationships have a generally lower degree of correlation as compared to those of Au.

Also of importance is the correlative triad of Ca, C and Mn. Not surprisingly Ca and C show a very strong positive R-value of 0.987, reflecting the calcite content in the system. Ca shares only one other positive correlation with Mn (0.675). This adds further weight to the XRF analysis of Mn-bearing calcite being the predominant dark carbonate mineral in the Mercedes vein and to the phase I origin of the precious metal mineralization.

	FA-Ag	FA-Au	Ag	As	Ba	Ca	Cu	Fe	Ga	Hg	Mg	Mn	Mo	Pb	Sb	Se	Zn	C	S
FA-Ag	1.000																		
FA-Au	0.517	1.000																	
Ag	0.767	0.284	1.000																
As	0.175	0.354	0.071	1.000															
Ba	-0.352	-0.299	-0.342	0.423	1.000														
Ca	-0.153	-0.131	-0.110	-0.321	-0.274	1.000													
Cu	0.448	0.851	0.345	0.341	-0.283	-0.152	1.000												
Fe	-0.072	0.120	-0.191	0.657	0.764	-0.416	0.074	1.000											
Ga	-0.187	-0.239	-0.197	0.417	0.863	-0.366	-0.195	0.745	1.000										
Hg	0.706	0.856	0.470	0.364	-0.291	-0.059	0.771	0.063	-0.189	1.000									
Mg	-0.135	-0.168	-0.102	0.258	0.441	0.145	-0.090	0.414	0.451	-0.054	1.000								
Mn	-0.077	-0.063	-0.028	-0.222	-0.240	0.675	0.053	-0.308	-0.318	0.035	0.226	1.000							
Mo	-0.237	-0.114	-0.188	0.225	0.156	-0.209	-0.103	0.107	-0.035	-0.178	-0.187	-0.210	1.000						
Pb	0.613	0.913	0.395	0.345	-0.335	-0.180	0.898	0.095	-0.234	0.811	-0.155	-0.024	-0.132	1.000					
Sb	0.600	0.686	0.510	0.123	-0.603	-0.140	0.753	-0.262	-0.418	0.688	-0.277	0.035	-0.209	0.760	1.000				
Se	0.719	0.808	0.383	0.304	-0.328	-0.200	0.682	0.114	-0.203	0.712	-0.141	-0.065	-0.172	0.843	0.631	1.000			
Zn	0.473	0.775	0.468	0.267	-0.315	-0.140	0.936	-0.006	-0.218	0.702	-0.060	0.078	-0.146	0.788	0.713	0.636	1.000		
C	-0.147	-0.122	-0.102	-0.280	-0.288	0.987	-0.142	-0.396	-0.389	-0.042	0.212	0.675	-0.163	-0.167	-0.133	-0.185	-0.136	1.000	
S	0.181	0.277	-0.020	0.152	0.002	-0.122	0.150	0.359	0.153	0.230	0.097	-0.127	-0.116	0.333	0.087	0.351	0.019	-0.111	1.000

Figure 46. Correlation matrix for selected elements, Mercedes vein. Green colors are significant positive correlations, yellows and oranges poor correlations and dark orange to red indicates significant negative correlations. N = 83.

THE KLONDIKE VEIN

Introduction

The Klondike vein (Fig. 47) is the second vein in production at the Mercedes property. The vein crops out along approximately 800 m with an average strike of 290° . Like Mercedes, it dips subvertically with an average dip of 77° to the south. It ranges between 1 and greater than 40 m in width, with the vein generally wider at depth. Unlike Mercedes, economic Au-Ag mineralization is restricted to only about 300 m of vertical extent.

Diamond drilling has defined two ore shoots, of lower grades than Mercedes. These are also localized in dilatational zones produced by changes in dip and strike of the fault-hosting vein. For the purposes of this study, two study cross sections (11080 and 11260) were chosen based on the access to core and underground exposures. The nomenclature reflects their positions within the Klondike zone exploration grid.

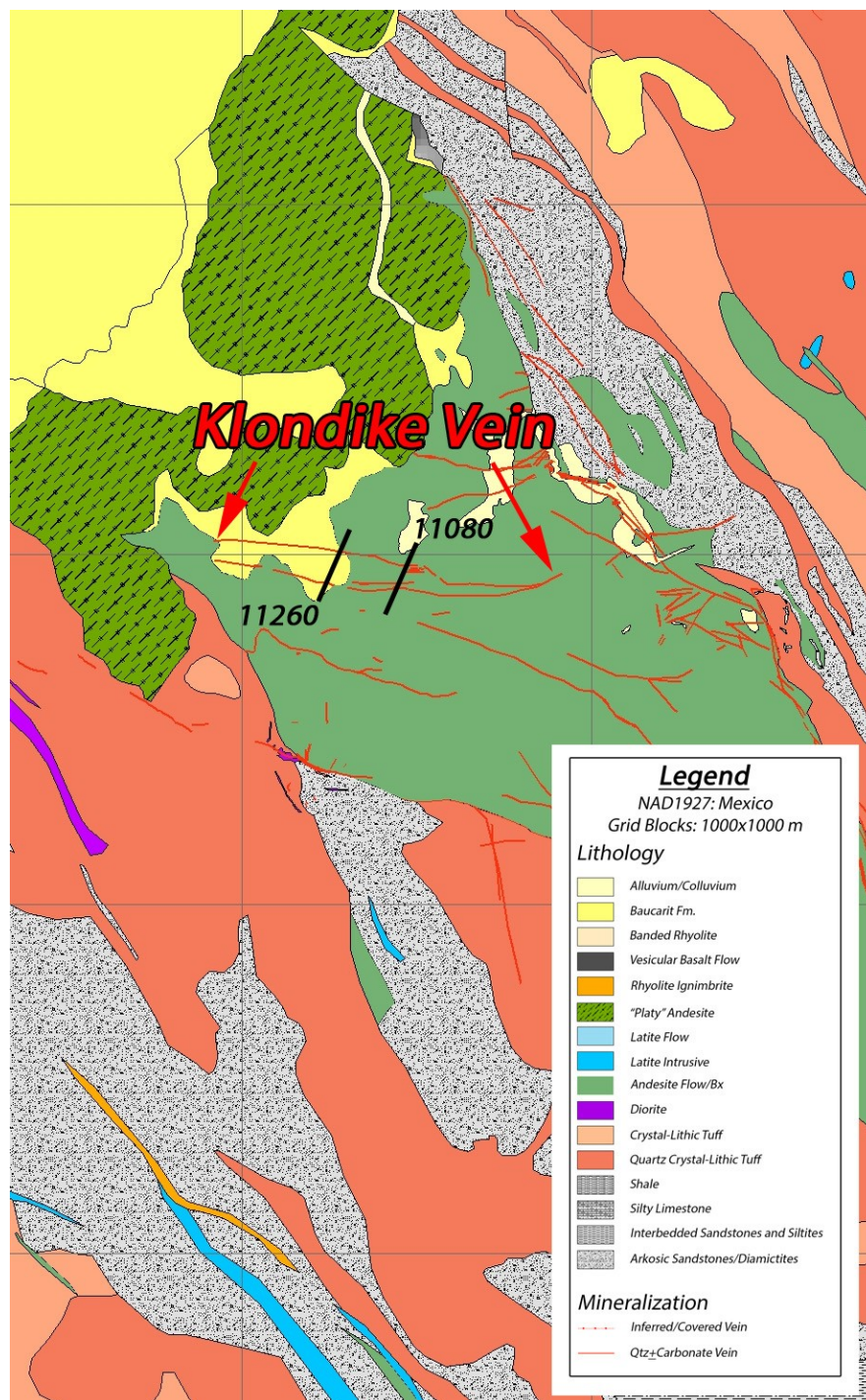


Figure 47. Geologic map of the Klondike vein zone. Black lines are the study cross sections, labeled according to the exploration grid nomenclature. Adapted from Yamana Geodatabase. (Yamana Exploration Staff, 2012)

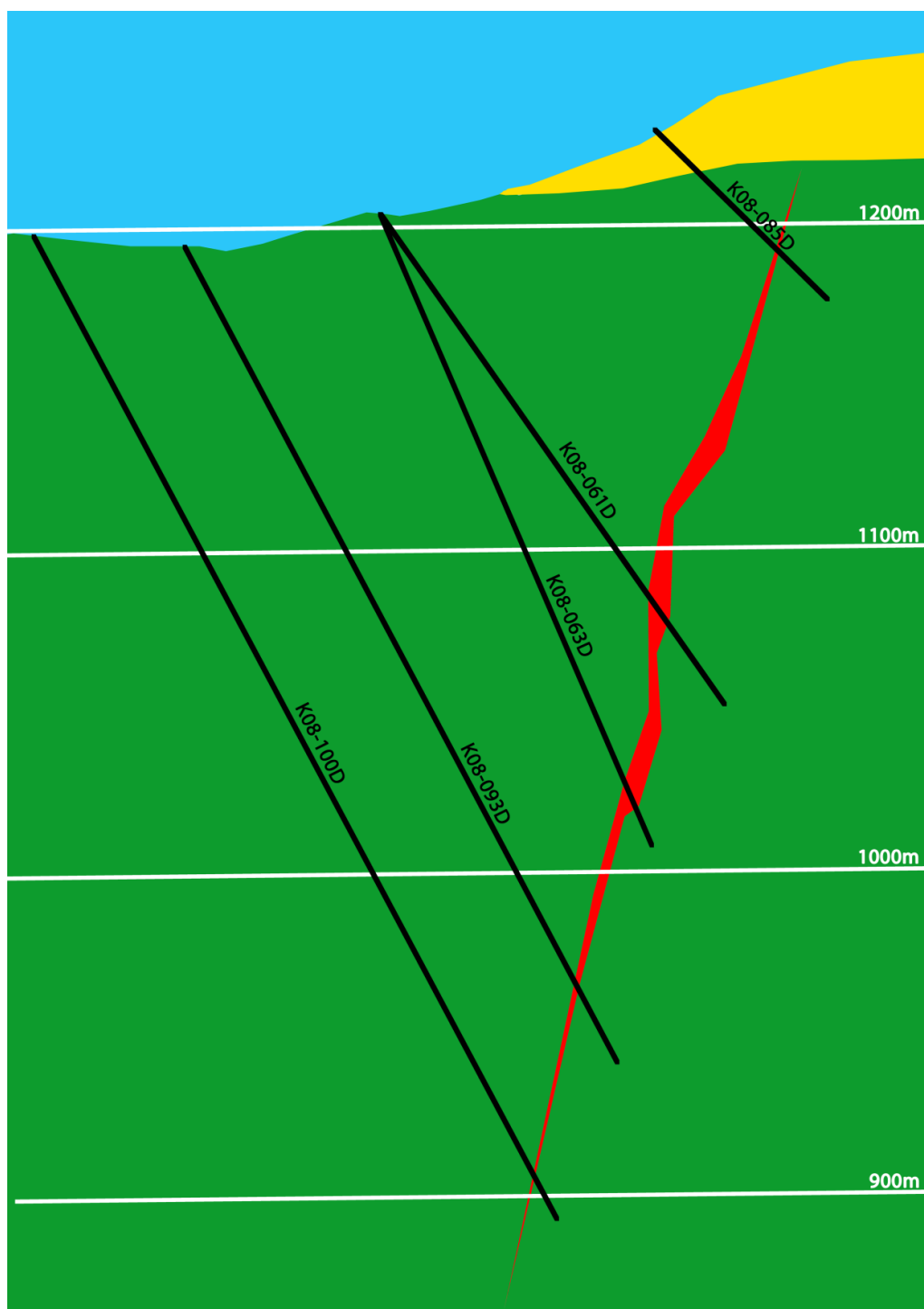


Figure 48. Cross section 11080 through the Klondike vein, looking east. Red polygon is vein material, green is host andesite, yellow is Baucarit Fm. and black lines are drill holes selected for sampling. Elevation is given at right in white. Figure created from unpublished interpretive cross-sections (Yamana Exploration Staff, 2008) and original work by the author.

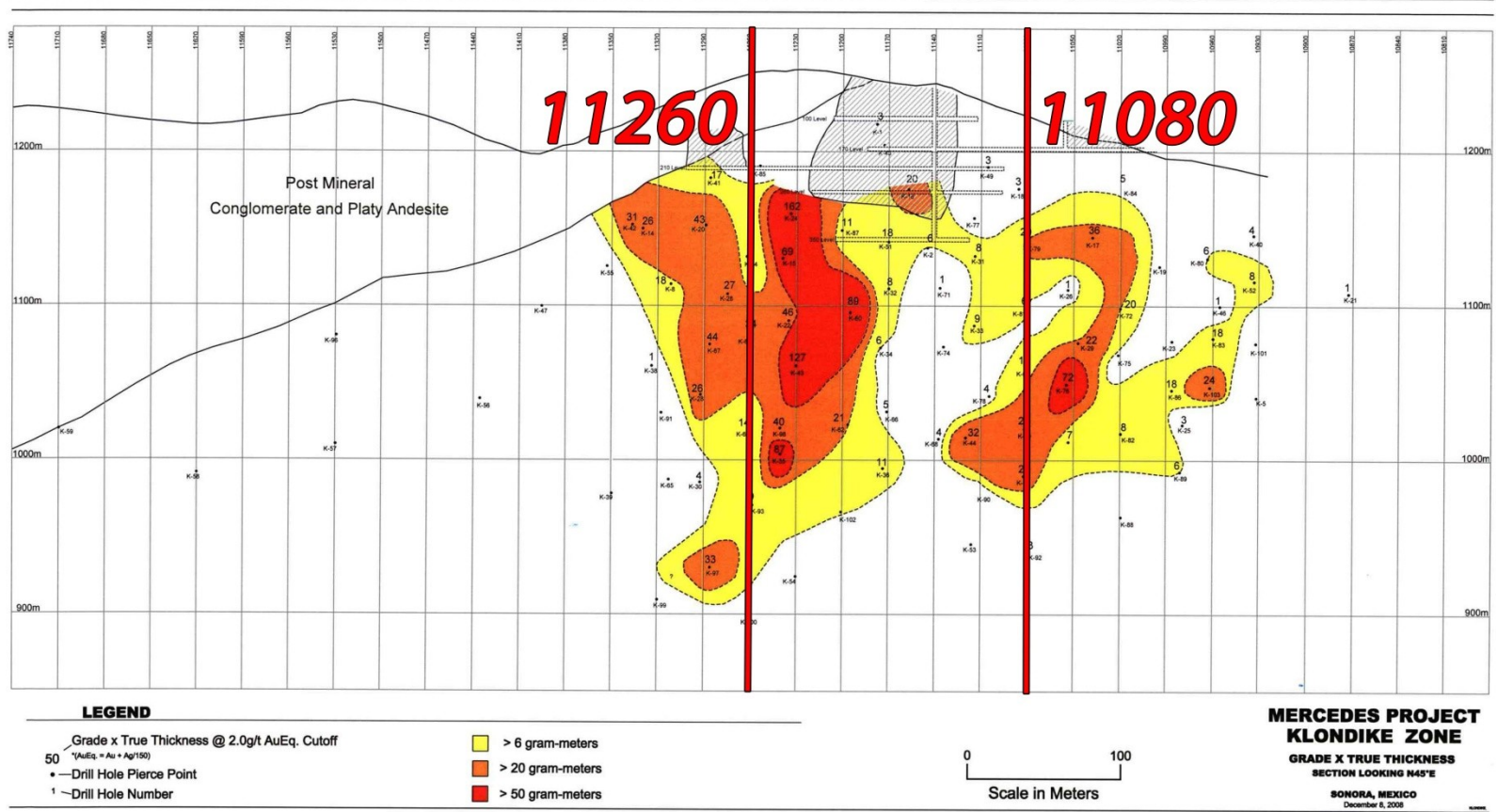


Fig. 49. Klondike vein long section showing grade-thickness values of the vein. Study cross sections are marked and labeled in red. (Yamana Exploration Staff, Unpublished Data, 2008)

Paragenesis

The paragenetic sequence of the Klondike vein (Fig. 50), like that of the Mercedes vein, consists of three major hydrothermal phases followed by a final phase of weathering and supergene effects upon the mineralogy of the ore body. At least one significant brecciation event separated Phases I and II, with additional brecciation likely ongoing during Phase II.

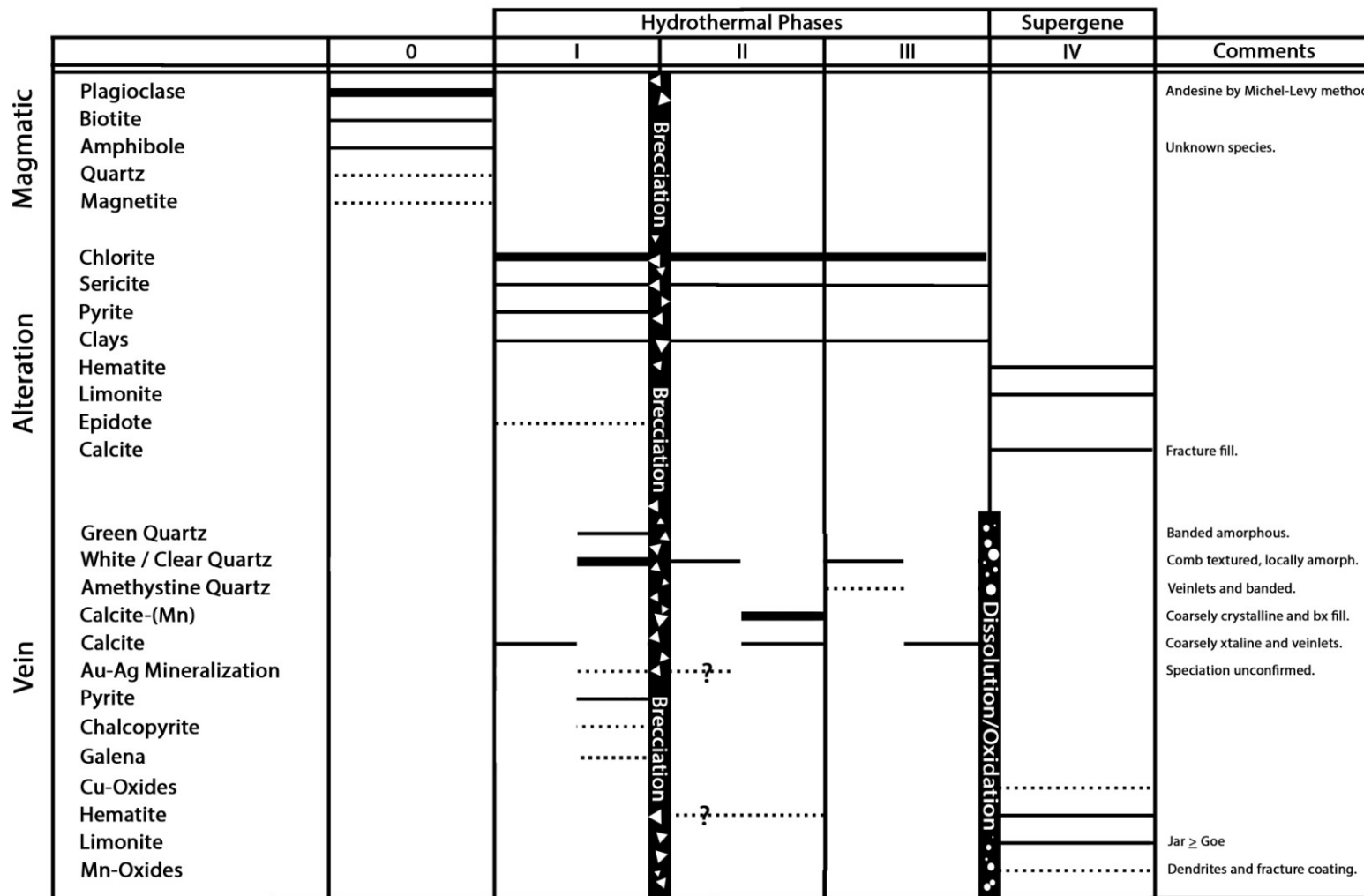


Figure 50. Klondike vein paragenetic diagram

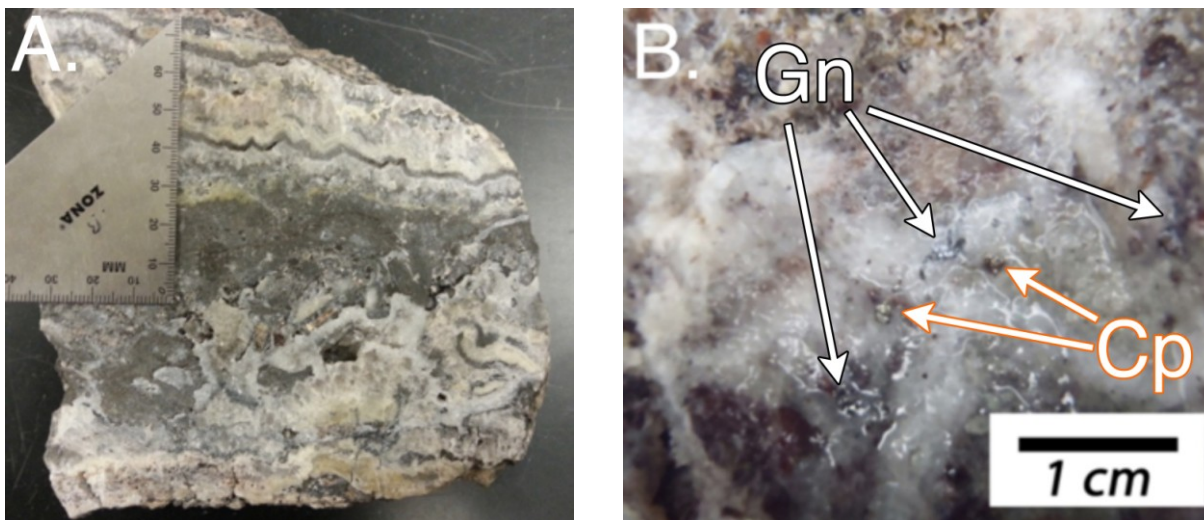


Figure 51. (A) Banded vein and vein breccia from the 1060 level of the Klondike mine with phase I green quartz and phase II dark carbonates. Note ductile deformation of banded vein material on bottom right. (B) Chalcopyrite (Cp) and galena (Gn) blebs in light phase I quartz in vein breccia from 279.80 m in hole K08-097D.



Figure 52. Vein proximal stockworks demonstrating paragenetic relationships. Phase II dark carbonate veinlets cutting phase I milky quartz veinlets. From 1080 level, Klondike mine.

Phase II

Phase II mineralization in Klondike closely resembles Phase II mineralization in the Mercedes vein. It is dominated by a dark, Mn-oxide bearing carbonate (Figs. 51, 52) with the local presence of a milky to clear quartz. However, the lower degree of brecciation within the Klondike system results in large sections of intact, banded vein material as well as Phase II cement surrounding Phase I vein clasts. In the banded section, a discrete boundary (see Fig. 55A) exists between the Phase I minerals and the Phase II carbonates, often with Phase I clasts peppering the boundary zone.



Figure 53. Phase II dark carbonate cement of oxidized andesite and local phase I quartz clasts. From 258.20 m in hole K08-093D. Scale in mm.

In some samples, hematite is found as massive, reddish streaks contained within the dark carbonates. These may represent relict sulfide bands that were oxidized.

While the bulk of the Au and Ag was associated with Phase I, the presence of Au and Ag grades within dominantly Phase II intercepts suggest that some precious metal mineralization must

have occurred during Phase II. While this may be the case, it is also possible that this low-grade mineralization is related to small amounts of Phase I material entrained within the Phase II carbonates that would be difficult to observe without quantitative mineralogy.

Phase III

The final phase of hydrothermal mineralization in Klondike is again similar to Mercedes, predominantly composed of white to clear crystalline quartz and calcite as both stockwork veinlets that cut through the vein into the country rock and drusy vug fill. However, in contrast to Mercedes, small and local amounts of amethystine quartz are present as druse within open spaces in the vein itself.



Figure 54. Crystalline Phase III calcite vein (top right) cutting oxidized andesite. From 154.90 m in hole K08-061D.

Phase IV

Phase IV represents supergene oxidation. It is characterized by the incomplete oxidation of the sulfide minerals to hematite and goethite. Some galena and pyrite has remained unoxidized due to encapsulation by silica and the relatively incomplete brecciation as compared to the Mercedes vein. Jarosite is more widespread than in Mercedes as both a pervasive staining in the wall rock as well as boxworks within the vein itself. Mn-oxides are also present as fracture coatings and dendrites.

Klondike also contains small amounts of copper oxides as stains and reaction rims around unoxidized chalcopyrite. The copper oxides have been observed in drill core from levels that cover the entire vertical extent of the vein system.

Vein and Mineral Textures

While sharing some of the same veining styles as the Mercedes vein, the Klondike vein differs in a few key ways, most notably the smaller magnitude of brecciation and a higher proportion of intact banded material.

Vein Textures: Macroscopic to Working-face Scale

The most significant dissimilarity between the Mercedes and Klondike veins is the amount of intact, non-brecciated banded vein material. Intact sections of vein on the scale of a 10 m working face were observed in several levels of the Klondike mine (notable the 1140 and 1060 levels, see Fig. 55 below) as well as in core and material from the mine dump.

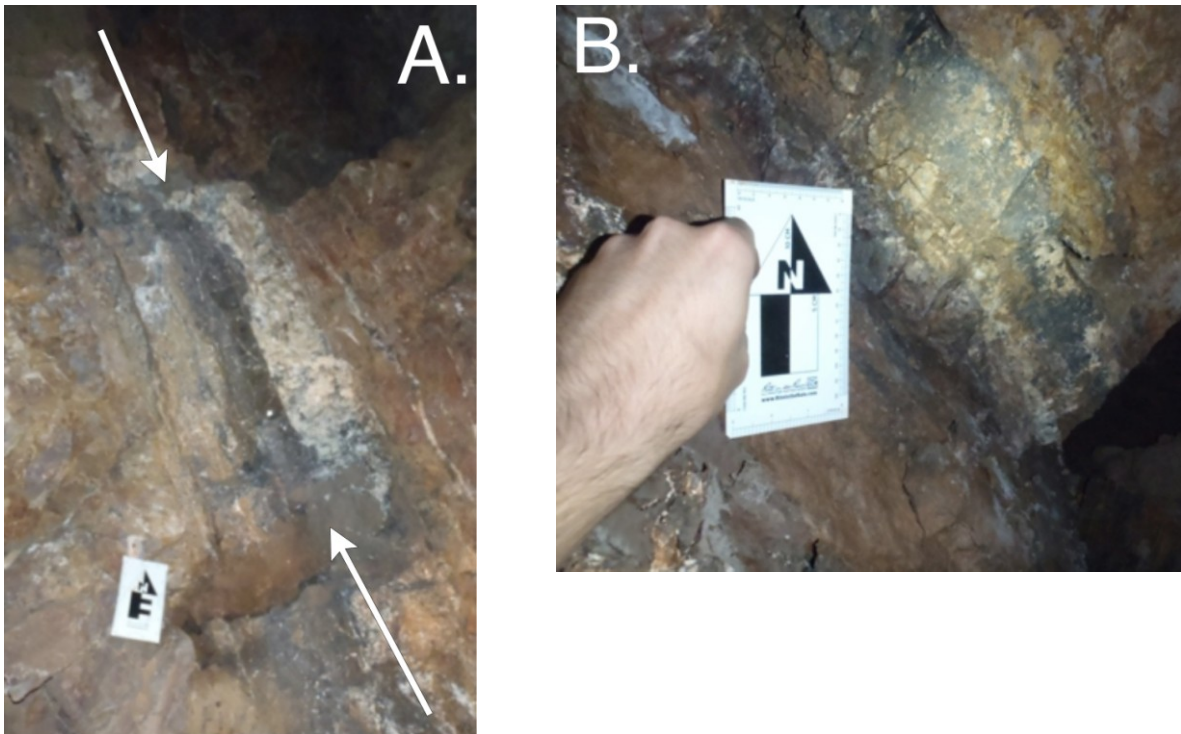


Figure 55. Banded vein material from Klondike. (A) Level 1060. Vein between arrows. Phase I quartz (white on right selvage) and dark carbonates (left selvage). Old workings are visible at top of image. (B) Level 1040. Comb-textured Phase I quartz and dark Phase II carbonates.

In the more massive banded sections, the vein was typically constructed of two or more thick (>10 cm) bands of either Phase I or Phase II material along with smaller, rhythmic banded sections of all three main hydrothermal phases. While these banded sections remained largely intact, local areas of brecciation and soft-deformation were abundant (Fig. 51A) but transport of the fragments was minimal and generally restricted to in-situ rotation, folding and juxtaposition.

Although the presence of intact vein material is common within the Klondike vein, large zones of brecciation are also common. Qualitatively, the banded and brecciated vein material is in a roughly 1:1 ratio as observed in the underground workings and in the drill core. The clasts are of both Phase I minerals and oxidized host andesites up to 10 cm across, and are much more angular than breccia clasts at Mercedes.. Breccia at Klondike ranges from clast-supported to matrix-supported styles, suggesting a lower degree of transport than the Mercedes system.

As with Mercedes, the vein is hosted within an oblique-normal fault with a slight dextral component. The Klondike fault displays nearly indistinguishable features from the Mercedes fault and is delineated by a 1-2 m zone of foliated, strongly flow banded clay gouge with local occurrences of slickenlines.

The high grade in Klondike appears to have the same general textural characteristics as that from Mercedes: a porous agglomeration of darker olive green clasts in a matrix of largely hematitic boxworks after sulfides with only minor amounts of Phase II carbonates. This material is less abundant within the Klondike vein, reflecting a lesser degree of brecciation, which likely resulted in lower grades at Klondike. Average grade for minable intervals are 6.3 ppm Au and 39 ppm Ag for Klondike versus 8.7 ppm Au and 95 ppm Ag for Mercedes (Hawksworth et al., 2009).

Macro- and Microscopic Textures: Phase I

Phase I textures in the Klondike vein are characterized by lower abundances of recrystallization textures and higher proportions of colloidal and amorphous silica within the banded vein and clasts within the vein breccia. As in Mercedes, jigsaw and saccharoidal quartz after calcite and local platy calcite are the most abundant habits of the Phase I minerals followed by more local feathery textures defined by zones of vapor inclusions (Fig. 56). However, unlike Mercedes, intact banded crustiform quartz with subordinate zones of earlier green colloform quartz are common (see Fig. 51, left), especially in higher level exposures within the Klondike mine.

Small amounts of calcite are present in the Phase I assemblage and it is distinguished from the later stages of calcite by its locally bladed habit and presence surrounded by colloidal silica. Also notable are the presence of unoxidized pyrite, chalcopyrite and galena (Fig. 51, right) found primarily as blebs encapsulated in crustiform milky quartz surrounding clasts of host andesite as well as within Phase II matrix-supported clasts of the same material.

The ubiquity of vigorous boiling textures in all the Phase I minerals and the spatial association of Au-Ag mineralization with the same minerals implies that boiling was the mechanism behind deposition of the precious metals in Klondike as well (Brown, 1986; Dong et al., 1995, Sillitoe, 1993; Cooke and Simmons, 2000; Moncada et al., 2012). Despite the lesser amounts of apparent hydrothermal transportation within the Klondike vein, these textures are apparent in clasts and banded veins at all levels and indicates a large vertical extent of boiling, multiple overprinted episodes of fracturing, depressurization and mixing of the vein material.

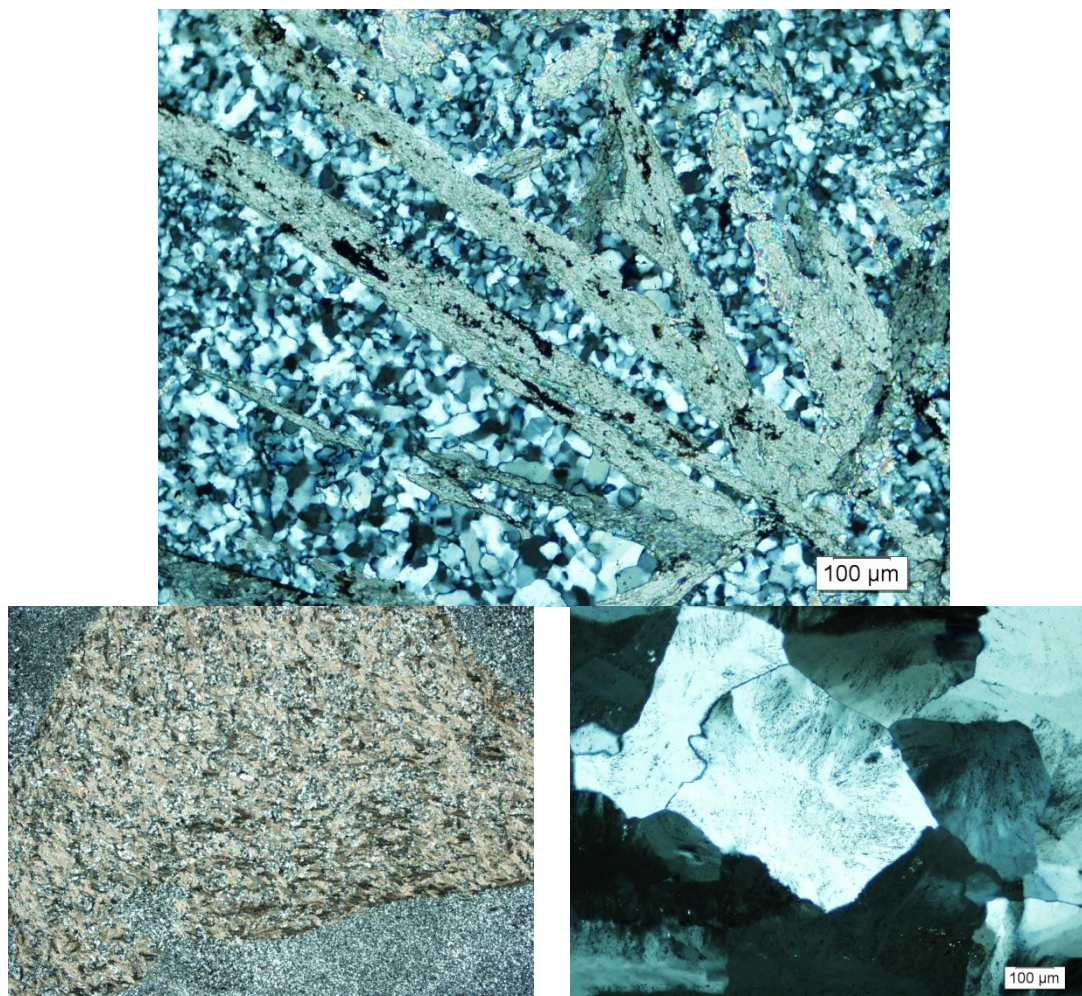


Figure 56. Typical Phase I mineral textures from the Klondike vein. Top: Mosaic quartz and platy calcite. From 220.74 m in hole K08-070D. Bottom left: Mosaic quartz replacing calcite, generating saccharoidal textures. From 219.0 m in hole M08-070D. Bottom right: Feathery textured quartz with abundant vapor inclusions. From 99.87 m in hole K08-079D.

Macro- and Microscopic Textures: Phase II

In contrast to the textural differences between Phase I mineralization in Klondike and Mercedes, Phase II in the two zones are markedly similar. The dominant mineral is again an intergrowth of Mn-oxides and calcite with up to 70% of the volume composed of the splotchy Mn minerals (Fig. 57). The calcite grains are small interlocking rhombic crystals with larger grains displaying twinning.

Locally, Phase II mineralization penetrates the wall rocks (see Fig. 52) as a stockwork of thin, 1-4 cm veinlets of identical textures and mineralogy to the main vein bands and breccia cement Phase II mineralogy.

As in Mercedes, the lack of boiling textures and the weak spatial associations between Phase II mineralization and Au-Ag suggest that this phase was not responsible for the precious metal endowment in the Klondike vein.



Figure 57. Typical Phase II textures. Dark brown Mn-oxide intergrowths in euhedral calcite. From 219.0 m in hole K08-070D.

Macro- and Microscopic Textures: Phase III

As in Mercedes, Klondike Phase III (Fig. 58) is a late, low-volume introduction of small clear quartz and calcite veinlets. The calcite is uniformly rhombic with coarser grains than the calcites of Phase II and twinning is common. The clear quartz is comb-textured and drusy where the Phase III minerals fill vugs and open space within the vein. The comb euhedra are locally growth zoned with two-phase vapor/liquid inclusions of constant ratio that locally grade into amethystine quartz.

These features suggest that this Phase II at Klondike, like at Mercedes, was a non-boiling, late phase that did not result in deposition of gold or silver..

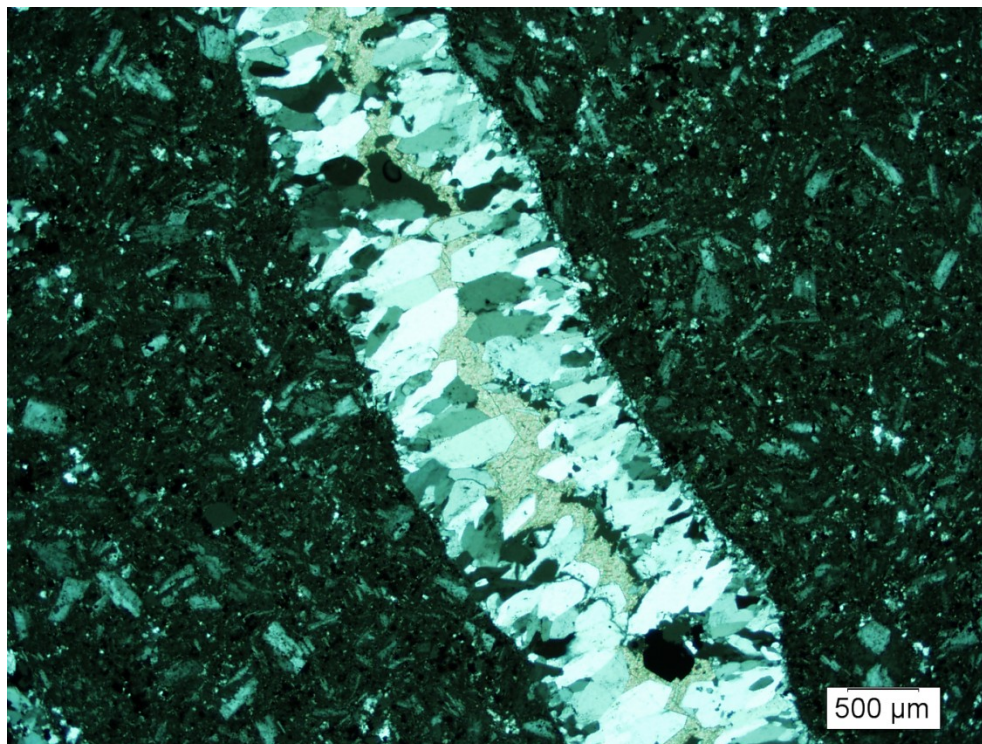


Figure 58. Typical Phase III textures. Clear comb quartz and calcite veinlet cutting altered andesite clast within vein breccia. From 203.50 m in hole K08-063D.

Macro- and Microscopic Textures: Phase IV

Phase IV represents a post-mineral period of weathering, oxidation, and supergene redistribution of precious and base metals. It is characterized by hematite and goethite staining of the wallrock and hematite replacement of vein sulfides as both isolated grains derived from the sulfide blebs as well as more extensive stockworks after sulfides.

No cerargyrite was observed, nor has it been reported from the Klondike vein, but high silver grades and mineralogy similar to the Mercedes vein suggests that it is present but unobserved. Cu-oxides are also locally present as staining and fracture coatings as well as oxidation halos surrounding smaller sulfide particles.

Finally, Mn-oxides are widespread in the vein system as fracture fill, dendrites and spongiform masses that occupy the location of former Phase II Mn-bearing calcites that have had the carbonate leached from the matrix leaving the intergrown Mn-oxides.

Variations in Textures

Similar to Mercedes, there does not appear to be any regular spatial controls of the distribution of these textures. Boiling textures appear at all levels and consistently along strike within the Phase I minerals. The distribution of breccias vs. intact vein segments also appears to be somewhat random, although brecciation appears to increase west along strike of the vein system.. This may be associated with increased proximity to Los Pinos graben, similar to the shearing and brecciation associated with extensional faulting in the Barrancas/Lagunas zone of the Mercedes vein.

There is a correlation between grade and the textures of the vein. The highest grade ore shoots Klondike vein system are clearly associated with breccias and fragmented banded veins,

while the more intact sections tend to be low- to mid-grade in Au and Ag. This observation has two main implications: First, these ore shoots were formed from tectonic or hydrothermal fracturing followed by rapid depressurization, brecciation and boiling resulting in deposition of high-grade material. Second, the porosity generated by these events made these areas more amenable to later supergene concentration and grade improvement of Au and Ag through the re-deposition of Ag and some Au and removal of carbonate during weathering, improving the ratio of Au to host rock.

Geochemistry

Composition of Green Quartz and Dark Carbonates

One sample of Phase I green quartz (Q-004) from the 1140 level and one sample of the Phase II dark carbonate (C-002) from the 1080 level was separated and submitted for XRF analysis (Appendix IV). The green quartz was very light green in color and contained 98.8% SiO₂, 0.14% Fe₂O₃, 0.06% MgO and 0.04% MnO with 0.01% C and 0.22% CaO. As with Mercedes, Fe⁺² ions are likely the causative factor behind the greenish color of the quartz.

Analysis of the dark carbonate showed a composition of 40.2% CaO, 8.75% C, 23.1% SiO₂, 0.67% Fe₂O₃, 0.09% MgO and 1.19% MnO. The dark carbonate contained a higher amount of other Phases than the Mercedes sample, predominantly stringers of lighter carbonate and small clasts of Phase I quartz. This contamination both increased the measured silica content (14.9% for Mercedes but 23.1% for Klondike) and diluted the signals of the pure dark carbonate, resulting in a lower value (1.19% vs. 3.78%) for the MnO that is the probable source of the dark coloration. However, the lack of any pinkish hue and the presence of the dark spongy boxworks of Mn-oxides in former Phase II sites within the Klondike core implies that the Mn-oxide/calcite intergrowth mechanism is responsible for the dark coloration of the Phase II carbonates in the Klondike vein as well.

Vertical Zonation

Figures 59 and 60 show the results of analyses on 30 samples from the Klondike vein, ranging in elevation from 909 m to 1141 m, representing 232 m of vertical extent within the vein.

Vertical zonation is very weakly defined for both the major metals (Ag, Au, Cu, Mo, Pb, Zn) and minor elements (As, Ba, Hg, Sb, Tl), and both display a roughly classical (Buchanan, 1981) epithermal distribution. Base metals (Cu, Pb, Zn) all show possible increases with depth, and this is reflected in the mineralogy of the deeper Klondike samples, specifically the increased presence of chalcopyrite and galena. Ag and Au also show slight increases in depth. The minor elements As, Ba, and Tl all show a possible tendency towards lower concentrations at deeper levels, while Sb increases with decreasing elevation. As in the Mercedes vein, Hg shows an anomalous increase with depth, with the Hg increase being much more pronounced in Klondike than in the Mercedes vein.

While the sample size is somewhat smaller for the Klondike vein than Mercedes (30 vs. 80 samples, respectively), the calculated trend lines have a much better statistical fit and the data overall displays much less scatter. In light of the less brecciated nature of the Klondike vein, it is interpreted that both the somewhat more identifiable trends in the zonation and the adherence of the elemental patterns to a classical epithermal zonation highlights the differences in texture and morphology of the two veins. This observation will be discussed in further detail in the "Conclusions" section of this paper.

The method outlined by Loucks and Petersen (1985) for the Ag-dominant veins at Topia, Durango was attempted (Fig. 61) for the geochemical data from the Klondike vein. No discernible pattern regarding the distribution of Ag/Zn and Pb/Zn ratios can be determined as is shown by the random "shotgun" pattern of the plotted data

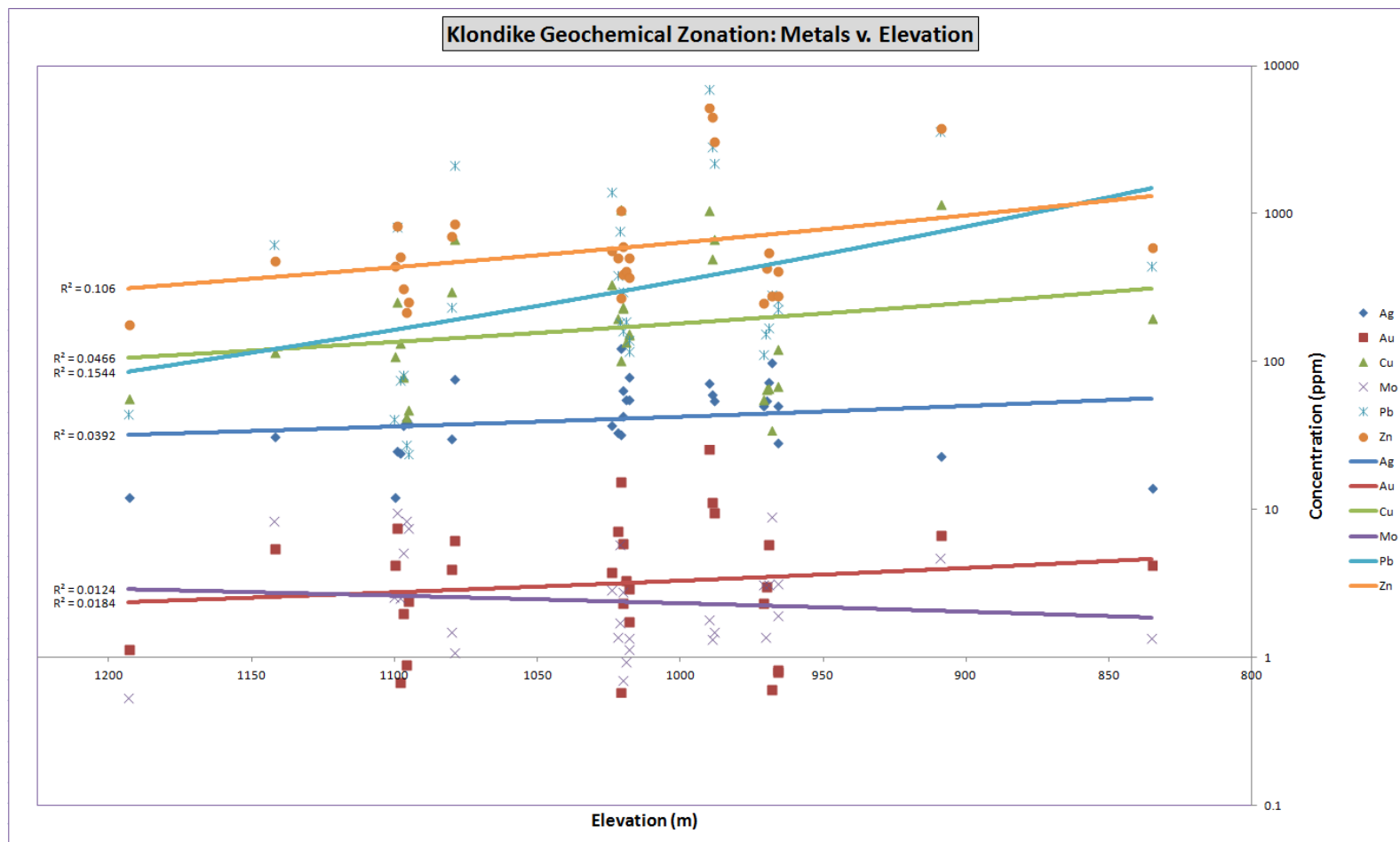


Figure 59. Klondike metals vs. elevation. Trend lines are power regressions with R-squared values listed. Note log scale on y-axis.

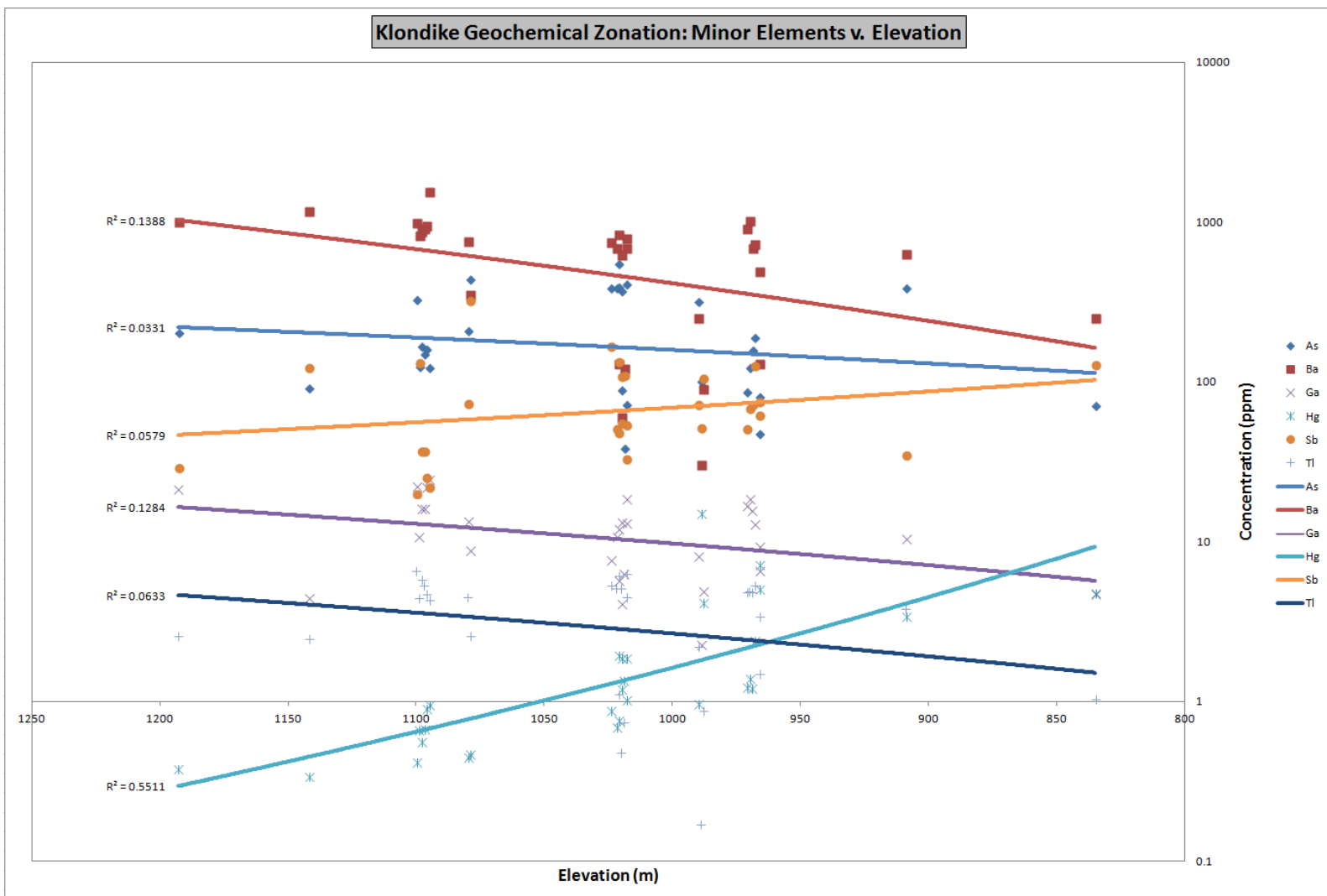


Figure 60. Klondike minor elements vs. elevation. Trend lines are power regressions with R-squared values listed. Note log scale on y-axis.

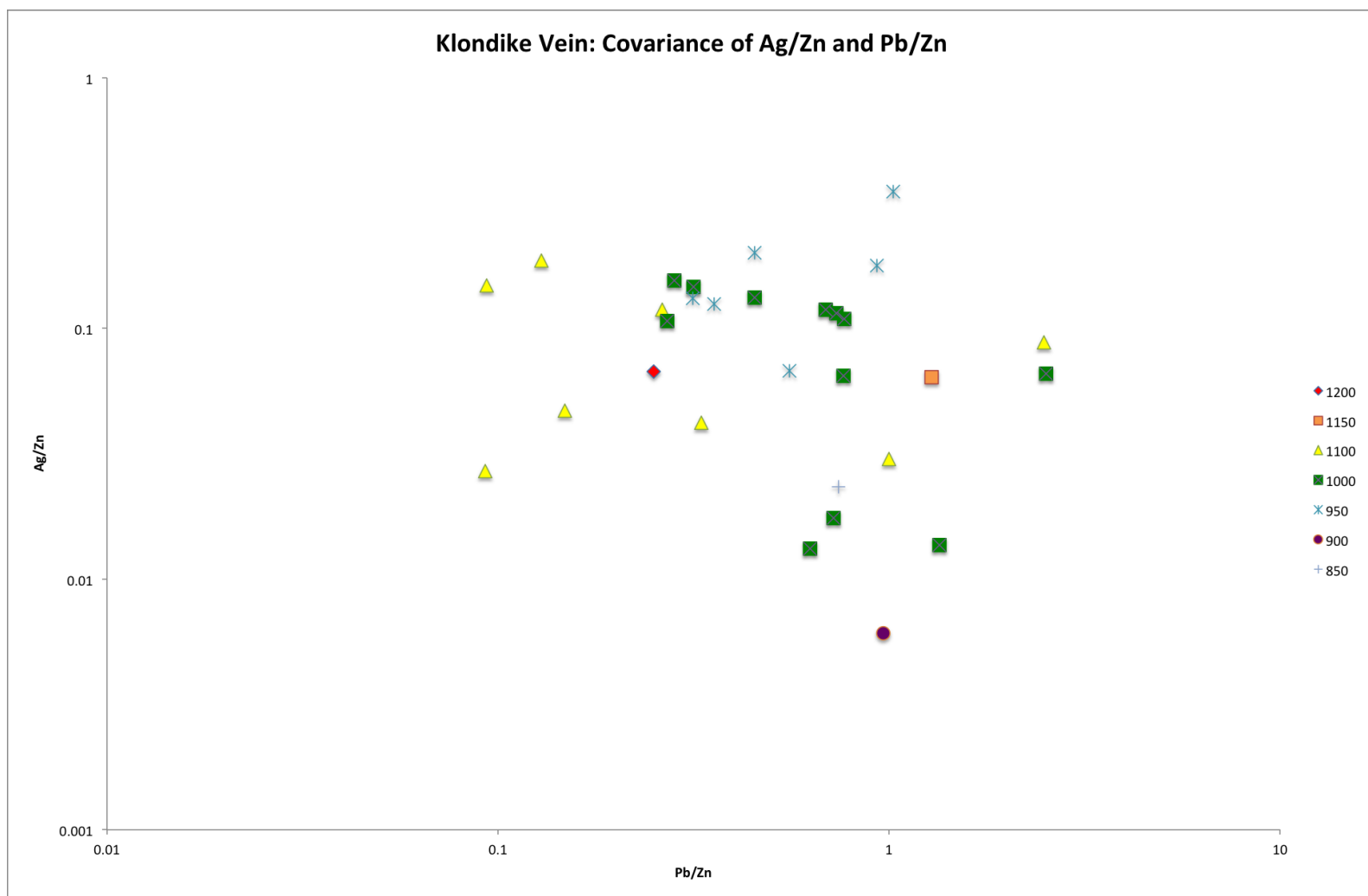


Figure 61. Covariation of Ag/Zn and Pb/Zn with elevation for the Klondike vein. Color spectrum reflects elevation in meters: red=higher, purple=lower. Method modified from Loucks and Petersen (1985).

Horizontal Zonation

The Klondike vein has a shorter mineralized strike length available to detect any elemental zonation along strike; study sections 11080 and 11260 are separated by only 180 m. 30 samples from both sections were used and the results of the ICP-AES analysis are shown in Figures 62, 63 and 64. As in seen in Mercedes, very slight variations in geochemistry are present along strike. Most elements display consistent abundances across the 180 m interval with Au, Zn, Mn, S, Se and Hg displaying slight decreases to the west along strike and Fe, C displaying slight increases. The strongest trends were in As, Ba, Tl and Au, with the first three increasing strongly towards the east and the Au with a decrease.

When compared to intervals of similar extent along the Mercedes vein (i.e. sections 9550 to 9880 or 8860 to 9100), variable and local opposite trends occur when compared to those of the vein system as a whole. It is conceivable that less brecciated nature imparts a more coherent zonation on strike as it imparts on the zonation down dip, however the restricted extent available to study the chemistry of the vein make it equally likely that these data represent local effects only and may not be representative of the Klondike vein system as a whole.

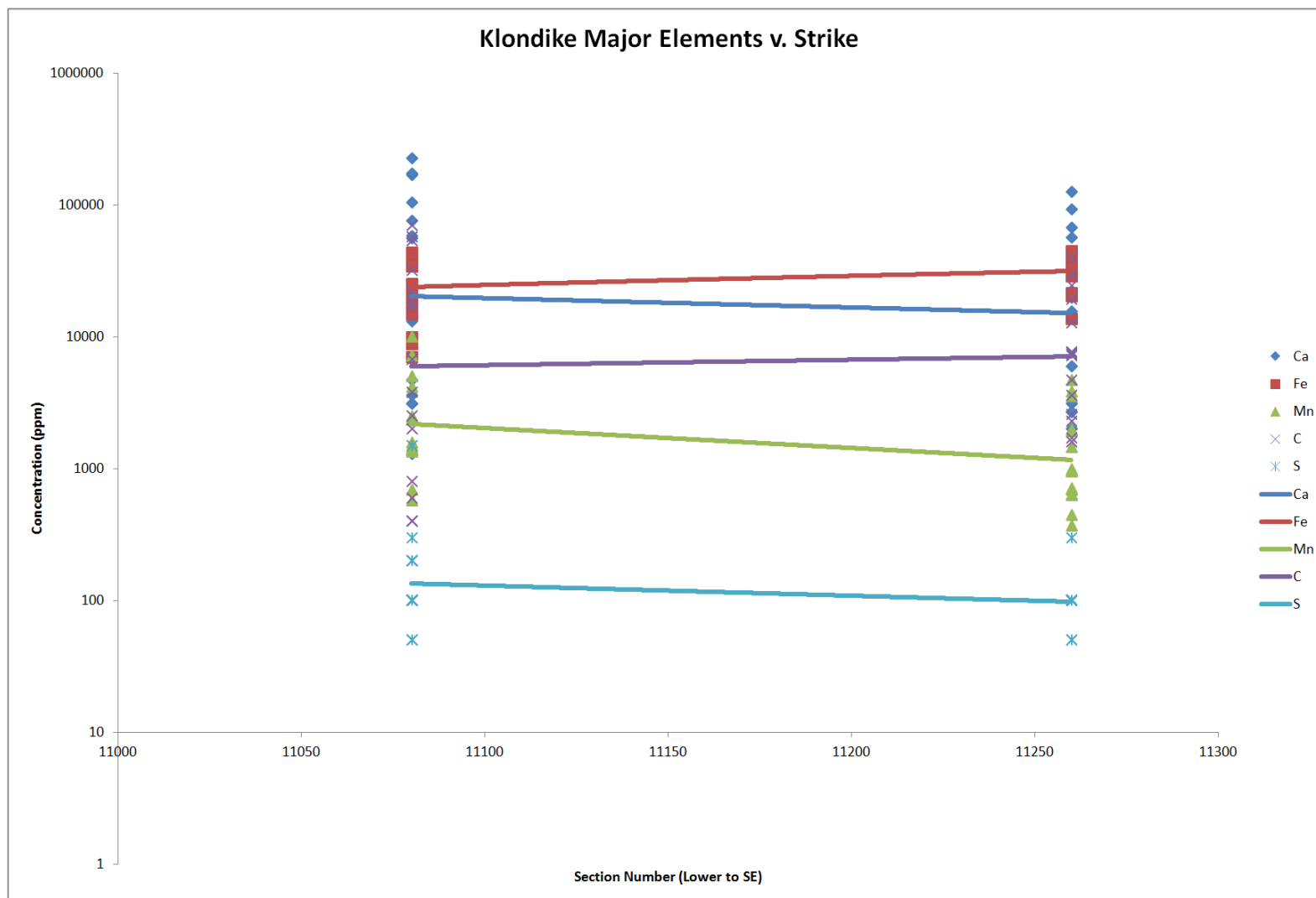


Figure 62. Klondike major elements vs. strike. Trend lines are power regressions. Note log scale on y-axis.

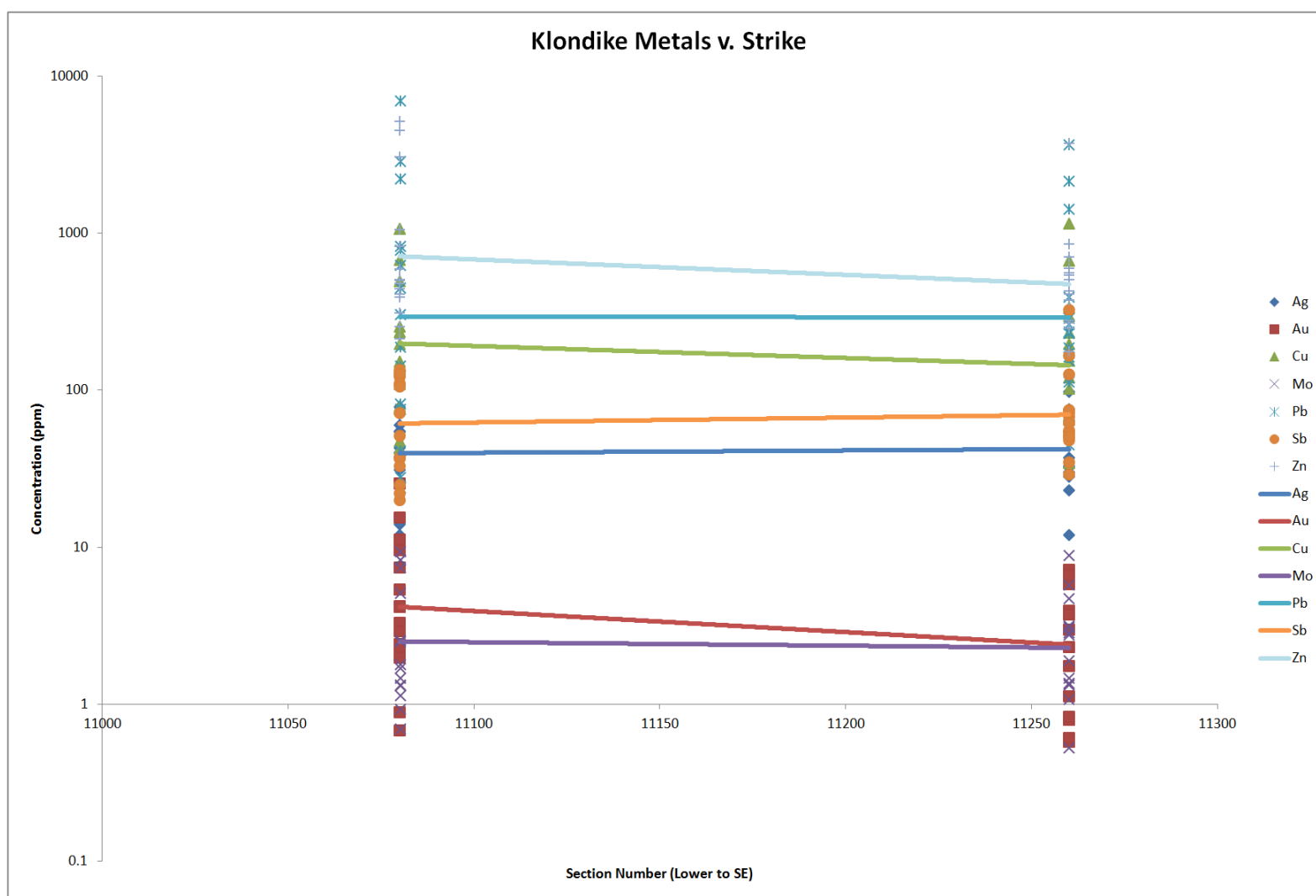


Figure 63. Klondike metals vs. strike. Trend lines are power regressions. Note log scale on y-axis.

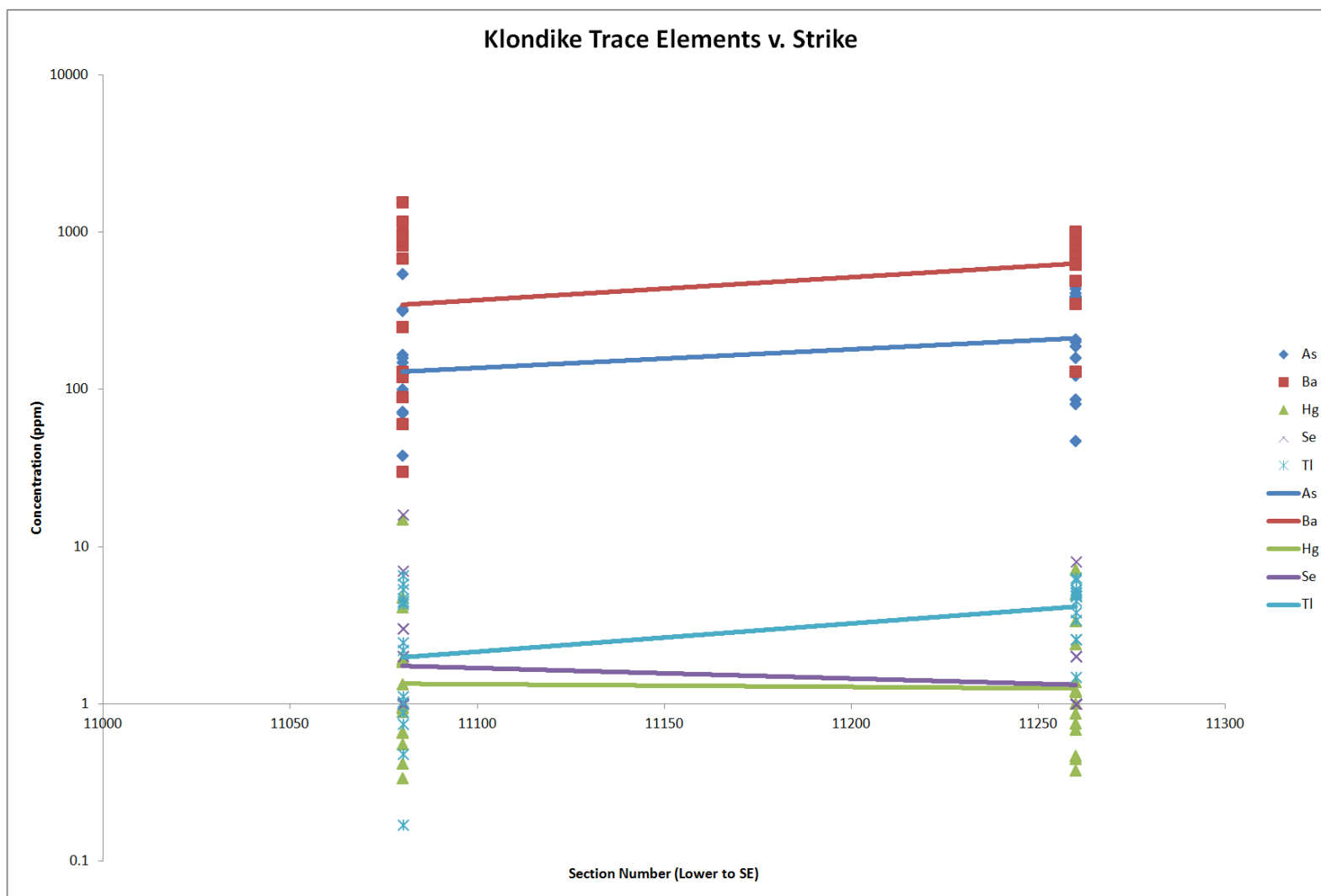


Figure 64. Klondike trace elements vs. strike. Trend lines are power regressions. Note log scale on y-axis.

Correlations

Statistical correlative analysis on the 48-element ICP-AES, fire assay (Au and Ag) and IR spectroscopy (C and S) data from the Klondike vein are displayed in Figure 65, below. As in Figure 46, the most salient 18 elements are used. Appendix V contains the entire suite of values. R-values with an absolute value greater than 0.5 are chosen to be statistically relevant while those greater than 0.75 are considered significant. Au grades are not strongly correlated with Ag ($R=0.398$ compared to Mercedes at $R=0.517$) and are most strongly correlated with Pb, V, Cu and Zn with coefficients of correlation of 0.821, 0.817, 0.785 and 0.777, respectively. Ag as a whole is much more statistically independent in Klondike than in Mercedes, with the greatest correlative relationship being to Au and Cu ($R=0.347$). The triad of Mn, C and Ca again represent a strong correlative group, however the correlation between Mn and Ca is weaker in the Klondike vein as compared with Mercedes (0.551 vs. 0.675), likely reflecting the absence of rhodochrosite in Klondike.

	FA-Ag	FA-Au	Ag	As	Ba	Ca	Cu	Fe	Ga	Hg	Mg	Mn	Mo	Pb	Sb	Se	Zn	C	S
FA-Ag	1.000																		
FA-Au	0.398	1.000																	
Ag	0.952	0.332	1.000																
As	0.253	0.331	0.201	1.000															
Ba	-0.354	-0.427	-0.434	0.011	1.000														
Ca	0.134	0.005	0.292	-0.258	-0.486	1.000													
Cu	0.347	0.785	0.339	0.509	-0.492	0.044	1.000												
Fe	-0.200	-0.300	-0.294	0.321	0.718	-0.816	-0.292	1.000											
Ga	-0.195	-0.402	-0.258	-0.007	0.780	-0.644	-0.455	0.859	1.000										
Hg	0.077	0.146	0.064	-0.308	-0.543	0.205	0.162	-0.482	-0.480	1.000									
Mg	-0.128	-0.146	-0.151	-0.266	0.435	-0.340	-0.229	0.436	0.681	-0.219	1.000								
Mn	-0.198	-0.048	-0.138	-0.211	0.234	0.552	-0.092	-0.397	-0.192	-0.148	-0.028	1.000							
Mo	-0.087	-0.189	-0.150	-0.108	0.543	-0.100	-0.221	0.184	0.233	-0.203	-0.054	0.465	1.000						
Pb	0.181	0.821	0.142	0.249	-0.396	-0.049	0.801	-0.236	-0.398	0.241	-0.156	-0.080	-0.127	1.000					
Sb	0.340	0.176	0.384	0.223	-0.366	0.386	0.298	-0.488	-0.516	-0.072	-0.332	0.349	-0.068	0.185	1.000				
Se	-0.200	0.095	-0.175	-0.144	-0.187	-0.201	0.196	-0.100	-0.216	0.197	-0.022	-0.168	-0.130	0.174	0.019	1.000			
Zn	0.156	0.777	0.108	0.120	-0.455	-0.059	0.768	-0.279	-0.414	0.496	-0.187	-0.186	-0.170	0.915	-0.018	0.199	1.000		
C	0.147	-0.002	0.304	-0.240	-0.496	0.997	0.045	-0.816	-0.659	0.187	-0.364	0.536	-0.116	-0.050	0.414	-0.186	-0.071	1.000	
S	-0.225	0.123	-0.194	-0.153	-0.294	-0.120	0.128	-0.212	-0.318	0.238	-0.098	-0.173	-0.164	0.150	0.138	0.886	0.155	-0.114	1.000

Figure 65. Correlation matrix for selected elements, Klondike vein. Green colors are significant positive correlations, yellows and oranges poor correlations and dark orange to red indicates significant negative correlations. N=30

THE LUPITA/DILUVIO SYSTEM

Introduction

The Lupita/Diluvio system (Fig. 66) is the northern-most mineralized system considered in this study and it lies approximately 2 km north-northwest of the Klondike vein. The system consists of two, genetically related mineralized zones: the Lupita vein with a 1500 m outcrop striking 070° along the contact between the lithic tuff and the overlying andesite flow breccias, and the buried Diluvio stockwork zone hosted within a block of lithic tuffs directly overlying the Lupita vein and buried under 150 to 300 m of andesite flows and flow breccias that appear to be identical to the host andesites of both Mercedes and Klondike.

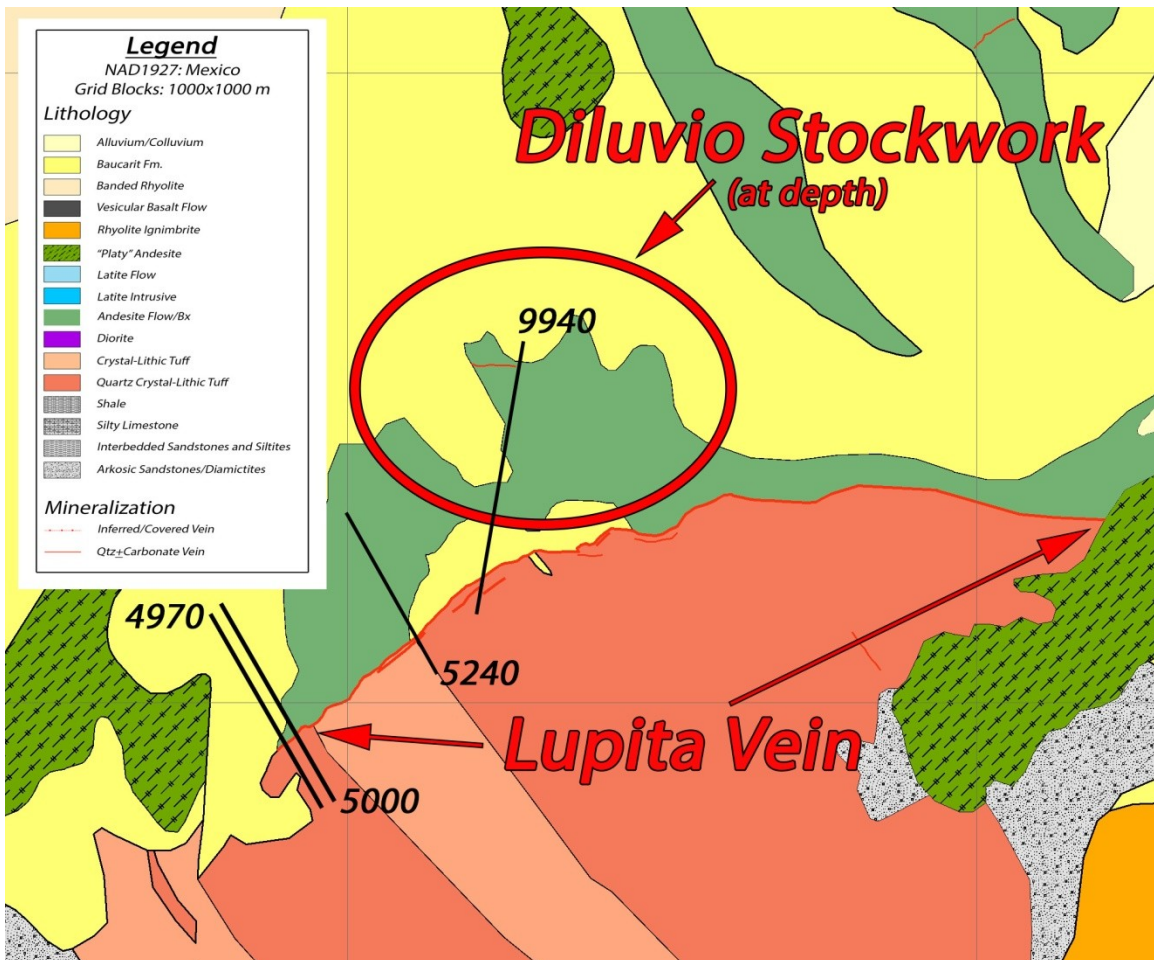


Figure 66. Geologic map of the Lupita/Diluvio zone. Study cross sections are shown in black and are labeled according to exploration grid nomenclature. Adapted from Yamana Geodatabase. (Yamana Exploration Staff, 2012)

The Lupita vein crops out as a resistant, silicified hogback 1-3 m in width and dips steeply between 50° and 70° to the north-northwest. Drilling on the vein indicates that the dip gradually shallows at depth to around 20° at depth (Fig. 67). It is bounded at higher levels on the hanging wall by the host andesite and on the footwall by the quartz and crystal-lithic tuff sequence. At approximately 1150 m elevation, the hanging wall rocks change abruptly to a heavily fractured and mineralized block of the lithic tuff sequence. This zone represents the Diluvio stockwork (Fig. 68). The network of fractures hosts quartz-carbonate mineralization as veins and veinlets 1-100 cm in

widths. The veins are similar in mineralogy to both Mercedes and Klondike as well as the underlying Lupita vein which continues under the block to at least 950 m elevation. Grades within both the vein and the stock work average between 1-3 ppm Au and 12-15 ppm Ag with local highs exceeding 85 ppm Au and 250 ppm Ag.

Given the location of the Lupita vein and the fractured nature of the overlying Diluvio stockwork, the Diluvio zone is interpreted here to represent a listrically-displaced block of the lithic tuff sequence. Fracturing caused by the normal faulting prepared the block for subsequent fluid introduction along the basal Lupita structure and mineralization occurred along both structures simultaneously. As such, both zones will be considered as one genetically related system for the purposes of this study.

Three cross-sections along the Lupita vein (4970, 5000 and 5240) and one through the Diluvio stockwork (9940) were evaluated. Only drill core was available from this zone, and the area is currently being drilled. As of mid-2012, there has been no underground development.

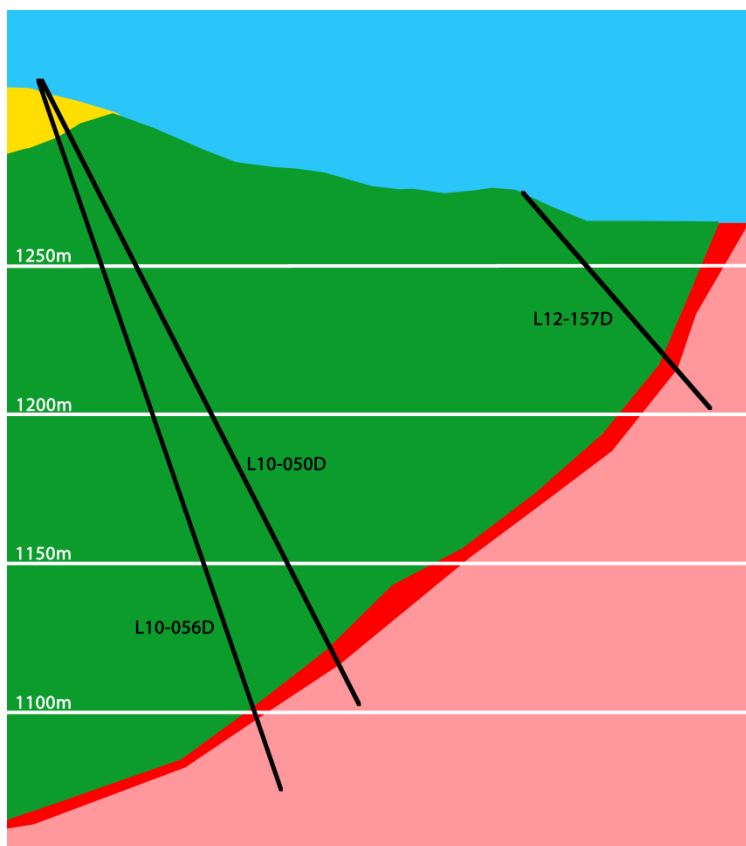


Figure 67. Cross section 5240, looking northeast. Pink=lithic tuffs, green=andesites, yellow=Baucarit Formation. Red is vein material designated on core logs and black lines are the drill holes selected for sampling. Figure created from unpublished interpretive cross-sections (Yamana Exploration Staff, 2008) and original work by the author.

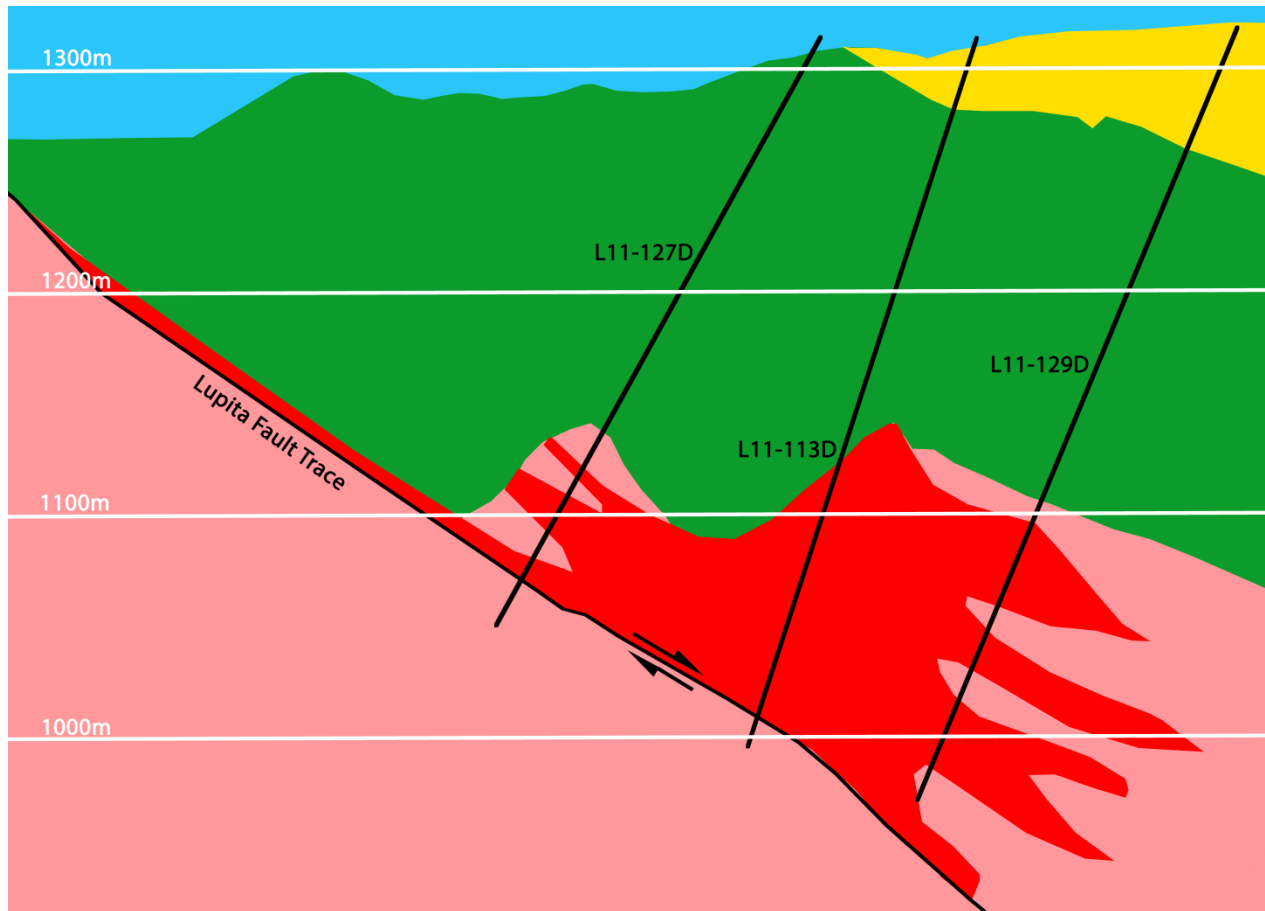


Figure 68. Cross section 9940 looking west-northwest through the Diluvio block. Pink=lithic tuffs, green=andesites, yellow=Baucarit Formation. Red is the 0.3 ppm Au grade shell and black lines are the drill holes selected for sampling. Figure created from unpublished interpretive cross-sections (Yamana Exploration Staff, 2008) and original work by the author.

Paragenesis

The paragenetic sequence of the Lupita and Diluvio vein systems (Fig. 69) consists of three major hydrothermal phases followed by a final phase of weathering and supergene effects on the mineralogy of the ore body. At least one significant brecciation event separated Phases I and II, with additional brecciation ongoing during Phase II. Detailed treatments of the mineralogy of each Phase follows.

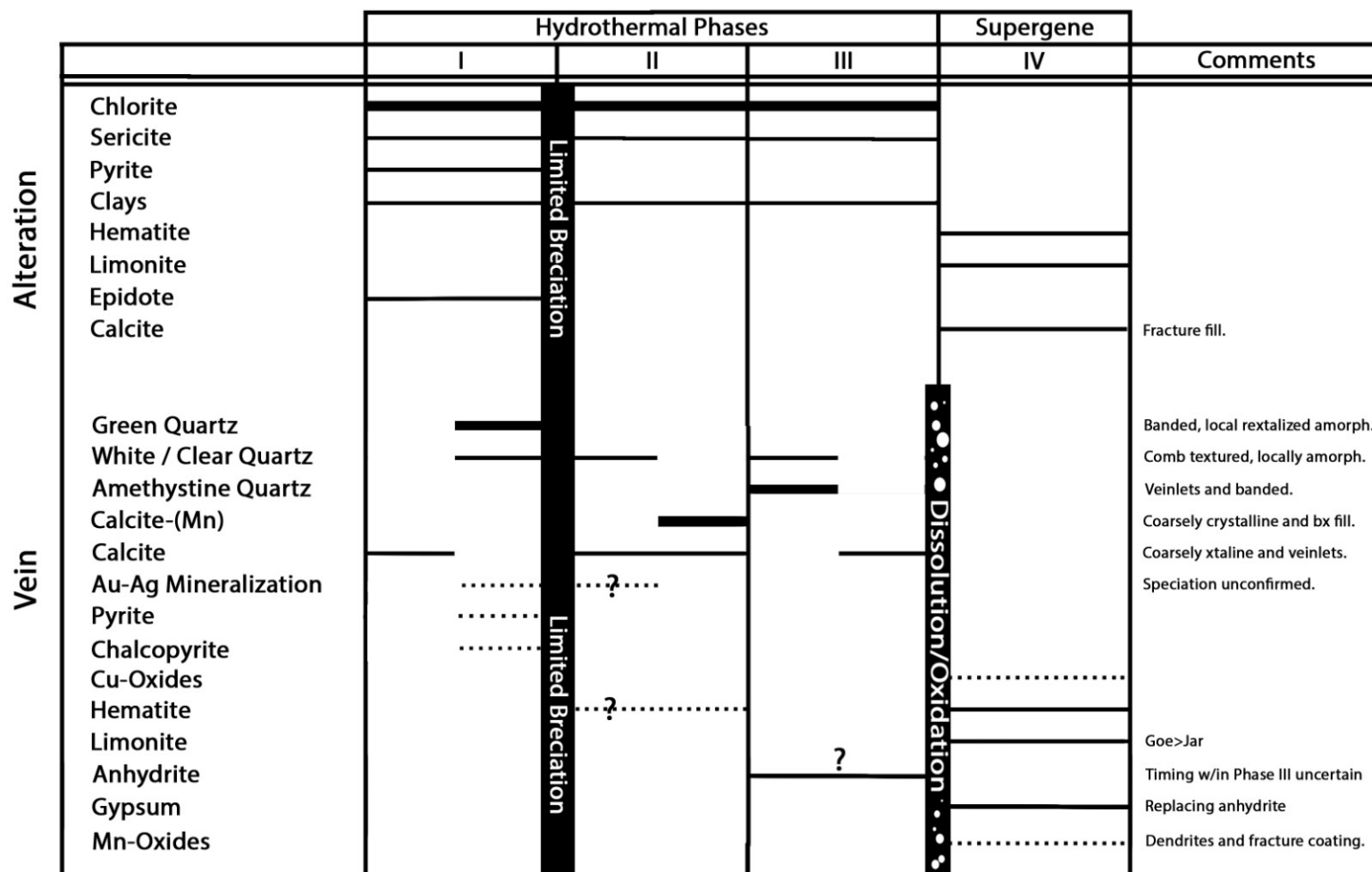


Figure 69. Paragenetic diagram for the Lupita/Diluvio system.

Phase I

As in both Mercedes and Klondike, the first phase of mineralization is dominated by greenish, ferruginous quartz along with lesser whitish to clear quartz. However, compared to the two southern zones the quartz has a generally lighter, milky green hue. Both color types are most commonly found as banded, chalcedonic intervals and less common crystalline and crustiform zones.

Local and uncommon blebs of unoxidized pyrite and chalcopyrite are present within the Phase I quartz, typically in proximity to andesites clasts in the more extensively brecciated segments of the vein.

Precious metal mineralization appears to be associated with the Phase I mineralization as the highest grades are linked with the green quartz-bearing zones. Neither quartz-carbonate nor precious metal mineralization appears to extend into the andesites covering the Diluvio block,

Phase II

Carbonate phases, both dark manganiferous calcites and clear calcites compose the second phase of mineralization. The Mn-calcite is again abundant, but the less manganiferous calcites form a greater proportion of the Phase II carbonates in Lupita/Diluvio than in either Klondike or Mercedes. These carbonates frequently retain platy textures. In some drill core (notably at the 329.52 m interval of hole L12-172D), small, braided veinlets of hematite are found containing clasts of Phase I quartz.

As in Klondike, deposition of Au and Ag may have continued during Phase II. But again, this typically low-grade mineralization may be due to small amounts of Phase I material contained within the dominantly carbonate intervals.

Phase III

Phase III mineralization is somewhat more complex in Lupita/Diluvio than in the other zones in this study. In addition to the late cross-cutting quartz and calcite veinlets that define this Phase III elsewhere in the district, Lupita/Diluvio contains appreciable amounts of amethystine quartz as late, comb-textured veinlets.

Furthermore, pseudomorphs of gypsum (included in Phase IV) after anhydrite are present in Lupita/Diluvio, especially at higher levels; hole L12-342D contains examples at <30 m below the current surface..

Phase IV

As at Mercedes and Klondike, Phase IV at Lupita-Diluvio is supergene oxidation related to weathering. Due to the burial of the Diluvio zone and the intact nature of the Lupita vein, supergene oxidation is less widespread and is most abundant at higher elevation along intersections of the Lupita vein.

Hematite and goethite are the most common products and have extensively permeated the wall-rocks as well. Jarosite appears to be absent in any quantity. Mn-oxides, likely pyrolusite, are widespread as fracture coatings, dendrites and spongy vug fill. This latter texture is related to the destruction of Phase II Mn-calcite by meteoric waters, leaving only the finely intergrown Mn-oxides. Gypsum is present as pseudomorphs after hydrothermal anhydrite.

Vein and Mineral Textures

Vein Textures: Macroscopic to Vein Scale

Similar to the Klondike vein, the Lupita/Diluvio system is dominated by both banded veins and vein breccias derived from the banded vein zones. In the Lupita vein outcrop, banded zones are common (Fig. 70) and show alternating zones of both Phase I quartz and what may be Phase II carbonates that have been silicified in outcrop, but retain their carbonate nature at depth (Fig. 71). Both brittle and soft deformation features are common within the banded section, especially notable within the green quartz zones. Transport of the clasts appears to be minimal and is restricted to rotation and minor displacement of the originally chalcedonic green quartz (Fig. 70). Brecciation is minimal to absent in much of the Diluvio stockwork, and most of the veins show either massive crystalline or banded amorphous textures. While the Phase I minerals dominate the bulk of the Lupita structure, Diluvio veinlets contain mostly Phase II carbonates or Phase III amethystine quartz with only minor amounts of the Phase I quartz present (Fig. 72).

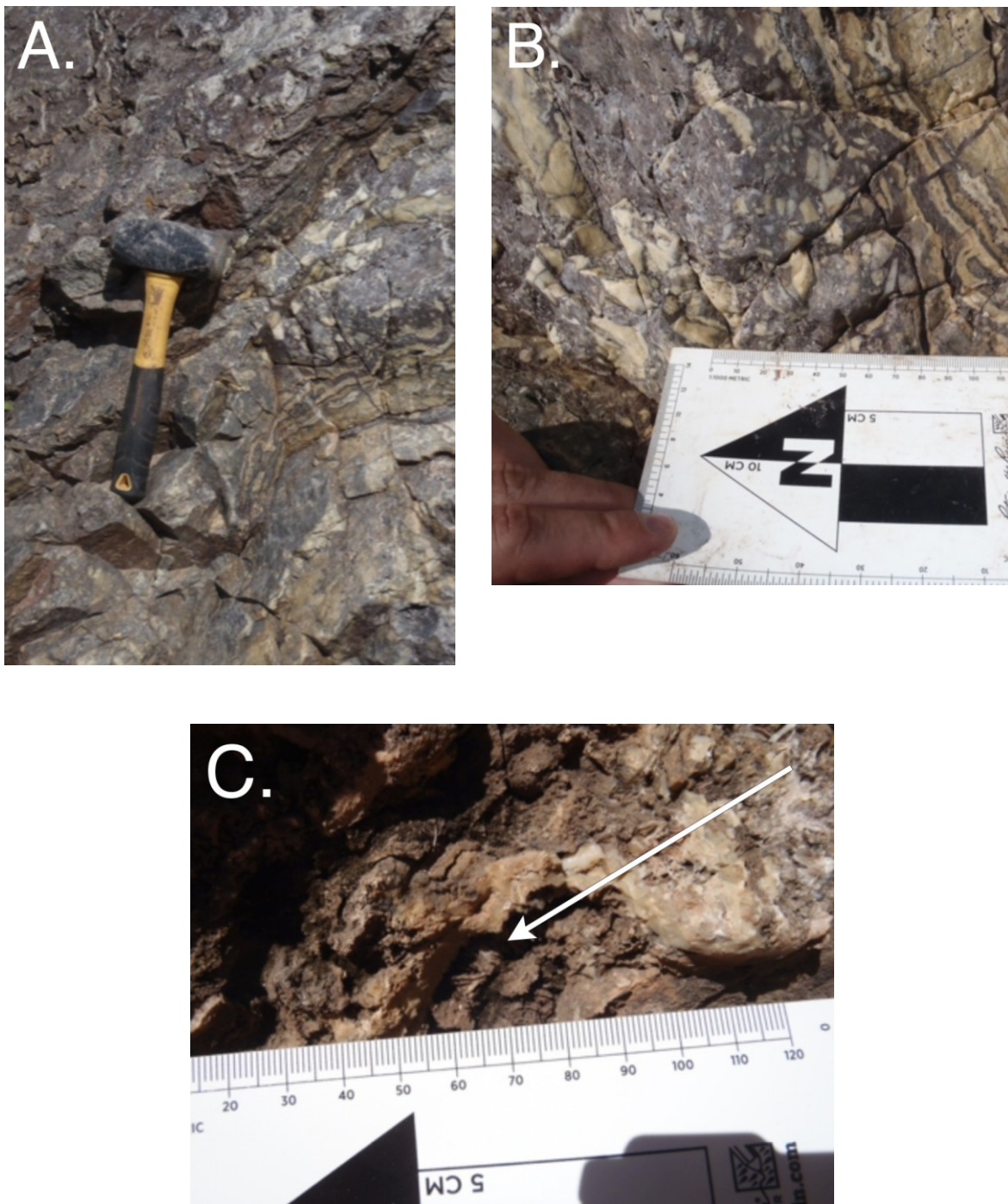


Figure 70. Outcrop textures of the Lupita vein. (A): Polyphase, silicified outcrop showing dark cherty quartz, green banded quartz and local silica pseudomorphs after platy carbonate. (B) Close-up of banded zone with green quartz clasts in dark cherty matrix and local soft-deformation textures within the green quartz bands. (C): Quartz pseudomorphs after platy carbonate (arrowed).

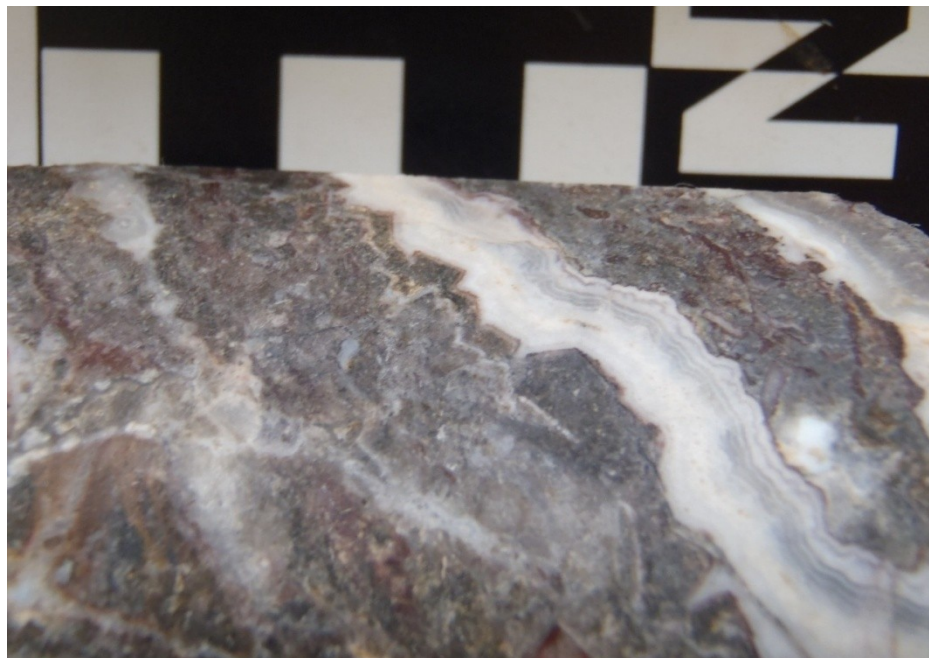


Figure 71. Phase III banded chalcedonic quartz and Phase II dark carbonate vein from the Lupita vein. From 303.31 m in Hole L12-172D. Scale blocks are 1 cm x 1 cm.



Figure 72. Massive dark carbonate w/ green quartz veinlet from Lupita vein. Hole L10-072, 276.50 m.

Vein breccias are present, but are less extensive than the banded veins. Unlike the Mercedes and Klondike veins, the clast types are almost exclusively fragments of banded, chalcedonic or amorphous Phase I green and light green quartz (Fig. 73) contained within a matrix of crystalline Phase II carbonates.

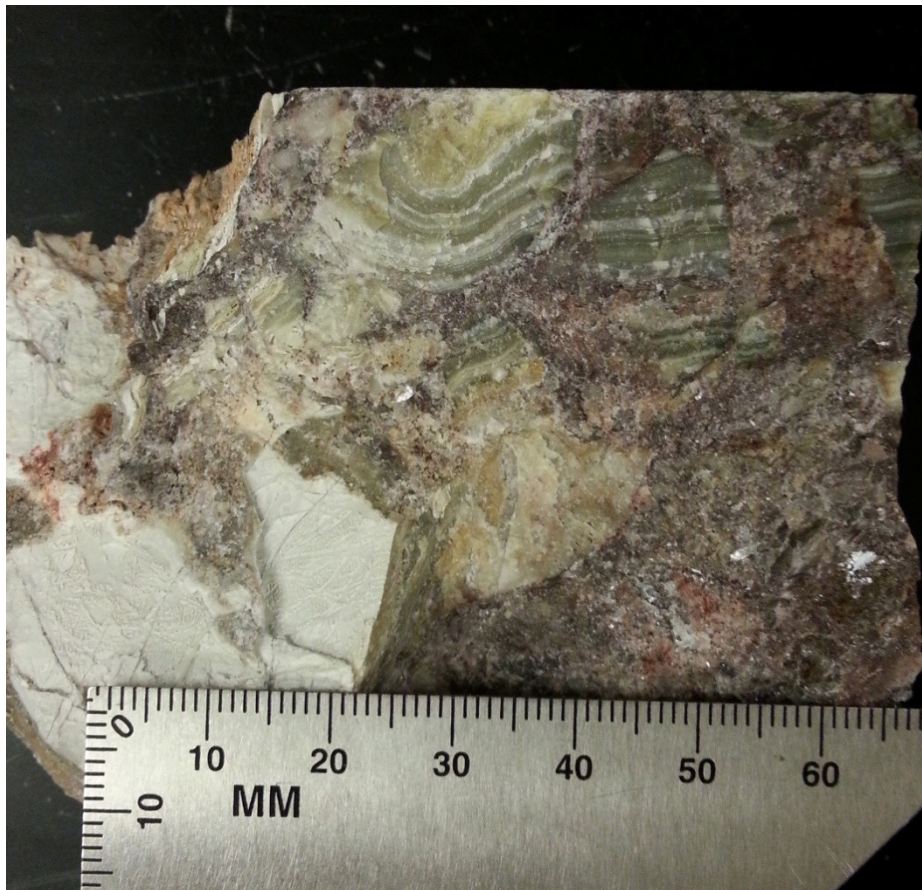


Fig. 73 Lupita vein breccia with clasts of chalcedonic green quartz in a carbonate/hematite matrix. From 226.17 m in hole L12-113D.

At higher levels within the Lupita vein, porous zones with significant amounts of open space are present. These zones are nearly devoid of carbonates and instead are variably silicified vein breccias and banded veins. Weathering has leached much of the carbonate from the matrix surrounding the Phase I quartz clasts, leaving behind a spongy residue of the Mn-oxides that were contained within the Phase II carbonates (Fig. 74, top). Local boxworks after sulfides (Fig. 74, bottom) contained within these intervals suggest that near-surface oxidative weathering of the sulfides generated an acidic fluid responsible for the destruction of the carbonates, leaving behind the banded silica and Mn-oxide residue.

Only limited amounts of high-grade material from the Lupita/Diluvio zones was available for examination, and these tended to be somewhat lower grade (25 ppm Au, 88 ppm Ag) than the samples examined from both Mercedes and Klondike. These samples were vein breccias containing considerable amounts of saccharoidal Phase I quartz with lesser amounts of carbonates, but there was little of the hematitic matrix material that was diagnostic of the Mercedes and Klondike high-grade.

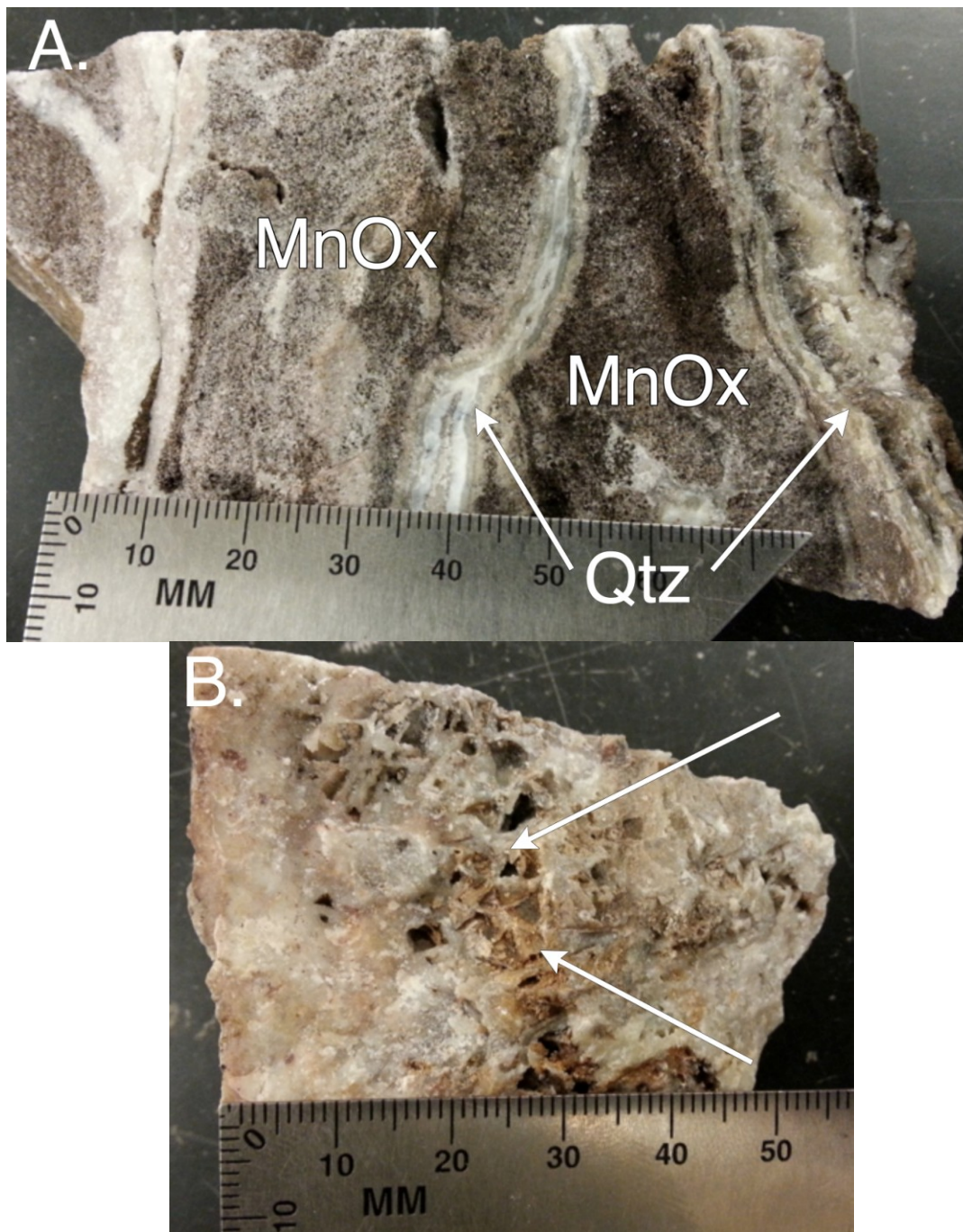


Figure 74. High level, vuggy vein material from the Lupita vein. (A): Dark Mn-oxide sponge after Phase II carbonate leaching surrounds chalcidonic quartz veins. From 73.20 m in hole L12-157D. (B): Vugs and boxworks after sulfides with quartz after platy carbonate (arrowed). From 69.58 m in hole L12-157D.

Macro- and Microscopic Textures: Phase I

While retaining the same overall mineralogy as Phase I in Mercedes and Klondike, the textural characteristics of the Lupita/Diluvio phase one are markedly different. The most significant differences are the abundance and preservation of primary crystallization textures in both the early silica and calcite phases and only partial subsequent replacement of the early calcite. Banded, colloform textures are profuse throughout both intact vein segments and breccia clasts in the Lupita vein as well as in the stockwork veinlets of the Diluvio system. These colloform zones display variable amounts of recrystallization textures under the microscope (Fig. 74, top), chiefly mosaic, feathery, flamboyant or plumose (Dong et al., 1995; Moncada et al., 2012) textures of different concentrations.

Silica replacement of calcite is only locally developed as pseudo-acicular or ghost-bladed textures (Dong et al., 1995, Moncada et al., 2012) and many intercepts, especially within the Diluvio stockwork (Fig. 75, bottom), retain feathery, bladed calcite wholly unreplaced by silica. Saccharoidal textures are rare within the Lupita/Diluvio system, but are consistently associated with the highest grade material.

The remaining pyrite and chalcopyrite within the veins are of similar character to that of Klondike, forming small blebs disseminated within the Phase I quartz, commonly in proximity to clasts of the host andesite and lithic tuffs entrained within the vein.

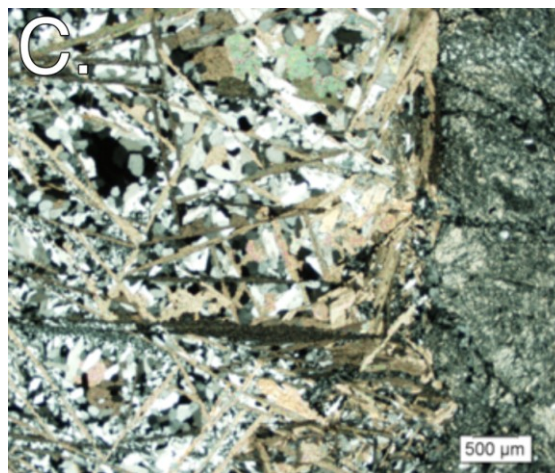
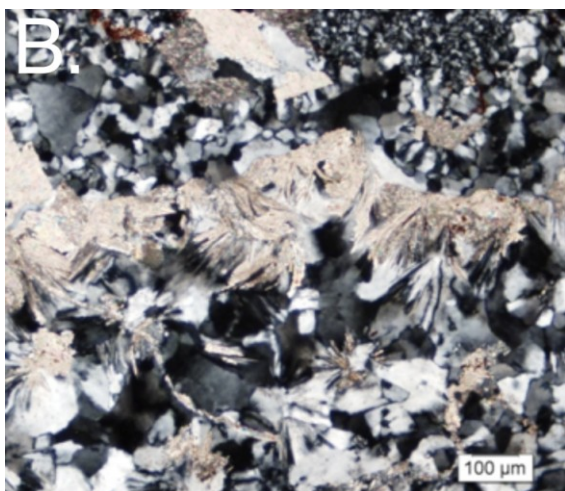
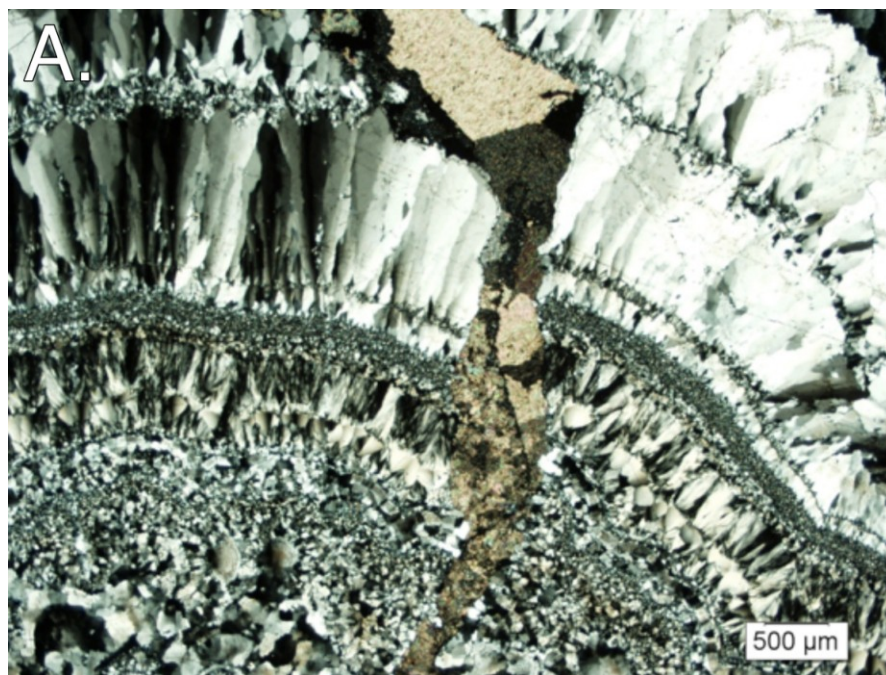


Figure 75. Typical Phase I mineral textures. (A): Mosaic, plumose and feather recrystallization textures after chalcedonic quartz cut and offset by a Phase II veinlet. Hole L10-072D, 284.18 m. (B): Pseudo-acicular quartz habits partially developed after quasi-platy calcite. Hole L11-113D, 239.62 m. (C): Platy calcite partially replaced by saccharoidal quartz. Argillized andesite clast can be seen at right. L10-072D, 249.28 m.

Vapor-rich fluid inclusions are common throughout the feathery quartz, but two-phase inclusions are also present. These suggest that the episodes of overpressurization, fracturing and boiling within the Lupita/Diluvio system was not as intense or widespread as in Mercedes or Klondike. This is supported by the apparent lack of significant hydrothermal brecciation and upward transport of vein material in Lupita/Diluvio. Furthermore, boiling textures are found at all depths within the system. These two facts suggest that mineralization may extend deeper within the Lupita vein and that the overall lower grades in the Lupita/Diluvio system are the result of a lack of conditions amenable of sudden depressurization due to hydrothermal or tectonic sources and a subsequent lack of flashing forming the localized bonanza-style deposition seen in the ore shoots of Mercedes and Klondike.

Macro- and Microscopic Textures: Phase II

Phase II mineralization is still dominated by massive Mn-oxide/calcite intergrowths composed of splotchy Mn-oxides mixed with crystalline calcite (Fig. 76). The Mn-oxide content is generally lower, with most samples visually estimated to be up to 40-50% Mn-oxide grading to near pure calcite in some intervals.

There is no evidence of boiling in any of the Phase II samples studied and the absence of high Au-Ag grades in the dominantly Phase II zones demonstrates that this Phase of mineralization was not responsible for the precious metal mineralization.

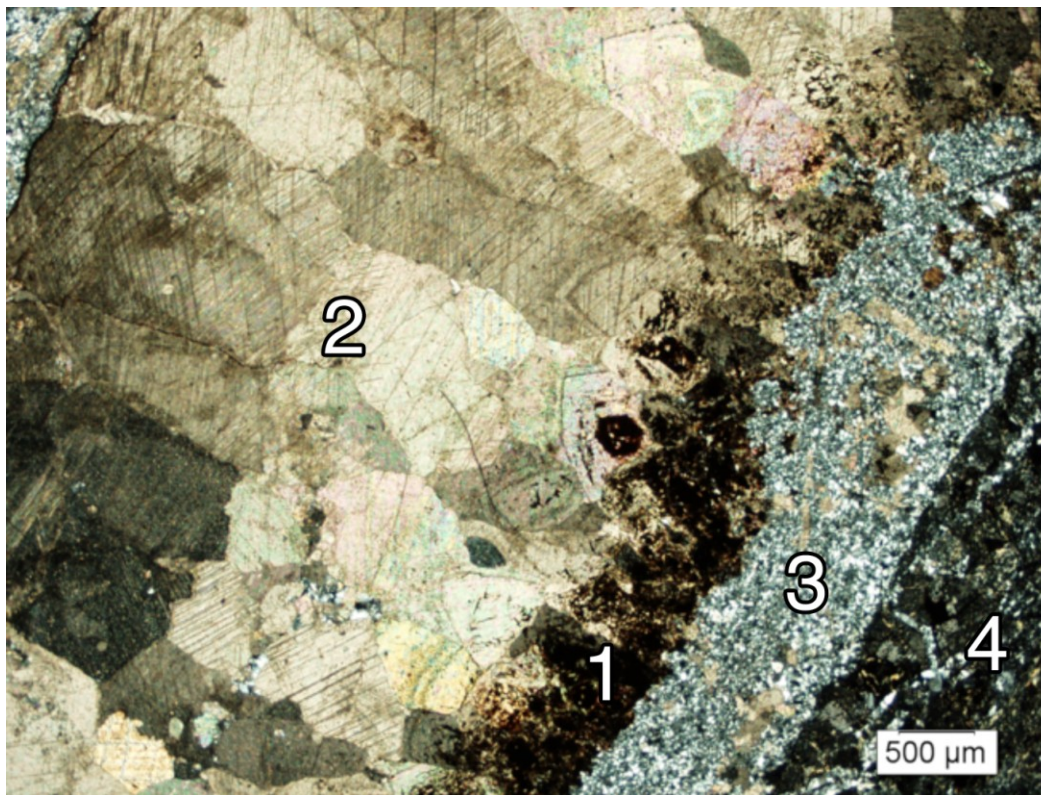


Figure 76. Dark, Phase II calcite+Mn-oxide intergrowths (1) grading to pure calcite (2) grown from a selvage of Phase I mosaic quartz and platy carbonate remnants (3) on a clast of intensely argillized andesite (4). Hole L11-113D, 290.23 m.

Macro- and Microscopic Textures: Phase III

Phase III mineralization is nearly identical in character to that in Mercedes and Klondike, consisting of coarse rhombic calcite and comb-textured quartz veins and veinlets cross-cutting the prior two Phases of mineralization. This Phase is especially well-developed in the Diluvio stock work, where some exclusively Phase III intercepts are up to 10 cm in true width.

Distinct from Mercedes and Klondike are the abundances of dark purple, comb-textured amethystine quartz and local crystalline anhydrite. Fluid inclusions within the amethystine quartz record constant ratios of liquid to vapor and indicate that these fluids were not boiling (Moncada et al., 2012).

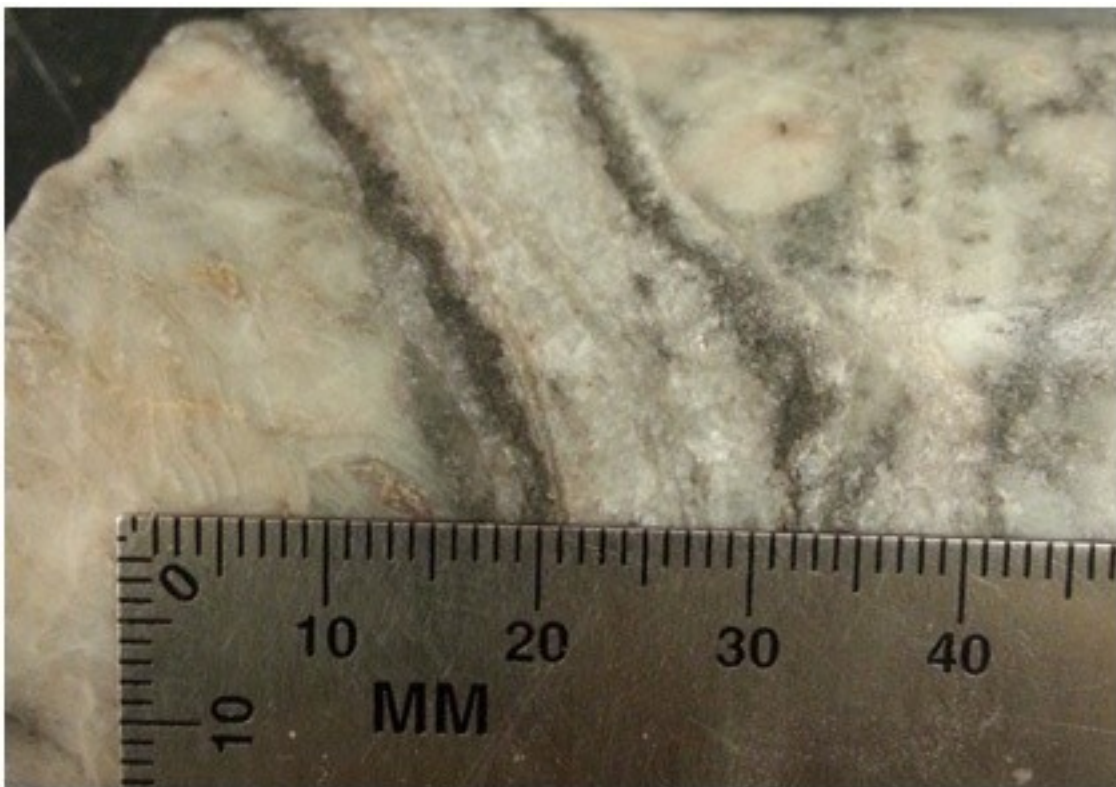


Figure 77. Phase III calcite veinlet with dark selvages cutting Phase I and II breccia.

Macro- and Microscopic Textures: Phase IV

Due to the overall lack of brecciation and the subsequent lack of permeability within the Lupita/Diluvio system, Phase IV oxidative mineralization is substantially less developed. While boxworks of hematite are present in association with the higher grade materials, only the higher levels of the Lupita vein show the extensive leaching and oxidation that the Mercedes and Klondike veins display. (Fig. 78). Where limonite occurs, it is goethitic and no occurrences of jarosite were seen.

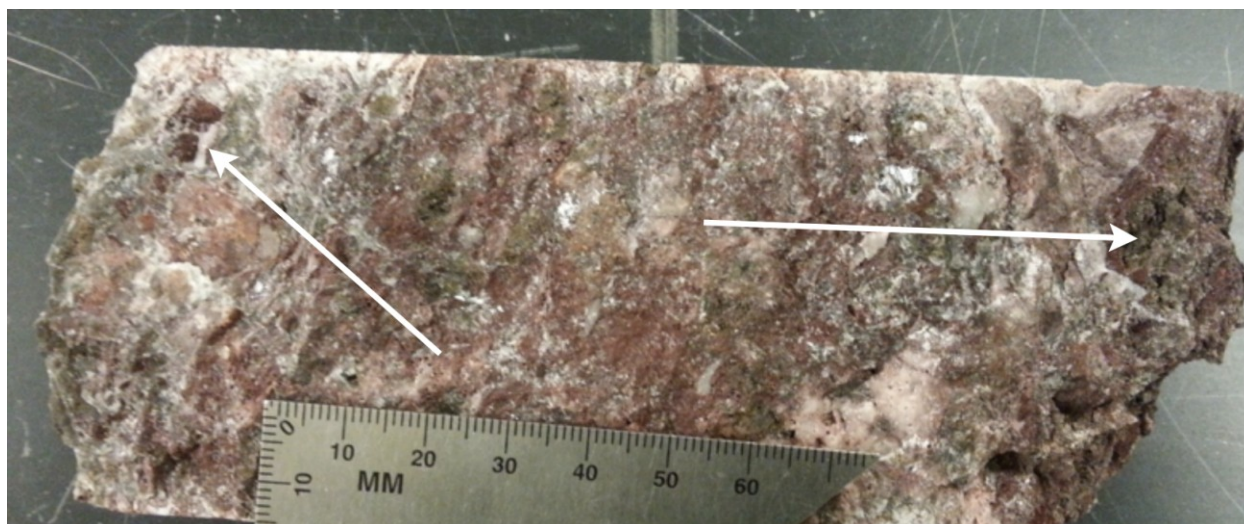


Figure 78. Phase IV oxidation of Lupita vein breccia with weak development of hematitic boxworks with green Phase I quartz (arrowed). Hole L11-172D, 300.84 m.

In the higher levels, leaching has removed much of the carbonate from the Phase II Mn-oxide/calcite assemblage, leaving spongy boxworks of Mn-oxides (chiefly pyrolusite) surrounding the Phase I banded quartz (see Fig. 74, top).

The locations where hematite boxworks are best developed correspond to the highest grade intervals of the Lupita vein. Compared to Mercedes and Klondike, these zones tend to have less saccharoidal green quartz and lower overall grades than comparable samples in the two southern zones

Variations in Textures

There is some variation down-dip in the Lupita vein, with more oxidized and vuggy material appearing higher in the system in general. These areas are sporadically distributed through the Lupita vein and are mostly absent from the overlying Diluvio stockwork. There was not enough data to determine if these textures vary along strike, but examination of the surface outcrop along its entire extent suggest that the vein is texturally homogenous along its length.

As with both Mercedes and Klondike, textural characteristics are a good proxy for grade. The highest grade intervals are located in the Lupita vein, in association with darker green quartz and hematitic boxworks.

Geochemistry

Vertical Zonation

As with both Mercedes and Klondike, quantitative chemical analysis was performed on assay pulps and selected core intervals (59 from the Lupita vein and 82 from the Diluvio stockwork) in order to discern any spatial patterns in the geochemistry of the systems.

Figures 79 and 80 illustrate the distribution of metals and trace elements across the 188 m of drilled vertical extent of the Lupita vein, from 1220 m to 1032 m of elevation. Given the limited extent compared to both the Mercedes and Klondike systems (450 m and 232 m, respectively), the trace element trends (Fig. 80) have predictably shallower slopes. As, Hg and Sb all show slight decreases with depth while Ba is nearly constant and Tl concentrations rise slightly. The metals in the system show somewhat more exaggerated trends. The base metals (Fig. 79) Cu, Mo, Pb and Zn all show marked increases with depth while Au and Ag decrease, with Au grades falling away faster.

In the Diluvio stockwork (Figs. 81 and 82), 177 m of vertical extent was represented from elevations of 1138 m to 961 m. Zonation patterns were broadly similar to that of the genetically-related Lupita system. As, Hg and Sb all showed slight decreases with depth. Ba and Tl were nearly constant with Ba displaying a very slight decline and Tl a very slight increase with depth in the system. The metals again possessed greater variations with Cu, Mo, Pb and Zn all showing strong increases with depth and Au and Ag showing strong decreases.

The statistical goodness of fit (R^2) of these trends tend to be somewhat better (often >0.15 compared with 0.01-0.05 commonly seen in Mercedes and Klondike) as well as showing a roughly classical (Buchanan, 1981) epithermal zonation pattern. Both of these characteristics likely result from the much lower degree of brecciation and transport of mineralized material that is observed within the Lupita/Diluvio system.

The method outlined by Loucks and Petersen (1985) for the Ag-dominant veins at Topia, Durango was attempted (Fig. 83) for the geochemical data from the Lupita vein and overlying Diluvio stockwork. The Lupita vein's recumbent orientation was accommodated by normalizing the true elevations according to a linear model of depth versus distance along dip in order to plot the Ag/Zn and Pb/Zn covariance along an approximate fluid flow path length similar to the supposed vertical paths of the Mercedes, Klondike and Diluvio systems. The resulting covariance plot for the Lupita system does not display any discernible patterns. However, the Ag/Zn-Pb/Zn covariance plot for the Diluvio system contains an obvious pattern (Fig. 84) related to the zonation of the Ag/Zn and Pb/Zn ratios. Figure 86 shows two theoretical elevation vs. element ratio zonation curves that would explain the observed pattern (Fig. 85) within the Diluvio data, namely an enrichment of Ag with respect to Zn at higher elevations with a corresponding decrease at lower elevations paired with an increasing Pb/Zn ratio at depth.

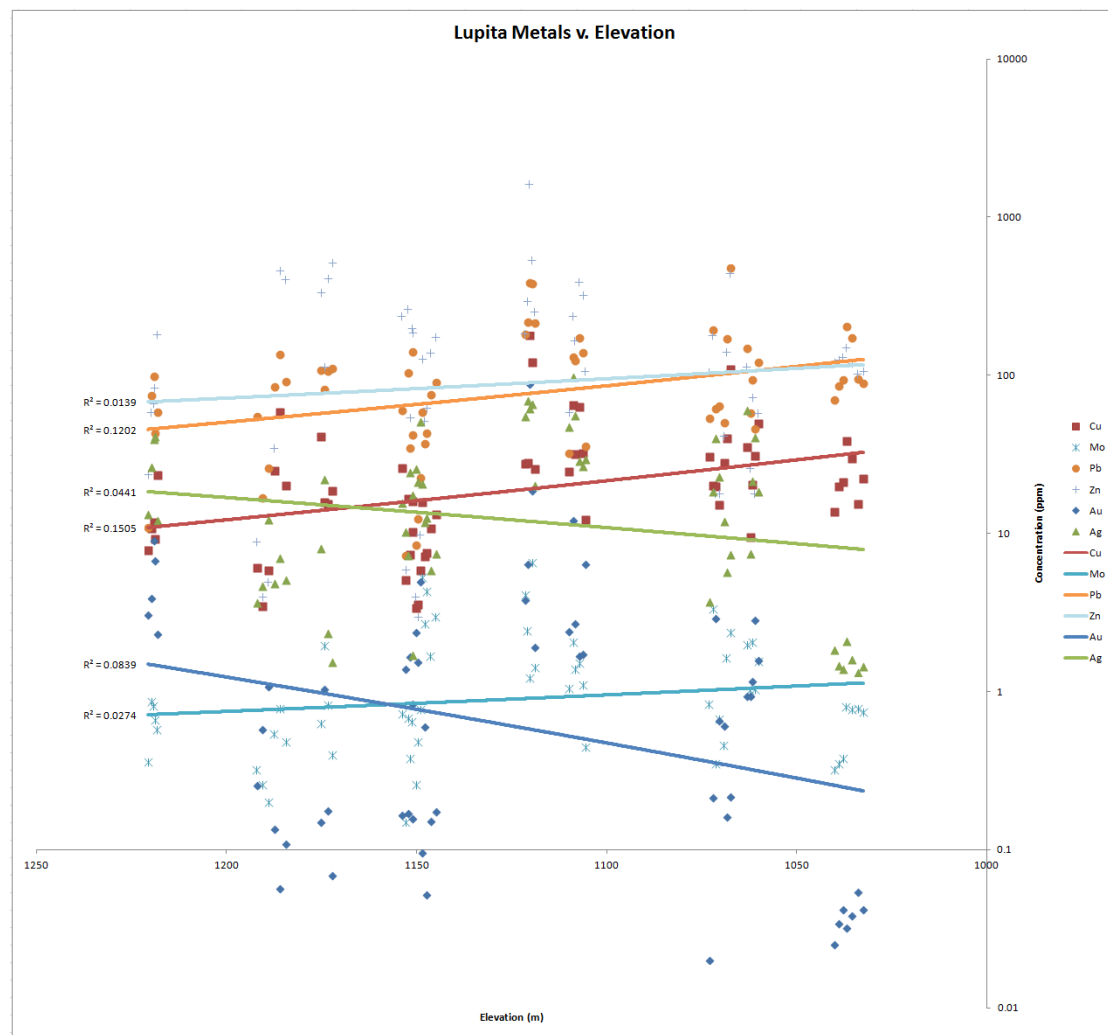


Figure 79. Lupita metals vs. elevation. Trend lines are power regressions with R-squared values listed. Note log scale on y-axis.

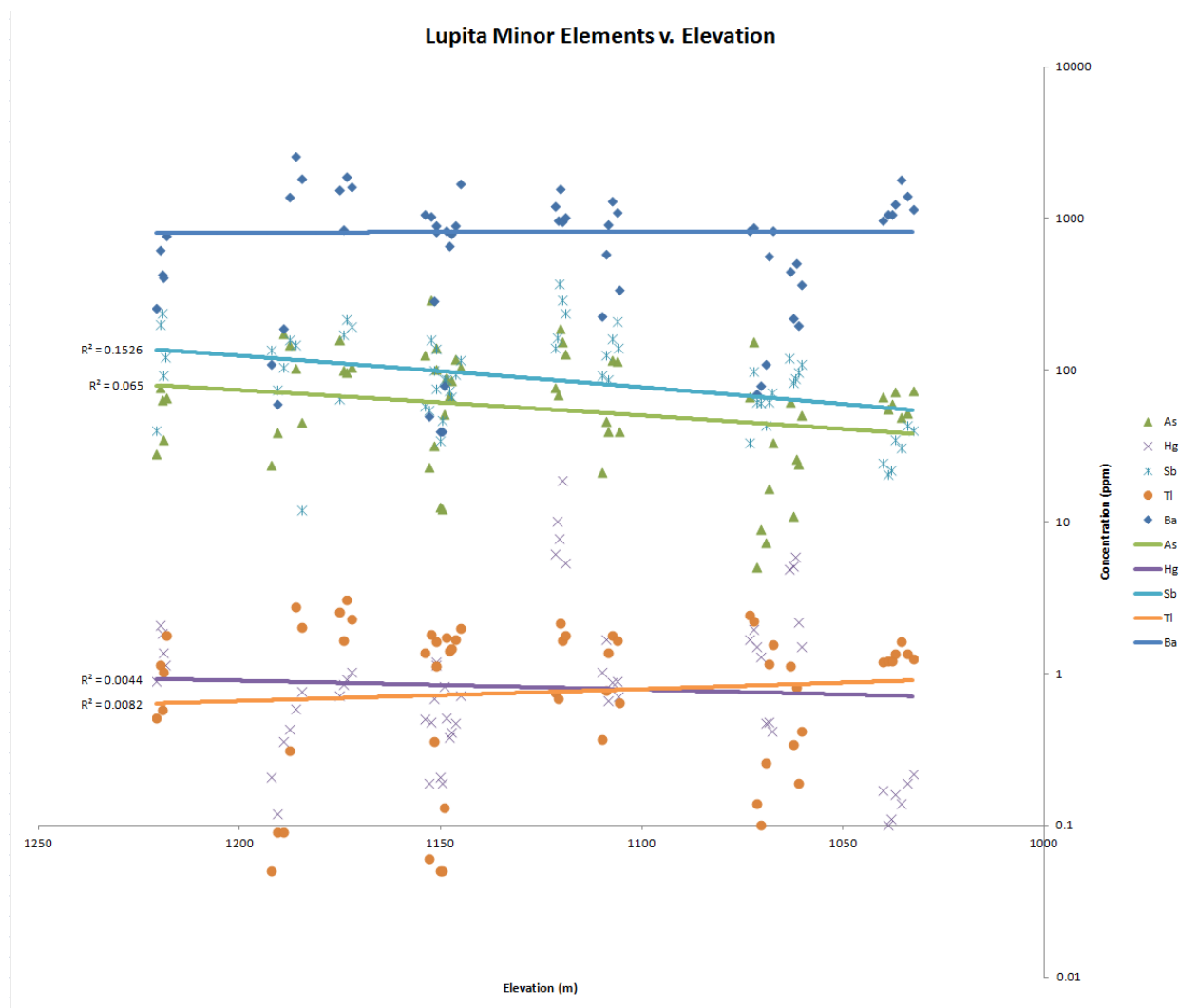


Figure 80. Lupita trace elements vs. elevation. Trend lines are power regressions with R-squared values listed. Note log scale on y-axis.

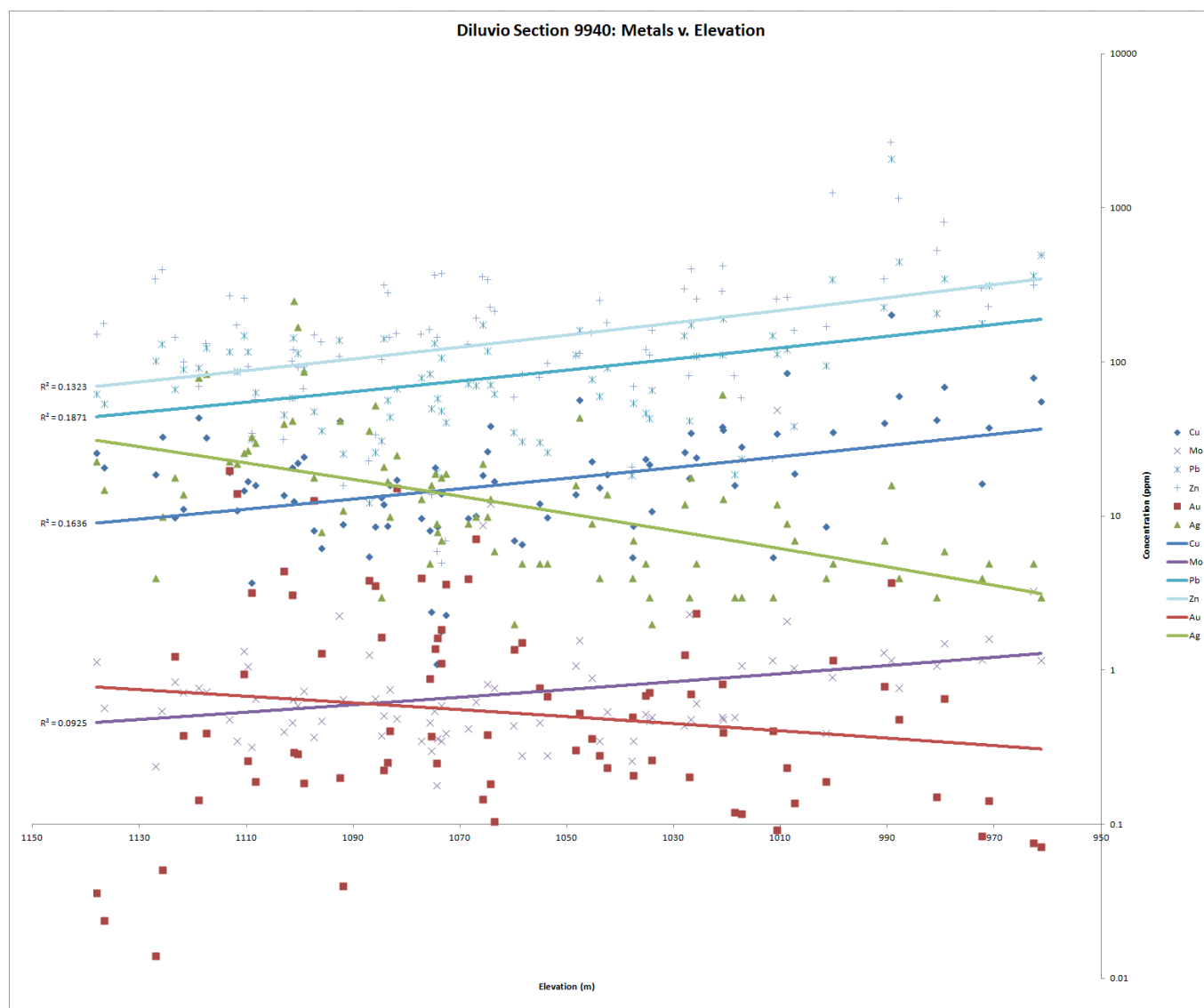


Figure 81. Diluvio metals vs. elevation. Trend lines are power regressions with R-squared values listed. Note log scale on y-axis.

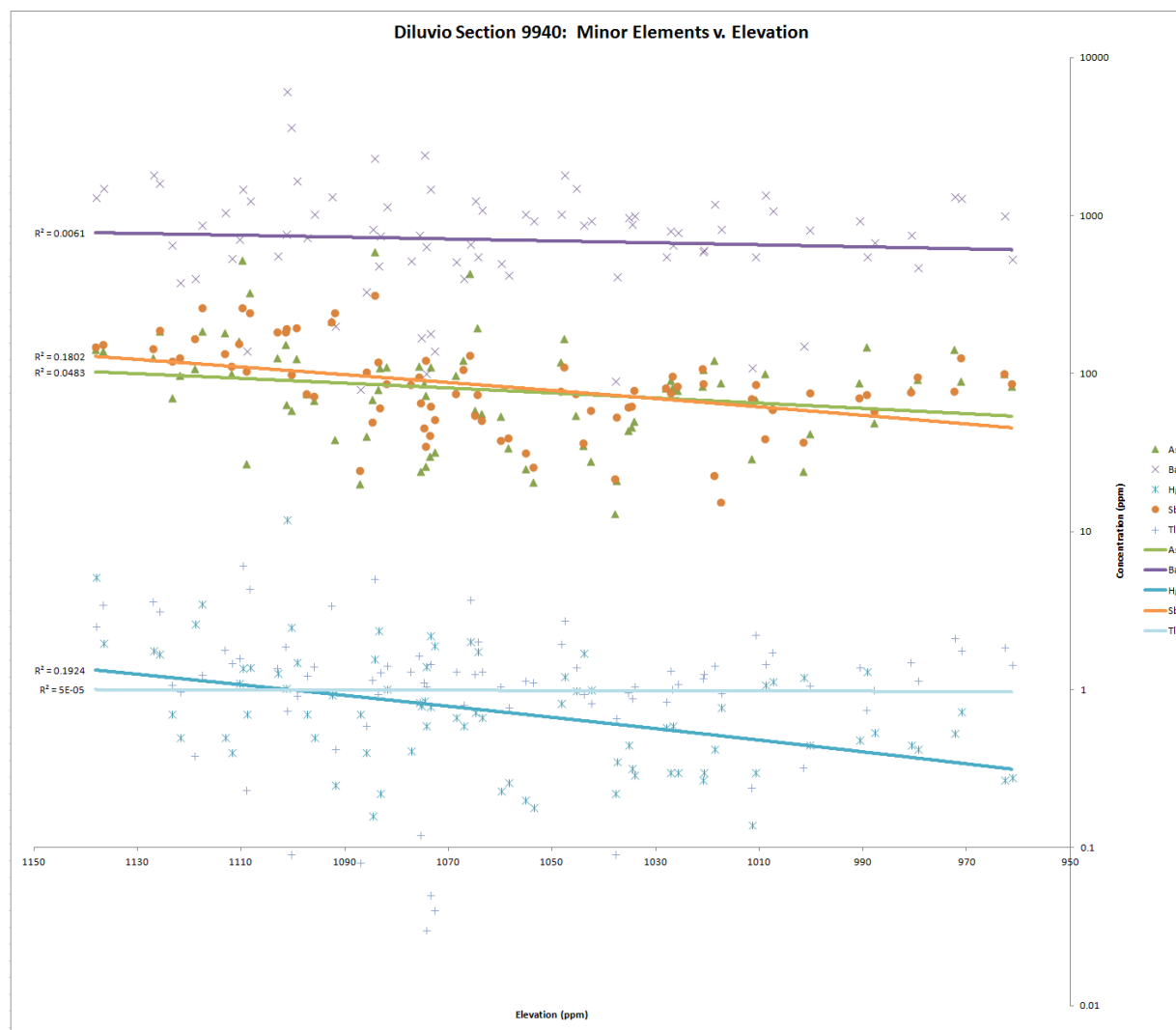


Figure 82. Diluvio trace elements vs. elevation Trend lines are power regressions with R-squared values listed. Note log scale on y-axis.

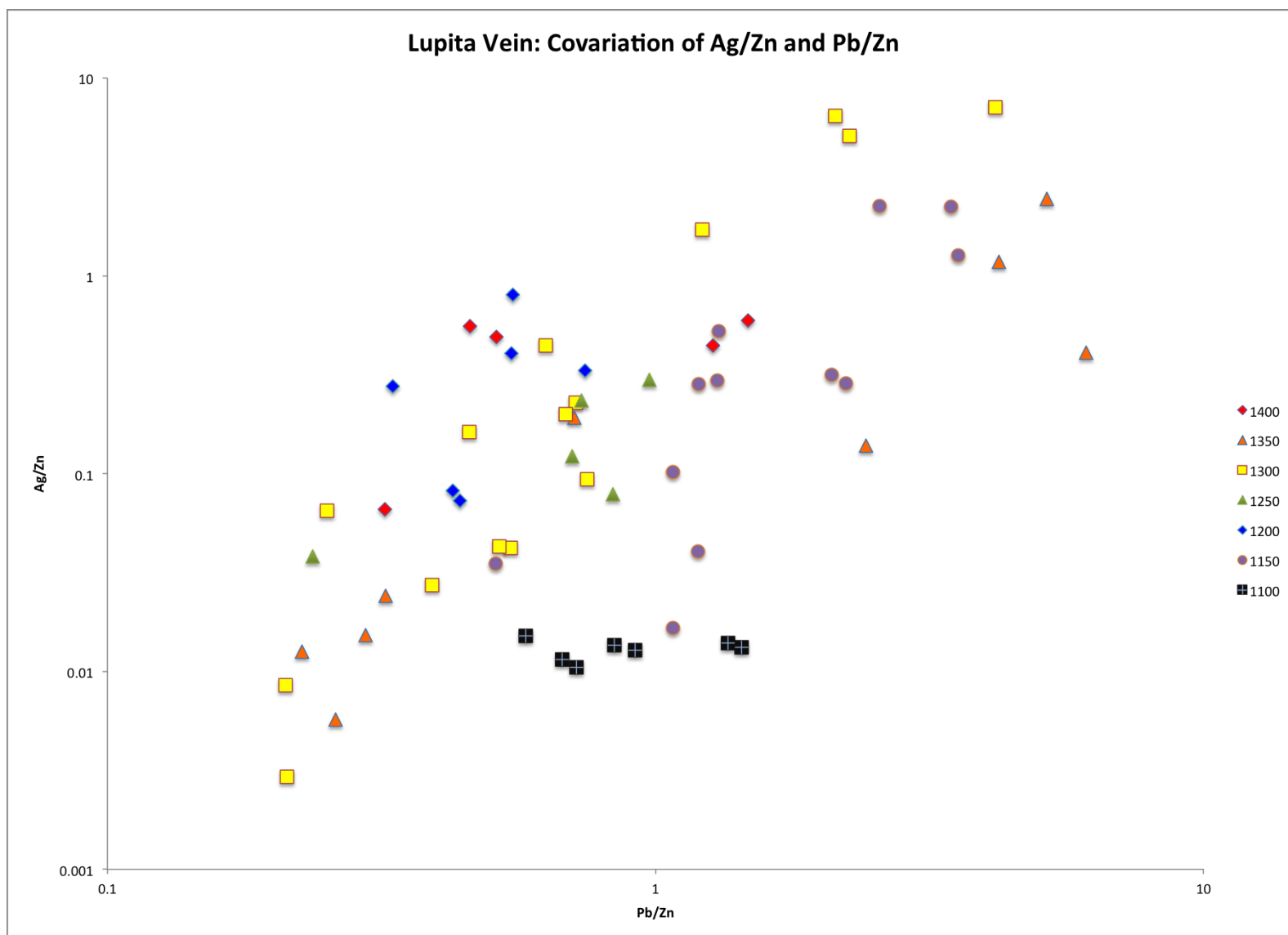


Figure 83. Covariation of Ag/Zn and Pb/Zn ratios with normalized elevation for the Lupita vein. Method modified from Loucks and Petersen (1985).

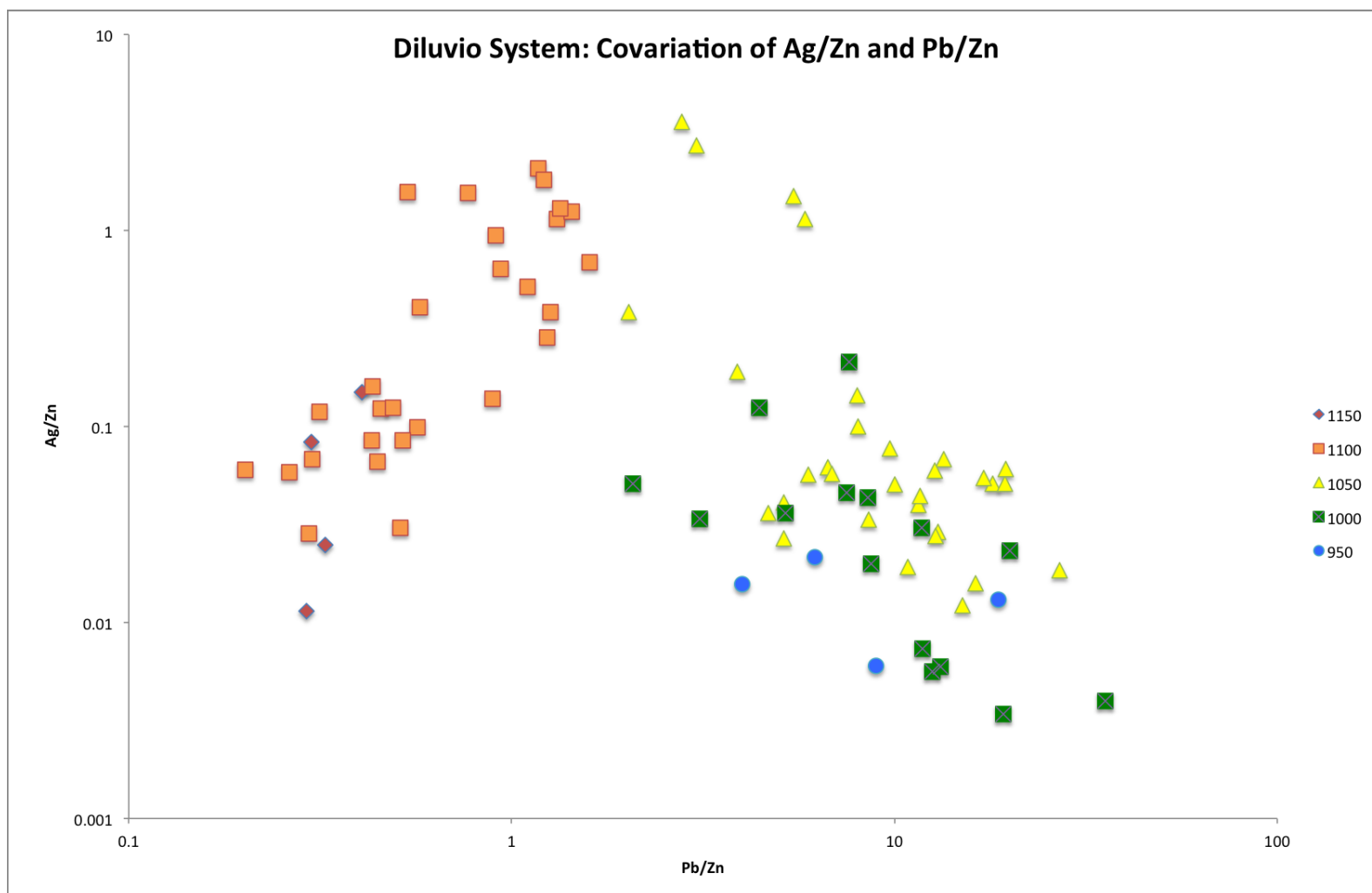


Figure 84. Covariance of Ag/Zn and Pb/Zn with elevation for the Diluvio system. Color spectrum reflects elevation in meters: red=higher, purple=lower. Method modified from Loucks and Petersen (1985).

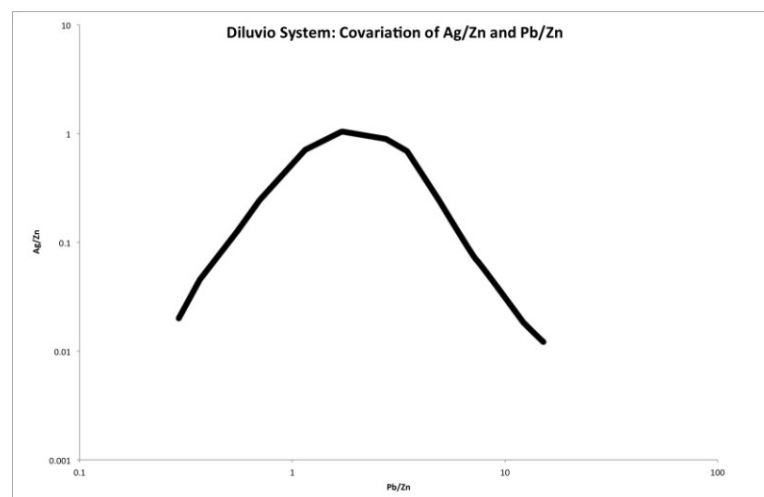


Figure 85. Interpretation of Ag/Zn-Pb/Zn covariation from Figure 84.

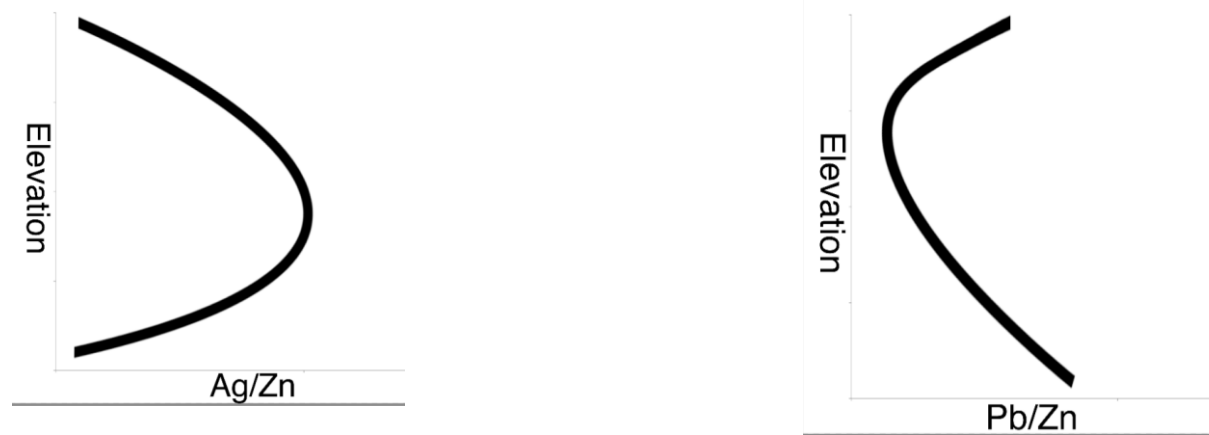


Figure 86. Relative Ag/Zn (left) and Pb/Zn (right) vs. elevation trends that would be responsible for the observed trends in the Diluvio system.

Correlations

Figure 87 is a correlation matrix for selected elements created using the combined 142 samples from both the Lupita vein and the Diluvio stockwork. Of note is the essentially non-correlated relationship ($R=0.166$, compare Mercedes at 0.517 and Klondike at 0.398) between Au and Ag. Both precious metals show only weak positive correlations to any other element with Au-Cu (0.462) and Ag-Hg (0.543) being the pairs with the greatest correlation. Cu, Pb and Zn all show strong correlations (>0.700) with one another as well as the Ca-C-Mn triad (C-Ca = 0.996, Ca-Mn = 0.704), further reinforcing the observation that the Phase II carbonates within the Lupita/Diluvio system are Mn-oxide bearing.

	Au	Ag	As	Ba	Ca	Cu	Fe	Hg	Mn	Mo	Pb	Sb	Se	Tl	Zn	C
Au	1.000															
Ag	0.166	1.000														
As	0.083	0.030	1.000													
Ba	0.014	0.528	0.299	1.000												
Ca	-0.086	-0.066	-0.324	-0.248	1.000											
Cu	0.462	0.088	0.137	0.134	-0.179	1.000										
Fe	0.052	-0.214	0.496	0.325	-0.293	0.219	1.000									
Hg	0.350	0.543	0.104	0.298	-0.034	0.314	-0.016	1.000								
Mn	-0.029	-0.008	-0.243	-0.076	0.704	0.051	-0.076	0.052	1.000							
Mo	-0.014	-0.008	0.075	-0.034	-0.092	0.112	0.074	0.072	-0.063	1.000						
Pb	0.129	0.007	0.131	0.067	-0.046	0.776	0.057	0.139	0.076	0.041	1.000					
Sb	0.392	0.362	0.572	0.268	-0.356	0.252	0.200	0.470	-0.219	0.024	0.098	1.000				
Se	0.294	-0.026	-0.058	-0.027	0.160	0.150	0.020	0.223	0.073	-0.026	0.061	0.030	1.000			
Tl	0.015	-0.116	0.788	0.433	-0.405	0.153	0.654	0.036	-0.331	0.157	0.071	0.447	-0.031	1.000		
Zn	0.370	-0.051	0.173	0.139	-0.062	0.785	0.253	0.138	0.108	0.042	0.858	0.171	0.137	0.173	1.000	
C	-0.089	-0.071	-0.336	-0.259	0.996	-0.187	-0.305	-0.043	0.714	-0.094	-0.056	-0.367	0.147	-0.419	-0.077	1.000

Figure 87. Correlation matrix for selected elements, Lupita/Diluvio system. Green colors are significant positive correlations, yellows and oranges poor correlations and dark orange to red indicates significant negative correlations. N=142.

STRUCTURE ON THE MERCEDES PROPERTY

Mercedes/Barrancas Structure

The Mercedes vein is localized within a fault zone that is generally parallel to the regional northwest-southeast trending structural fabric as defined by the axes of the anticlines, andesite basins and faults that transect the property. The Mercedes fault is accessible at a number of underground exposures and is characterized by a zone of 1-4 m thick foliated clay gouge with entrained clasts of vein and host rock with abundant examples of ductile deformation textures within the clays. The foliations in the gouge reveal several generations of fault movement, with slickenlines (Fig. 88) revealing a dextral-normal sense of faulting. Some foliation generations display an entirely normal sense of slip, while others show a record of episodic displacement with oblique slickenlines. No observations of purely strike-slip motion were observed.

In the Barrancas/Lagunas extension, the highly sheared and discontinuous structure of the vein (see Fig. 21) is likely controlled by a combination of horsetailing of the Mercedes fault and additional deformation related to the formation of Los Pinos graben. Poor core recovery and a lack of underground access prevent the direct assessment of the structure of this zone. Measurements of the strike and dip were taken at 16 underground exposures of the Mercedes fault to record a mean strike of 144°, dipping 83° to the southwest (Fig. 89).



Figure 88. "Foliated" clay gouge on the Mercedes fault trace at the 910 level of the Corona de Oro ore shoot. Note the slickenlines indicating normal dip-slip kinematics. This particularly well-developed example is likely to be related to tectonic activity, though it cannot be ruled out that these are related to ongoing mining.

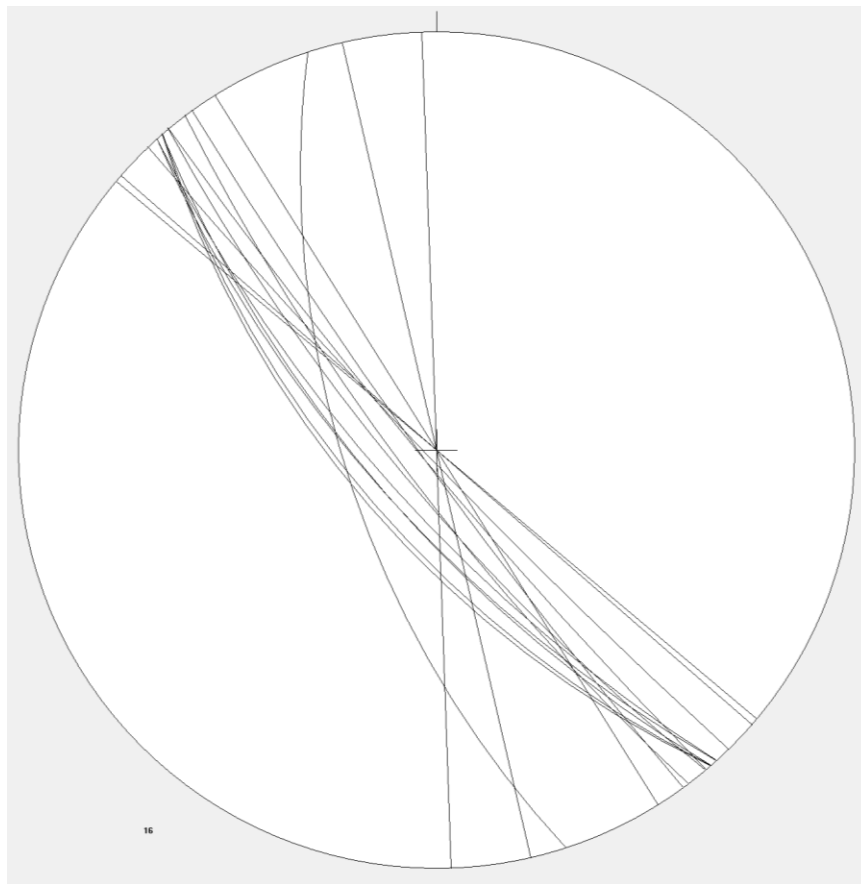


Figure 89. Stereographic projection of Mercedes fault trace measurements. N=16, average orientation is 324° , dipping 83° to the southwest. Plot made with GEORient software by Rod Holcombe.

Klondike Structure

The Klondike vein is hosted in a west-northwest trending fault zone that lies sub-parallel to the northwest-southeast structural fabric in the region. The Klondike fault (Fig. 90B) is accessible within the current underground workings and is characterized by a 1-2 m thick zone of foliated clay gouge with local inclusions of host andesite. These foliations record several generations of fault motion, with slickenlines indicating dextral-oblique kinematics. Measurements were taken at 10 underground exposures and revealed a mean strike (Fig. 90A) of 280° dipping 77° to the south.

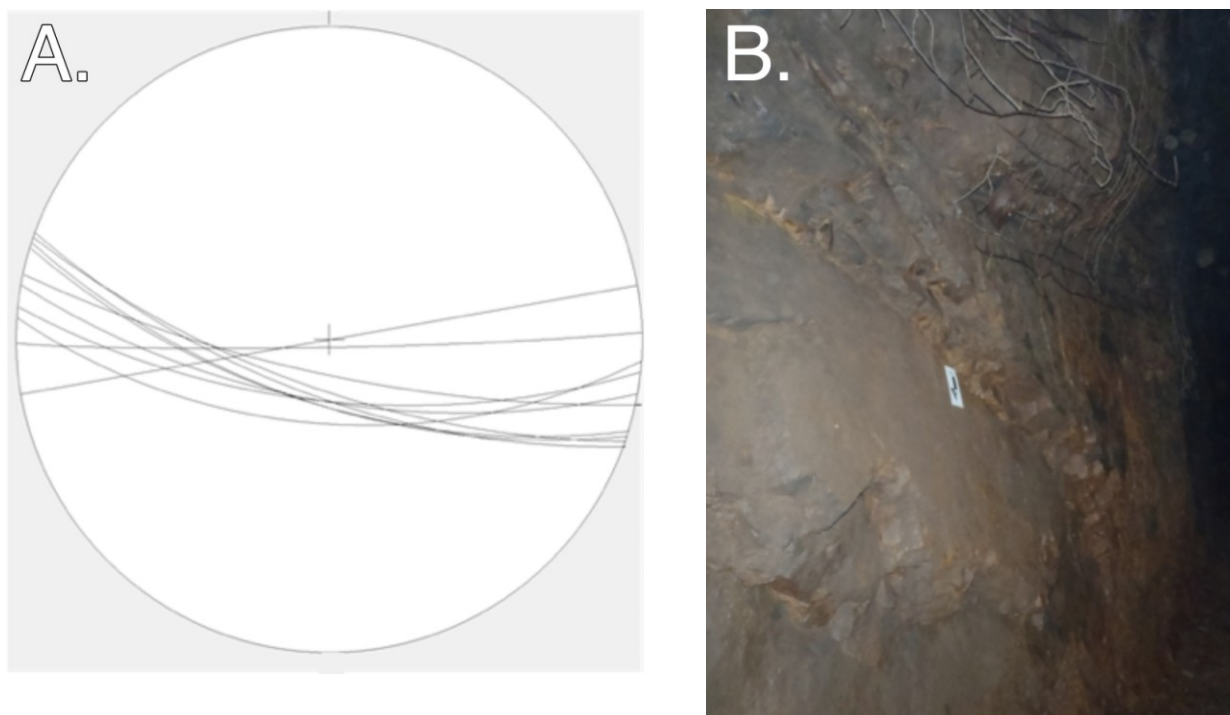


Figure 90. Left: Stereographic projection of Klondike fault trace measurements. $N=10$, average orientation is 280° dipping 77° southwest. Plot made using GEORient software by Rod Holcombe. Right: The exposed fault surface at the 1080 level of the Klondike mine. The arrow on the scale card points along faint slickenlines indicating oblique -slip kinematics with a slight dextral component.

Lupita/Diluvio Structure

The Lupita fault, hosting the Lupita vein and forming the footwall of the Diluvio stockwork zone, is unusual in the context of the structural fabric of the property. The outcrop of the fault and

vein has an average strike of 272° . The footwall of the fault is made up of the lithic tuff package, while the hanging wall is composed of andesites down to roughly 1100 m elevation when it changes to variably altered rock of the tuff package. The Diluvio block is highly fractured and veinlet/fracture orientations within the Diluvio stockwork appear to be random (work by the author and M. Hawksworth, F. Cazares, pers. comm., 2012). No kinematic indicators were found within the available core, but the geometry of the fault and the block of the tuffs suggest the Diluvio stockwork is hosted within a normally-displaced block down-dropped along the listric Lupita structure and covered by post-faulting andesites and Baucarit Formation rocks.

Discussion

The three mineralized structures studied on the Mercedes property are dominated by characteristics of extensional tectonics. Normal dip-slip motion indicated by slickenlines dominates the displacement in all three zones, and there is a minor dextral component of slip present in both the Mercedes and Klondike faults. The recognition of this strike-slip component has implications for the geometry of the veins, as both changes in dip and changes in strike will have produced dilatational openings with favorable conditions for ore deposition (Sibson, 1987; Bogie and Lawless, 2001; Hudson, 2003; Begbie et al., 2007; Spörli and Cargill, 2011). Additionally, the presence of strike-slip kinematics raises the possibility of sympathetic fracturing in step-over or accommodation zones between parallel fault zones. As the drilling pattern to date has focused on delineating the known mineralized veins, most drill holes have been directed perpendicular to the strike of the main veins--an orientation that would run roughly parallel to the strike of any off-shoots oriented perpendicular to the main fault -hosted mineralization and reduce the chances of intercepting such a feature.

As a whole, the structural fabric on the Mercedes property reflects the trans-tensional regime that has been sporadically active in northern Mexico since at least the Jurassic (Molina-Garza and Iriondo, 2007). Extensional tectonics in northern Sonora are coeval and genetically related to basin and range extension throughout southwestern North America (Henry and Aranda-Gomez, 1992). Unaltered biotite and hornblende phenocrysts entrained within the clay gouge suggest that motion on the fault began prior to the hydrothermal activity and continued during the hydrothermal mineralization.

The Mercedes district appears to occupy a stepover linkage or accommodation zone between normal faults of Los Pinos graben to the west of the property and the Aconchi graben to the southeast (Fig. 91). The orientation of the normal faults that host the Mercedes, Klondike, and Lupita systems as well as the rotation of the faulting from northwest-southeast to east-west strikes from south to north in the district superficially matches modeling (Fig. 92) done of graben stepovers by Fossen et al. (2010) and matches well with work done by Faulds et al. (2011) regarding the structural setting of active hydrothermal systems in the northern Great Basin (Fig. 93).

The Lupita fault, with its east-west orientation and listric nature is more problematic to explain. The lack of detailed structural data for the fault and the property as a whole only permits speculation. Given the late Mesozoic age of the tuff sequence and the orientation of the Lupita fault, it may represent a Mesozoic compressional structure that has been reactivated as a normal fault during subsequent extension. Henry (1986) and others (Turner et al., 1986) have established the presence of east-northeast trending structural fabrics both south and north of the Mercedes property and it seems likely that this framework directs the structure in the Mercedes district as well. This reactivation may also be due to the linkage between the Aconchi and Los Pinos grabens.

Further evidence of extensional tectonic control on the structure in the region comes from the presence of the gently plunging anticline that separates the Mercedes and Klondike basins (see Fig. 4.). Antiformal structures are known to form (Varga et al., 2000) at step-over zones between adjacent graben structures and this is a possible mechanism for the creation of the upwarping of the stratigraphy within the Mercedes property.

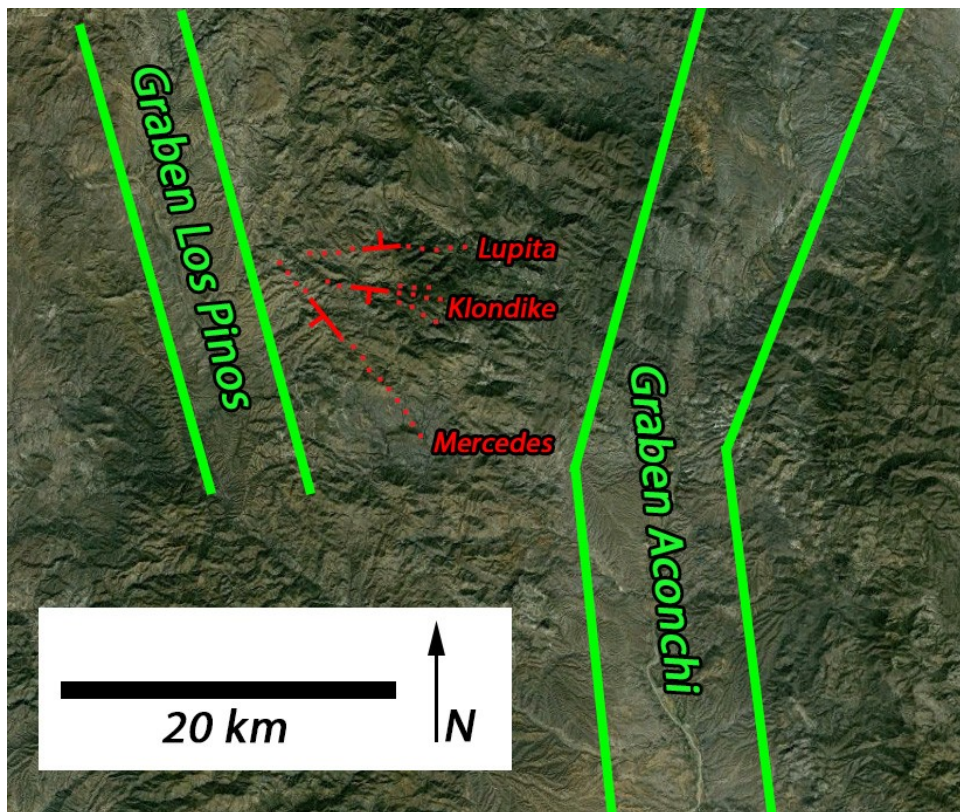


Figure 91. Structural context of the Mercedes, Klondike and Lupita fault-hosted veins. Dotted lines are extensions of the fault traces for clarity. Green lines bounding the grabens correspond to the theoretical location of range-front normal faults. Compare to Fig. 87.

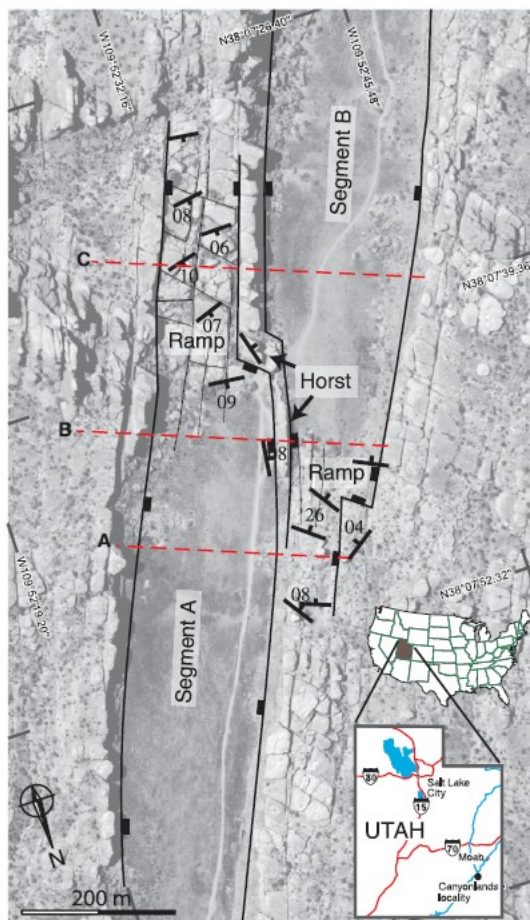


Figure 92. Graben linkage structures from Canyonlands, Utah. The Mercedes district may represent a similar, mirror-image system. From Fossen et al., 2010.

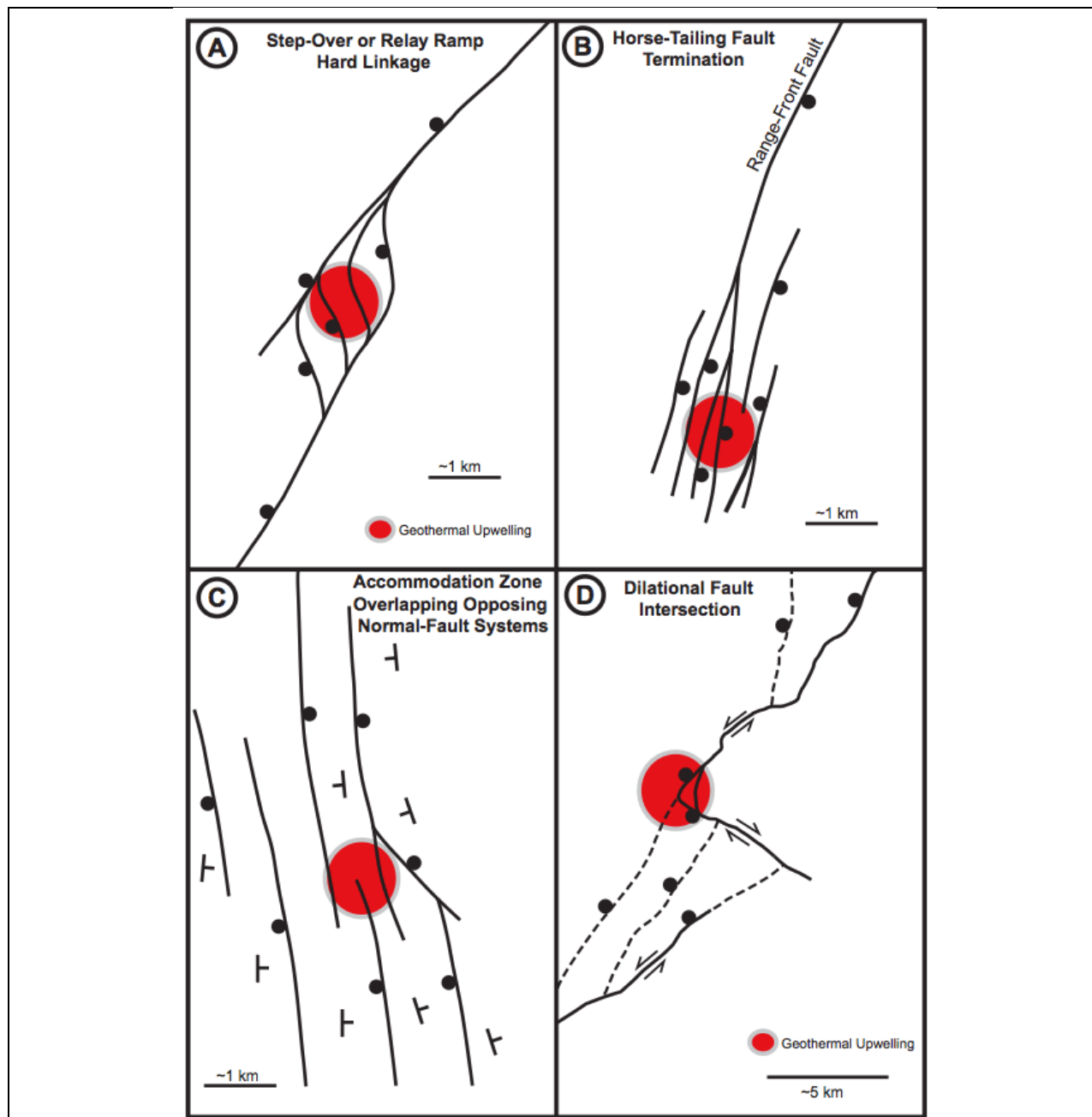


Figure 93. Illustrations of various structural regimes controlling geothermal systems in the Great Basin. Note the superficial similarities between examples (A) and (B) to the Mercedes district as shown in figure 91. From Faulds et al., 2011.

CONCLUSIONS

The similarities in the mineralogy and paragenesis between the Mercedes, Klondike and Lupita/Diluvio zones within the district suggest that they are all parts of a genetically-related, low-sulfidation hydrothermal system. The system is characterized by early phase reduced Fe-bearing green quartz spatially and temporally associated with precious metal mineralization and a Mn-oxide+calcite second phase that chiefly acted as a cement between clasts of Phase I and host rock breccia. Of note are the lack of adularia, extensive oxidation and variable amounts of brecciation that directly controlled the degree of the supergene reworking of the precious metal and trace element distributions.

Mineralization is localized by a series of normal faults with a slight component of dextral slip that appear to be part of a step-over linkage or accommodation zone between the adjacent Aconchi and Los Pinos grabens. Assuming these grabens are part of the widespread Basin and Range extensional episode, an age on the mineralization can be placed between the earliest known expressions of extension at 30 Ma (Henry and Aranda-Gomez, 2001) and the adjacent and unaltered glassy latite at 26.15 Ma (this study). This corresponds to the second wave of epithermal mineralization in Mexico defined by Camprubi et al. (2003) occurring between 36 and 27 Ma and linked to the emplacement of the giant ignimbrite province of the Sierra Madre Occidental. This date also appears to be the most northerly occurrence of epithermal mineralization of that Oligocene age. While the constraint created by the glassy latite only directly applies to the Mercedes vein, the similarities of the Klondike and Lupita/Diluvio systems in mineralogy, structural setting and paragenetic sequence to Mercedes suggests that these veins are all of the same age.

Table 1. Comparison of the Mercedes District to a selection of other epithermal Au-Ag deposits.

ac=acanthite, adu=adularia, Ag-ss=silver sulfosalts, bms=base metal sulfides, cc=calcite, chal=chalcedony, ec=electrum, hm=hematite, ill=illite, Mnnox=manganese oxides, pg=pyrargyrite, pr=proustite, py=pyrite, qtz=quartz, smect=smectite, tet=tetrahedrite.

Deposit	Au Reserves or Production	Ag Reserves or Production	Mineralogy	Host Rock	Age	Source
Mercedes District	0.96 Moz	10.1 Moz	qtz + co3 + Au + Ag + hm	Andesite flows/breccias	?	Yamana Gold, 2011
Midas (Ken Snyder), NV, US	3 Moz	35 Moz	qtz + adu + ec + bms + Se	Rhyolite Tuffs and Lacustrine Sediments	15.4 Ma	Leavitt et al., 2004
Waihi, New Zealand Martha Favona	6.71 Moz 0.025 Moz	42.1 Moz 0.116 Moz	qtz + adu + ill + ec + sl + gn	Andesite flows/pyroclastics	6.0-6.1 Ma	Christie et al., 2007
McLaughlin, CA, USA	2.93 Moz	?	qtz/chal + ec + pg + Hg	Sinters and breccias in basalt	0.75 Ma	Tingley and Bonham, 1986
Guanajuato, Zacatecas, MX	5.1 Moz	1016 Moz	qtz + adu + cc + ac + ec + bms + Se	Andesite volcanics	27-31 Ma	Randall R. et al., 1994
Fresnillo, Zacatecas, MX	0.61 Moz	32.2 Moz	qtz + cc + clays + adu + Ag-ss + tet + bms	Marine sediments/Volcanics	28-32 Ma	Ruvalcaba-Ruiz and Thompsom, 1988 Camprubi et al., 2003
Topia, Durango, MX	0.025-0.050 Moz	15-30 Moz	qtz + cc + adu + tet + pr-pg + bms + ec	Andesite volcanics	43.5-44.0 Ma	Loucks et al., 1988
Hishikari, Japan	7.6 Moz	?	qtz + adu + smect + ec + cc + bms	Andesite flows/pyroclastics	0.9-1.15 Ma	Etoh, et. Al, 2002

Table 2. Summary of characteristics of the Mercedes, Klondike and Lupita/Diluvio Zones.
 qtz=quartz, cc=calcite, Mnox=Mn-oxides, hm=hematite, jar=jarosite, cer=cerargyrite.

	Mercedes	Klondike	Lupita/Diluvio
Orientation	324°, dips 83° SW	280°, dips 77° SSW	070°, dips 20-70° N
Strike Length	Up to 3 km	1200 m	1500 m
Mineralized Vertical Extent	≥600 m	~400 m	~400 m
Average Grade (max. grade)	8.7 (640) ppm Au 95 (3700) ppm Ag	6.3 (60) ppm Au 39 (200) ppm Ag	~2 (18) ppm Au ~20 (65) ppm Ag
Mineralogy	Phase I: green qtz+cc Phase II: cc+Mnox Phase III: qtz+cc Phase IV: hm+jar+cer	Phase I: green qtz+cc Phase II: cc+Mnox Phase III: qtz+cc Phase IV: hm+jar	Phase I: green qtz+cc Phase II: cc+Mnox Phase III: qtz+cc Phase IV: hm
Textures	Vein Breccia	Vein Breccia Banded Vein	Banded Vein Local Vein Breccia
Boiling Textures	Abundant	Common	Less Common
Structural Setting	Dextral-normal fault hosted	Dextral-normal fault hosted	Listric Normal Fault Stockwork (Diluvio)
Age	30-26 Ma	30-26 Ma	30-26 Ma
Elemental Zonation	Anomalous	Slightly Anomalous	Roughly Classical

Geochemically, the system fits the profile of the C-type, low-sulfidation epithermal system in the Camprubi and Albinson (2007) classification system of Mexican epithermal deposits, and in general is best classified as an intermediate-sulfidation epithermal deposit based on the high precious/base metal ratio, dominance of quartz, calcite and Mn-oxides/carbonates over adularia, and the district's location within andesites in an extensional continental setting (Sillitoe and Hedenquist, 1993; Albinson et al., 2001; Gemmell, 2004, Simmons et al., 2005) These systems are interpreted to form distally to deeper, parental felsic magmas from reduced, low-salinity fluids resulting in the high Au/Ag and precious/base metal ratios. (Sillitoe and Hedenquist, 2003) Deposition of the precious metals is controlled by tectonically-initiated rapid depressurization of hydrothermal fluids and destabilization of the dissolved metal-bisulfide complexes (Weissberg, 1969; Brown, 1986; Sibson, 1987; Sillitoe, 1993, Cooke and Simmons, 2000; Moncada et al., 2012).

The early-stage quartz from these zones preserves a number of textures related to flash boiling (Brown, 1986; Dong et al., 1995, Cooke and Simmons, 2000; Moncada et al., 2012). These textures are found throughout the vertical extent of all three systems, though this observation may be of less significance in the Mercedes zone where significant amounts of vertical hydrothermal transport make interpretation of the original extent of boiling impossible.

The tectonic and hydrothermal activity introduced textural controls on the mineralization and geochemistry in the form of physical transport and increased permeability that controlled the location of the ore shoots. Extensive brecciation and upward transport of fragments of vein material more than 400 m has been documented in the Mercedes vein, with lesser amounts in Klondike. No transport and relatively little brecciation was observed within the Lupita/Diluvio system and the stockworking of the Diluvio block appears to be related to tectonic fracturing related to slip along the Lupita fault and not hydrothermal overpressuring. This apparent lack of

disruption within the Diluvio system provides a useful test of the methods used to interpret the geochemical zonation in the Mercedes, Klondike and Lupita zones. For the Diluvio system, the Loucks and Petersen (1985) graphical method shows a clear gradation from an increased Ag/Zn (and presumably precious/base metal) ratio at higher levels to a higher Pb/Zn (and lower precious/base metal) ratio at lower levels in the system typical of low-sulfidation epithermal systems (Weissberg, 1969; Goodell and Petersen, 1974; Cooke and Simmons, 2000, Echavarria, 2006). The direct plotting method for Diluvio agrees well with this zonation pattern and shows the least spread among the data out of all the systems studied. Further, the obvious lack of zoning patterns in most of the metals as shown by the low R^2 values of the calculated regressions correlates well with the relative amount of physical disruption within the systems.

It is again worth stressing that the actual regressions and poor R^2 values are not intended to indicate any real, spatial geochemical zonation. The interpretation of the poor quality of these values (commonly <0.1), and the apparent correlation of R^2 degradation to a higher degree of brecciation is meant to highlight the textural-geochemical relationships within each vein system.

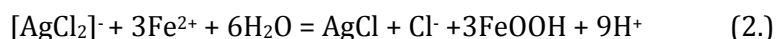
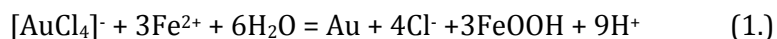
As the amount and severity of brecciation increases, the zoning patterns deteriorate. This inverse correlation is entirely due to both the physical mobilization of brecciated vein material that later allowed for significant penetration of post-mineral, oxidized, meteoric fluids into the vein system. These fluids pervasively oxidized the veins in the district down to the deepest observable levels, more than 400 m below the current surface. These fluids mobilized As, Ag, Hg and Sb (among others), smearing out the geochemical zonation within the highly brecciated and permeable Mercedes and Klondike veins. As a result of these processes, geochemical zonation can not be used as a vector towards ore or as an evaluation of the erosion level or any other characteristic of the brecciated orebodies.

The highest grade material is associated with the porous, saccharoidal green quartz breccia formed during paragenetic Phase I mineralization and hematitic boxworks with texturally-controlled grade enhancement created during Phase IV oxidation favorable zones of high porosity and a chemistry favoring the destabilization of the complexed Au and Ag. The Au is now present largely as native Au and minimal amounts of high-fineness electrum, as implied by the poor correlations between Au and Ag grades. Ag is now present as cerargyrite, argentojarosite and a number of unidentified species that likely resulted from oxidation and remobilization of silver sulfides, sulfosalts and native metal. Very poor Au and Ag correlations within the relatively unmodified Lupita and Diluvio systems ($R=0.166$) compared with the slightly better, but not significant, correlations in the Mercedes and Klondike system ($R=0.517$ and 0.398 , respectively) hint at a relict vertical zonation to the Au and Ag. A spatial and mineralogical disconnection between Au and Ag would explain the poor correlation between the two in the Lupita/Diluvio system. The better correlation between Ag and Au at Mercedes and Klondike suggests redeposition of the precious metals was controlled by a single mechanism, enhancing the spatial and mathematical association between the two. This mechanism was apparently not efficient enough to generate a stronger statistical link.

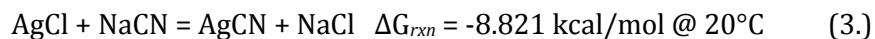
The fault-hosted nature of these veins suggests that the high-grade ore shoots reflect individual zones of tectonic depressurization and bonanza-grade precious Au-Ag deposition during multiple pressurization-depressurization events. The grade has been further enhanced with the selective destruction of relatively barren carbonate by supergene fluids as well as by the porosity of the high-grade breccias leading to a lower bulk density and thus a higher precious metal grade.

The chemical and physical modification of the ore body has a significant effect on the grade distribution within the Mercedes district. Ag: Au ratios are highly erratic, ranging from less than 1:1

to over 1000:1 with no discernible spatial pattern. The presence of cerargyrite and in association with the highest grade intervals and the spongy, hematite-associated coarse Au implies that supergene remobilization via acidic, chloride-containing fluids has reworked the Ag mineralization within the deposit (Saunders, 1993; Butt, 1998). Both Au and Ag are meta-stable as chloride complexes ($[\text{AgCl}_2]^-$ and $[\text{AuCl}_4]^-$) and susceptible to deposition in the presence of Fe^{2+} ions (Webster and Mann, 1984; Saunders, 1993) through the equations:



The products of these supergene processes have implications for recoveries of the precious metals as well. Ag recoveries on the property are in the neighborhood of 30% (M. Hawksworth, pers. communication). A number of possible causes related to both supergene and hypogene effects are plausible. Most likely, encapsulation within oxides and silica as a result of the precipitation of Fe-oxyhydroxides and argentojarosite during paragenetic Phase IV (see eq. 2) and replacement of calcite by saccharoidal quartz and recrystallization of chalcedonic quartz sequestering the Ag during Phase I are the causes behind the poor Ag recovery. It is also possible that the efficiency of the vat leach is poor regarding cerargyrite and argentojarosite dissolution (Sillitoe, 2009 and references therein), though the thermodynamics of the reaction for cerargyrite are somewhat favorable (T. Seal, pers. comm., 2013) as shown in eq. 3, below:



These supergene effects may also affect the economics of the Lupita/Diluvio system. Some textural features of the visible Au in Mercedes suggest enhancement of the grades resulting from supergene transport of Au and Ag from higher levels to zones of favorable chemistry for reprecipitation. (Webster and Mann, 1984; Butt, 1998). The lower amounts of permeability, reduced Fe⁺² content and exposure of the Lupita/Diluvio system do not present the same environment conducive to supergene enhancement that the Mercedes and Klondike veins possess. Further exacerbating this are the relative lack of brecciation and explosion textures in quartz in the Lupita/Diluvio system. In contrast to the Mercedes and Klondike systems, platy carbonate and variable ratio vapor+fluid inclusions within the veins suggest a more quiescent hydrothermal depositional environment for the precious metals resulting in a lack of bonanza ore grades (Sillitoe, 1993) during the hypogene mineralization.

There are indications that mineralization in all three zones may extend deeper than has been drilled, which bears on exploration potential. Long sections of the Mercedes and Klondike zones (Figs. 20 and 49) portray mineralization as dropping off at depth, but given the irregular nature of the higher-level mineralization, it is possible that further ore shoots are to be found at deeper levels. Mineralogical and textural indications of boiling are found in even the deepest samples examined in the Mercedes zone. Thus it seems likely that more ore-grade material exists at depth. The morphology of the Klondike vein seems to suggest that this is the case. The less extensive brecciation and limited fluid inclusion thermometry (Warren, 2008A) imply that the current Klondike exposures represent formation depths up to 500 m greater than the Mercedes vein.

The possibility and geometry of undiscovered mineralization is further complicated by the uncertainties regarding the nature of the fluid pathways. There appears to be a slight lateral zonation in Ag, Au, Mo and Hg within the Mercedes system, with Au, Mo and to a lesser extent Pb and Cu increasing towards the northwest and a drop in Ag and Hg. Using a classical zonation model for the distribution of elements within an epithermal system (Buchanan, 1981), this would indicate that the Barrancas/Lagunas zone represents a deeper level or source proximal zone of the Mercedes vein system. Conversely, this pattern can be interpreted as a supergene effect that is enhanced due to the sheared and permeable nature of the Barrancas/Lagunas zone. High-level relative depletion suggests that Hg may have been removed entirely in the higher elevations whereas less soluble Au, Ag, Cu and Pb complexes may have been leached from higher zones and redeposited within the remaining portions of the vein breccia. This interpretation is supported by the slight lateral depletion of Ca and enrichment of Mn consistent with the leaching and destruction of carbonate from Phase II calcite+Mn-oxide intergrowths that has been documented elsewhere on the Mercedes property. Thus, while the horizontal zonation present along the 3 km strike of the Mercedes vein may have some implications for further exploration, the true processes behind this zonation remain uncertain.

EXPLORATION IMPLICATIONS

As of 2013, exploration in the Mercedes district is ongoing. Both modern discoveries and historic production show that epithermal mineralization is widespread in the region. The conclusions drawn by this thesis have direct implications on the continuing exploration within the district and in the surrounding region. High-grade mineralization is controlled through structural and subordinate textural preparation born of the oblique-normal tectonic regime of the vein systems. The complex structural story allows for a number of targets, including blind veins, sheared extensions of the main veins, anastomosing stockworks or cross-over zones with bulk-tonnage potential and dilatational bonanza shoots. The likelihood of further mineralization at depth in Mercedes and Klondike suggests that historic workings on the other veins on the property may not have exhausted ore., it may well be worth revisiting the limited exploration core from these zones and including those veins in future drill programs with an eye for structural and textural indicators that may reveal the presence of high-grade zones at depths beyond what has been explored. In particular, the supergene effects on the precious metal distributions have not been taken into account in exploration targeting models, and incorporating the repercussions of this concept into these models may prove useful to reevaluating the district.

Additionally, the oblique kinematics of the Mercedes and Klondike faulting suggests that mineralized structures may exist in orientations that would run parallel or sub-parallel to the pattern of the exploration drilling that defined the Mercedes and Klondike veins. More detailed structural mapping may reveal the presence of structures that have not been intersected by the drilling due to their unfavorable orientation. Any such structures found may have economic mineralization, especially given the probable dilatational nature of their formation.

While the southern parts of the district appear to be moderately dissected, the widespread propylitic alteration in the andesite packages allows for a significant probability that blind veins or unknown offshoots of the main veins exist. Veins may also exist under the post-mineral latite and platy andesite volcanic cover. Projections of the Mercedes and Klondike trends under these units, as well as vectoring using structural indications of faulting at the surface and detailed mapping of the propylitic alteration could reveal further mineralization under these units.

SUGGESTIONS FOR FUTURE WORK

This study provides the first detailed look at the geology, geochemistry and structure of the Mercedes district but it is by no means an exhaustive survey of the mining camp. Additional framework studies of the volcanic stratigraphy, relative timing verification of the correlations between the Mercedes units and the regional volcanic sequence could aid in locating similarly productive areas.

Little detailed work has been done on the nature of the alteration halos surrounding the veins. The underground drilling program currently under way could provide samples for characterizing the effects of hydrothermal circulation on the host andesites that could provide geochemical or mineralogical vectors towards blind ore shoots.

Work on the mineralogy of the precious metals within the veins would help illuminate the deportment of the Au and Ag and the reasons for the poor silver recoveries. Systematic XRD crystallography and electron microscopy of the high grade ore would be the best approach. More detailed fluid inclusion thermometry would help to identify the depth of formation, the possible extent of mineralization and the sequence of hydrothermal events that formed the ore mineralization as well as the amount of exhumation that has occurred in each of the areas.

Finally, regional and district-scale structural studies of the Mercedes district would prove highly useful for identifying further zones of favorable weaknesses that could host veins beneath the post-mineralization Baucarit, andesite and ignimbrite sequences as well as identify other accommodation/step-over zones in the region that may also host paleohydrothermal systems with economic mineralization. Integrating the regional study with age dates of volcanics in the region, focusing on the timeframe between 30 and 25 Ma may prove especially fruitful.

The work this thesis presents is only the first look at the unique hydrothermal system of the Mercedes district. The findings presented here are meant to help guide the exploration and research into this productive district, with the hopes that many more ounces of Au and Ag will be found and exploited.

REFERENCES

-
- Adams, S.F. (1920) **A Microscopic Study of Vein Quartz.** *Economic Geology*. v. 15 no. 8 pp. 623-644.
- Alba Pascoe, J.A. (1998) **Current situation and prospectives of the Santa Gertrudis mining district, Municipality of Cucurpe, Sonora.** *Society of Economic Geologists Guidebook Series*. no. 30 pp. 21-34.
- Albinson, T. et al. (2001) **Controls on Formation of Low-Sulfidation Epithermal Deposits in Mexico: Constraints from Fluid Inclusion and Stable Isotope Data.** Society of Economic Geologists Special Publication 8: New Mines and Discoveries in Central America. pp. 1-32.
- Anderson, T.H. and Silver, L.T. (2005) **The Mojave-Sonora Megashear--Field and analytical studies leading to the conception and evolution of the hypothesis.** *The Mojave-Sonora Megashear Hypothesis: Development, Assessment and Alternatives*. Geological Society of America Special Paper 393, pp. 1-50.
- Anderson, T.H., and Silver, L.T. (1977) **U-Pb Isotope Ages of Granitic Plutons near Cananea, Sonora.** *Economic Geology*. v. 72 pp. 827-836.
- Begbie, I and Lawless, J.V. (2001) **Precipitation of Gold in a Low-Sulfidation Epithermal Deposit: Insights from Submillimeter-scale Oxygen Isotope Analysis of Vein Quartz—A Discussion.** *Economic Geology*. v. 96 pp. 1701-1703. Discussing Hayashi et al., 2001. *Economic Geology*. v. 96 pp. 211-216.

- Begbie, M.J. et al. (2001) **Structural Evolution of the Golden Cross Epithermal Au-Ag Deposit, New Zealand.** *Economic Geology*. v. 102 pp. 873-892.
- Berger, B.R., and Silberman, M.L. (1985) **Relationships of Trace-Element Patterns to Geology in Hot-spring Type Precious-Metal Deposits.** *Reviews in Economic Geology—Volume 2: Geology and Geochemistry of Epithermal Systems*. pp. 233-246.
- Boise State, Prepared for I. Warren. (2008). **Report of Investigation.** Unpublished internal document, Yamana Gold. Accessed 8 July 2012. Boise State University Isotope Geology Laboratory
- Brown, K.L. (1986) **Gold deposition from geothermal discharges in New Zealand.** *Economic Geology*. v. 81 no. 4 pp. 979-983.
- Buchanan, L.J. (1981). **Precious metal deposits associated with volcanic environments in the southwest.** In Dickenson, W.R. and Payne, W.D., Eds. *Relations of Tectonics to Ore Deposits in the Southern Cordillera. Arizona Geological Society Digest XIV*. pp. 237-262.
- Butt, C.R.M. (1998) **Supergene gold deposits.** *Journal of Australian Geology & Geophysics*. v. 14 no. 4 pp. 89-98
- Camprubi, A. and Albinson, T. (2007) **Epithermal deposits in Mexico-Update of current knowledge and an empirical reclassification.** The Geological Society of America, Special Paper 422-Geology of Mexico: Celebrating the Centenary of the Geological Society of Mexico. pp. 377-415.

- Camprubi, A. et al. (2003) **Ages of Epithermal Deposits in Mexico: Regional Significance and Links with the Evolution of Tertiary Volcanism.** *Economic Geology*. v. 98 no. 5 pp. 1029-1037
- Centeno-Garcia, E. et al., (2008). **The Guerrero Composite Terrane of western Mexico: Collision and subsequent rifting in a supra-subduction zone.** The Geological Society of America Special Paper 436.
- Chiaradia, M. et al., (2013) **How Accurately Can We Date the Duration of Magmatic-Hydrothermal Events in Porphyry Systems?—An Invited Paper.** *Economic Geology*. v. 108 no. 4 pp. 585-604
- Christie, A.B. et al. (2007) **Epithermal Au-Ag and Related Deposits of the Hauraki Goldfield, Coromandel Volcanic Zone, New Zealand.** *Economic Geology*. v. 102 no. 5 pp. 785-816.
- Cooke, D.R. et al. (2005) **Giant porphyry deposits; characteristics, distribution, and tectonic controls (in: A special issue devoted to giant porphyry-related mineral deposits)** *Economic Geology*. vol. 100 no. 5 pp. 801-818.
- Cooke, D.R. and Simmons, S.F. (2000) **Characteristics and Genesis of Epithermal Gold Deposits:** *Reviews in Economic Geology—Volume 13: Gold in 2000.*, p. 221-244.
- Damon, P.E. et al. (1983) **Geochronology of the porphyry copper deposits and related mineralization of Mexico.** *Canadian Journal of Earth Sciences*. v. 20 no. 6 pp. 1052- 1071.
- Dong, G. et al. (1995) **Quartz Textures in Epithermal Veins, Queensland-Classification, Origin and Implication.** *Economic Geology*. v. 90 no. 6 pp. 1841-1856

- Echavarría, L. et al. (2006) **Geologic Evolution of the Caylloma Epithermal Vein District, Southern Peru.** *Economic Geology*. v. 101 pp. 842-863.
- Faulds, J. E. et al. (2011) **Assessment of Favorable Structural Settings of Geothermal Systems in the Great Basin, Western USA.** *Transactions of the Geothermal Reference Council*. v. 35 pp. 777-783
- Ferrari, L. et al. (2007). **Magmatism and tectonics of the Sierra Madre Occidental and its relation with the evolution of the western margin of North America.** The Geological Society of America, Special Paper 422-Geology of Mexico: Celebrating the Centenary of the Geological Society of Mexico. pp. 1-39
- Franchini, M. et al. (2011) **Porphyry to epithermal transition in the Agua Rica polymetallic deposit, Catamarca, Argentina: An integrated petrologic analysis of ore and alteration parageneses.** *Ore Geology Reviews*. v. 41 no. 1 pp. 49-74.
- Gemmell, J.B. (2004) **Low- and intermediate-sulfidation epithermal deposits.** *CODES Special Publication 5—24 ct Au Workshop*. pp. 57-65.
- Glazner, A.F. (1980) **Frequency distribution of plagioclase extinction angles: precision of the Michel-Levy technique.** *American Mineralogist*. v. 65 no. 9-10 pp. 1050-1052.
- Goodell, P.C. and Petersen, U. (1974) **Julcani Mining District, Peru: A Study of Metal Ratios.** *Economic Geology*. v. 69 pp. 347-361.

Hawksworth, M.A. et al. (2009). **Geology and Low Sulfidation Epithermal Au-Ag Vein Mineralization of the Mercedes Area, Sonora, Mexico.** Unpublished internal manuscript, Yamana Gold Company.

Heald, P. et al. (1987). **Comparative Anatomy of Volcanic-Hosted Epithermal Deposits: Acid-Sulfate and Adularia-Sericite Types.** *Economic Geology*. v. 82 no. 1 pp. 1-26.

Hayaba, D.O. et al. (1985) **Geologic, Mineralogic, and Geochemical Characteristics of Volcanic-Hosted Epithermal Precious Metal Deposits.** *Reviews in Economic Geology Vol. 2—Geology and Geochemistry of Epithermal Systems*. pp. 129-167.

Henry, C., and Aranda-Gomez, J. (1992). **The real southern Basin and Range: Mid- to late Cenozoic extension in Mexico.** *Geology*, vol. 20 pp. 701-704.

Henry, C.D. (1986) **East-northeast trending structures in western Mexico: Evidence for oblique convergence in the late Mesozoic.** *Geology*. v. 14 pp. 314-317.

Holcombe, R. (2011) **GEORient Software v. 9.5.0.** Version Date: 29 January 2011, accessed August 2012.
<http://www.holcombecoughlinoliver.com/holcombe>.

Hudson, D.M. (2003) **Epithermal Alteration and Mineralization in the Comstock District, Nevada.** *Economic Geology*. v. 98 pp. 367-385.

Itoh, J. et al. (2002) **Bladed Quartz and its Relationship to Gold Mineralization in the Hishikari Low-Sulfidation Epithermal Gold Deposit, Japan.** *Economic Geology*. v. 97 no. 8 pp. 1841-1851.

- Gonzalez-Leon, C.M. et al. (2000) **Cretaceous and Tertiary sedimentary, magmatic and tectonic evolution of north-central Sonora (Arizpe and Bacanuchi Quadrangles), northwest Mexico.** *GSA Bulletin*. v. 112 no. 4 pp. 600-610.
- Fossen, H. et al. (2010) **Fault linkage and graben stepovers in the Canyonlands (Utah) and the North Sea Viking Graben, with implications for hydrocarbon migration and accumulation.** *AAPG Bulletin*. v. 94 no. 5 pp. 597-613.
- Leavitt, E.D. et al. (2004) **Geochronology of the Midas Low-Sulfidation Epithermal Gold-Silver Deposit, Elko County, Nevada.** *Economic Geology*. v. 99 no. 8 pp. 1665-1686.
- Lewis, W.J. (2005) **Technical Report on the San Francisco Mine Property, Estacion Llano Sonora, Mexico.** National Instrument 43-101 filing. Accessed 3 April 2013.
- Loucks, R.R. et al. (1988) **Polymetallic Epithermal Fissure Vein Mineralization, Topia, Durango, Mexico: Part I. District Geology, Geochronology, Hydrothermal Alteration and Vein Mineralogy.** *Economic Geology*. v. 83 no. 8 pp 1499-1529.
- Michel-Levy, A. (1894) **Etude sur la determination de feldspathes.** *Librairie Polytechnique du Paris*.
- McDowell, F.W., and Clabaugh, S.E. (1981) **The Igneous History of the Sierra Madre Occidental and its Relation to the Tectonic Evolution of Western Mexico.** *Revista-Instituto de Geologia*. v. 5 no. 2 pp. 195-206.

- McDowell, F.W. and Keizer, R.P. (1977) **Timing of mid-Tertiary volcanism in the Sierra Madre Occidental between Durango City and Mazatlan, Mexico.** *GSA Bulletin*. v. 88, pp. 1479-1487.
- Molina-Garza, R.S. and Iriondo, A. (2007) **The Mojave-Sonora megashear: The hypothesis, the controversy and the current state of knowledge.** The Geological Society of America, Special Paper 422-Geology of Mexico: Celebrating the Centenary of the Geological Society of Mexico. pp.233-259
- Moncada, D. et al. (2012) **Mineral textures and fluid inclusion petrography of the epithermal Au-Ag deposits at Guanajuato, Mexico: Application to exploration.** *Journal of Geochemical Exploration*. v. 114 pp. 20-35
- Noble, A. et al. (2010) **Technical Report and Resource Estimate on the Santa Gertrudis Gold Project, Sonora Mexico.** Animas Resources Ltd. National Instrument 43-101 filing. Accessed: 12 February 2013.
- Railsback, L.B. (2003) **An earth scientist's periodic table of the elements and their ions.** *Geology*. v. 31 no. 9.
- Randall R., J.A. et al. (1994) **Exploration in a Volcano-Plutonic Center at Guanajuato, Mexico.** *Economic Geology*. v. 89 no. 8 pp. 1722-1751.
- Robb, L. (2005) **Introduction to Ore-Forming Processes.** Blackwell Science Ltd. 373 pp.
- Ruvalcaba-Ruiz, D.C., and Thompson, T.B. (1988) **Ore Deposits at the Fresnillo Mine, Zacatecas, Mexico.** *Economic Geology*. v. 83 no. 8 pp. 1583-1596.

- Sander, M.V. and Black, J.E. (1988) **Crystallization and Recrystallization of Growth-Zoned Vein Quartz Crystals from Epithermal Systems-Implications for Fluid Inclusion Studies.** *Economic Geology*. v. 83 no. 5 pp. 1052-1060.
- Saunders, J.A. (1993) **Supergene oxidation of bonanza Au-Ag veins at the Sleeper Deposit, Nevada, USA: implications for hydrogeochemical exploration in the Great Basin.** *Journal of Geochemical Exploration*. no. 47 pp. 359-375.
- Schwertmann, U. and Cornell, R.M. (2000) **Iron Oxides in the Laboratory: Preparation and Characterization. 2nd Ed.** Wiley. 183 pp.
- Servicio Geologico Mexicano (1999) **Carta Geologico-Minera Saracachi H12-B72 Sonora.** Scale 1:50,000.
- Sibson, R.H. (1987) **Earthquake rupturing as a mineralizing agent in hydrothermal systems.** *Geology*. v. 15 pp. 701-704.
- Simmons, S.F. and Christenson, B.W. (1994) **Origins of Calcite in a Boiling Geothermal System.** *American Journal of Science*. v. 294 pp. 361-400.
- Simmons, S.F. et al. (2005) **Geological Characteristics of Epithermal Precious and Base Metal Deposits.** *Economic Geology 100th Anniversary Volume*. pp. 485-522.

- Silberman, M.L. and Berger, B.R. (1985) **Relationship of Trace-element Patterns to Alteration and Morphology in Epithermal Precious-metal Deposits.** *Reviews in Economic Geology—Volume 2: Geology and Geochemistry of Epithermal Systems.* pp. 203-230.
- Sillitoe, R.H. (1993) **Giant and Bonanza Gold Deposits in the Epithermal Environment: Assessment of Potential Factors.** *Society of Economic Geologists—Special Publication 2: Giant Ore Deposits.* pp. 125-156.
- Sillitoe, R.H. (2009) **Supergene Silver Enrichment Reassessed.** *Society of Economic Geologists—Special Publication 14: Supergene Environments, Products and Processes.* pp. 15-32.
- Sillitoe, R.H. and Hedenquist, J.W. (2003) **Linkages between Volcanotectonic Settings, Ore-Fluid Compositions, and Epithermal Precious Metal Deposits.** *Society of Economic Geologists—Special Publication 10: Volcanic, Geothermal, and Ore-Forming Fluids: Rulers and Witnesses of Processes within the Earth.* pp. 315-343.
- Spörli, K.B. and Cargill, H. (2011) **Structural Evolution of a World-Class Epithermal Orebody: The Martha Hill Deposit, Waihi, New Zealand.** *Economic Geology.* v. 106 pp. 975-998.
- Suter, M. (2001) **The historical seismicity of northeastern Sonora and northwestern Chihuahua, Mexico (28-32°N, 106-111° W).** *Journal of American Earth Sciences.* v. 14 pp. 521-532.
- Tingley, J.V. and Bonham, Jr., H.F. (1986) **Precious-metal Mineralization in Hot Springs Systems, Nevada-California.** *Nevada Bureau of Mines and Geology Report 41.*

- Turner, R.L. et al. (1982) **Regional Northeast-Trending Structural Control of Mineralization, Northern Sonora, Mexico.** *Economic Geology*. v. 77 no. 1 pp. 25-37.
- Valencia, V.A. et al. (2008) **Hydrothermal Evolution of the Porphyry Copper deposit at La Caridad, Sonora, Mexico, and the Relationship with a Neighboring High-Sulfidation Epithermal Deposit.** *Economic Geology*. v. 103 no. 3 pp. 473-491.
- Varga, R.J. et al. (2000) **Miocene extension and extensional folding in an anticlinal segment of the Black Mountains accommodation zone, Colorado River extensional corridor, southwestern United States.** *Tectonics*. v. 23 19 pgs.
- Warren, I. (2008A). **Memorandum: Fluid inclusion analyses of quartz from the Mercedes and Klondike veins.** Unpublished internal document, Yamana Gold.
- Warren, I. (2008B) **Memorandum: Geochemical and alteration vectors to mineralized veins at Mercedes.** Unpublished internal document, Yamana Gold.
- Webster, J.G. and Mann, A.W. (1984) **The influence of climate, geomorphology and primary geology on the supergene migration of gold and silver.** *Journal of Geochemical Exploration*. v. 22 pp. 21-41.
- Weissberg, B.G. (1969) **Gold-Silver Ore-Grade Precipitates from New Zealand Thermal Waters.** *Economic Geology*. v. 64 pp. 95-108.

White, N.C., Hedenquist, J.W. (1990) **Epithermal environments and styles of mineralization: variations and their causes, and guidelines for exploration.** *Journal of Geochemical Exploration*. v. 36 pp. 445-474.

Wodzicki, W.A. (2001) **The Evolution of Magmatism and Mineralization in the Cananea District, Sonora, Mexico.** Society of Economic Geologists Special Publication 8: New Mines and Discoveries in Central America. pp. 243-263.

Yamana Exploration Staff (2012) **Yamana Unpublished Mapping Geodatabase.** Accessed July, 2012. Unpublished.

Yamana Gold Mineral Reserve and Mineral Resource Estimates as of December 31, 2011

<http://www.yamana.com/Operations/ReservesAndResources>, retrieved 10 January, 2013.

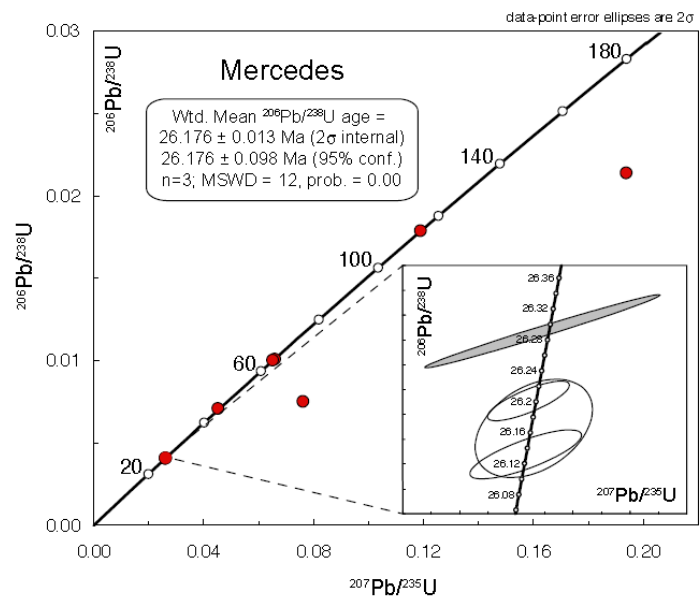
APPENDICES

I. Boise State U-Pb Date

Sample	Compositional Parameters										Radiogenic Isotope Ratios					Isotopic Ages							
	Wt. mg	U ppm	Th U	Pb ppm	$^{206}\text{Pb}^*$ $\times 10^{-11}$ mol	mol % $^{206}\text{Pb}^*$	Pb^*/Pb_c	Pb_c (pg)	$^{206}\text{Pb}/^{207}\text{Pb}$	$^{206}\text{Pb}/^{208}\text{Pb}$	$^{206}\text{Pb}/^{209}\text{Pb}$	% err	$^{206}\text{Pb}/^{238}\text{U}$	% err	$^{206}\text{Pb}/^{235}\text{U}$	% err	corr. coef.	$^{206}\text{Pb}/^{206}\text{Pb}$	$^{206}\text{Pb}/^{238}\text{U}$	$^{206}\text{Pb}/^{235}\text{U}$	$^{206}\text{Pb}/^{238}\text{U}$	$^{206}\text{Pb}/^{235}\text{U}$	$^{206}\text{Pb}/^{238}\text{U}$
(a)	(b)	(c)	(d)	(c)	(e)	(e)	(e)	(e)	(f)	(g)	(g)	(h)	(g)	(h)	(g)	(h)		(i)	(h)	(i)	(h)	(i)	(h)
z1	0.009	289	0.400	2.4	0.8425	99.27%	44	0.51	2563	0.198	0.073412	0.147	0.076149	0.197	0.007523	0.068	0.810	1025.33	297	74.52	0.14	48.32	0.03
z2	0.008	227	0.777	1.1	0.3224	97.43%	12	0.70	723	0.230	0.046383	1.229	0.026123	1.291	0.004067	0.199	0.382	27.88	29.43	26.18	0.33	26.17	0.05
z3	0.006	375	0.833	1.9	0.3676	97.22%	12	0.86	669	0.267	0.046452	0.841	0.026085	0.903	0.004073	0.080	0.793	21.16	20.17	26.15	0.23	26.20	0.02
z4	0.006	322	0.629	3.9	0.7929	96.36%	8	2.46	511	0.202	0.047335	1.066	0.063878	1.138	0.010094	0.103	0.723	66.16	25.36	64.78	0.71	64.74	0.07
z5	0.006	1124	0.256	24.5	5.5207	99.67%	89	1.30	5640	0.108	0.065720	0.128	0.193807	0.200	0.021388	0.086	0.898	797.46	2.69	179.87	0.33	136.42	0.12
z6	0.003	387	0.577	4.5	0.5189	97.43%	12	1.13	723	0.184	0.047118	0.756	0.069097	0.813	0.010020	0.082	0.717	55.21	18.03	64.04	0.50	64.27	0.05
z7	0.004	259	0.887	1.3	0.1690	96.23%	9	0.54	494	0.285	0.046541	1.155	0.026066	1.231	0.004062	0.099	0.787	25.76	27.67	26.13	0.32	26.13	0.03
z8	0.001	895	0.217	16.6	0.8168	97.78%	12	1.53	837	0.069	0.048239	0.636	0.118985	0.691	0.017889	0.105	0.585	111.02	15.00	114.15	0.75	114.30	0.12
z10	0.003	271	0.784	1.5	0.1281	93.31%	5	0.76	278	0.252	0.046468	2.441	0.026184	2.586	0.004087	0.147	0.989	21.95	38.50	26.24	0.67	26.29	0.04
z12	0.002	214	0.328	1.9	0.1422	93.31%	4	0.84	278	0.104	0.046196	2.197	0.045157	2.324	0.007090	0.174	0.748	7.85	52.82	44.85	1.02	45.54	0.08

(a) z1, z2 etc. are labels for fractions composed of single zircon grains or fragments; all fractions annealed and chemically abraded after Mattinson (2005).
(b) Nominal fraction weights estimated from photomicrographic grain dimensions, adjusted for partial dissolution during chemical abrasion.
(c) Nominal U and total Pb concentrations subject to uncertainty in photomicrographic estimation of weight and partial dissolution during chemical abrasion.
(d) Model Th/U ratio calculated from radiogenic $^{206}\text{Pb}/^{206}\text{Pb}$ ratio and $^{207}\text{Pb}/^{235}\text{U}$ age.
(e) Pb^* and Pb_c represent radiogenic and common Pb, respectively; mol % $^{206}\text{Pb}^*$ with respect to radiogenic, blank and initial common Pb.
(f) Measure ratio corrected for spike and fractionation only. Mass fractionation correction of 0.22 ± 0.02 (1-sigma) ‰/amu (atomic mass unit) was applied to all single-collector Daly analyses, based on analysis of NBS-981 and NBS-982.
(g) Corrected for fractionation, spike, and common Pb; all common Pb was assumed to be procedural blank; $^{206}\text{Pb}/^{204}\text{Pb} = 18.60 \pm 0.80\%$; $^{207}\text{Pb}/^{204}\text{Pb} = 15.69 \pm 0.32\%$; $^{208}\text{Pb}/^{204}\text{Pb} = 38.51 \pm 0.74\%$ (all uncertainties 1-sigma).
(h) Errors are 2-sigma, propagated using the algorithms of Schmitz and Schoene (2007) and Crowley et al. (2007).
(i) Calculations are based on the decay constants of Jaffey et al. (1971). $^{206}\text{Pb}/^{238}\text{U}$ and $^{207}\text{Pb}/^{206}\text{Pb}$ ages corrected for initial disequilibrium in $^{230}\text{Th}/^{238}\text{U}$ using Th/U [magma] = 3.

Appendix II-1. Raw data, zircons, Platy Andesite, Boise State, 2008.



Appendix II-2. Concordia diagram for samples from Appendix II-1. Orange dots represent the individual samples.

III. Geochemical Data

File #	Sample #	Depth From	Depth To	Section	Elev	FA.Ag	FA.As	Ba	Bi	Cs	Cu	Fe	Ga	Hg	Mn	Mo	Pb	Sb	Tl	Zn	C'	S'	
		m	m		m	ppm	ppm	ppm	ppm	ppm	ppm	ppm	ppm	ppm	ppm	ppm	ppm	ppm	ppm	ppm	ppm	ppm	
M08-38SD	ME-123630	152.4	153.92	8880	1022	51.7	0.609	6.7	790	0.2	20600	21.6	15800	17.75	0.3	643	1.38	36.7	45.6	1.6	81	8800	100
M08-38SD	ME-123631	154.92	154.82	8880	1021	108	0.114	17.2	730	0.23	43900	18.7	19900	14.7	0.55	1270	4.1	147	65.6	2.2	138	16500	100
M08-38SD	ME-123632	155.45	155.45	8880	1020	137	1	11.5	140	0.34	68700	14.8	7700	4.63	0.48	1260	1.23	127.5	208	0.46	79	22600	100
M08-38SD	ME-123633	155.45	156.53	8880	1019	280	7.84	72	610	1	26700	86	18100	10	1.16	1495	4	88	132	5	230	0	0
M08-38SD	ME-123637	156.97	158.5	8880	1018	95.1	0.791	186.5	700	1.28	3300	67.1	28400	19.8	1.16	913	11.85	52.5	74.6	5.26	107	8000	100
M08-38SD	35128427	234.27	234.4	8880	921	189	11.1	70	180	0.05	22100	58.5	12400	5.62	0.3	494	4.28	467	304	1.11	856	8400	400
M08-286D	28653735	537.35	537.55	8880	653	<5	0.13	93.7	700	0.01	4500	35.5	43300	23.6	0.19	735	0.35	7.1	25.9	3.43	71	2300	9400
M08-286D	28653498	534.98	535.1	8880	655	<5	0.09	119	670	0.01	30200	44.9	37600	20	0.49	1520	0.5	17.3	30.1	2.83	113	11800	8900
M08-071R	M71-44	43.69	44.7	9550	1103	49	1.2	64.4	190	0.03	700	38.5	11300	4.25	0.48	141	9.9	18.2	237	0.73	81	2900	300
M08-071R	M71-45	44.7	45.72	9550	1102	102	7.53	32.1	30	0.01	400	39	7800	4.55	0.51	143	7	54	138.5	0.15	66	2100	100
M08-071R	M71-46	45.72	46.74	9550	1101	47	2.23	114	130	0.02	400	27.1	10800	5.33	0.61	894	6.92	21.4	300	2.04	58	1900	1200
M07-83D	8318228	182.28	182.41	9550	1009	180	3.89	174	470	0.04	38700	63	22300	18.1	0.29	136	0.65	25.7	133	2.25	166	13500	100
M07-83D	8318229	182.49	182.79	9550	1009	228	2.55	227	750	0.06	19900	56.6	27100	22.6	3.2	390	0.69	22.8	89.8	4.02	161	7700	900
M07-83D	8318345	183.45	183.49	9550	1009	103	0.51	37	220	0.01	139000	31.8	5300	2.89	0.95	7330	0.79	10.3	27.3	0.44	58	112500	200
M07-189D	ME110455	249.67	249.1	9550	935.8	303	1.08	167.5	360	0.05	2100	31.2	16800	13.2	0.5	241	0.7	10.4	496	2.32	114	2200	300
M07-189D	ME110456	240.1	240.79	9550	935.3	707	8.73	92.2	200	0.02	17300	41.4	13300	9.67	3.1	819	0.55	81.3	332	1.33	325	7700	100
M07-189D	ME110457	240.79	241.87	9550	934.5	698	51.8	113.5	80	0.02	4200	221	10900	9.09	3.6	410	0.57	396	474	0.53	390	2800	200
M07-189D	ME110458	241.87	242.58	9550	933.7	586	341	265	30	0.09	700	837	37200	5.67	5.8	51	1.01	3760	687	0.07	679	2900	7800
M07-189D	ME110459	242.58	243.28	9550	933.1	955	223	163.5	70	0.02	700	361	25000	6.15	6.3	54	0.66	1825	532	0.3	416	1600	3500
M07-189D	ME110460	243.28	243.84	9550	932.5	374	398	273	70	0.03	14700	2200	23600	5.04	9.8	2480	1.91	3600	1080	0.21	4080	6400	400
M07-189D	ME110461	244.26	244.26	9550	932.1	272	496	196.5	30	0.06	6700	694	36500	3.54	5.7	827	0.87	1935	619	0.18	2460	4000	200
M07-189D	ME110462	244.26	244.76	9550	931.7	450	70.1	78	110	0.01	133500	203	15200	2.68	2.9	4450	0.57	962	289	0.27	1120	43500	400
M07-189D	ME110464	245.71	246.65	9550	930.2	601	5.06	103	180	0.02	3300	94.2	13700	16.3	3	302	0.84	201	238	0.87	902	2000	100
M07-189D	ME110470	248.02	249.39	9550	928	165	0.46	118.5	1010	0.06	3200	44	34200	19.75	0.3	316	0.46	28.9	42.2	3.68	149	1700	100
M07-189D	ME110473	251.19	252.08	9550	925.4	43	0.13	98.6	970	0.05	13100	36.5	94300	21.6	0.2	719	0.35	23.5	37.5	4.59	282	4400	100
M07-91D	912591	259.31	259.21	9550	892	314	95.7	207	80	0.02	3500	552	18200	8.9	0.6	251	1.59	1250	425	0.26	1620	3400	700
M07-91D	912594	259.31	259.36	9550	793	21	0.17	11.9	42000	0.6	31200	23.3	18700	10.8	0.19	3120	0.08	27.4	7.8	4.45	76	14700	100
M07-91D	9125466	354.66	354.86	9550	790	8	0.84	125.5	680	0.03	37800	35.7	29800	19.45	0.6	1580	3.31	21.2	76.4	3.54	85	13600	100
M08-439D	4195710	57.1	57.2	9100	1097	<5	0.07	54.7	290	0.05	41100	29.7	29700	20.1	0.17	589	0.45	13.5	27.1	3.41	68	14800	100
M08-314D	ME-119492	147	148.24	9100	996	27	1.24	206	770	0.02	2100	89.2	11600	6.42	0.6	490	0.42	12.5	47.6	0.56	390	1000	100
M08-314D	ME-119493	148.24	149.35	9100	995	66	1.67	65.6	210	0.02	82400	15.2	8800	7.55	0.48	1570	0.32	31.9	285	1.15	71	26000	100
M08-314D	ME-119494	149.35	149.99	9100	995	25	0.46	65.8	240	0.02	97200	12.4	11200	5.32	0.61	2810	1.2	10.3	188	0.86	43	31300	200
M08-315D	ME119527	172.1	172.1	9100	943	69	4.2	64.2	11700	0.6	6430	106.2	7	4.52	199	0.83	0.32	328	3500	200	100	100	100
M08-315D	ME119529	174.2	175.26	9100	943	69	2.72	26	100	0.01	62000	24.7	8400	6.36	0.8	2050	1.18	29	400	0.59	57	20200	200
M08-315D	ME119530	175.26	176.24	9100	942	38	2.33	42.4	30	0.005	46600	7.2	10800	4.15	0.5	1160	0.88	9.7	376	0.12	21	18400	200
M08-315D	ME119531	177.02	177.02	9100	941	18	0.02	99	1020	0.01	84900	6.7	17700	3.93	1.11	3300	0.86	10.1	188.8	0.47	20	34600	100
M08-074R	M74-17	16.25	17.27	8860	1089	45	0.2	49.4	410	0.03	3300	55.5	20800	11.65	0.53	471	1.87	4.2	367	2.62	81	1100	100
M08-074R	M74-18	17.27	18.28	8860	1088	55	1.48	43.5	400	0.02	42800	20.2	16600	9.64	0.42	1110	1.37	16.7	263	2.18	54	12700	100
M08-074R	M74-19	18.28	19.3	8860	1088	28	0.23	219	840	0.14	5100	23.9	31700	33	0.29	491	0.35	7.3	34	5.94	32	1000	100
M08-074R	M74-20	19.3	20.32	8860	1087	19	1.17	74.3	610	0.03	7700	22.6	24300	17.25	0.39	1650	0.79	15.2	170	3.45	74	2000	50
M08-324D	ME-117348	95.36	96.42	8860	1011	95	2.5	80.4	200	0.01	71700	47	10800	8.55	0.8	1870	0.51	64.8	515	0.49	82	23200	200
M08-324D	ME-117349	96.42	97.42	8860	1010	41	1.5	84	130	0.005	222000	8	13500	2.02	1.16	3970	0.48	9.9	89.2	0.08	51	93400	300
M08-324D	ME-117350	97.42	98.75	8860	1009	101	2.55	74.1	190	0.01	69500	30.2	10200	10.6	0.92	1940	0.35	42.5	367	0.61	105	22800	200
M08-227D	ME-112644	297.13	297.63	8860	936	51	0.51	279	1050	0.05	8500	43.1	37100	23.5	0.73	408	0.34	20.7	51.5	6.58	92	1800	50
M08-227D	ME-112645	297.63	298.54	8860	936	143	1.11	202	360	0.04	88800	30	22800	7.28	2.02	4210	0.53	17.5	178	2.31	69	41500	200
M08-227D	ME-112646	298.54	299.58	8860	935	139	2.37	84.2	250	0.02	70300	23.9	13600	6.45	1.1	2340	0.41	16.7	236	0.96	53	22100	300
M08-227D	ME-112650	299.58	240.18	8860	935	117	0.025	159	880	0.16	6200	30.8	34300	22.5	0.45	818	0.25	7.7	36.8	6.48	61	1300	50
M08-227D	ME-112651	240.18	241.68	8860	934	40	0.23	219	840	0.14	5100	23.9	31700	33	0.29	491	0.35	7.3	34	5.94	32	1000	100
M08-227D	ME-112652	241.68	243.23	8860	933	2.5	0.18	203	980	0.08	5200	24.6	33200	22.9	0.35	725	0.28	11.8	36.2	1.15	55	2500	100
M10-589D	ME-146605	218.54	219.76	11950	1019.2	39.6	0.708	188	1010	0.02	6000	48.7	38700	17.05	0.34	1990	1.74	41.3	54.4	3.77	133	2000	400
M10-589D	ME-146606	220.23	220.98	11950	1018.16	189	10.6	67.6	270	0.06	2200	237	12700	7.3	1	7110	1.58	682	397	0.74	554	2100	200
M10-589D	ME-146607	220.98	221.59	11950	1017.59	53	0.468	92.1	360	0.03	3500	77.9	26800	9.12	0.23	1980	1.76	21.1	135	1.39	183	2200	200
M10-589D	ME-146608	221.59	222.81	11950	1016.96	22.8	0.337	128.3	740	0.06	6900	40.1	50000	18.4	0.14	888	2.38	14.8	37.9	1.45	137	1800	500
M11-600D	ME-145896	261.06	261.06																				

Hole #	Sample #	Depth From m	Depth To m	Section	Elev m	FA-Ag ppm	FA-Au ppm	As ppm	Ba ppm	Bi ppm	Ca ppm	Cu ppm	Fe ppm	Ga ppm	Hg ppm	Mn ppm	Mo ppm	Pb ppm	Sb ppm	Tl ppm	Zn ppm	C ppm	S ppm
K08-79D	K799987	99.87	100.25	11080	1142	31	5.41	91	1170	0.01	168500	117.5	10000	4.44	0.34	10050	8.33	622	122	2.45	484	53800	100
K08-081D	KR-104089	127.1	128.3	11080	1100	12	4.19	324	980	0.11	3100	110	43700	22.2	0.42	1580	2.57	41.1	20	6.56	444	600	50
K08-081D	KR-104090	128.3	129.01	11080	1099	25	7.46	124.5	820	0.05	55700	255	21400	10.85	0.66	7160	9.45	826	131	4.44	827	16800	100
K08-081D	KR-104094	129.01	130	11080	1098	24	0.68	166.5	870	0.03	3100	135	34500	16.25	0.56	1380	2.5	75.7	37.1	5.78	511	800	100
K08-081D	KR-104095	130	131.06	11080	1097	37	1.99	147.5	900	0.02	13100	79.4	34400	16.1	0.67	2480	5.1	82	36.7	5.32	312	3800	50
K08-081D	KR-104096	131.06	132	11080	1096	40	0.89	158.5	940	0.02	3600	42.6	36900	22	0.9	2480	8.33	27.8	25.1	4.66	215	400	100
K08-081D	KR-104097	132	133	11080	1095	38	2.41	122	1550	0.02	4700	47.8	42200	24.5	0.95	5000	7.48	23.9	22.1	4.31	256	400	100
K08-070D	KR-102654	218.36	219.46	11080	1021	122	15.5	542	130	0.02	104500	1075	14800	5.74	1.96	2370	1.71	776	134.5	1.11	1060	32100	100
K08-070D	KR-102655	219.46	220.52	11080	1020	43	2.33	89	60	0.01	226000	237	7100	4.13	1.88	4170	0.7	302	108	0.48	394	70400	200
K08-070D	KR-102656	220.52	221.86	11080	1019	55	3.29	38	120	0.02	173500	136.5	9100	6.34	1.35	2370	0.93	187.5	110.5	0.74	414	57400	100
K08-070D	KR-102660	221.86	222.5	11080	1018	78	2.91	71.7	680	0.02	14200	153	35300	18.5	1.86	1480	1.14	142	33	4.48	502	6700	100
K08-073D	KR-102681	239.51	240.16	11080	990	71	25.5	315	250	0.08	6600	1070	25500	8.13	0.97	693	1.8	6970	71.9	2.2	5190	2500	300
K08-073D	KR-102682	240.16	240.79	11080	989	60	11.2	100.5	30	0.03	76000	498	8800	2.27	15	1340	1.32	2850	51.6	0.17	4540	22400	200
K08-073D	KR-102683	240.79	241.59	11080	988	54	9.58	92.5	90	0.03	57800	679	17000	4.92	4.14	1410	1.48	2220	106	0.88	3080	18300	200
K08-092D	KR-102832	279.75	280.42	11080	835	14	4.23	70.5	250	0.02	1300	199	18700	4.74	4.79	573	1.34	445	127.5	1.03	598	2000	1500
K08-085D	KR-103471	49.35	50.9	11260	1193	12	1.13	201	1000	0.05	19900	56.4	44900	21.5	0.38	1980	0.53	44.6	29.2	2.58	178	4700	100
K08-061D	KR-103022	151.49	152.5	11260	1080	30	3.93	207	750	0.05	15600	298	29000	13.5	0.45	1460	1.48	235	72.9	4.51	711	7400	100
K08-061D	KR-103023	152.5	153.52	11260	1079	76	6.22	437	350	0.04	67700	674	20600	8.87	0.47	3840	1.08	2150	325	2.57	863	24600	100
K08-063D	KR-103084	195.59	196.9	11260	1024	37	3.75	387	740	0.04	56500	337	29200	7.73	0.88	4700	2.86	1420	166.5	5.32	562	19300	100
K08-063D	KR-103085	196.9	198.42	11260	1022	33	7.15	382	680	0.05	13700	198	37800	10.85	0.69	711	1.37	389	51.1	5.07	508	7200	100
K08-063D	KR-103086	198.42	199.95	11260	1021	32	0.58	392	830	0.03	6000	103	37700	12.1	0.76	370	5.77	185	48.2	6.09	269	3600	100
K08-063D	KR-103087	199.95	201.47	11260	1020	64	5.89	370	620	0.03	14000	234	35800	13.25	1.2	689	2.77	162.5	55.7	5.1	599	7600	100
K08-063D	KR-103088	201.47	203	11260	1018	55	1.75	408	790	0.01	21200	156	37900	13.1	1.02	448	1.34	119	54	6.3	376	7700	100
K08-093D	KR-104297	252.07	253.57	11260	971	50	2.32	86	900	0.09	2700	56.2	31000	16.9	1.23	962	3.12	113	50.7	4.85	249	1600	50
K08-093D	KR-104298	253.57	255.12	11260	970	54	3	122.5	1010	0.07	3100	65.6	32400	18.5	1.39	947	1.37	154.5	67.9	4.87	432	2600	100
K08-093D	KR-104299	255.12	255.42	11260	969	72	5.8	158	680	0.1	2700	66.7	33700	15.75	1.22	630	3.1	171	72.2	4.83	544	1700	100
K08-093D	KR-104300	255.42	256.7	11260	968	98	0.61	188.5	720	0.07	35200	34.7	35600	12.85	2.42	635	8.92	286	127	5.29	279	12700	100
K08-093D	KR-104302	257.3	258.1	11260	966	50	0.8	80.4	490	0.04	92200	122	21500	9.4	5.04	1940	3.16	261	74.9	3.41	280	29600	50
K08-093D	KR-104303	258.1	258.9	11260	966	28	0.83	47	130	0.03	125500	68.7	13800	6.56	7.2	3540	1.91	230	61.9	1.48	413	39900	100
K08-100D	KR-104529	327.3	328.12	11260	909	23	6.67	384	630	0.17	2000	1160	34000	10.55	3.4	991	4.71	3640	35	3.79	3770	2300	300

Klondike Vein Geochemical Data

Hole #	Sample #	Depth From m	Depth To m	Elev m	Section	Au-FA ppm	Ag-FA ppm	As ppm	Ba ppm	Bi ppm	Ca %	Cu ppm	Fe ppm	Ga ppm	Hg ppm	Mn ppm	Mo ppm	Pb ppm	Sb ppm	Tl ppm	Zn ppm	C ppm	S ppm
U11-127D	LU109420	198.42	199.95	1138.06	4970	0.036	22.6	143	1300	0.07	0.6	25.7	22000	15.25	5.15	736	1.14	62.1	148.5	2.51	153	2900	<100
U11-127D	LU109421	199.95	201.47	1136.72	4970	0.024	14.9	139	1490	0.12	0.29	20.8	23600	17.5	1.98	562	0.57	54	153	3.42	180	2700	<100
U11-127D	LU109431	210.92	212.45	1127.07	4970	0.014	4.42	126.5	1810	0.1	1.94	18.8	28000	14.35	1.78	813	0.24	102	144.5	3.62	350	3700	<100
U11-127D	LU109432	212.45	213.97	1125.83	4970	0.051	10.2	187	1600	0.07	0.36	32.9	29900	15.15	1.69	476	0.55	131.5	187.5	3.1	404	1500	<100
U11-127D	LU109439	220.18	221.59	1119.01	4970	0.145	79.7	107	400	0.01	0.71	43.6	6900	2.55	2.62	389	0.77	92.1	167	0.38	70	4000	<100
U11-127D	LU109440	221.59	223.11	1117.62	4970	0.393	80.7	185	880	0.03	4.8	32.6	13400	4.35	3.51	1490	0.73	124.5	261	1.23	133	16000	<100
U11-127D	LU109448	230.73	232.25	1107.77	4970	0.259	25.9	523	1470	0.03	0.26	18.9	27100	9.72	1.37	230	1.06	117.5	262	6.08	95	1400	<100
U11-127D	LU109449	232.25	233.78	1106.38	4970	0.191	29.2	326	1250	0.03	0.15	15.9	19900	9.32	1.39	128	0.66	69.8	242	4.32	58	1400	<100
U11-127D	LU109456	241.18	241.55	1101.25	4970	0.296	>100	63.5	6100	0.01	9.66	12.6	4600	2.68	1.19	2370	0.65	143.5	192.5	0.73	122	3000	8400
U11-127D	LU109457	241.55	242.93	1100.41	4970	0.287	>100	58.4	3640	0.01	4.65	22.2	3600	2.41	2.49	1340	0.59	114	98.4	0.09	94	15500	700
U11-127D	LU109458	242.93	243.75	1099.35	4970	0.185	85.8	124	1660	0.02	1.54	24.4	7200	3.4	1.49	387	0.74	113	195.5	0.91	68	5000	<100
U11-127D	LU109465	250.5	251.77	1092.62	4970	0.202	39.9	214	1330	0.07	1.57	42	26500	15.5	0.93	366	2.28	139	213	3.39	110	4100	<100
U11-127D	LU109466	251.77	252.07	1091.95	4970	0.04	11.1	38.5	200	0.01	2.84	8.9	4600	9.8	0.25	475	0.65	25.6	245	0.42	16	8400	<100
U11-127D	LU109478	259.88	261.21	1084.32	4970	0.227	21	587	2300	0.1	0.67	12	25500	9.56	1.57	418	0.51	142	312	5	318	2500	<100
U11-127D	LU109479	261.21	261.81	1083.63	4970	0.254	14.15	79	480	0.02	16.5	8.7	8500	4.08	2.37	2050	0.25	57.2	118.5	0.93	284	52600	<100
U11-127D	LU109490	270.36	271.38	1075.44	4970	0.376	15.15	24	170	0.01	11.55	2.4	2100	1.13	0.79	1360	0.3	49.9	65.1	0.12	14	36100	<100
U11-127D	LU109491	271.38	272.4	1074.38	4970	0.251	8.33	26	100	<0.01	26.2	1.1	1600	1.11	1.41	2930	0.18	19.3	34.7	0.03	6	83800	<100
U11-127D	LU109492	272.4	273.41	1073.57	4970	1.84	16.9	30	180	<0.01	23.5	1.8	1700	1.35	2.21	3720	0.35	48.3	40.5	0.05	5	77500	<100
U11-127D	LU109498	273.41	274.43	1072.73	4970	3.65	17.15	32	140	<0.01	22.5	2.3	1900	0.03	1.9	2590	0.39	40.9	51.5	0.04	7	73400	<100
U11-127D	LU109500	281.02	282.55	1065.86	4970	0.146	22.4	428	660	0.1	0.42	18.6	42100	23.9	2.03	227	8.83	174.5	130.5	3.69	363	2300	<100
U11-127D	LU109501	282.55	284.07	1064.39	4970	0.183	13.25	196	550	0.06	0.78	38.6	38800	20.4	1.74	473	12.15	71.3	73.4	2.01	230	2800	<100
U11-113D	LU107343	200.86	202.39	1123.4	4970	1.24	19.75	70	650	0.05	13.05	9.9	11300	6.32	0.7	1860	0.85	66.5	119.5	0.70	146	40700	<100
U11-113D	LU107344	202.39	203.91	1121.84	4970	0.377	10.75	98	380	0.14	12.2	11.2	12800	8.59	0.5	1580	0.72	89.9	126	0.97	101	34900	<100
U11-113D	LU107351	211.53	213.06	1113.26	4970	19.95	24.3	181.5	1050	0.18	1.39	19.3	23800	16.2	0.5	459	0.48	117.5	133.5	1.78	272	4300	<100
U11-113D	LU107352	213.06	214.58	1111.86	4970	14.1	14.4	99.6	540	0.18	5.11	10.9	17300	15.8	0.4	586	0.35	86.8	111	1.46	177	14900	<100
U11-113D	LU107358	220.67	222.2	1110.46	4970	0.954	25.1	161.5	710	0.17	6.39	14.8	20400	14.6	1.1	809	1.34	148.5	155	1.57	262	19000	<100
U11-113D	LU107359	222.2	223.3	1109.06	4970	3.19	34.1	27	140	0.02	18.15	3.7	4300	2.85	0.7	2210	0.32	31.8	104	0.23	35	55000	<100
U11-113D	LU107365	228.3	229.82	1097.41	4970	12.75	17.9	74.5	730	0.12	5.68	8.1	12500	11.7	0.7	905	0.37	47.9	74.7	1.22	152	17500	<100
U11-113D	LU107367	229.82	231.34	1096.02	4970	1.295	75.3	67.6	1030	0.1	9.15	6.2	10700	10.35	0.5	926	0.47	36	71.8	1.4	157	27000	<100
U11-113D	LU107377	239.52	240.49	1087.12	4970	3.86	35.2	20	80	0.01	12.25	5.5	5300	2.11	0.7	2910	1.26	12.3	24.3	0.08	23	39800	<100
U11-113D	LU107378	240.49	242.01	1085.93	4970	3.54	55.2	40	330	0.03	11.8	8.6	6500	3.72	0.4	1900	0.66	26.2	30.3	0.59	34	37300	<100
U11-113D	LU107388	249.63	251.16	1077.35	4970	3.99	11.6	87.9	520	0.14	9.06	9.8	12100	8.19	0.41	1070	0.35	79.4	85.9	1.29	153	29400	<100
U11-113D	LU107389	251.16	252.68	1075.75	4970	0.889	5.48	112	760	0.12	6	8.1	12800	11.55	0.83	805	0.46	83.9	95	1.64	164	21600	<100
U11-113D	LU107390	252.68	254.21	1074.35	4970	1.63	78.2	72.8	640	0.08	9.87	8.6	9600	7.49	0.58	630	0.36	58	121.5	1.04	147	3600	<100
U11-113D	LU107394	258.78	260.3	1068.56	4970	3.92	8.36	98	510	0.08	12.1	9.8	10500	7.69	0.67	852	0.42	72.1	74.8	1.3	132	42200	<100
U11-113D	LU107395	260.3	261.82	1067.11	4970	7.15	9.3	121	400	0.1	16.75	10.1	12300	5.18	0.59	1180	0.63	71	106.5	0.8	196	57200	<100
U11-113D	LU107401	267.92	269.44	1060	4970	1.365	4.03	53.6	500	0.12	8.22	7	6000	8.56	0.23	521	0.44	35.3	38	1.04	60	26800	<100
U11-113D	LU107402	269.44	270.97	1058.48	4970	1.51	4.38	34	420	0.1	14.6	6.6	7500	5.54	0.26	1100	0.28	30.7	39	0.77	84	47300	<100
U11-113D	LU107414	280.11	281.63	1048.36	4970	0.903	14.2	119	1020	0.13	8.97	13.9	14200	9.68	0.82	1190	1.08	112	77.9	1.94	111	27700	<100
U11-113D	LU107415	281.63	283.15	1047.65	4970	0.536	44.4	167.5	1810	0.12	9.02	56.9	15100	9.09	1.2	434	0.58	162	119.5	2.74	115	16800	<100
U11-113D	LU107427	291.7	292.3	1037.85	4970	0.499	3.7	13	90	0.01	16.85	5.4	5300	2.02	0.22	2010	0.26	18.4	21.7	0.09	21	55400	<100
U11-113D	LU107428	292.3	292.48	1037.6	4970	0.209	6.35	21	410	0.04	18.2	8.7	8200	3.62	0.35	3750	0.35	54.2	52.9	0.66	70	59200	<100
U11-113D	LU107435	301.45	302.97	1028.08	4970	1.26	11.7	81	550	0.06	21.3	26.1	13600	5.77	0.58	7060	0.44	148.5	81.7	0.84	301	66000	<100
U11-113D	LU107436	301.45	302.97	1028.84	4970	0.702	16.65	81	650	0.06	17.85	34.8	16200	6.88	0.59	6060	0.48	175.5	95.9	1.01	407	55300	<100
U11-113D	LU107440	307.54	309.06	1021	4970	0.819	49.9	83.3	590	0.12	8.04	38	19200	9.52	0.27	3060	0.5	111.5	107	1.18	290	28600	<100
U11-113D	LU107441	309.06	310.59	1020.84	4970	0.986	13.75	106.5	610	0.14	9.91	36.3	23400	11.35	0.3	3900	0.48	192.5	86.9	1.25	427	34200	<100
U11-113D	LU107450	319.74	320.13	1011.55	4970	0.407	2.48	29	110	0.01	12.25	5.4	4500	2.46	0.14	2500	1.16	149.5	69.3	0.24	24	41900	<100
U11-113D	LU107452	320.13	321.26	1010.79	4970	0.092	9.66	68.3	550	0.04	4.75	34.6	13000	5.99	0.3	1300	48.9	113	85.3	2.22	260	16700	<100
U11-129D	LU109540	227.69	229.21	1103.08	4970	4.39	59.6	125.5	560	0.02	0.64	13.8	15400	8.44	1.27	221	0.4	45.9	183	1.37	32	4400	<100
U11-129D	LU109541	229.21	230.73	1101.49	4970	3.09	41.7	153	770	0.03	1.56	20.8	23500	11.2	1.03	433	0.46	59.2	184	1.88	103	6300	<100
U11-129D	LU109555	247.49	249.02	1084.74	4970	1.64	5	48.8	800	0.23	0.53	13.3	9100	15.15	0.16	230	0.38	31.1	48.3	1.15	105	9900	<100
U11-129D	LU109556	249.02	250.54	1083.26	4970	0.405	10.1	108.5	750	0.2	0.54	16	20700	19.25	0.22	302	0.75	44.4	60.8	1.28	147	3300	

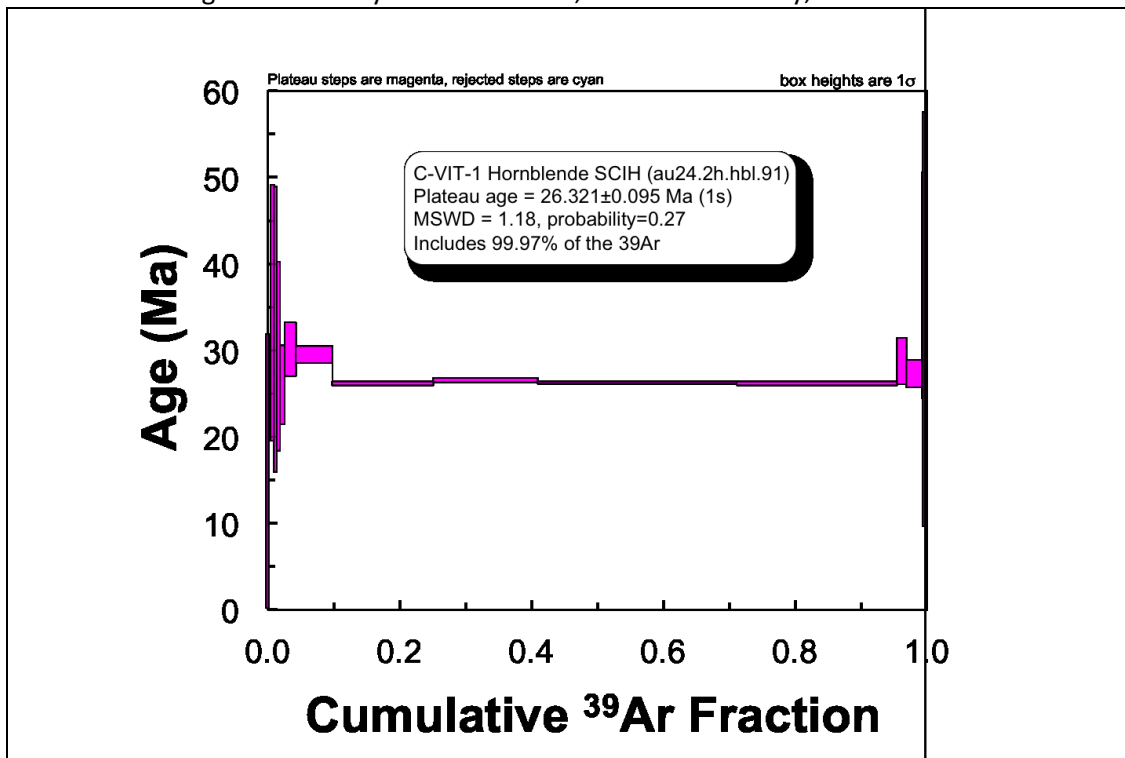
IV. XRF Data on Green Quartz and Dark Carbonate

Sample	Sample Type	Location	C %	SiO ₂ %	Al ₂ O ₃ %	Fe ₂ O ₃ %	CaO %	MgO %	Na ₂ O %	K ₂ O %	Cr ₂ O ₃ %	TiO ₂ %	MnO %	P ₂ O ₅ %	SrO %	BaO %
Q-001	Green Qtz.	Mercedes	0.06	95.9	1.3	0.32	0.48	0.22	0.22	0.16	<0.01	0.03	0.01	<0.01	0.01	0.01
Q-002	Green Qtz.	Mercedes	0.06	98.1	0.39	0.09	0.34	0.08	0.05	0.05	<0.01	<0.01	0.05	<0.01	<0.01	<0.01
Q-003	Green Qtz.	Mercedes	0.23	95.2	0.57	0.28	1.37	0.21	0.04	0.05	<0.01	0.01	0.05	<0.01	0.01	0.01
Q-004	Green Qtz.	Klondike	0.01	98.8	0.89	0.14	0.22	0.06	0.15	0.14	<0.01	0.02	0.04	<0.01	<0.01	<0.01
C-001	Dark Carbonate	Mercedes	9.67	14.9	0.29	0.89	46.3	0.15	0.02	0.23	<0.01	<0.01	3.78	0.02	0.08	0.3
C-002	Dark Carbonate	Klondike	8.75	23.1	0.18	0.67	40.2	0.09	0.01	0.12	<0.01	0.01	1.19	0.03	0.05	0.15

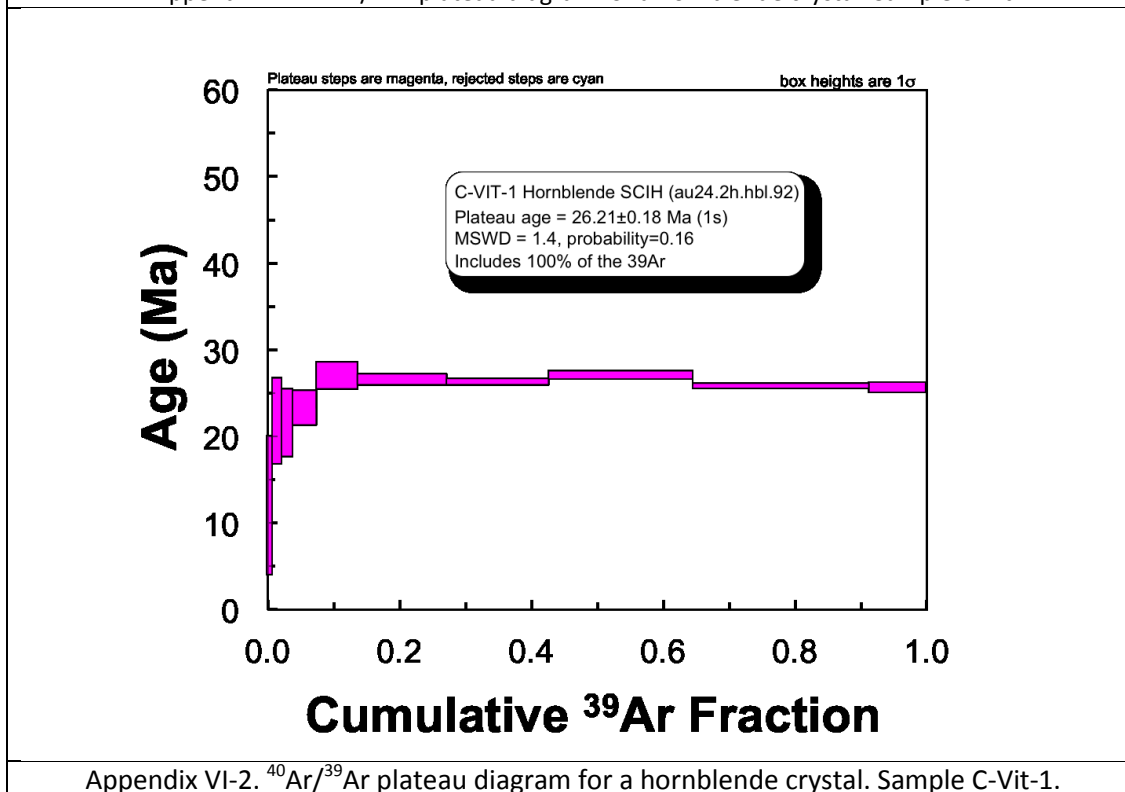
	Ag	Au	Cd	Co	Cu	Fe	Ga	Ge	Hf	Hg	In	K	Li	Ni	Pb	Rb	Sb	Se	Sn	Sr	Ta	Tl	Ti	V	W	Zn	Zr	C	S																	
Ag	1.000																																													
Au	0.993	1.000																																												
Cd	0.377	-0.021	1.000																																											
Co	0.014	0.081	0.030	1.000																																										
Cu	0.474	0.014	0.520	0.379	1.000																																									
Fe	0.176	0.034	0.137	-0.098	0.154	1.000																																								
Ga	-0.242	0.141	-0.235	0.487	0.116	0.113	-0.243	1.000																																						
Ge	0.055	-0.095	0.066	-0.377	-0.124	-0.248	-0.316	-0.162	1.000																																					
Hf	0.227	0.076	0.223	-0.222	-0.086	0.084	-0.225	0.093	0.143	1.000																																				
Hg	-0.324	-0.064	0.300	0.904	0.369	0.417	-0.081	0.345	-0.390	-0.205	1.000																																			
In	-0.245	-0.050	-0.228	0.674	0.274	0.273	0.004	0.296	-0.090	-0.205	0.478	1.000																																		
K	0.055	0.049	0.050	0.031	0.053	0.028	0.225	0.010	-0.356	-0.184	-0.008	0.177	1.000																																	
Li	-0.152	-0.042	-0.140	0.521	0.345	0.163	0.134	0.151	-0.225	-0.147	0.462	0.488	0.068	1.000																																
Ni	0.104	-0.462	-0.098	0.153	0.137	0.134	-0.183	0.314	-0.175	0.414	0.136	0.067	0.086	0.024	1.000																															
Pb	0.227	0.082	0.214	0.909	0.496	0.351	0.063	0.384	-0.395	-0.188	0.819	0.898	0.182	0.326	0.215	1.000																														
Rb	0.357	-0.007	0.331	0.954	0.367	0.333	0.029	0.457	-0.361	0.257	0.844	0.702	0.006	0.592	0.106	0.788	1.000																													
Sb	0.088	0.050	-0.077	0.443	0.454	0.192	-0.096	0.224	-0.497	0.192	0.014	0.289	-0.115	0.267	0.439	0.096	0.096	1.000																												
Se	0.366	-0.104	-0.357	0.909	0.296	0.396	-0.102	0.402	-0.147	-0.222	0.938	0.572	0.033	0.482	0.136	0.875	0.874	0.273	1.000																											
Sn	0.518	0.350	0.541	0.178	0.104	0.298	0.027	-0.082	-0.034	0.169	-0.160	-0.100	0.066	-0.103	0.314	-0.016	-0.203	0.066	-0.227	1.000																										
Sr	0.315	0.030	0.298	0.808	0.298	0.273	-0.142	0.618	-0.170	-0.141	0.445	-0.297	0.143	0.453	0.205	0.839	0.808	0.204	0.731	0.143	1.000																									
Ta	0.312	-0.064	-0.294	0.912	0.435	0.384	-0.174	0.480	-0.443	-0.191	0.907	0.491	0.089	0.392	0.256	0.699	0.800	0.387	0.667	0.074	0.682	1.000																								
Tl	0.317	-0.079	-0.291	0.876	0.318	0.416	-0.063	0.318	-0.397	-0.209	0.994	0.450	0.017	0.471	0.122	0.810	0.820	0.314	0.931	-0.166	0.610	0.867	1.000																							
Ti	0.218	0.047	0.137	-0.427	-0.265	-0.207	0.111	-0.298	-0.101	0.035	-0.160	-0.375	0.304	-0.208	-0.099	-0.294	-0.469	-0.302	-0.586	0.063	-0.505	-0.148	-0.556	1.000																						
V	0.282	0.006	-0.242	0.675	0.177	0.246	-0.047	0.319	-0.116	-0.161	0.499	0.267	0.467	0.147	0.834	0.704	0.239	0.602	-0.102	0.777	0.521	0.475	-0.337	0.900																						
W	-0.001	-0.029	-0.008	0.300	-0.243	-0.076	-0.205	-0.096	0.704	0.318	-0.292	0.088	-0.133	-0.150	0.051	-0.070	-0.263	0.300	0.240	0.052	-0.030	-0.368	-0.292	-0.120	0.083	1.000																				
Zn	-0.005	-0.014	-0.008	0.025	0.075	-0.014	-0.089	-0.096	-0.092	0.039	0.084	0.033	0.006	0.050	0.112	0.074	0.015	-0.014	-0.029	0.072	-0.012	0.071	0.008	0.111	0.036	-0.063	1.000																			
Zr	0.283	-0.049	-0.259	0.545	0.037	0.105	-0.141	0.360	-0.012	-0.019	0.370	0.122	-0.007	0.332	0.054	0.493	0.554	0.247	0.413	-0.190	0.604	0.328	0.336	-0.426	0.510	-0.014	-0.051	1.000																		
C	0.146	-0.050	-0.140	0.474	0.267	0.219	0.086	0.140	-0.113	-0.179	0.338	0.768	0.626	0.360	0.026	0.679	0.447	0.253	0.413	-0.058	0.548	0.392	0.509	-0.219	0.712	0.016	-0.037	0.294	1.000																	
S	0.189	-0.117	-0.173	0.978	0.529	0.356	0.115	0.189	-0.266	-0.199	0.586	0.816	0.301	0.600	0.045	0.834	0.808	0.472	0.605	-0.081	0.607	0.592	0.564	-0.360	0.782	0.132	0.233	0.190	0.756	1.000																
Co	0.011	0.123	0.007	0.088	0.131	0.067	-0.200	0.288	-0.046	0.432	0.077	-0.070	-0.079	-0.018	0.778	0.057	0.025	0.144	0.069	0.139	0.124	0.143	0.066	-0.112	-0.002	0.076	0.041	0.998	-0.066	-0.024	1.000															
Fe	0.319	0.045	-0.300	0.918	0.426	0.314	-0.132	0.545	-0.368	-0.220	0.811	0.595	0.016	0.527	0.182	0.763	0.864	0.444	0.834	-0.122	0.794	0.929	0.812	-0.048	0.580	-0.289	0.133	0.421	0.379	0.621	0.071	1.000														
Ga	0.072	0.040	0.062	0.001	0.039	0.185	0.073	0.047	-0.114	-0.059	0.009	0.014	0.084	0.002	0.011	0.014	-0.011	0.073	0.002	-0.046	-0.016	0.069	0.039	0.106	0.012	0.095	0.011	-0.085	0.006	0.046	0.014	0.041	1.000													
Ge	0.380	0.392	0.362	0.023	0.572	0.268	0.286	-0.032	-0.356	0.048	-0.001	-0.006	0.166	0.010	0.252	0.300	-0.068	0.166	-0.111	0.470	-0.066	0.135	-0.007	0.147	-0.096	-0.219	0.024	-0.211	0.051	0.237	0.998	0.073	0.070	1.000												
Hf	-0.344	-0.198	-0.245	0.971	0.431	0.317	-0.060	0.382	-0.123	-0.217	0.688	0.883	0.121	0.415	0.065	0.894	0.745	0.243	0.672	-0.163	0.878	0.611	0.559	-0.497	0.796	0.024	-0.012	0.526	0.703	0.794	0.021	0.689	0.026	0.034	1.000											
In	0.025	0.294	-0.026	0.012	0.068	0.027	-0.106	0.057	0.160	0.063	0.003	-0.022	0.001	-0.074	0.156	0.020	-0.040	0.065	-0.008	0.213	0.078	0.037	-0.006	-0.100	-0.010	0.071	-0.026	0.184	-0.024	-0.060	0.061	0.033	0.065	0.030	1.000											
Ni	0.229	-0.007	-0.314	0.771	0.253	0.264	-0.244	0.777	-0.275	-0.093	0.682	0.477	-0.009	0.350	0.255	0.603	0.731	0.812	0.738	0.051	-0.477	0.520	-0.179	-0.006	0.523	0.300	0.461	0.231	0.782	0.007	-0.054	0.604	0.604	0.026	1.000											
Pb	-0.113	-0.009	-0.101	-0.372	-0.151	-0.185	-0.305	-0.088	0.014	0.441	-0.213	0.041	-0.306	-0.084	-0.214	-0.127	-0.193	0.008	-0.393	-0.067	-0.063	-0.163	-0.227	-0.362	0.017	0.513	0.101	0.006	-0.070	-0.113	-0.200	-0.084	-0.265	0.022	0.145	-0.148	1.000									
Rb	0.330	-0.061	-0.365	0.618	0.019	0.114	-0.201	0.317	-0.197	-0.094	0.747	0.051	-0.240	0.138	0.127	0.819	0.611	0.027	0.762	-0.227	0.352	0.643	0.752	-0.483	0.146	0.283	-0.020	0.164	-0.057	0.062	0.189	0.562	0.040	-0.284	0.191	-0.031	0.524	-0.235	1.000							
Sb	0.028	0.057	0.015	-0.183	-0.135	-0.147	-0.083	0.033	0.029	-0.177	-0.127	0.023	-0.071	0.078	0.141	-0.189	0.095	-0.188	-0.004	-0.168	-0.159	-0.173	0.073	-0.115	0.013	0.126	-0.114	-0.108	-0.139	-0.023	-0.149	-0.025	-0.061	-0.163	0.001	-0.140	-0.024	-0.133	1.000							
Se	0.287	0.031	0.266	0.467	0.029	0.119	-0.172	0.244	-0.158	-0.132	0.593	0.006	-0.208	0.114	0.117	0.178	0.541	-0.013	0.748	-0.146	0.285	0.645	0.708	-0.399	0.097	-0.309	-0.002	0.144	-0.088	0.011	0.099	0.544	-0.020	-0.212	0.116	0.001	0.413	-0.278	-0.043	0.113	1.000					
Sn	0.252	-0.077	0.236	0.802	0.220	0.222	0.029	0.312	-0.192	-0.233	0.612	0.036	0.151	0.056	0.930	0.772	0.466	0.605	-0.144	0.843	0.645	0.582	-0.470	0.799	-0.063	0.038	0.499	0.715	0.903	-0.013	0.727	0.016	0.117	0.951	-0.020	-0.034	0.116	-0.154	0.090	1.000						
Ta	0.122	0.031	-0.116	0.729	0.798	0.413	-0.004	0.212	-0.405	-0.174	0.448	0.448	0.129	0.145	0.153	0.854	0.576	0.520	0.570	0.036	0.485	0.714	0.623	-0.377	0.382	0.331	0.157	0.123	0.418	0.713	0.071	0.657	0.064	0.447	0.596	-0.031	0.505	-0.187	0.222	-0.100	0.229	0.487	1.000			
Tl	0.283	0.023	-0.264	0.796	0.288	0.253	-0.247	0.305	-0.297	-0.074	0.788	0.151	-0.226	0.175	0.202	0.427	0.693	0.053	0.884	-0.205	0.585	0.745	0.625	-0.429	0.367	-0.220	-0.001	0.381	0.079	0.209	0.245	0.689	-0.001	-0.223	0.427	0.044	0.673	-0.201	0.882	-0.140	-0.060	0.353	0.330	1.000		

VI. Glassy Latite Age Date

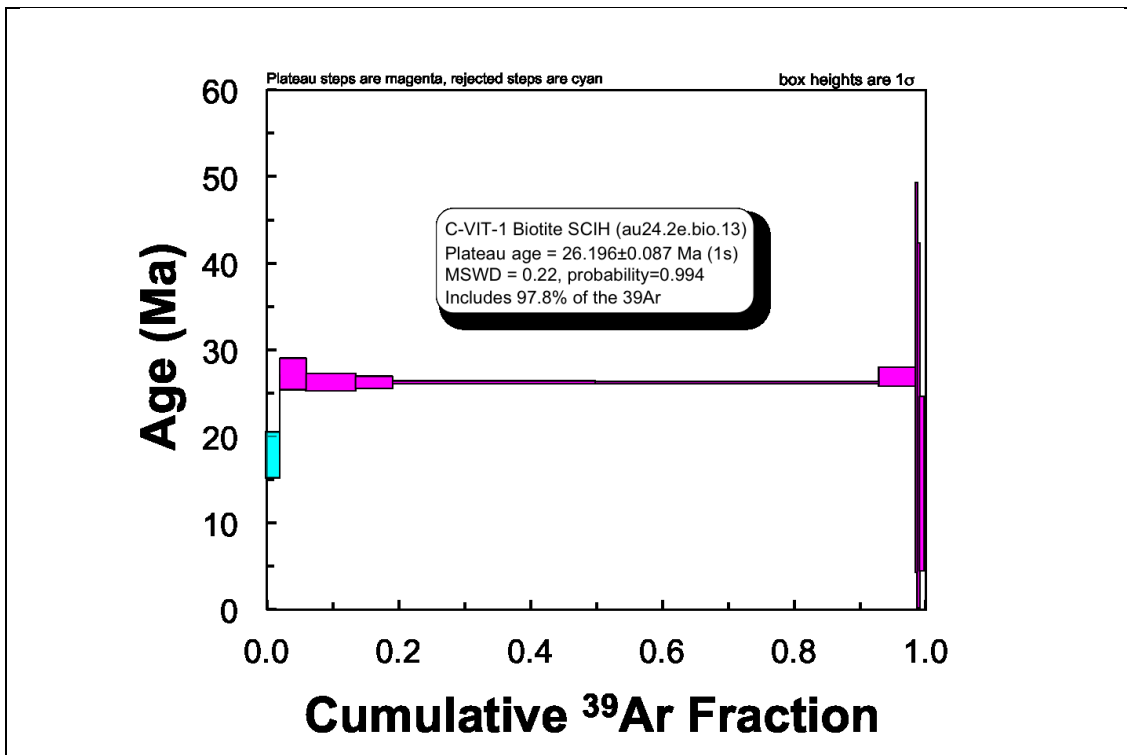
Plateau diagrams courtesy of Willis Hames, Auburn University, 2013.



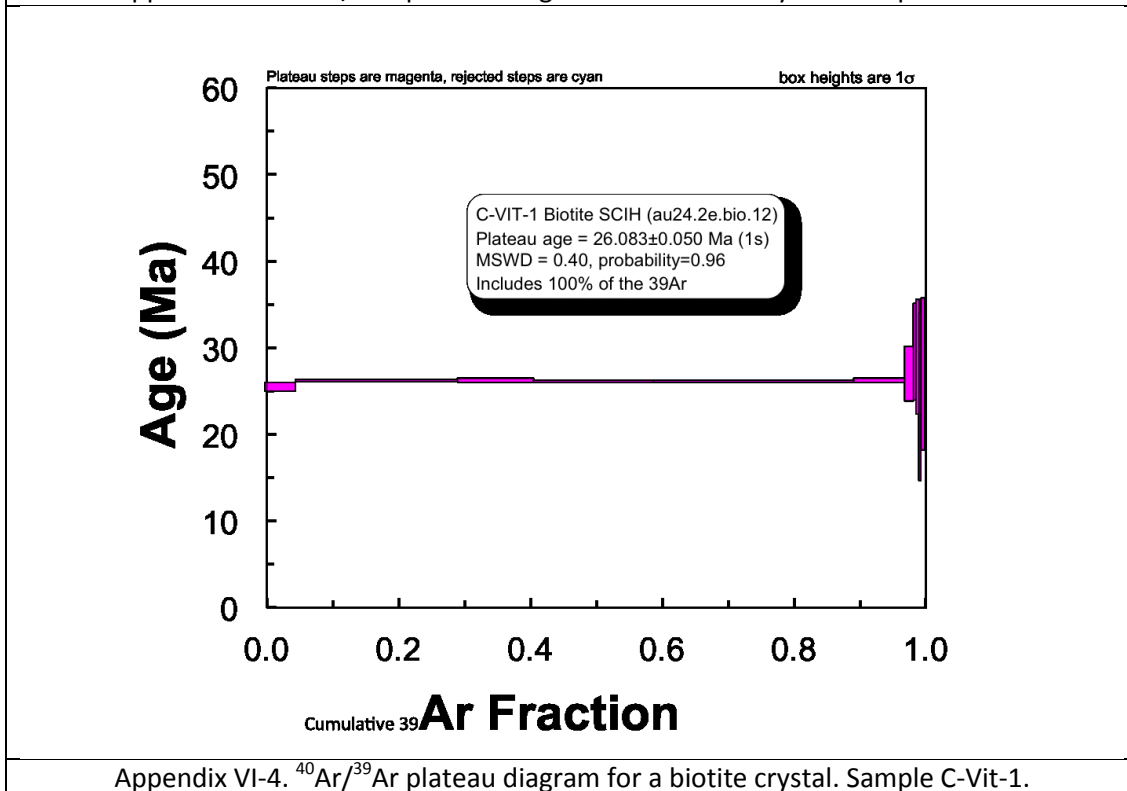
Appendix VI-1. $^{40}\text{Ar}/^{39}\text{Ar}$ plateau diagram for a hornblende crystal. Sample C-Vit-1.



Appendix VI-2. $^{40}\text{Ar}/^{39}\text{Ar}$ plateau diagram for a hornblende crystal. Sample C-Vit-1.



Appendix VI-3. $^{40}\text{Ar}/^{39}\text{Ar}$ plateau diagram for a biotite crystal. Sample C-Vit-1.



Appendix VI-4. $^{40}\text{Ar}/^{39}\text{Ar}$ plateau diagram for a biotite crystal. Sample C-Vit-1.